University of Cincinnati

Date: 6/19/2014

I, Aniket Vyas , hereby submit this original work as part of the requirements for the degree of Doctor of Philosophy in Materials Science.

It is entitled:

MORPHOLOGY AND PROPERTIES OF CLAY/NYLON-6-EPOXY NANOCOMPOSITES, COATINGS AND FILMS

Student's name: **Aniket Vyas**

This work and its defense approved by:

Committee chair: Jude Iroh, Ph.D.

Committee member: F James Boerio, Ph.D.

Committee member: Raj Manglik, Ph.D.

Committee member: Rodney Roseman, Ph.D.

10564

Morphology and Properties of Clay/Nylon-6-Epoxy Nanocomposites, Coatings and Films

A dissertation submitted to the
Division of Research and Advanced Studies
University of Cincinnati
In Partial Fulfilment of the requirements for the degree of
Doctorate of Philosophy (Ph.D.)
December, 2014
By
Aniket Vyas
B.Tech – Surface Coating technology (ICT, Mumbai)

Committee Members: Dr. Jude O. Iroh (Chair)
Dr. F. James Boerio
Dr. Raj M. Manglik
Dr. Rodney D. Roseman

Program of Material Science and Engineering

University of Cincinnati

ABSTRACT

This research is focused on the synthesis, characterization and properties of epoxy based coatings, blended and cured with thermoplastic nylon-6 and organoclay modified nylon-6. Epoxy resins has 2 major drawbacks: (1) extremely brittle nature and (2) moisture absorption. The first problem is solved by incorporation of nylon-6 in epoxy, and the second problem is solved by incorporation of nano-clay in the nylon-6/epoxy system.

The storage modulus in glassy region for nylon-6/epoxy composites decreased linearly as nylon-6 weight % increased, along with decrease in glass transition temperature from 70 °C to 30 °C. The storage modulus in rubbery region increased compared to control epoxy. The control epoxy used in the system was water based EPIREZ5522-WY-55, thermally heated without using curing agent. The curing agent was not used to study the effect of nylon-6 on storage modulus in rubbery region. These results indicated that sole nylon-6 increased cross-link density of epoxy resin, which was verified by determining fractional epoxy conversion by monitoring characteristic epoxy peak at 914 cm^{-1} in FTIR, which increased with increase in nylon-6 wt.%. The nylon-6/epoxy coatings applied on Al-2024 T3 substrate were tested for anti-corrosion. The coating containing 10% of nylon-6 in epoxy showed the best performance, compared to other compositions. Comparison with formulation cured by thermal treatment of epoxy showed that nylon-6 alone without standard curing agent is effective in improving the properties, while comparison with standard epoxy-amine system suggested that the novel technology can be effectively used in practical applications. Then clay/nylon-6 nanocomposites were synthesized using in-situ solution polymerization. As the concentration of clay was increased to 0.5 % by weight, molecular weight of nylon-6 increased from 10362 g/mol to 10659 g/mol. On further increasing clay weight %, the molecular weight of nylon-6 decreased. The melting point of

nylon-6 increased from 209 to 217 °C on addition of clay at 0.5 weight%. But on increasing clay to 1 wt%, it decreased with broadening in peak. On further increasing clay, the melting peak was not observed.

Then clay/nylon-6-epoxy nanocomposites were prepared for improving thermo-mechanical and corrosion inhibition properties of epoxy matrix. The storage modulus in glassy as well as rubbery region were found to increase upto a clay concentration of 1 weight% with respect to nylon-6, while after that it began to decrease. After incorporation of clay, the corrosion current reduced by 4 orders of magnitude in Direct Current Polarization tests, while impedance value increased by 2 orders of magnitude as observed in Bode plots.

The nylon-6/epoxy composite showed a multiphase morphology with distinct amorphous and crystalline zones. The nylon-6 crystals were found to be distributed among the epoxy resin, which increased in number with increase of nylon-6 concentration in epoxy from 5 to 30 wt.%., and lead to decrease in glass transition temperature and storage modulus. At the surface of coating, the nylon-6 crystals were found to be growing in the cracks and crevices of epoxy formed during the curing process. This lead to improved barrier properties of nylon-6/epoxy coating

Acknowledgments

I have written this dissertation in loving memory of my grandmother, Late Mrs. Motibala Joshi (1947-2011).

I am extremely grateful to my academic advisor Dr. Jude Iroh who guided, supported and motivated me to carry out independent experimental research in polymer science, which enabled me to hone my creativity in scientific manner. I am highly indebted to him for providing me with significant worldly experience which has allowed me to grow into a wise and pragmatic person.

I dedicate my dissertation to my parents (Mr. Jitendra Vyas and Mrs. Sunita Vyas) who supported me in every form and prayed for my success continuously. Their blessings kept me focused for the entire duration of PhD and made my will stronger to reach my goal without stopping.

I would also like to convey my appreciation to my dissertation committee members Dr. F. James Boerio, Dr. Rodney Roseman and Dr. Raj Manglik, who took time out of their busy schedule to serve in my committee and provided valuable feedback during my progress review.

This PhD would not be possible without motivation from my academic mentor Dr. T C Gupta (Professor – Mechanical Engineer, Malviya National Institute of Technology, Jaipur, India) and my lab mates Jimmy Longun, Jaspreet Beemat and Linqian Feng who provided instant technical support whenever required, participated in valuable scientific discussions, regulated a strong work ethic and partook equally in every moment of success and failure.

I highly appreciate Soumyarwit Manna at Advanced Material Characterization Center (AMCC), UC for assisting me greatly with microscopic techniques that enabled me to witness wonderful

novel morphologies in the system I developed as a part of my research. I would also like to extend my appreciation to Dr. Necati Kaval in Chemistry department, who trained me with spectroscopy instrumentation.

I also acknowledge the support from Padmanabh Joshi, who inspired and motivated me to work efficiently while maintaining a balance between work and extra-curricular activities. I am also grateful for his technical suggestions during my research.

I am thankful to UC Racquetball Club and World Peace Yoga, Clifton which provided me a medium to maintain a daily routine with recreational activities, enabling me to work with strong focus and determination, and helped me to stay calm and peaceful in challenging times.

I would like to extend my appreciation to my other lab mates Anushree Deshpande. Shirley Peng, Nathan Holliday, Patricia Okafor, Wajeeh Marashdeh, Yujie Zhang and Praveen Kumar for supporting me during the course of PhD.

I am also grateful to my friends for their love, support and memorable times gifted to me by Prachi Gupta, Anubhav Mathur, Som Bahadur, Amit Joshi, Raghav Aditya, Pratik Sogani, Sonam Chourasiya, Amit Arbune, Shrishti Pant, Rutooj Deshpande, Suraj Nagpure, Brad Ruff, Patrick Welage, Nivedita Singh , Chaitanya Kane, Dara Pultorak O' Loughlin and Rachit Malik.

Table of Contents

Chapter 1. Introduction/Background

Chapter 2. Experimental

2.2. Processing

2.3 Analytical Techniques

Chapter 3. Results and Discussion

3.1. Hybrid Blends of Nylon-6 and Epoxy

3.2. 15A Clay/nylon-6 Nanocomposite

3.3. Hybrid Blends of Clay/Nylon-6 Nanocomposite and Epoxy

List of Figures

Figure 60 – Dynamic Mechanical Properties (storage modulus and tan(δ) as a function of temperature) of Clay-nylon-6/epoxy componensts at epoxy: nylon ratio of 90:10 by weight (a-0 wt.% clay, b- 0.05 wt.% clay, c- 0.1 wt.% clay, d- 0.5 wt.% clay and 1wt.% clay with respect to solid content of epoxy)

Figure 61 –Storage Modulus of clay/nylon 6-epoxy nanocomposite films as a function of clay weight% (a) in glassy region at T=-10^{O}C (b) in transition region at T=10^{O}C

Figure 62 –Storage Modulus of clay/nylon 6-epoxy nanocomposite films as a function of clay weight% in rubbery region at T=45^{O}C

Figure 63 –Glass transition temperature of clay/nylon 6-epoxy nanocomposite films as a function of clay weight% for epoxy: nylon-6 ratio of 90:10.

Figure 64 – Weight of nylon-6 reacted with epoxy as a function of clay weight%.

Figure 65 - DCP Plots for epoxy/nylon-6 (90:10) coatings on Al 2024-T3 alloy substrate filled with clay after (a) 1 day of exposure (b) after 2 months of exposure to 3.5 weight% salt solution (1- thermally cured neat epoxy, 2- epoxy/nylon-6(10wt.%), 3 - 0.05wt.% clay, 4 – 0.1 wt.% clay, 5- 0.5 wt.% clay, 6- 1 wt.% clay with respect to solid content in epoxy)

Figure 66 - Bode Plots for clay modified nylon-6 filled epoxy coatings on Al 2024-T3 alloy substrate after exposure to 3.5% salt solution for 2 months at epoxy: nylon-6 ratio of 90:10 (a) after 1 day of exposure (b) after 2 months of exposure to 3.5 weight% salt solution. (1- thermally cured neat epoxy, 2- epoxy/nylon-6(10wt.%), 3 - 0.05wt.% clay, 4 – 0.1 wt.% clay, 5- 0.5 wt.% clay, 6- 1 wt.% clay with respect to solid content in epoxy)

List of Abbreviations

NY	Nylon
PA	Polyamide
EPNY	Epoxy/Nylon
EPNYCL	Epoxy/Nylon/Clay
MMT	Montmorillonite-Clay
NMP	N-Methyl-Pyrrolidone
AA	AA-2024-T3
FTIR	Fourier Transform Infrared Spectroscopy
DSC	Differential Scanning Calorimetry
XRD	X-ray Diffraction
SEM	Scanning Electron Microscope
TEM	Transmission Electron Microscope
DMS	Dynamic Mechanical Spectroscope
DCP	Direct Current Polarization
EIS	Electrochemical Impedance Spectroscopy
Rp	Polarization Resistance
OCP	Open Circuit Potential
SCE	Saturated Calomel Electrode
WE	Working Electrode
CE	Counter Electrode
RE	Reference Electrode

CHAPTER 1

INTRODUCTION

1.1. Epoxy Resin

Epoxy resins are extensively used as coatings and adhesives in automotive, construction, and aerospace industries primarily because of their excellent physical, chemical and mechanical properties [1-4]. The outstanding stiffness and strength of epoxy resin make it a useful matrix material in advanced structural composites [5, 6].

Epoxy resin contains one or more reactive epoxide ring which can simultaneously react (cross-linked) either with themselves through catalytic homopolymerisation, or with a wide range of co-reactants including polyfunctional amines, acids (and acid anhydrides), phenols, alcohols, and thiols. [7-9]. Increasing the crosslink density increases the tensile modulus, glass transition temperature (Tg), thermal stability as well as chemical resistance of the epoxy resin [10, 11]. The crosslink density is affected by factors such as the number of epoxide groups per molecule, spacing between them and functionality of the curing agents. Increasing the functionality of the curing agent increases the cross-link density of epoxy resin [10].

Epoxy functional group is a highly reactive three membered ring with oxygen bonded to two carbon atoms. The high electronegativity of oxygen makes it electron withdrawing, it therefore attracts electrons from the adjacent carbon atoms, thereby making the carbon atoms partially positively charged, and the epoxide ring extremely strained. As a consequence, the epoxide ring is unstable and susceptible to breakage in the presence of a curing agent (figure 1) [12, 13]. For epoxy resins dispersed in water (such as EPIREZ, which is used in this research), Walker [9] has reported that it can be cured without using any curing agent. The polymer when applied to substrate and heated to 110°C for 30 minutes, hardness of coating begins to develop.

On further increasing baking temperature upto 160°C, the hardness and solvent resistance of coating increases and becomes comparable to the epoxy cured with standard curing agent. The commercially available water dispersible epoxy resin is discussed in more detail in experimental part.

1.1.1. Types of Epoxy Resins

There are various kinds of epoxy resins including the diglycidyl ether of bisphenol A based resin, cycloaliphatic epoxy resin, and the tetraglycidyl methylene dianiline based epoxy resin (TGMDA)[14]. The description of the various types of epoxy resin is presented below.

i. Diglycidyl ether of bisphenol A (DGEBA) is the most commonly used epoxy resin especially in surface coating industries (Figure 2(a)). The usage of DGEBA based epoxy resin is limited to low temperature applications floor coatings, household adhesives and paints [15].

ii. Cycloaliphatic epoxies (Figure2 (b)) contain one or more non-aromatic cycloaliphatic rings in the molecule to which the oxirane ring is fused. The cycloaliphatic structure refers to a six-membered carbon atom ring. They generally have low zero shear rate viscosity and they are easy to process. The cycloaliphatic epoxy resins have distinct advantages over the glycidyl ether epoxy resin in their ability to adhere strongly to poorly cleaned and oily surfaces[16, 17].

iii. For high service temperatures applications in aerospace industry, tetraglycidyl methylene dianiline (TGMDA) are often used (figure 2(c)) [12]. This is due to its high Tg and high strength retention capacity even after prolonged exposure to elevated temperatures which is in stark contrast to DGEBA and cycloalipahtic epoxies [18]. The extra-ordinary properties of

TGMDA epoxy is due to presence of more epoxide functional groups in polymer chain which results in high crosslink density of cured epoxy.

1.1.2. Curing of Epoxy

Epoxy can react with amines and other co-reactants to produce a 3-D cross-linked polymer network. The curing of epoxy resins can be accomplished at ambient or elevated temperature. The rate of curing and temperature for full cure of epoxy resin is dependent on the type of hardener used[19] [10]. The aliphatic primary amines are ambient temperature, fast curing agents, while the aromatic primary amine such as methylene dianiline is a high temperature curing agent for epoxy resin [20, 21]. Acid Anhydride is another type of hardener which reacts with epoxy at elevated temperature and is used in the presence of strong bases such as tertiary amines. Anhydrides are preferred over amines, when protection against thermal ageing is required [22, 23].

1.1.3. Limitations of Epoxy

In spite of the desirable properties of cured epoxy resin such as good adhesion, and excellent chemical and thermal stability, there are notable shortcomings which prevent their widespread use in aircraft and automobile industries, as discussed below.

1.1.3.1. Moisture Absorption

The presence of polar hydroxyl groups makes cured epoxy resins susceptible to moisture absorption, which has adverse effects on tensile strength and modulus of the resins. This may lead to decrease in the performance of epoxy during its service life. The equilibrium moisture uptake depends upon the type of epoxy resin used[24]. Li et al. [25] reported that tetra (glycidyl methylene dianiline) (TGMDA) has higher equilibrium moisture uptake than diglycidyl ether of bisphenol A (DGEBA), given the same humid conditions and the same curing agent [25] . The moisture acts as a plasticizer when imbibed by epoxy resins and results in reduction of the glass transition temperature (T_g) and modulus of rigidity [10, 26].

Fumed silica is often added to epoxy resin during processing to minimize the water uptake. The reduction in the water uptake by the fumed silica particles is accomplished by reducing the free volume that can be occupied by moisture otherwise [27].

1.1.3.2. Brittle Nature

Cured epoxy resins are inherently brittle in nature due to their high cross-link density and glassy nature[28]. They are stiff and brittle and fracture easily in the presence of sharp cracks. Hence, an improvement in the toughness of epoxy resin is greatly desired. Toughening of epoxy resin has often been successfully done by incorporation of a rubber such as carboxyl terminated butadiene acrylate (CTBN) or hydroxyl terminated polybutadiene (HTPB) [29] or thermoplastic polymer such as polyetherimide [30], polycaprolactone [31] and polyethersulfone [32]. Yee et al. [33] has thoroughly investigated the mechanism behind toughening of epoxy resin in presence of carboxyl-terminated butadiene nitrile liquid rubber as second phase. The second phase precipitates during the curing process and produces a two phase microstructure consisting of small rubber particles with a size distribution of 0.5 μm to 10 μm dispersed in a matrix of epoxy [33]. The presence of the second phase in epoxy resin triggers a variety of toughening mechanisms including crack termination, particle de-bonding, particle delamination and particle plastic deformation [5, 33, 34].

1.2. Modification of Epoxy

1.2.1. Modification by rubber

Early studies on toughening of epoxy resin were based on inclusion of rubber such as CTBN and HTPB in epoxy matrix. The rubber modified epoxy is toughened mainly due to enhanced shear deformation of matrix material as reported by Bucknall et al. [35]. The shear deformability of epoxy resin is affected by the cross-link density and glass transition temperature. The epoxy with high crosslink density possess high glass transition temperature and is more brittle in nature, which in turns reduces the shear deformability of cured epoxy.

The modification of epoxy with reactive rubbers such as amine-terminated butadiene acrylonitrile (ATBN) has been reported to produce a significant decrease in elastic modulus and glass transition temperature (Tg) as a result of the presence of partially dissolved rubber in the epoxy phase [36].

Other major problem associated with the use of rubber such as butadiene-acrylonitrile rubber is the high level of unsaturation in their structure, which provides sites for degradation in oxidative and high-temperature environment. The high level of unsaturation exist in this rubbers due to presence of carbon-carbon double bond and carbon-nitrogen triple bond in the polymer structure[37]. In case of carboxyl terminated polybutadiene rubbers, the presence of unsaturation also causes an increase in the viscosity of liquid polymer due to disappearance of terminal functional group [37]. Furthermore, the presence of double bonds in the polymer chain causes oxidation reaction leading to further crosslinking, and loss of elastomeric properties and ductility of the rubber-epoxy blend [38]

Despite the advantage of rubber in the modification of epoxy resin for increasing toughness, they cause delay in gel time lowering the cross-link density of epoxy resin, reduces tensile strength and flexural properties [39]. Therefore, use of rigid materials to toughen and improve the processability of epoxy resin is necessary.

1.2.2. Modification by thermoplastics

In order to overcome the drawbacks in the use of rubber as modifying agent, ductile engineering thermoplastics like polysulfone, polyester [40], poly(ether-imides), poly(ϵ-caprolactone) [2] and polyamides [5, 41] have been studied as alternate modifiers. These thermoplastics are found to be promising since they do not decrease the inherent properties of epoxy matrix such as crosslink density, tensile strength and flexural properties[39]. Pearson et al. [42, 43]investigated the toughening mechanism of epoxy by rubber such as carboxyl-terminated butadiene acrylonitrile (CTBN) and metha-acrylated butadiene styrene (MBS), and thermoplastic such as phenylene oxide. They concluded that the most compelling toughening mechanism with MBS rubber is cavitation of the rubber particles and associated shear banding in the matrix. On the other hand, thermoplastics provide a wider variety of toughening mechanisms such as (1) crack pinning, (2) particle bridging, (3) crack path deflection, (4) particle yielding, (5) particle-yielding induced shear banding, and (6) micro cracking. As thermoplastics toughens epoxy resin by several mechanisms as mentioned above in contrast to rubber which toughens epoxy resin essentially by cavitation along with reducing cross-link density, they suggested this difference in mechanism as a reason behind ability of thermoplastics to toughen highly cross-linked epoxy more effectively relative to rubbers.

Bragg et al. [44] investigated the tensile properties of DGEBA based epoxy containing nylon-6,6 oligomer and cured with dodecenylsuccinic anhydride (DDSA). The nylon-6,6 oligomer was extracted from residues of industrial nylon-6,6 polymerization in this research and no information is reported on molecular weight of nylon-6,6 oligomers used in this work by authors [44]. The effect of nylon 6,6 oligomer on tensile properties of epoxy resins as a function of composition is shown in Figure 3. The addition of 2 weight % of nylon-6,6, resulted in an increase in the tensile strength of epoxy resin by 22 %. Additional increase in the concentration of nylon-6,6 upto 35 weight% resulted in decrease in tensile strength of epoxy resin [44]. The authors provided reasoning for such behavior based on morphological evaluation in nylon-6,6 oligomer/epoxy composites. From 0 to 2 wt.% nylon-6,6 in epoxy, a homogenous surface was observed with no phase separation under Scanning Electron Microscope (SEM). For 5 wt. % nylon-66 in epoxy resin, phase separation was observed along with scattered clusters of irregularly shaped particles. For 10 and 35 wt.% nylon-6,6 in epoxy, phase separation was observed along with random clusters of irregularly shaped particles and elongated fibers protruding from surface flaws [44].

Thermal analysis of these blend with differential Scanning Calorimeter (DSC), showed that the blends containing up to 5 weight % of nylon-6,6 had a single glass transition temperature (T_g). However, the blends containing > 5 weight % of nylon-6,6 had two T_gs. On basis of this observation, the authors suggested that, 2 weight % of nylon-6,6 is the miscibility limit for this system after which separation of the phases begins to occur. Bragg et al. [44] suggested that the second phase acts as a plasticizer which increases the flexibility and hence the ultimate strain.

Polyamide (nylon) is a class of thermoplastic polymer known to react chemically with epoxy. In 1960s, Gorton [45] studied the reaction between epoxy (epon 828) and alcohol soluble nylon (commercially available as Zytel 61 with number average molecular weight of 25,000) by swelling tests, and reported that the amide functional group in nylon reacts with the epoxide functional group. After that, Zhong et al [41] studied the cure kinetics of reaction between alcohol soluble nylon (copolymerized by 50% caprolactam and 50% hexamethylenediammonium adipate salt, intrinsic viscosity $[\eta]=0.98\ dlg^{-1}$ measured in 93% H_2SO_4 at 25^oC) and DGEBA based epoxy resin in absence of standard curing agent in 1998. They proposed the nucleophilic attack by nitrogen of amide group in nylon on oxirane ring of epoxide as the main reaction mechanism. Since then, various groups have studied epoxy/nylon composites for mechanical properties [46], thermal properties[44], morphology[5, 47, 48] and rheology [47] but no significant work has been done to explore the underlying chemical reaction.

1.3 Nylon-6

Nylons are characterized by the amide functional group. Synthetic polyamides are called nylons. The equation for synthesis of nylon-6,6 and nylon-6 and the repeat units of these polymers are shown in Figure 4. The amide functional group is responsible for the strong intermolecular attraction due to hydrogen bonding interaction and van der walls forces between the methylene chains[49, 50]. The reaction of the amide group with epoxy may lead to disordering of the nylon chains there-by lowering the extent of crystallinity [41].

Nylon-6 consists of three polymorphic crystalline forms (Figure 5): The α-phase is most commonly observed at room temperature and can be obtained by slowly cooling from the melt state [51, 52]. The crystal structure of the α-phase is monoclinic, and the hydrogen-bonded sheets are composed of neighboring chains traversing in opposite or antiparallel directions. In the X-ray diffraction pattern of Nylon 6, two peaks characteristic of the α phase at room temperature are at about $2\theta = 20$ and 23.7° and are indexed as (200) and (002)/(202) reflections, respectively [49].

The γ phase can be obtained by fast quenching from the melt state or by treating α phase in iodine–potassium iodide aqueous solution, followed by removal of the absorbed iodine by sodium thiosulfate. For the γ phase, the diffraction peaks at about $2\theta = 10.7$ and 21.4° are indexed as (020) and (001) reflections, respectively [53].

The β phase (or pleated α) is generally formed in quenched samples. The β crystal is assumed to be a metastable phase with variable degree of disorder or stacking faults: it includes stacking of parallel and antiparallel chains, paracrystalline disorder, faults in the hydrogen bond sheet-like setting, and hydrogen bonded layers normal instead of parallel to the chain axis [49].

1.5. Montmorillonite 15A Clay

The principal building blocks of nanoclay minerals are 2-D arrays of silicon oxygen tetrahedral and 2-D arrays of Al or Mg oxygen hydroxyl octahedral. The apex oxygen atom in the silica tetrahedral is shared with adjacent octahedral sheet. The clay particles are bundles of such platelets that are roughly 1nm in thickness and 100-1000nm in breadth. For example, an 8µm clay particle has approximately 8000 platelets of 1nm thickness and 200nm in lateral dimensions [54, 55]. In montmorillonite clay, which is an aluminosilicate mineral, some tetravalent Si atoms in the tetrahedral sheet are partly replaced by trivalent atoms such as Al. Also, in the octahedral sheet, some trivalent Al atoms are replaced by divalent atoms such as Mg, Fe, Cr, Zn etc. This results in a deficit of positive charge or an excess of negative charge being imparted to the clay platelet. This negative charge is compensated by adsorption, on the clay surface, of cations such as Na^+ and Ca^{2+}. In the presence of aqueous solution, these cations can be exchanged for others that are present in the solution. This property of ion exchange of aluminosilicate clay is used to treat the surface of the clay with organic cations, to make it compatible with an organic phase, such as a polymer [56, 57]. Several types of commercial organoclay are available. The main difference among them is the organic modifier, whose organic cations can replace the sodium cations on the clay surface[58].

15A is natural montmorillonite clay which is modified with 2M2HT: dimethyl, dihydrogenated tallow, quaternary ammonium (Figure 6). The HT, or hydrogenated tallow, contains (~65% C18; ~30% C16; ~5% C14) [59].

1.5 Epoxy Based Coatings for Anti-Corrosion

In past several decades, significant research is carried out on use of organic and inorganic coatings for protection of metals against corrosion[60]. In the field of organic coatings, extensive research has been carried out on epoxy based coatings due to their high dimensional stability and strong adhesion to the substrate [61, 62]. Most widely used metal in structural and aerospace applications are Al-2024 alloy and carbon steel which contains inter-metallic inclusions [62, 63]. Several epoxy based formulation have been studied in past couple of years by Beemat et al [56, 64] and Bagherzadeh et al [61] to protect Al-2024 using silane coupling agents, preparation of epoxy-silane hybrid binders, and epoxy/clay nanocomposites [61]. Silanes increases the adhesion between metallic substrate and coating, while clay improves the barrier properties and reduces the water uptake by coating due to formation of intercalated or exfoliated morphologies [65].

One of the most widely used techniques to study corrosion inhibition behavior is Electrochemical Impedance Spectroscopy (EIS). In this technique, impedance is measured over a range of frequency for a given system. Impedance is the opposition of flow of alternating current. Electrochemical impedance is normally measured using a small excitation signal. This is done so that the cell's response is pseudo-linear. In a linear (or pseudo-linear) system, the current response to a sinusoidal potential will be a sinusoid at the same frequency but shifted in phase. The excitation signal is expressed as function of time as $E_t = E_o\text{Sin}(\omega t)$, where E_t is at potential at time t, E_o is amplitude of signal and ω is radial frequency. In a linear system, the response signal I_t is shifted by phase ϕ and has a different amplitude than I_0. $I_t = I_0\text{Sin}(\omega t + \phi)$. The expression to calculate impedance is analogous to ohm’s law $Z = E_t/I_t = E_o\text{Sin}(\omega t) / I_0\text{Sin}(\omega t + \phi) = Z_o \text{ Sin}(\omega t)/ \text{Sin}(\omega t + \phi)$. the impedance is therefore in terms of magnitude Z_o and a phase shift ϕ.

Bagherzadeh et al [61] reported 99.21% reduction in water uptake and improved anti-corrosion properties of epoxy/clay nanocompoistes using electrochemical impedance spectroscopy. They used DGEBA based epoxy (Araldite Razeen LR-2257), polyamide hardener (Aradur 43 SBD) and modified montmorellonite closite 30 B clay as filler material. The coatings were applied on sandblasted metallic panels by spray and dried at 23°C for a week, which resulted in dry film thickness of 60 ± 5 µm.

Foyet et al [62] reported the Bode plots obtained by electrochemical impedance spectroscopy for epoxy-amine system. They used bisphenol A based epoxy (epikote 828) cured with aromatic amine 4,4-methylene dianiline, and the coating was applied on aluminum alloy Al 2024. The impedance value at lowest frequency, which is indicative of coating resistance showed a drop from 1×10^9 to 1×10^6 Ω in a time period of 7 days.

Several other researchers such as chen et al[66] and Shi et al [67] have studied epoxy based nanocomposite coatings for anti-corrosion performance using electrochemical impedance spectroscopy, where incorporation of nano Clay particles enhanced the corrosion inhibition properties. Chen et al [66] studied the anti-corrosion performance of Epon 828 (bisphenol-A epoxy) cured with amine based curing agent 8290-Y-60, reinforced with monmorillonite Closite Na clay. The coating was applied on Al 2024-T3 and was allowed to cure for 1 week at room temperature. They reported small increment in impedance value for coating systems containing organoclay [66]. Shi et al [67] studied the anti-corrosion performance of liquid epoxy blend of low molecular weight diluents and DGEBA cured with aliphatic amines, reinforced with Halloysite nanoclay. A cylindrical Steel coupon was used as substrate on which coating was applied and cured at room temperature for 7 days. They reported that Halloysite nanoclay significantly increased the coating resistance from 352.5 Ωcm^2 to 3.60×10^4 Ωcm^2 exposed to 3.5 wt.% salt solution for 7 days [67].

In contrast to the above mentioned research, in this work anti-corrosion performance for DGEBA based aqueous epoxy emulsion (EPI-REZ 5522-WY-55) is studied cured and modified with thermoplastic nylon-6 (polyamide) and clay modified nylon-6. The substrate used is Aluminum alloy Al-2024 T3, on which polymer blend was applied by solution casting and cured by step-wise heating initially at 70^{O}C for 3 hours, 100 ^{O}C for 2 hours, 120 ^{O}C for 2 hours and 150 ^{O}C for 2 hours. Conventional amine based curing agent is not used in this research, in order to determine the sole effect of thermoplastic nylon-6 and clay modified nylon-6 on properties of epoxy. It has been reported by Dow Chemicals [68] that the reaction of polyamides with epoxies is similar to that of the aliphatic amines. Moreover, the polyamides are relatively large polymers (compared to amines), the ratio of polyamide to epoxy is varied largely to obtain properties from hard to semi-flexible. In this sense, the polyamides can be considered resin modifiers as well as curing agents [68]. Use of thermoplastics are widely reported to improve mechanical properties of epoxy resin [46, 47], but in this research anti-corrosion properties of nylon-6/epoxy and clay/nylon-6-epoxy composites are determined along with thermo-mechanical properties.

1.6 Effect of morphology on properties of epoxy based coatings and films

This section is dedicated to the literature reported on the effect of morphology on thermo-mechanical and corrosion inhibition properties of epoxy based composite systems.

1.6.1 Effect of morphology on thermo-mechanical properties

In past, several researchers have reported co-relation between morphological evaluation, and corresponding effect on thermo-mechanical behavior for thermoplastic toughened epoxy and epoxy/clay nanocomposites [47, 69-71].

Wu et al [69] synthesized polyphenylene oxide toughened epoxy composites using EPON 828 as epoxy, cured with multifunctional cyanate ester. It is necessary to use curing agent in this case because polyphenylene oxide does not contain any functional group available to react with epoxide rings except terminal hydroxyl group. They reported that morphology of final cured epoxy/PPO blends is dependent on concentration of PPO. The SEM images of fractured surface of the films showed that films containing PPO less than 30 phr consisted of continuous epoxy matrix with PPO-rich domains existing as finely dispersed particles [69]. For blends containing 30 phr of PPO, partial phase inversion was found in morphology [69]. When PPO concentration was increased to 50 phr, complete phase inversion with honeycomb morphology was observed [69].

A direct effect of such variation in morphology was found on corresponding thermo-mechanical properties. The DMA result clearly showed the presence of 2 phases and partial mixing in the cured epoxy/PPO system [69]. A two-step decrease in dynamic storage modulus (E') was observed along with and two tan(δ) peaks for PPO/epoxy blends. PPO has a high glass transition temperature and shows change in modulus at higher temperature (230°C). But for PPO/epoxy blends, the transition in storage modulus began took place at lower temperature (100-150°C). Moreover, two transition were observed in storage modulus curve along with two peaks of glass transition temperature in tanδ at 125°C and 200°C, which is in direct agreement with the two phase morphology observed in SEM. Moreover, neat PPO showed highest tanδ peak of around 2.2, but for epoxy/PPO composites, the peak height reduced with increase in epoxy concentration. For epoxy/PPO (50 phr), peak heights were 0.5 and 0.45, while for epoxy/PPO (30 phr), peak heights were at 0.2 and 0.25 which is in direct agreement with morphology, where with increase in epoxy phase in the composition, tanδ peak height decreases. Also, the storage modulus in rubbery region for blends was higher than that of neat PPO, due to increased crosslink density of overall system.

Kishi et al [70] synthesized epoxy based films cured with dicyandiamide (DICY) and toughened with polyamide-12 (nylon-12). The curing agent was necessary to cure epoxy because pre-formed polyamide-12 thermoplastic solid particles (diameter 6 μm) were added to liquid epoxy, which doesn't dissolve in liquid epoxy and hence cannot chemically interact.

The SEM micrograph of the fractured surface of the resin after compact tension test showed that the particles of polyamide-12 in the epoxy matrix were highly deformed during crack propagation [70]. This suggests that the particles adhered well to the epoxy matrix and were capable of large plastic deformation to absorb the external energy. This indicates that particles worked as 'bridges' for advancing cracks and thus suppressed crack propagation [70].

Kishi et al [70] has compared the storage modulus of polyamide-12/epoxy system as a function of temperature to unmodified epoxy cured with DICY as control material. There was no significant difference in the storage modulus and the glass transition temperature of the modified resin with 10 phr polyamide-12 particles to that of the unmodified resin. For resin modified with 20 phr polyamide-12 particles, the glass transition temperature of the resin was slightly reduced, but the storage modulus below 100°C was still high. They concluded that using particulate polyamide-12 were efficient in decreasing the cracks [70].

Wang et al [71] studied epoxy/clay nanocomposite using aromatic epoxy (DER332) cured with 4,4'-diamino-diphenylsulphone in presence of pristine clay. They reported the SEM image of control epoxy and its composite with clay. The SEM image of neat epoxy was very smooth and amorphous in appearance with no features due to its brittle nature. At 1 weight% of nanoclay in epoxy, numerous micro cracks were observed, generated at interface of clay particles and epoxy matrix, travelled along clay platelets and resulted in a highly tortuous surface. On the other hand, at 3 weight% clay, the morphology was dominated by clay clusters. Clay aggregates were observed around 1-4 µm with typical trail structure, which are caused when two secondary crack fronts separated by a particle meet with each other [71]. The authors then co-related the morphology with dynamic mechanical properties of clay/epoxy nanocmoposite. An increase in storage modulus in glassy region was observed by 31% at incorporation of clay at 3 weight%, which is in good association with morphology observed, where clay particles acts as hindrance to chain motion. However, T_g increased at 1 weight% clay, but decreased on further increasing clay weight%. In literature, decrease as well as increase of T_g is reported for epoxy modified with clay. They hypothesized that Chemical bonding between silicate and epoxy matrix at the interface could lead to hindered relaxational mobility in the polymer segments near the interface, which increases Tg at low concentration of clay. However, at higher concentration of clay lack of surrounding entanglements and reduced crosslink density at the interface can cause decrease of Tg [71].

1.6.2 Effect of morphology on anti-corrosion properties

Organic coatings are usually applied on metallic substrates, in order to protect them from corrosion due to several reasons such as strong adhesion between coating and metal, high resistance of coatings to solvents and chemicals, good scratch resistance and hardness, high modulus and strength. Several researchers have reported that the morphology of the coatings plays a major role in deciding anti-corrosion performance. Hence, it is crucial to study the morphology of coatings and its co-relation with corrosion inhibition properties.

Palraj et al [72] reported the co-relation between morphology and anti-corrosion properties of epoxy polyamide system applied on galvanized steel, treated with zinc phosphate, manganese phosphate and calcium phosphate coatings. They used 3 weight% salt solution as electrolyte (corrosive environment), saturated calomel electrode (SCE) as reference electrode, coated steel plate as working electrode in order to carry out electrochemical testing.

The Bode plots for galvanized steel substrate treated with different types of phosphate solutions coated with epoxy-polyamide primer coatings are reported by authors [72]. After 1 day of exposure, system treated with calcium phosphate coating showed the highest impedance value of $1\times10^{8.2}$ Ω at frequency of 0.1 Hz showing best anti-corrosion performance, but after 50 days of exposure (7 weeks), calcium phosphate coating degraded with impedance value of 1×10^{7} Ω but manganese phosphate coating showed the best performance with impedance value of $1\times10^{8.1}$ Ω at frequency of 0.1 Hz. The coating with zinc phosphate showed lowest impedance value throughout the exposure time, but all the systems treated with phosphate solutions showed better performance compared to system coated with epoxy-polyamide primer without phosphate treatment. These results were then co-related with the surface morphology. It was observed from the figures that calcium modified phosphate coatings were uniformly distributed throughout the surface and pattern of deposit was dendrite in nature [72]. However in the zinc phosphate coating system the coating was non-uniform and randomly distributed on the steel surface [72]. The grains were spherical in nature, and the deposition was selective in nature. The manganese modified phosphate system exhibited the combination of needle and spheroid structures, distributed uniformly throughout the surface [72].This particular coating exhibited better corrosion protection compared to other systems, due to the reduction of porosity and roughness [72]. The possible reason for difference in morphology shown by different phosphate coatings is due to difference in ionic radius of calcium, zinc and manganese.

Beemat and Iroh [73] reported effect of morphology on corrosion resistant properties of epoxy ester – polymethylhydroxysiloxane coatings and its hybrid with rigid aromatic polyurea using direct current polarization (DCP) technique and scanning electron microscopy. The DCP curves for epoxy ester – polymethylhydroxysiloxane (EE-PMHS) containing various concentrations of polyurea (PU) were reported by authors[73]. The corrosion current (I_{corr}) for the EE-PMHS coating was lower than the EE-PMHS-PU hybrid coatings after 1 day of exposure. All the coatings except the EE-PMHS-PU 15 wt % hybrid coating showed passivation behavior in the anodic curves. The passivation behavior is shown by aluminum alloys when exposed to corrosive environment. After 5 days of exposure, the EE-PMHS coating had higher I_{corr} than the EE-PMHSPU 15 wt % hybrid coating, but less than the other hybrid coatings [Figure 17(b, d)]. The I_{corr} for the EE-PMHS coating became comparable to the hybrid coatings of EE-PMHS containing 20 and 25 wt % PU and was remarkably higher than EE-PMHS-PU 15 wt % hybrid coating after 14 days of exposure time [Figure 17(c, d)] [73]

The electro-chemical properties were then co-related with the surface morphology of these coatings. For epoxy ester, uniformly distributed self-assembled nano snaps were observed in morphology consisting of collapsed long aliphatic chains of fatty acids [73]. As the polyurea was added to epoxy ester at 15 weight%, the small dots disappears and no morphological feature were seen from the SEM images [73], suggesting formation of inter-penetrating network, such that the mesh of rigid PU did not allow the soft EE chains to collapse, a reason reported for increased durability and anti-corrosion performance [73]. As polyurea was further increased to

25 weight%, the morphology began to open up as polyurea began to dominate over epoxy ester matrix, due to its higher rigidity [73]. As polymethylsiloxane was added to the system consisting of epoxy ester-polyurea (25%), the morphology became very compact due to coupling of epoxy ester and polyurea which lead to better anti-corrosion performance [73].

CHAPTER 2

EXPERIMENTAL

2.1 Materials

Polyfunctional water dispersible DGEBA based epoxy resin (EPI-REZ 5522-WY-55) was purchased from Hexion Chemicals, Houston, USA. The pH value of EPI-REZ 5522-WY-55 was estimated using pH paper, and it was around 4-5. This suggests that the epoxy resin emulsion was prepared by manufacturers in acidic medium. The polymerization reaction of aqueous epoxy resin emulsion is catalyzed by acid, hence thermal treatment of such resin can lead to curing of epoxy [9]. EPIKURE 8290-Y-60 was used as curing agent. ϵ -caprolactam, 95% pure dry sodium hydride, N-acetylcaprolactam and NMP solvent were purchased from Sigma-Aldrich, USA for solution polymerization ε-caprolactam. The Al-2024-T3 Q-panels were purchased from Q-Labs, Cleveland, Ohio. Cloisite 15A clay was purchased from Southern Clay. All the reagents mentioned above are of analytical grade. The nylon-6 synthesized by solution polymerization was used to cure epoxy resin.

2.2. Processing

2.2.1. Synthesis of Nylon-6 and in-situ Clay/Nylon-6 Composites

Polymerization was carried out in an oil bath assembly. 100 ml of NMP was taken in a 3 neck flask and 30 g of monomer (ϵ -caprolactam) was added and stirred until it formed a colorless solution at room temperature. It was followed by addition of montmorillonite 15A clay. Nitrogen supply was turned on and temperature was raised to 80^{O}C. 0.72 g of NaH (catalyst) was then added to the solution and stirred till it dissolved completely. This process of dissolution was accompanied by a series of color changes from colorless to dark blue which eventually turned black upon complete dissolution. Temperature was then gradually raised by setting the knob of heater to 160°C, which took approximately 30-45 minutes to reach 160°C, followd by addition of 0.396 g of N-acetyl Caprolactam (Initiator) to the solution while maintaining the stirring. After addition of initiator, solution was stirred for 30 minutes, then nitrogen supply was turned off, and the black solution was observed to gently turning into a dark orange viscous solution. Nylon-6 existed as a homogeneous solution at higher temperature but while transferring to a glass jar at room temperature it began to phase separate and existed in a suspension form.

In order to obtain clay/nylon-6 nanocomposites, clay was added to the solution of NMP solvent and monomer ε-caprolactam in the beginning, and reaction was carried out in a similar manner as stated above. Various compositions were synthesized with varying amount of clay as 0, 0.5, 1, 5 and 10% by weight to obtain clay/nylon-6 nanocomposite.

2.2.2. Preparation of Nylon-6/Epoxy and Clay/Nylon-6-Epoxy Hybrid Blends

2.2.2.1. Nylon-6/Epoxy Hybrid Composition

25 ml (~13.75 g) of epoxy resin (EPI-REZ 5522-WY-55, 50-55% solid by volume) was transferred to a glass jar, Nylon-6 suspension (20-30% solid by volume) was added in various amounts and NMP was further added to the blend in order to maintain the total volume of all the compositions to around 45 ml (sample volume). Moreover, extra NMP diluted the solution and reduced the viscosity that resulted in ease of processing in order to have defect-free films and coatings. Nylon-6 was added as 5 wt.% (2.5 ml, ~0.68 g), 10 wt.% (5.1 ml, 1.33 g), 15 wt.% (8 ml, ~2.06 g), 20 (11.45 ml, ~2.75 g) & 30 (14.5 ml, ~4.3 g) wt. %. The weight % of nylon-6 was estimated with respect to solid content of epoxy resin. The mixture was then stirred using

mechanical stirrer for 1 hour at room temperature to obtain homogeneous solution and then ultra-sonicated for 5 minutes.

2.2.2.2. Clay/Nylon-6-Epoxy Hybrid Composition

Clay/nylon-6-epoxy composite systems were prepared using same technique as was used to prepare Nylon-6/ epoxy blend. Instead of nylon-6 suspension, clay/nylon-6 system obtained in a suspension form was used in order to modify epoxy resin. Four clay/nylon-6 systems were prepared with clay loading as 0.5 wt.% (0.15 g), 1 wt.% (0.3 g), 5 wt.% (1.5 g) and 10 wt.% (3 g). The weight % of clay was with respect to weight of monomer used for polymerization. Each system was blended with epoxy resin in varying amount as 1, 5, 10, 15, 20 and 30 weight %. Table 1 shows the individual percentage composition of nylon-6 and clay with respect to solid content of epoxy. The mixture was then stirred using mechanical stirrer for 1 hour at room temperature to obtain homogeneous solution and then ultra-sonicated for 5 minutes.

Table 1 - The individual percentage composition of nylon-6 and clay with respect to solid content of epoxy.

Composition	**Epoxy**	**% Nylon**	**% Clay**
EPNYCL0.5-5	~13.75 g	4.9975 (~0.68 g)	0.0025 (~0.34 mg)
EPNYCL1-5	~13.75 g	4.95 (~0.68 g)	0.05 (~6.87 mg)
EPNYCL5-5	~13.75 g	4.75 (~0.65 g)	0.25 (~34.38 mg)
EPNYCL10-5	~13.75 g	4.5 (~0.618 g)	0.5 (~68.75 mg)
EPNYCL0.5-10	~13.75 g	9.95 (~1.37 g)	0.05 (~6.87 mg)
EPNYCL1-10	~13.75 g	9.9 (~1.36 g)	0.1 (~13.75 mg)

EPNYCL5-10	~13.75 g	9.5 (~1.31 g)	0.5 (~ 68.75 mg)
EPNYCL10-10	~13.75 g	9 (~1.23 g)	1 (~137.5 mg)
EPNYCL0.5-15	~13.75 g	14.925 (~2.06 g)	0.075 (~10.31 mg)
EPNYCL1-15	~13.75 g	14.85 (~2.04 g)	0.15 (~ 20.62 mg)
EPNYCL5-15	~13.75 g	14.25 (~1.95 g)	0.75 (~103.25 mg)
EPNYCL10-15	~13.75 g	13.5 (~1.85 g)	1.5 (~206.25 mg)
EPNYCL0.5-20	~13.75 g	19.9 (~2.73 g)	0.1 (~13.75 mg)
EPNYCL1-20	~13.75 g	19.8 (~2.72 g)	0.2 (~27.5 mg)
EPNYCL5-20	~13.75 g	19 (~2.61 g)	1 (~137.5 mg)
EPNYCL10-20	~13.75 g	18 (~ 2.47 g)	2 (~275 mg)

2.2.3. Sample Preparation

5 ml of neat nylon-6 (20-30 weight% solid by volume) and nylon-6/clay suspensions (approximate clay loadings in 5 ml suspension – 7.5 mg, 15 mg, 75 mg and 850 mg) were taken in a Teflon mold and gradually heated up to 200°C for 24 hours in vacuum oven to fully evaporate the solvent. The residual nylon-6 and its composites with nanoclay were obtained as granules and weighed in range of 1 – 1.5 g.

The coatings were prepared by solution casting method onto 1" x 4" x 1/8" Al 2024-T3 coupons. 2 ml of polymer blend was taken in syringe and poured at the edges of coupon and then was allowed to spread uniformly on the substrate. The viscosity of polymer blend was in the range of 35-55 cP measured at spindle speed of 100 rpm in Brookfield viscometer. The heating of polymer blend on substrate was carried out in a stage wise manner starting with 70°C for 3 hours followed by 100°C for 2 hours, 120°C for 2 hours and 150°C for 2 hours, in order to obtain coatings. The thickness of the coatings was maintained at about 60±5 μm. Free standing films for dynamic mechanical testing were casted in Teflon molds with cavity dimensions of 1.5" x 1.5" x 1/4". In order to obtain free standing films, the polymer blend in Teflon mold was heated in step-wise manner with 50°C for 13 hours followed by 70°C for 3 hours, 100°C for 2 hours, 120°C for 2 hours and 150°C for 2 hours.

2.3. Analytical Techniques

2.3.1. Differential Scanning Calorimeter (DSC)

Differential scanning Calorimetry (DSC) was used to measure thermal properties of nylon-6/clay nanocomposite. DSC was performed at the heating rate of 5°C/min using DSC6200, Seiko Instruments Inc. Glass transition temperature was indicated by a gradual shift in the baseline of during the DSC cycle, melting point was determined by a melting peak during heating cycle and crystallization point was determined by a peak during cooling cycle. A sample DSC run is shown in Figure 7.

2.3.2. Dynamic Mechanical Analysis (DMA)

The viscoelastic behavior of the films was studied by using dynamic mechanical analyzer, DMS6000, from Seiko Instrument Inc. under tensile loading at a heating rate of 5°C per minute and a frequency of 1 Hz. The dynamic mechanical analysis data is plotted in the form of storage modulus against temperature and tan delta against temperature as shown in Figure 8. The plot of storage modulus against temperature shows the variation of elastic modulus of the film with temperature. The glass-rubber transition (T_g) is measured from the temperature corresponding to the peak of tan delta curve in the tan delta vs. temperature curve.

2.3.3. Scanning Electron Microscopy (SEM)

Surface morphology of the coatings and morphology of the fractured surface of film was observed under Scanning Electron Microscope, Philips model FEI XL 30 ESEM-FEG. The software used to capture images was Scandium. Aluminum stubs with carbon tape were used as sample holders. Coatings for surface analysis were prepared by solution drop method onto 10mm x 10mm Al 2024-T3 panels. The samples were sputter coated with Ag by using Polaron SC7640.

2.3.4. X-Ray Diffraction (XRD)

Wide angle X-ray diffraction (WAXD) was carried out by using Philip X-Ray Diffractometer. X-ray diffraction tests were performed by using a Cu-K radiation source at a wavelength of 1.54 A° between 2θ angles of 0.5° - 30°. The d-spacing of the organoclay platelets was calculated using Bragg's law (equation 1) and length of crystal was calculated using Sherrer equation (equation 2).

$$n\lambda = 2dsin\theta \qquad [1]$$

Where n is a constant integer (1 in our case), λ is wavelength, d is d-spacing and θ is diffraction angle in degrees.

$$D(hkl) = \frac{K\lambda}{\beta(hkl)\, cos\theta} \qquad [2]$$

Where D (hkl) is the mean crystal size along [hkl] direction, K is the shape factor (scherrer constant, value of 0.94 is used in this case), β (hkl) is the line broadening at half the max intensity in radians and θ is the half scattering angle.

2.3.5. Fourier Transform Infrared Spectroscopy (FTIR)

Nicolet 6700 FT-IR instrument equipped with a Smart Orbit ATR accessory with diamond crystal was used to determine the chemical composition of the samples. ATR was performed over a wavenumber range between 4000 cm^{-1} and 400 cm^{-1}

2.3.6. Electrochemical Impedence Spectroscopy (EIS)

Reference 3000 from Gamry Instruments was used for the electrochemical impedance spectroscopic studies. A cylindrical glass cell with a rubber O-ring of inner area 2.8cm^2, attached to the grooved bottom of the cylindrical cells and a clamp fixture was used to hold the samples. A saturated calomel electrode (SCE) and a graphite electrode were used as reference and auxiliary electrode respectively. The potential was applied in a range of ±10mV from open circuit potential and the frequency was varied from 10^6 to 10^{-2} hz. All the tests were performed on non-scribed samples in 3.5wt% NaCl solution as otherwise mentioned in the discussion. Data from EIS measurement is presented in the impedance vs. frequency plot (known as Bode plot). A typical representation of Bode plot is shown in Figure 9 [74]

2.3.7 *Direct Current Polarization* (DCP)

Direct Current Polarization is a potential dynamic corrosion testing technique in which a polarized electrode generates currents in the electrolyte via electrochemical reactions that occur at the electrode surface. The electrochemical cell consists of counter electrode, reference electrode, working electrode and electrolyte, all connected to a potentiostat. The current flows through the electrodes. The open circuit potential is the potential at which the cathodic and anodic currents are in equilibrium. Tafel plots are generated by measuring the current density on a logarithmic scale as a function of applied potential (Figure 10). Tangents are drawn to the anodic and cathodic curves of the Tafel plot and the intersection is projected on the X-axis and Y-axis to give the corrosion current (I_{corr}) and corrosion potential (E_{corr}) values [75].

Reference 3000 gamry potentiostat equipped with echem analyst software was used to analyze the DC polarization curves. The DC curves were generated by applying a potential in the range from -250 mV to + 250 mV from the open circuit potential against a saturated calomel reference electrode, SCE, at a scan rate of 2mV/s. The corrosion protection properties were evaluated on the coated aluminum alloy (working electrode) in the testing solution of 3.5 weight% NaCl by using a cylindrical glass cells constantly clamped to the sample with an exposed area of 2.8 cm^2. Graphite rod was used as counter electrode.

2.3.8 Transmission Electron Microcopy (TEM)

The TEM machine used for imaging was JEOL 2100F with digital micrograph software with a voltage of 200Kv. A single tilt holder with samples disbursed on a lacey carbon grid was used to observe the structure of sample. Sample was prepared by spreading a drop of polymer solution on carbon grid and was allowed to dry overtime naturally till a dry polymer film was obtained.

CHAPTER 3

RESULTS AND DISCUSSIONS

3.1. Hybrid Blends of Nylon-6 and Epoxy

3.1.1. FTIR Analysis

Figure 11 shows the FTIR spectrum of the monomer (ε-caprolactam) used to synthesize nylon-6. The ε-caprolactam contains carbonyl (C=O) and secondary amine (-NH) functional group. Table 2 shows the characteristic peaks associated with ε-caprolactam.

Table 2- Characteristic absorbance peaks for ε-caprolactam

Functional Group	**Absorbance Peak (cm^{-1})**
-NH group	3278
-C=O group	1651
Hydrocarbons ($-CH_2$ and $-CH_3$)	2926, 2954

Figures 12 shows the FTIR spectrum for neat nylon-6 synthesized from neat nylon-6. From the FTIR spectrum of nylon-6 (Figure 12), the peak at 1651cm^{-1} confirms the presence of carbonyl group (C=O) of amide group, i.e. formation of nylon-6 via solution polymerization. The peaks at 2926 cm^{-1} and 2954 cm^{-1} represents hydrocarbons ($-CH_2$ and $–CH_3$). The peaks at 3295 cm^{-1} and 3360 cm^{-1} represents -NH stretching, and duplet indicates primary amine group. The peak at 1161 cm^{-1} represents –CONH skeletal motion [76], which was not observed in FIR spectrum on monomer, which further confirms the formation of nylon-6. Peak at 791 cm^{-1} is due to –NH wagging and peak at 1351 cm^{-1} is due to –CN bond. The nylon-6 was synthesized using NaH as catalyst and N-acetyl caprolactam as initiator. The possible end groups can be amine or acetyls group. Chains formed before introduction of initiator are terminated with amine end groups which is indicated by primary amine peaks at 3295 cm^{-1} and 3360 cm^{-1}. The peaks at 1351 cm^{-1} (-CN), 1161 cm^{-1} (-CO and –CONH overshadowed) and 2854 cm^{-1} (alkane) indicates presence of acetyl group[47]. The characteristic absorbance peak for nylon-6 is shown in table 3.

Table 3 - Characteristic absorbance peak for nylon-6

Functional Group	**Absorbance Peak (cm^{-1})**
Amide group (C=O)	1651
Hydrocarbons (-CH_2 and -CH_3)	2926, 2954
-NH stretching	3295, 3360
-NH wagging	791
-CN group	1351

Figure 13 and 14 shows the FTIR spectrum for uncured liquid emulsion of epoxy resin (EPI-REZ 5522-WY-55) and thermally treated epoxy resin heated stepwise in oven for 9 hours (70° C -3h, 100°C -2h, 120°C -2h, 150°C – 2h) respectively. The broad peak corresponding to –OH stretching at 3393 cm^{-1} (Figure 13) was very broad and prominent due to presence of water in emulsion, while in thermally heated neat epoxy (EPI-REZ 5522-WY-55), it became smaller and narrow due to evaporation of excess water while formation of heating (Figure 14). The characteristic peaks for epoxy are listed in table 4. A significant information was obtained about curing of epoxy by thermal heating, by comparison of FTIR spectrum of uncured epoxy (Figure

13) and cured epoxy (Figure 14). The intensity of peak at 1036 cm^{-1} due to C-O-C ether linkage increased, suggesting increased bond formation between oxygen and carbon of oxirane ring among different epoxy chains during heating. The peak at 1506 cm^{-1} due to C-C stretching characteristic to benzene does not take part in reaction, hence it was taken as standard and area under 914cm^{-1} was calculated with respect to area under 1506 cm^{-1} for both uncured and cured epoxy. The ratio of area under 914 cm^{-1} (with respect to area under 1506 cm^{-1}) for uncured to that of cured epoxy came around 0.25-0.30, suggesting fractional conversion of 25-30% for epoxy by heating.

Table 4- Characteristic absorbance peak for epoxy

Functional Group	**Absorbance Peak (cm^{-1})**
-OH stretching	3393
Oxirane ring (C-O)	914
Oxirane ring (C-O)	831
C-C (benzene ring)	1506
C=C (benzene ring)	1608
C-O-C ether stretching	1036

Figure 15 shows the FTIR spectrum for epoxy resin containing 20 weight% of nylon-6 thermally cured stepwise in oven for 9 hours (70° C -3h, 100°C -2h, 120°C -2h, 150°C – 2h). The peak at 3392 cm^{-1} became relatively sharp and narrow (Figure 15) indicating the presence of amine group in the system which indicates hydrogen bonding. Previously, many authors have done a time based study for curing of epoxy using FTIR, maintaining the same composition [77, 78]. The characteristic peak of epoxide ring is observed at 914 cm^{-1} and 863 cm^{-1} [79, 80].

On close observation of these two peaks in Figure 16, nylon-6 prepared in suspension form was found to be assisting in the curing of epoxy. All of the samples were cured under same conditions of time and temperature, but with the increase in nylon-6 wt. % the peak corresponding to epoxide group gradually lowered.

Following the same guidelines, a composition based study was carried out for the curing of epoxy as a function of wt. % of nylon 6. Nylon-6 suspension was added as 5 wt.% (2.5 ml, ~0.68 g), 10 wt.% (5.1 ml, 1.33 g), 15 wt.% (8 ml, ~2.06 g), 20 (11.45 ml, ~2.75 g) & 30 (14.5 ml, ~4.3 g) wt. % to liquid emulsion of epoxy resin, the concentration for which was same in all the compositions (25 ml (~13.75 g) of EPI-REZ 5522-WY-55, 50-55% solid by volume). The weight % of nylon-6 was estimated with respect to solid content of epoxy resin. The mixture was then stirred using mechanical stirrer for 1 hour at room temperature to obtain homogeneous solution and then ultra-sonicated for 5 minutes. The coatings were prepared by solution casting method onto 1" x 4" x 1/8" Al 2024-T3 coupons. 2 ml of polymer blend was taken in syringe and poured at the edges of coupon and then was allowed to spread uniformly on the substrate. The heating of polymer blend on substrate was carried out in a stage wise manner starting with 70°C for 3 hours followed by 100°C for 2 hours, 120°C for 2 hours and 150°C for 2 hours, in order to obtain coatings. The step-wise heating was done for slow evaporation of solvent (NMP) in order to obtain uniform and defect-free coating. Moreover, 150°C was chosen as final temperature as thermal heating of EPI-REZ 5522-WY-55 upto 150°C leads to development of hardness in coating [9]. All the samples were cured for same period of time and epoxy fractional conversion was calculated based on the peak area variation of epoxy group’s absorption at 914 cm^{-1}. The internal standard was chosen as stretching vibration of C-C at 1506 cm^{-1} characteristic peak of benzene to quantify the variation. The epoxy fractional conversion with respect to epoxy cured by heating is calculated as:

$$\alpha = 1 - \left(\frac{\left(\frac{Aepoxy}{Abenzene}\right)without\ nylon}{\left(\frac{Aepoxy}{Abenzene}\right)with\ nylon}\right) \qquad [3]$$

where A is the area under absorption peak.

Figure 17 show the variation of epoxy fractional conversion with respect to cured epoxy without nylon-6 as a function of weight % of nylon-6 in epoxy resin and was found to be increasing with the loading of nylon-6. The conversion is found to be low at low loading (5%) which increases sharply at 10 and 15% and then reaches a plateau at 20%, after which the conversion becomes almost constant.

3.1.2 Thermal Properties

For the nylon-6/epoxy composites of varying weight% of nylon-6, associated melting peak was well observed but with the reduction in nylon-6, the melting peak began to narrow down. As the nylon-6 wt.% decreased in the system, the degree of crystallinity of the composite decreased (Table 2), which lead to reduction in melting peak and increment in glass transition temperature. These results clearly suggested that degree of crystallinity of nylon-6 in nylon-6/epoxy composites depends on concentration of nylon-6 which directly effects the thermal properties. Figure 18(a) and 18(b) represents the DSC thermogram showing the melting peak and T_g of nylon-6/epoxy composites respectively.

Heat of fusion was calculated using the area under the melting peak. It was observed that heat of fusion was very high for neat nylon-6 compared to that of composites. In few compositions of composite, distinct multiple peaks over a broad range were observed. This suggests a wide distribution of nylon-6 crystals in epoxy matrix and relatively more energy was required to melt the crystals. The value of heat of fusion was used to calculate degree of crystallinity in samples by following formula $\Theta = \Delta H_f / \Delta H_f^{\circ}$, where Θ is degree of crystallinity, ΔH_f is heat of fusion of samples, and ΔH_f° is theoretical value of heat of fusion for 100% crystalline nylon-6. A commonly accepted value for ΔH_f° of nylon-6 is 230 (±20) J/g [81].

The glass transition temperature was found to be decreasing with increase in nylon-6 concentration. It was reported by Bragg et al. [44] that second phase of nylon may act as plasticizer which increases the flexibility of epoxy. The smaller molecular weight of nylon-6 can coat the stiff epoxy matrix, acting as a lubricant [82], which allows the chains to slide over each other causing reduction in glass transition temperature.

As nylon-6 was crystallized in presence of epoxy matrix, epoxy can be considered as a diluent in present case. The results on melting of nylon-6 in epoxy matrix (the decrease in melting point in presence of epoxy) were in agreement with Flory's theory of depression of melting point, where melting point of semi-crystalline substance decreases when melted in presence of diluent [83]. The T_m for neat nylon-6 was 209^{O}C, which was more than T_m of nylon-6 in epoxy for all nylon-6/epoxy compositions. But when T_m was analyzed only for composites, it was found to decrease with increase in nylon-6 concentration (decrease in epoxy as diluent) which is in disagreement with Flory's theory, where T_m is expected to decrease with increase in diluent. The values for T_g, T_m and approximate values of heat of fusion are listed in table 1.

Table 5 – Thermal parameters for composites

Composition	**T_g (^{0}C)**	**T_m (^{0}C)**	**ΔH (J/g)**	**Θ - Degree of Crystallinity**

Neat nylon-6	25	209	119.81	57.05 %
EPNY30	42	202	8.23	3.91%
EPNY20	54	190, 196, 206, 211 (a small peak)	7.14	3.4%
EPNY15	57	195, 206	11.82	5.3%
EPNY10	50	208	2.73	1.3%

3.1.3 Effect of Nylon-6 on morphology and thermo-mechanical properties of nylon-6/epoxy films

The morphology of the bulk of composite film was investigated by studying the fractured surface of the film, quenched in liquid nitrogen. The effect of composition on nature of crystals was noticeable at the fractured surface. Figure 19(a) is the fractured surface of neat epoxy, where no crystalline features were observed. It was a flat polymeric surface, possibly due to amorphous nature of epoxy caused by high cross-link density. As the nylon-6 was added in epoxy resin at 5% by weight with respect to solid content of epoxy, various crystalline zones were observed. Figure 19(b) shows one of the crystalline zones with large number of small crystals. Few crystals were protruding out of the amorphous matrix and few were embedded in the matrix. Presence of crystals was also observed in all the cracks developed during the fracture of film. This indicates that growth of nylon-6 crystals in epoxy matrix were isotropic in distribution i.e. nylon-6 crystallized uniformly in all directions. Figure 19(c) shows further increase in crystals as nylon-6 was increased to 10 weight%. Few voids were also observed in the morphology. Choi et al [84] studied the occurrence of voids in carbon fiber/epoxy composites. The epoxy used in their study was DGEBA based epoxy resin (Epikote 825) and carbon fibers (commercially available as VGCF) had diameter of 10-20 μm and diameter of 150 nm. They reported that number of voids increased with increase in carbon fiber concentration. Moreover, compositions with low viscosity had lesser number of voids then that of higher viscosity compositions, as due to higher viscosity fillers can aggregate that may act as defects which can lead to formation of voids in fibers[84]. Similarly, in the present case, nylon-6 crystals were fiber-like and increased concentration can cause increase in agglomeration of crystals causing defects such as voids in the composite.

Effect of further increasing the concentration of nylon-6 up to 15% can be seen in figure 19(d). Large crystals growing inside the epoxy matrix were seen coming out of the fractured surface. This suggests that nylon crystals after growing, begins to form network overlapped by amorphous zone. Several folds were observed in morphology along with large crystals, which were large and inter-connected (Figure 19d). As the nylon-6 concentration was increased, it seems crystals began to agglomerate and formed a larger bundle of crystals which were encapsulated by epoxy matrix. On brittle fracture in liquid nitrogen, these networks were broken which can be easily seen in SEM image. On further increasing the concentration of nylon-6, the crystals began to play an important role by acting as bulk material in composite by dominating epoxy as matrix material, and a phase inversion was observed at 20 weight% nylon-6 as shown in Figure 19(e). On further increasing nylon-6 at 30 weight %, a complete different morphology was observed where only one phase was present, as shown in figure 19(f). A stacked morphology was observed with large number of folds under SEM. Hama et al [85] has studied stacking in crystal morphologies of melt cooled polyoxymethylene crystals. They speculated that stacked morphology exists due to the existence of bundle of taut tie chains which continuously pass through the several sheets of lamellae and amorphous region between them. In the present case, nylon-6 was 30 wt.% with respect to solid content of epoxy resin (more than phase inversion concentration of 20 wt.%). it is possible that not enough space was not available for nylon-6 crystals to grow, and they began to form bundles of nylon-6 crystal chains which began to stack onto each other on cooling, eventually leading to stacked morphology with large number of folds.

A direct co-relation was found between the morphological evaluation and corresponding thermo-mechanical properties of nylon-6/epoxy films. Figures 20 and 21 show the dynamic mechanical properties for the neat and nylon-6-loaded epoxy films. The storage modulus and tangent-to-loss modulus are studied as a function of temperature beginning in the glassy state, through the T_g, and ending as a rubbery plateau. The storage modulus, which is a measure of material stiffness under tensile deformation of a solid sample at room temperature[86], was highest for the neat epoxy, whereas the systems with nylon-6 showed lowering of storage modulus in glassy region. The variation of storage modulus with different nylon-6 loading in glassy region is shown in Figure 22.

The decrease of storage modulus in the glassy region suggests the plasticizing effect of nylon-6 with an increase in flexibility of epoxy. As can be seen Figure 22, the storage modulus of composites decreased almost linearly with addition of nylon-6. This is due increase in degree of crystallinity in epoxy matrix as were observed in SEM images. In glassy state, stiffness is related to changes in the stored elastic energy upon small deformation as the molecular segments resist motion [87, 88]. The presence of nylon-6 crystals also causes increase in free volume, thereby lowering the T_g as discussed later, which is other possible reason for increased plasticity.

An increase in storage modulus in rubbery region was observed from neat epoxy to epoxy/nylon-6 blend. In composite systems, storage modulus was highest for 5% but decreased gradually with increase in nlyon-6 weight % though it was greater than neat epoxy for all blends as shown in Figure 23. This phenomenon can be attributed to the occurrence of reaction between epoxy and nylon-6 which causes increase in crosslink density evident by the rise in storage modulus in rubbery region, which was further verified by FTIR. The presence of unreacted nylon-6 for higher amounts acts as plasticizer [89] which causes fall in T_g, with increase in fraction of nylon-6, which is clearly evident with increase in degree of crystallinity in epoxy matrix with increase in nylon-6 concentration. The average number of moles of cross-links can be calculated from storage modulus in rubbery region using the formula G=nRT, where G is rubbery region storage modulus, R is gas constant and T is temperature.

The dependence of T_g on nylon-6 weight % is shown in Figure 24. The T_g decreases from neat epoxy (70^{0}C) to 5% (41.2^{0}C), then decreases gradually from 5 to 30 % (25.7^{0}C).The reason for drop of T_g has been cited as under-curing of epoxy due to partial miscibility of second phase in epoxy [89]; another reason can be flexible aliphatic nature of thermoplastic backbone [2].The increased storage modulus in rubbery region with increase in nylon-6 concentration suggests chemical interaction between nylon and epoxy. Moreover FTIR results are also in agreement with increase in fractional conversion of epoxy. Hence, a possible reason for lowering of T_g by addition of nylon-6 should be the plasticizing effect of low molecular weight nylon-6 crystals, i.e. it increases the free volume of epoxy and essentially lubricates the macromolecular chains.

Furthermore in the given temperature range, presence of single peak for α-transition in tan (delta) vs. temperature plot indicates the existence of a single amorphous phase in cured epoxy/nylon-6 blend. If the two starting materials had different phases in amorphous region and prevented reaction, then two T_g peaks would be expected, one for each amorphous phase which is observed for immiscible or partially miscible thermoplastic blends. Moreover, only one amorphous phase was observed in under SEM as well.

Calculation of amount of nylon-6 reacted in the nylon-6/epoxy composites using storage modulus in rubbery region (E'_R)

Storage modulus in rubbery region (E'_R (Pa)) can be used to calculate moles of crosslinks in the given sample using the equation

$$E'_R = n_v RT \quad [4]$$

where n is moles of crosslinks per unit volume, R is universal gas constant (8.314 $m^3PaK^{-1}mol^{-1}$), and T is temperature in Kelvin. Moles of crosslinks per unit volume is shown in table 6

Table 6 – Moles of crosslinks per unit volume (n_v) calculated form Storage Modulus (E'_R) for each composition

Composition	Storage Modulus (E'_R)	Moles of crosslinks per unit volume (n_v) (n/m^3)
Thermally cured neat epoxy	29000	9.34
EPNY 5	51000	16.43
EPNY 10	48000	15.47
EPNY 15	40000	12.89
EPNY 20	45000	14.50
EPNY 30	43500	14.02

The molecular weight of nylon-6 used in nylon-6/epoxy composites is 10362.87 (calculated by dilute solution viscometry). Moreover, weight of nylon-6 added to the system was known in grams. Hence total moles of nylon-6 added to the epoxy/nylon-6 blend can be obtained by using equation

$$no.\,of\ moles = \frac{wt.\,in\ grams\ of\ nylon-6}{molecular\ weight\ of\ nylon-6} \quad [5]$$

The no. of moles of nylon-6 in the sample used for dynamic mechanical analysis can be obtained by equation

$$no.\,of\ moles\ of\ nylon\ 6\ in\ film = \frac{total\ no.\,of\ moles\ of\ nylon\ 6}{total\ volume\ of\ blend} \times volume\ of\ film$$

[6]

Total no. of moles of nylon-6 in film used for dynamic mechanical analysis is shown in table 2.

Table 7- Total no. of moles of nylon-6 in film used for dynamic mechanical analysis

composition	weight of nylon-6 (grams)	Total moles of nylon-6 ($n_{nylon-6}$)	Total volume of blend (mm^3)	Volume of films (mm^3)	Moles of nylon-6 in film
Thermally cured neat epoxy	0.68	0.0000656189	27500	285.6	NA
EPNY 5	1.33	0.000128343	30100	119.78	2.85812E-07
EPNY 10	2.06	0.000198787	33000	171.75	7.32322E-07

EPNY 15	2.75	0.000265371	36450	183.35	1.10447E-06
EPNY 20	4.3	0.000414943	39500	261.39	1.90302E-06
EPNY 30	0.68	0.0000656189	27500	278.4	2.92456E-06

The moles in sample (film for DMA) per unit volume (m^3) can be calculated using equation:

$$moles\ per\ unit\ volume = \frac{moles\ in\ film}{total\ volume\ of\ film} \quad [7]$$

The molecular weight of nylon-6 synthesized is 10362.87, and the repeat unit of nylon-6 ($C_6H_{11}NO$) has molecular weight of 113, hence total number of repeat units in nylon-6 are (10362.87/113 = 91.70) 92 units.

The average moles of nylon-6 reacted in the composites per unit volume (N_{1v}) can be calculated by equation:

$$N_{1V} = \frac{moles\ of\ crosslinks\ of\ composites - moles\ of\ crosslinks\ in\ neat\ epoxy}{92} \quad [8]$$

The average moles of nylon-6 reacted in the epoxy/nylon-6 composite is shown in table 8.

Table 8 - The average moles of nylon-6 reacted in the epoxy/nylon-6 composite.

Composition	Total volume of film (m^3)	Moles of nyon-6 per unit volume (n/m^3)	Moles of nylon-6 reacted /m^3 (N_{1V})
Thermally cured neat epoxy	2.856E-07	NA	NA

EPNY 5	1.1978E-07	1.00074234	0.077079943
EPNY 10	1.7175E-07	6.113888755	0.066569042
EPNY 15	1.8335E-07	6.430687404	0.038539972
EPNY 20	2.6139E-07	10.37918291	0.056058141
EPNY 30	2.784E-07	11.18849242	0.05080269

The total weight of nylon-6 reacted per unit volume (g/m^3) can be calculated using equation:

$$reacted\ weight\ of\ nylon\ per\ unit\ volume\ \left(\frac{g}{m3}\right) = moles\ of\ nylon\ 6\ reacted\ per\ unit\ volume\ \times molecular\ weight\ (10362) \qquad [9]$$

Once, the weight of nylon-6 reacted per unit volume is knows, the total weight of nylon-6 reacted while curing can be obtained by using equation:

$$total\ weight\ of\ nylon\ 6\ reacted\ in\ composite = weight\ of\ nylon\ 6\ reacted\ per\ unit\ volume\ \times total\ volume\ of\ blend \qquad [10]$$

Table 9 - The weight of nylon-6 reacted in the nylon-6/epoxy composite.

Composition	Weight of nylon-6 reacted in composite sample film (g/m^3)	Total reaction volume (m^3)	Total weight of nylon-6 reacted in composite (g)
EPNY 5	798.7694336	0.0000275	0.021966
EPNY 10	689.846329	0.0000301	0.020764

EPNY 15	399.3847168	0.000033	0.01318
EPNY 20	580.9232244	0.00003645	0.021175
EPNY 30	526.4616721	0.0000395	0.020795

Once, the total weight of nylon-6 reacted while curing is obtained, the total weight of unreacted nylon-6 in the composite can be calculated using equation:

$$weight\ of\ unreacted\ nylon6\ (g)\ =$$

$$total\ weight\ of\ nylon\ 6\ in\ blend\ (g) - weight\ of\ reacted\ nylon\ 6(g) \qquad [11]$$

Table 10 shows the fraction of reacted and unreacted nylon-6 in the composite

Table 10 – Total weight in grams of nylon-6 added to the epoxy/nylon-6 system along with fraction of reacted and unreacted nylon-6.

Composition	Weight of nylon-6 added to system (g)	Weight of nylon-6 reacted in composite (g)	Weight of nylon-6 unreacted in composite (g)	Weight fraction of nylon-6 reacted in composite (%)	Weight fraction of nylon-6 unreacted in composite (%)
EPNY 5	0.68	0.021966	0.658034	3.230318	96.76968

EPNY 10	1.33	0.020764	1.309236	1.561231	98.43877
EPNY 15	2.06	0.01318	2.04682	0.639791	99.36021
EPNY 20	2.75	0.021175	2.728825	0.769987	99.23001
EPNY 30	4.3	0.020795	4.279205	0.48361	99.51639

These results suggests that nylon-6 reacts only upto a certain point with epoxy resins to form crosslinks, irrespective of concentration of nylon-6 in composition. Increasing the concentration of nylon-6 beyond that point results in more of unreacted nylon-6, which potentially crystallizes. The increased nylon-6 phase in the composite leads to reduction in glass transition temperature and storage modulus in gassy region. The amount of nylon-6 that remains unreacted as a function of total weight of nylon-6 added to system shows a perfect linearly increasing trend as shown in Figure 25.

3.1.4 Effect of nylon-6 on surface morphology and anti-corrosion properties of nylon-6/epoxy coatings

Figure 26(a) shows the SEM micrograph of surface of thermally treated EPI-REZ 5522-WY-55 epoxy coated on Al-2024 T3 aluminum alloy surface. Very sharp and long cracks were observed at the surface, which is possibly due to the brittle nature of epoxy resin caused by high cross-link density. The epoxy resin was then blended with nylon-6 suspension followed by curing to form a coating on Al alloy coupon as a substrate. Morphology of the surface of composite coating containing 10% of nylon-6 in composition by weight can be seen in figure 26(b). As discussed earlier, multilayered crystals with spherulites have tendency to grow radially outwards along with high level of branching to occupy free volume, as once crystals are nucleated over inhomogeneous surface, nylon-6 chains begins to fold over previously formed crystals in all directions [90].

During thermal curing of nylon-6/epoxy blends, where coating was heated upto 150°C, the cross-link density of epoxy begin to increase. As coating began to cool down after the process was completed, cracks begin to develop in coating due to thermal gradient developed between metallic substrate and coating. Since nylon-6 chains have tendency to crystallize while cooling in all direction, they begin to crystallize in the space created by cracks and crevices in epoxy matrix. The sharp brittle cracks were filled with ductile nylon-6 phase. The nylon-6 phase begin to fill the voids and cracks of epoxy, which lead to plasticization of epoxy along with increase in toughness and reduction in brittleness. On closely spotting a crack filled with nylon-6 crystals at higher magnification, long fibril crystals were observed with length ranging from 0.5-2 μm. On further increasing nylon-6 concentration to 20%, a significant variation in surface morphology was observed as shown in figure 26(c). The number of cracks was found to be reduced and the cracks that were present were also very small in size. The nylon-6 crystals reduced in size but increased in number and were found to be dispersed on the surface. On closely observing the morphology at higher magnification, each nylon-6 phase can be seen to be followed by one tail or crack.

Such kind of surface morphology had direct effect on the anti-corrosion properties of nylon-6/epoxy composite coatings, coated on Al-2024 alloy substrate.

3.1.4.1 Direct Current Polarization

DC Polarization test was performed to obtain information about corrosion rate which is determined by using corrosion potential (E_{corr}) and corrosion current (I_{corr}). Since, corrosion rate is directly proportional to I_{corr}, the coating with least I_{corr} value is considered to be most efficient coating for anti-corrosion purpose[91]. Effect of increasing weight % of nylon-6 in epoxy resin was studied for corrosion inhibition using DCP.

Figure 27 represents the TAEFL plots for nylon-6/epoxy coatings after exposure to 3.5wt% NaCl solution. The corresponding values for E_{corr} and I_{corr} are shown in table 11. Just after one day of exposure, neat epoxy coating showed lesser corrosion current then nylon-6/epoxy, but as exposure time increased, the neat epoxy coating began to fail and obtained higher value of I_{corr} compared to nylon-6 filled epoxy coatings. Moreover, multiple shoulders in the anodic arm for epoxy coating were observed which suggests the passivation mechanism. This indicates that, neat epoxy coating failed and passive Al oxide film was getting formed on substrate that was saying it from corrosion. But such passivation phenomenon was not observed in any other coating indicating increased durability of epoxy coatings by incorporation of nylon-6.

Table 11 - Parameters obtained from direct current polarization for nylon-6/epoxy coatings on Al 2024-T3 alloy substrate

Composition	I_{corr} (A/cm^{-2}) – after 1 day	E_{corr} (V) – after 1 day	Corrosion rate (mpy) after 1 day	I_{corr} (A/cm^{-2}) – after 2 months	E_{corr} (V) – after 2 months	Corrosion rate (mpy) after 2 months	Morphology
Neat Epoxy	3.7×10^{-7}	-0.66	576×10^{-3}	2.2×10^{-6}	-0.90	9.081	Large and sharp cracks
EPNY 5	6.9×10^{-6}	-0.73	489×10^{-3}	4.6×10^{-6}	-0.75	2.983	Small cracks

							filled with small crystals
EPNY 10	4.0×10^{-6}	-0.79	422×10^{-3}	9.0×10^{-7}	-0.54	2.184	Cracks uniformly filled with larger crystals
EPNY 15	8.8×10^{-6}	-0.62	515×10^{-3}	4.2×10^{-6}	-0.73	5.817	Inter-connected network of crystals accompanied with smaller cracks
EPNY 20	2.2×10^{-6}	-0.73	448×10^{-3}	1.9×10^{-5}	-0.76	3.082	Large cluster of crystals with small cracks
EPNY 30	5.0×10^{-6}	-0.69	537×10^{-3}	5.1×10^{-6}	-0.80	6.984	Rubber like morphology with stacks and folds

Figure 28 a and b shows the DCP Plots for comparison of epoxy/nylon-6 (10% by weight) and thermally treated neat epoxy coatings on Al 2024-T3 alloy substrate after1 day of exposure and 2 months of exposure to 3% NaCl solution. It was clearly observed that epoxy coating containing 10 weight% of nylon-6 had lower corrosion current then thermally treated neat epoxy after 2 months of exposure.

3.1.5.2 Bode Plots

The EIS study was performed on Al alloy substrate coated with epoxy containing nylone-6 in various concentrations. The coatings were exposed to 3.5wt% NaCl solution.

The Bode plots of nylon-6/epoxy composite coatings applied on aluminum alloy Al-2024 T3, and cured with step-wise heating by 70°C for 3 hours followed by 100°C for 2 hours, 120°C for 2 hours and 150°C for 2 hours, are presented in Figure 29 (a) and (b) before exposure and after 2 months of exposure. To determine the effect of nylon-6 on the anti-corrosion properties of nylon-6/epoxy coatings, the control material used was thermally heated EPI-REZ 5522-WY-55 epoxy resin, without using curing agent, but corrosion experiments were carried out on standard epoxy-amine (EPIKURE 8290-Y-60) coating system to compare it with nylon-6/epoxy system. The amine based curing agent was added in stoichiometric ratio (79:21) recommended by manufacturers for maximum conversion of epoxy. Epoxy-amine coating showed higher impedance value (1×10^{6} Ω) as shown in Figure 30 compared to thermally cured epoxy without curing agent ($1\times10^{4.2}$ Ω) after exposure to 3.5 weight% solution. This lead to conclusion that nylon-6 had a profound effect on improving the anti-corrosion properties without curing-agent, moreover, comparison with standard epoxy-amine system suggests that the novel nylon-6/epoxy composites can be effectively used in practical applications.

The impedance modulus, |Z| at the lower end of frequencies provides the information about the corrosion protection quality of the coatings. The higher impedance value at low frequency implies better corrosion protection. The |Z| at frequency of 0.001 (hz) as a function of exposure time for the various nylon-6 loadings in epoxy coatings are shown in Figure 31.

The coating with 15 and 30 wt% nylon-6 loading showed the lowest impedance than other coatings at all exposure times. Coating containing 20 wt% of nylon-6 shows higher impedance during the initial exposure time and then attained the same value of impedance as that 15 and 30% coating after few days of exposure. The coating with 5 and 10 wt.% nylon-6 showed highest impedance value at all exposure time compared to other coatings.

It was observed that all the coating containing nylon-6 showed better corrosion performance than epoxy coating without nylon-6. When surface morphology of thermally cured EPI-REZ 5522-WY-55 epoxy coating was observed under SEM (Figure 26a), large number of micro cracks were observed. The cracks provides convenient path for electrolyte to diffuse and pass through it, which can readily reach the surface of metal substrate (Al2024 T3) on exposure. Hence, this coating shows poor anti-corrosion performance. Among the nylon-6/epoxy coatings, the coating containing 10 weight % of nylon showed the best corrosion performance with highest impedance value of $1\times10^{8.5}$ ohms. The morphological study of this coating revealed that nylon-6 crystals began to form in the cracks and crevices formed during the curing. These crystals filled the cracks and hence provided a better barrier to diffusion of electrolyte, resulting in a better corrosion performance.

3.2. 15A Clay/Nylon-6 Nanocomposites

3.2.1. Thermal Behavior

In this section, thermal properties of neat nylon-6 and clay/nylon-6 nanoocomposites has been discussed[90]. DSC is employed to obtain information about the glass transition temperature (T_g), melting temperature (T_m) and crystallization temperature (T_c) of the polymer composites [92]. The experiment was carried out in 4 runs. The 1st run was to remove thermal history of polymer, where sample was heated just beyond T_g (around 40°C) and then cooled with liquid nitrogen to -5°C. The 2nd run was started from -5°C up to the melting point (T_m) of polymer sample (250°C). Then it was quenched in presence of liquid nitrogen, and the temperature was lowered to -5°C. The 3rd run was then started after quenching from 250°C, to analyze the effect of quenching on T_g and T_m. Then the sample was allowed to cool by turning off the heat in DSC, followed by fourth run, in order to compare the thermal parameters with and without quenching. Effect of clay composition on the thermal properties of nylon-6 has been discussed. Each parameter, i.e., T_c, T_m and T_g are distinctly discussed. The observed values for these parameters are shown in listed in table 12 for comparison, and degree of crystallinity for each run is listed in table 13.

The effect of clay on the crystallization temperature of nylon-6 containing 0.5% clay by weight and 1% clay by weight is shown in Figure 32. When the samples were allowed to cool by turning off the heat of DSC from the melt, a sharp narrow crystallization peak was observed with T_c at 170°C for neat nylon-6. At clay loading of 0.5 wt.%, the T_c increased to 176°C. On further increasing clay to 1% by weight, the T_c dropped to 171°C. Moreover, the crystallization peak broadened comparatively, indicating formation of structure of nancomposite with a wide distribution of crystals. Hence, it can be concluded that in presence of clay at very low concentration (0.5%), when caprolactam is polymerized in presence of organoclay to give clay/nylon-6 nanocomposites, a composite with increased crystallinity is obtained. Degree of crystallinity was 57.05% for neat nylon-6, while it increased to 65.75% at clay loading of 0.5 weight%. Further addition of clay beyond 1 wt.% (65% degree of crystallinity at 1 wt.% clay) leads to decrease in crystallinity (melting and crystallization peaks were not detected at 5 wt.% and 10 wt.% of clay). As the clay stacks are increased, they pose hindrance to the chain addition during polymerization step leading to formation of short polymer chains [93]. The shorter the chain, the lesser are the chances of crystallinity in polymer, as crystallization is directly dependent upon molecular weight of polymer [94]. The effect of concentration of clay on molecular weight of nylon-6 synthesized by in-situ solution polymerization is discussed in section 3.3.4.

Table 12 – DSC parameters at different clay composition

Clay Composition	T_g (°C) (4th run)	Tc (°C)	T_m (°C) (2nd run)	T_m (°C) (3rd run)	T_m (°C) (4th run)
0%	24	170	212.8	201.2, 209.8	209.2
0.5%	23	176	218	216	217.6
1%	18	171	219	204	200, 210

Table 13 – Heat of fusion and degree of crystallinity for clay/nylon-6 nanocomposites

Clay Composition	ΔH (J/g) (2nd run)	ϴ - Degree of Crystallinity (2nd run)	ΔH (J/g) (3rd run)	ϴ - Degree of Crystallinity (3rd run)	ΔH (J/g) (4th run)	ϴ - Degree of Crystallinity (4th run)

0%	119.81	57.05	72.58	34.56	89.71	42.71
0.5%	138.08	65.75	66.36	31.60	90.01	42.86
1%	136.51	65.01	47.21	22.48	49.27	23.46

Figure 33 shows the comparison of melting temperature of nylon-6 with different clay loadings. Figure 33(a) refers to the samples, when they were freshly prepared by precipitation from solution in oven. Figure 33(b) refers to the samples that were quenched after melting in second run. Figure 33(c) refers to the samples that were recrystallized under slow cooling after melting in third run. When clay/nylon-6 nanocomposites were subjected to DSC just after processing, a single peak was observed in all the samples, suggesting that samples obtained were high in crystallinity with stable crystal structure. When these samples are quenched and re-melted, two melting peaks are observed for neat nylon-6 at 201°C and 209°C, while a single peak is observed for nylon-6/clay (0.5%) at 216°C and nylon-6/clay (1%) at 204°C. This indicates that in presence of clay, stable crystal structures are obtained on fast cooling due to preferred secondary crystals compared to mixture of α- and γ-crystals formed in neat nylon-6. When these samples were allowed to cool slowly (by turning off the heat of DSC) and re-melted as shown in Figure 41(c), single peak for nylon-6 re-emerged at 209.8°C and peak related to 201°C vanished. The γ-crystals that melted at 201°C recrystallized to form more stable α-crystals. For nanocomposite with 0.5% clay loading, position of melting peak remained almost unaffected at 217°C. However, for nylon-6/clay (1%) two melting peaks were observed.

This is possibly due to presence of more clay particles which reduces the room for polymer chains to crystallize and gives rise to various metastable crystals. This leads to a metastable crystal structure which is a partially disordered crystal structure of nylon-6, and it is a phase intermediate between α-form and γ-form [49, 95] On further increasing clay concentration to 5 and 10%, crystallinity of nylon-6 was reduced significantly.

Hence, it can be concluded that 0.5% by weight is the optimum concentration for nylon-6/clay nanocomposite to be synthesized by solution polymerization, which constantly leads to formation of stable crystal structure with narrow distribution and high crystallinity, irrespective of slow or fast cooling conditions for crystallization. Figure 42 represents the effect of clay on the T_g of nylon-6. A sharp fall in the base line was observed which occur near T_g. Such sharp and clean transition was not observed in the second and third run, probably due to thermal stresses.

A sharp transition in the baseline was observed for all the samples in fourth run. The T_g was found to be decreasing with increase in clay loading. The T_g for neat nylon-6 dropped from 26^0C to 24^0C at 0.5% clay loading and to 18^0C at 1% clay loading. The range of temperature in which T_g transition occurred, was found to be decreasing with increase in clay percentage. The reinforcement of polymers by organoclay depends on the interaction of polymer matrix and the clay platelets [96]. There are two factors that can poosibaly contribute to lowering of T_g; 1) free volume existing at the polymer surface interface due to poor wetting and 2) plastcization of polymer due to incorporation of nanoclay [96].

3.2.2. Structural Analysis

When nylon-6/clay composite granules are subjected to X-Ray diffraction, two kinds of peaks are observed. One corresponding to ordered clay stacks at lower angle and other corresponding to the polymers chains arranged in an orderly fashion to form a crystal at higher angle[97]. The location of peak at a particular angle gives information about nature of crystalline form, d-spacing, length of crystals and stability of crystals.

The crystal length and corresponding d-spacing were calculated using Scherrer equation and bragg's law respectively [98, 99]. The Scherrer equation is given as follows:

$$D(hkl) = \frac{K\lambda}{\beta(hkl)\cos\theta} \qquad [12]$$

Where D (hkl) is the mean crystal size along [hkl] direction, K is the shape factor (scherrer constant, value of 0.94 is used in this case), β(hkl) is the line broadening at half the max intensity in radians and θ is the half scattering angle. According to Bragg's law, d-spacing was calculated using the following equation:

$$n\lambda = 2d\sin\theta$$

[13] Where n is a constant integer (1 in our case), λ is wavelength, d is d-spacing and θ is diffraction angle in degrees.

The x-ray diffraction pattern at lower angle for pristine 15A clay and nylon-6/clay composites is shown in Figure 34. The peak corresponding to pristine clay was found at 2θ angle of 2.5^{0}, but the peak position shifted to lower angle of 2.05^{0} for composite. The decrease in the angle for peak location suggests that intercalated structure was obtained with increase in the distance of clay galleries. The peak location, d-spacing and crystallite length among clay galleries are shown in Table 14.

Table 14 – XRD peak location, d-spacing and crystallite size for nylon-6/clay composite system at lower angle (for nanoclay)

	2θ (^{o})	d-spacing (A^{o})	Crystallite length (A^{o})
Neat Clay 15A	2.5	34.48	103.48
Nylon-6/clay (0.5%)	2.05	43.25	113.35

Nylon-6/clay (1%)	1.95	45.26	125.19
Nylon-6/clay (5%)	1.95	45.26	137.42
Nylon-6/clay (10%)	2.05	43.25	131.73

The increase or decrease in the d-spacing depends upon the processing technique used to obtain polymer/clay composite [100, 101]. Hegde et al [102] reported a slight increase in d-spacing at low clay concentration while slight decrease at higher concentration of clay for nylon-6/clay composites processed by melt compounding. Zhang et al [103] reported decrease in d-spacing for clay with increase in composition for composites processed by twin screw extruder. Swain and Isayev [104] demonstrated increase in d-spacing when composites are processed by continuous sonication process. The d-spacing increased by in-situ solution polymerization of ε-caprolactam in presence of clay. It is speculated that during polymerization reaction, a fraction of polymer chains enter the clay galleries which eventually crystallizes leading to formation of intercalated composite system. The d-spacing for clay increased from 34.48 A° to 43.25 A° for nylon-6/clay (0.5% by weight), but remains almost in the same range with further increase. Hence, the composition of the composite has no effect on the d-spacing of clay galleries after a threshold. It can be inferred that polymerization lead to increase in inter-gallery distance for clay up to a limit, but was not able to break the oriented or regular structure of clay, which is essential for exfoliation. On increasing clay concentration to 5%, a new peak is observed at 2θ angle of 3.23° which increases to 4.14° on increasing clay to 10% by weight, indicating that at high clay loading, the polymerization and crystallization process lead to change in the orientation of a fraction of clay stacks with decreased d-spacing.

Clay has a pronounced effect on the crystal structure of nylon-6 [95, 98, 105]. Nylon-6 has two major crystalline forms, due to difference in packing of nylon-6 chains by hydrogen bonding. It may occur in an anti-parallel (α form) or parallel way (γ form) [106, 107]. On subjecting nylon-6 to x-ray diffraction, the polymers crystals show a peak in diffraction pattern. Figure 35 is the X-Ray diffraction pattern for the polymer crystals of neat nylon-6 and its composites with clay at different loading. Along with a considerable effect on the d-spacing of clay galleries due to in-situ solution polymerization, a marked effect on crystalline form and structure of nylon-6 was also observed due to clay composition in intercalated composite system.

α polymorph of nylon-6 crystal shows major peaks near 17.4^{o}, 19.9^{o} and 24^{o}. [108-110] and γ polymorph usually shows peak at 18.2^{o} and 21^{o} [108, 109]. As the polymer was crystallized from solution, a mixture of both forms was observed in neat nylon-6 without clay. But α form was found to be dominating over γ form as indicated by the position of crystal peaks at 19.9^{o} corresponding to [200] plane and 24.1^{o} corresponding to [202] plane, while relatively small peaks were observed at 18.15^{o} and 21.6^{o} corresponding to [002] plane suggesting presence of γ phase in minority. But as the clay loading was increased, γ form began to stabilize gradually.

When clay was introduced as 0.5% by weight (Figure 35), peaks related to α form were still dominant at 19.8^{o} and 24.09^{o}, but peaks corresponding to γ phase were narrow relative to neat nylon-6 with increased intensity suggesting formation stable γ form of crystals. On further increase in clay concentration to 1%, peak corresponding to α form at 24^{o} almost vanished and the one at 19.8^{o} reduced in intensity. Moreover, peak at 17.03^{o} and 18.15^{0} increased and new small peak at 22.8^{0} appeared. This suggests a swift transition from α to γ phase as the peak at

18.15° grew up along with a small peak at 21.9°. On further increasing clay upto 5 and 10 weight %, the overall crystallinity reduced substantially as indicated by relatively small peaks. Furthermore, the peak at 18.15° shifted to lower angle of 17.7° and 17.3°, i.e. d-spacing among crystals corresponding to this angle was increased. Few small crystalline peaks were observed at 17.7°, 19.8° and 21.2° suggesting mixture of α and γ crystals. Hence, it can be concluded that at lower clay loading crystallinity increases with γ-crystals attaining stability, but as clay is further increased up to 5 and 10%, crystallinity of nylon-6 decreased. The results obtained by XRD concerning dispersion of clay and crystallinity of nylon-6 were further supported by TEM. The dark shady lines represent layered clay platelets. TEM images of composites are shown in Figure 36.

3.2.3. Morphological Analysis

The morphology of neat clay and the composite systems containing varying concentration of clay was observed under SEM. Observed morphologies are shown in Figure 37 at lower magnification with corresponding higher magnification. In case of nylon-6 without clay synthesized by solution polymerization and heated to obtain solid nylon-6 powder, small crystals dispersed in an amorphous matrix were observed throughout the sample. At higher magnification, large spherulites were observed grown radially outwards from a single point (Figure 37a). Then, effect of clay was analyzed on subsequent samples. At a clay loading of 0.5% by weight, a highly crystalline and unique spherulitic morphology was observed at a lower magnification grown from a common center. At higher magnification, large crystals were observed but the appearance was different from that of neat nylon-6. They appeared to be more flat, like an array of ribbon tied at a common center. The unique flat appearance suggests that the crystallization process begin to take place inside the clay galleries which then continued outside clay in order to fulfill the space (Fig 37b).

When clay was increased to 1 weight %, a morphology consisting of distinct crystalline zones were observed throughout the sample at lower magnification. The crystals appeared to be numerous but reduced in size. On closely observing at higher magnification, a noodle type crystalline morphology was observed, where cylindrical small crystals were observed distributed over a wide zone, unlike nylon-6 and it's composite with clay at 0.5 weight %. This suggests that on increasing clay particles, the amount of nucleating agents increased and various crystals had different origins, instead of a common center (Fig 37c).

On further increasing clay to 5 and 10 weight % (Fig 37d and 37e), a drastic change in the morphology was observed with significant reduction in amount of crystals. At 5 weight % clay loading, cylindrical crystals uniformly protruding outwards were observed at low magnification. Large clay chunks were observed surrounded and encapsulated by nylon-6 crystals. Since the clay loading was high, it leads to reduction in the space for crystals to grow. Hence, the crystals that grew were found to be impinged on each other intensely as observed at higher magnification. At 10% clay loading, large clay stacks were observed with almost no crystallinity. At higher magnification small fiber like structures impinged into each other were observed surrounded by large clay chunks. This suggests that at this concentration of clay, large aliphatic chains were not created due to stearic hindrance and no space was available for small chains to grow as crystals. Clay stack dominated in the nylon-6 matrix.

3.2.4 Molecular Weight Analysis

The effect of clay concentration on the intrinsic viscosity [η] of nylon-6 was analyzed using ubbelhold viscometer[90]. The intrinsic viscosity was obtained from a plot of Log (Rel η)/C and Sp η/C Vs. C, where C is the concentration in g/dl and η is the measure of viscosity. The following formulae were used in this experiment [111]:

Relative Viscosity (rel η) = t/t_o [14]

Specific Viscosity (Sp η) = $(t - t_o)/t_o$ [15]

Where t is the elusion time of the solution and t_o is the elusion time of solvent.

By extrapolating the reduced viscosity plots to zero concentration, as shown in Figure 38(a-d), intrinsic viscosity were obtained for different clay/nylon-6 systems. The values of intrinsic viscosity were used to calculate viscosity average molecular mass for different systems by using Mark-Houwink equation [112]:

$$[\eta] = KM^{\alpha} \quad [16]$$

Where the parameters K and α are Mark-Houwink constants, which depends upon the type of polymer and corresponding solvent. In the present case, nylon-6 was dissolved in conc. H_2SO_4. For this system $K = 3.32 \times 10^{-4}$ and $\alpha = 0.72$ [113]. The variation in the intrinsic viscosity and the calculated molecular weight as a function of clay concentration in nylon-6 matrix is shown in Figure 39a and 39b respectively. It was observed that molecular mass initially increased by 2.8% when 0.5 mass % clay was incorporated in nylon, but on further increase in clay concentration, molecular mass of clay began to fall sharply. It is spaculated that high amount of clay stacks during the ring opening anioninc addition polymerization reaction acts as hinderance to the addition reaction and growth of chains. Hence, at low clay concentration of clay, it is hypothesized that nylon chain growth occurs rapidly with intercalated clay platlets bein the part of chain therby increasing the molecular mass. While, at higher clay loading, chain growth is retared, hence, lower molecular mass. The values of intrisic viscosity and molecular mass are shown in Table 15.

Table 15 – Values of Intrinsic Viscosity and Molecular Weight

Clay Concentration (weight %)	Intrinsic Viscosity (dLg^{-1})	Molecular Weight (g/mol)
0	0.45	10362.87
0.5	0.46	10659.03
1	0.22	4140.297
5	0.16	2752.46
10	0.08	1131.839

The moleculare weight obtained by solution polymerization is very close to nylon-6 synthesized by hexamethylene diamine-initiated polymerization of ϵ-caprolactam at 220°C by melt polymerization (337 – 10940) [114]. Molecular weight was also found to be close to nylon-6 and clay/nylon-6 composite synthesized by Toyota using ring opening reaction of caprolactam via melt polymerization in presence of 12-montmorillonite and 6-caproic acid (3200-5100) [115].

3.3. Hybrid Blends of Clay/Nylon-6 Nanocomposite and Epoxy

3.3.1 FTIR Analysis

Figure 49 and 50 are the FTIR spectra of Cloisite 15 A clay and clay/Nylon -6 nanocomposite respectively, used in this work. Table 16 shows the characteristic peak related to commercially available organoclay and table 17 shows the characteristic peak related to clay/nylon-6 nanocomposites.

Table 16 – Characteristic peaks for 15 A clay

Functional Group	**Absorbance Peak (cm^{-1})**
-OH stretching	3636
Si-O-Si stretching	1040, 470
Al-OH-Al deformation of aluminates	917
-CH vibrations from methylene groups (asymmetric stretching, symmetric stretching and bending) from surfactant	2924, 2842, 1475

Table 17 – Characteristic peaks for clay/nylon-6 nanocomposites

Functional Group	**Absorbance Peak (cm^{-1})**
Amide group (C=O)	1651
Hydrocarbons ($-CH_2$ and $-CH_3$)	2926, 2954, 1475
-NH stretching	3360

γ-crystals of nylon-6	980
Si-O-Si stretching	1040, 470
Al-OH-Al deformation of aluminates	917

Figure 51 shows the FTIR spectrum of clay/nylon-6-epoxy composite coating. Table 18 shows the characteristic peaks for clay/nylon-6-epoxy composite coating.

Table 18 – characteristic peaks for clay/nylon-6-epoxy composite coating

Functional Group	**Absorbance Peak (cm^{-1})**
-OH stretching	3393
Oxirane ring (C-O)	914
Oxirane ring (C-O)	831
C-C (benzene ring)	1506
C=C (benzene ring)	1608
C-O-C ether stretching	1036
Si-O-Si stretching	470
Si-O-Si out of plane vibration	980

The major peaks associated with clay are observed at the wavenumber of 470cm^{-1} due to the Si-O-Si deformation [116]. The neat epoxy sample, nylone-6 loaded epoxy and epoxy resin filled with clay modified nylon-6 were analyzed by FTIR. For pristine epoxy and nylon-6 filled epoxy, no peak was observed at 470, but as clay modified nlyon-6 was introduced to the system, a new peak at 470 was clearly observed. Figure 52 represents the FTIR for system focused at 470 cm^{-1} due to Si-O-Si deformation.

As discussed in section 1.1.1, epoxy fractional conversion was calculated as a function of clay content in composites. On close observation of the peak at 914 cm^{-1} in Figure 53,clay was found to have effect on curing of epoxy. All of the samples were cured under same conditions of time and temperature, but with the increase in clay wt. % the peak corresponding to epoxide group lowered at low concentration of clay, but increased at higher clay concentration.

The epoxy fractional conversion with respect to epoxy cured by heating is calculated as:

$$\alpha = 1 - \left(\frac{\left(\frac{Aepoxy}{Abenzene}\right)without\ nylon}{\left(\frac{Aepoxy}{Abenzene}\right)with\ nylon}\right) \qquad [3]$$

where A is the area under absorption peak.

Figure 54 show the variation of epoxy fractional conversion with respect to cured epoxy without nylon-6, as a function of weight % of clay in epoxy/nylon-6 resin The conversion initially increased at low concentration of clay (0.05% by weight), but on further increasing clay the conversion was less than that of composite without clay.

Infra-red spectroscopy is a widely used technique to monitor the effect of corrosion on the coating at chemical level [65, 117-120]. Figure 55 a and b shows the FTIR spectra of neat epoxy, nylon-6/epoxy and clay/nylon-6/epoxy coating containing 10 weight% of nylon-6 and 1 weight% of clay, before and after exposure to a 3.5 weight% NaCl solution. It can be seen in figure that the coatings containing clay showed a significant reduction in the intensity for spectra, but for coatings not containing clay, the reduction in intensity was very minimal. The organoclay aliphatic group shows peak at 2925 and 2852 cm^{-1} and the silicon oxide shows a peak 1054 and 470 cm^{-1}. The peaks at 2925, 2852 and 1054 cm^{-1} were masked by epoxy but a prominent peak at 470 cm^{-1} was clearly observed. The intensity of the IR absorption peak at 465cm^{-1} was found to be increasing with increasing clay concentration, moreover after exposure intensity of clay peak at 465 relatively increased while overall intensity of the coatings decreased.

The hydroxyl peak at 3361 cm^{-1} was examined for increment in absorption intensity for nylon-6/epoxy coatings with and without clay loading. The samples were exposed to 3.5 weight% salt solution for two months, and were then subjected to infra-red spectroscopy to determine the water absorption by each sample, in order to investigate the corrosion mechanism. For better understanding, hydroxyl peak height was measured for each sample, before and after exposure to electrolyte and the ratio of peak height was noted. The ratio of peak height at 3361 was directly proportional to water uptake by coatings in 8 weeks. The effect of clay on the water uptake is shown in Figure 56, where peak height ratio is plotted as a function of clay weight%. It can be seen that, the water uptake by samples without clay was very high with a ratio of 1.1 for epoxy/nylon (90:10) and 2.8 for epoxy/nylon (80:20). But when clay was introduced in the system, the ratio for the peak height decreased significantly to 0.46 and 0.45 at lay loading of 0.5 and 1 weight%, with epoxy to nylon ratio maintained at 90:10. For the epoxy to nylon ratio of 80:20, the ratio of peak height decreased to 0.99 and 0.41 at clay concentration of 0.5 and 1 weight%.

3.3.2 Thermal Properties

The 3 component system was investigated for melting and crystallization behavior of nylone-6 in presence of clay and epoxy resin using DSC. For nylon-6 containing clay, it was noted before that at clay content of 5 and 10 wt.%, degree of crystallinity reduces to such an extent that it is not detected in DSC. Similar results were observed for present systems, when 5 and 10 wt. %

clay modified nylon-6 was incorporated in epoxy matrix, no melting or crystallization peak was observed in DSC runs. Hence, only the systems with 0.5 and 1 wt.% clay modified nylon-6 were investigated for melting and crystallization behavior.

For the epoxy system containing 0.5 wt. % of clay, a melting peak was observed in the range of 206-210 °C for different composition (Figure 57). As the clay-nylon 6 concentration was increased, the melting peak begin to broaden as the degree of crystallinity increased with increasing amount, along with wide distribution of crystals. For the epoxy system loaded with 1 wt.% crystals, the peak temperature for melting was also found in the range of 205-210 °C.

The objective of this study was to see the effect of nano-clay on the crystallization of nylon-6 in epoxy matrix. Multiple melting peaks were not observed in DSC thermogram for the compositions with clay unlike the samples without clay. In case of crystallization of neat nylon-6 in epoxy, different melting peaks were observed due to formation of a broad distribution of type of crystals, but in presence of clay, crystals grew in a narrow distribution. It was possibly because in presence of clay, nylon-6 could use clay particles as nucleating agent instead of epoxy template, as nanoclay has larger surface area and higher surface energy, which makes them better nucleating agent.

For epoxy: nylon 6 ratio of 95:5, 2 melting peaks were observed at 194 and 208 °C, but in case of composite containing 0.0025 and 0.05 wt.% of clay, single and short melting peaks were observed at 209 °C and 206 °C respectively. At a ratio of 90: 10 the melting peak remained unchanged at 208 °C for clay weight% of 0.05 but at 0.1 wt.% of clay, it dropped to 205 °C. A similar trend was observed in all ratios where at little increase of clay, T_m increases but at further increase it begins to drop.

Melting point is a property which is directly related to the molecular weight of the polymer [121]. At low concentration of clay during polymerization reaction, larger chains were obtained as indicated by higher melting point for 0.5% clay modified nylon-6 but as the clay was increased, the resultant T_m began to fall down suggesting lower molecular weight. Hence, initially crystallinity of sample increases at lower clay loading but at higher amount, it begins to fall. The values for peak T_m and T_c (from Figure 57 and 58)are shown in table 19.

Table 19 – Melting and crystallization peak values for epoxy resin filled with clay modified nylon-6.

Composition	**T_m (^OC)**	**T_c(^OC)**	**ΔH (J/g) (app.)**	**Θ - Degree of Crystallinity**
EPNYCL0.5-5	209	163	12.62	6.009524
EPNYCL0.5-10	208	162.1	18.91	9.004762
EPNYCL0.5-15	211	164.9	20.32	9.67619
EPNYCL0.5-20	210	168.5	24.89	11.85238
EPNYCL0.5-30	209	169	27.91	13.29048
EPNYCL1-5	206	170	10.43	4.966667
EPNYCL1-10	205	170	11.91	5.671429
EPNYCL1-15	205	164.5	16.08	7.657143
EPNYCL1-20	208	164	21.75	10.35714
EPNYCL1-30	205	157.9	26.46	12.6

3.3.3 Effect of clay on morphology and thermo-mechanical properties of clay/nylon-6-epoxy films

The effect of clay on the morphology of nanocomposite is shown in Figure 59, for epoxy: nylon-6 ratio of 90:10. For the system containing lowest concentration of nano clay, a high degree of crystallinity was observed in morphology. A high degree of crystallinity was observed with crystals impinged into each other. The amorphous matrix was filled with several crystalline zones, but as the clay was increased, the morphology became more amorphous in nature. For all the epoxy:nylon 6 ratios, at the lowest level of clay concentration (for 0.5% clay modified nylon-6), a high degree of crystallinity was observed with crystals grown radially in all directions protruding outwards. As the clay was increased (by blending 1% clay modified nylon-6), the crystalline morphology was still maintained. When nylon-6 synthesized in presence of clay with loading of 5 wt.% was introduced in epoxy resin, the morphology changed significantly. Since the nylon chains were not formed during polymerization step (indicated by lower molecular weight) at higher concentration of clay where clay begins to act as hindrance to chain growth, the matrix was mainly dominated by clay instead of crystals. A large number of cracks were found in brittle epoxy matrix formed near agglomerated clay stacks. Owing to brittle nature, cracks were formed which were deflected by clay particles but due to absence of large nylon-6 chains (lower molecular weight at higher clay concentration), nylon crystals were not able to grow in the cracks and crevices of epoxy. On further increasing clay, a compact morphology with large number of clay particles distributed in epoxy matrix along with small crystals was observed. The cracks were significantly reduced from the previous composition.

This kind of morphological evaluation had a direct impact on thermo-mechanical properties of clay/nylon-6-epoxy nanocomposite system. The dynamic mechanical properties for the 3 component system were analyzed for the effect of clay at epoxy: nylon 6 ratio of 90:10. The storage modulus and tan (δ) as a function of temperature are shown in Figure 60. The present discussion is mainly focused on variation is storage modulus in glassy and rubbery region and glass transition temperature with varying concentration of clay at fixed epoxy: nylon 6 ratio.

Figure 61a represents the storage modulus in glassy region as a function of clay composition at constant epoxy: nylon 6 ratio of 90:10 at -10°C, where a linear increase was observed with increase in clay concentration. This phenomenon can be attributed to the presence of nanoclay in the system as reinforcing agent. Figure 61b represents the storage modulus in the beginning of transition region at 10°C. Figure 62 represents the rubbery region as a function of clay composition at 45°C and Figure 63 represents the variation in T_g with increase in clay concentration.

In the glassy region, a material has the highest value of storage modulus which is largely independent of temperature, frequency, molecular weight between cross-links and crosslink functionality. This region occurs due to immobility of molecular chains within polymer network, due to close packing of molecular chains. The large scale molecular motion does not take place in this region. On the other hand in rubbery region, material exhibit lowest storage modulus. In this state molecular chains are free from random coiling and hindrances and can slip past each other, but they are restricted only by crosslinks in the network. In the glass transition zone, storage modulus drops significantly from glassy to rubbery region due to large scale molecular motion of polymeric chains. The T_g is inferred by the peak in tan(δ) curve [86, 87, 122].

As seen in morphology (Figure 59), when nylon-6 was modified with 0.5% of clay, it lead to formation of larger crystals while at 1%, the degree of crystallinity increased with reduction in size. For clay/nylon-6-epoxy composite containing 5 wt.% and 10 wt.% of clay with respect to nylon-6, degree of crystallinity reduced significantly due to hindrance possessed by clay stacks during polymerization which lead to shorter chains. It is inferred that such clay modified nylon-6 system when incorporated in epoxy; the properties of matrix will be controlled mainly by crystals at lower level of clay while at higher concentration, the properties of matrix will be mainly controlled by nano-clay. When clay modified nylon 6 was maintained at weight ratio of 90:10, the storage modulus initially increased at clay concentration upto 0.1% (crystal controlled) but then began to decrease (clay controlled) in rubbery region suggesting increased crosslink density of epoxy at low clay loading.

Clay has been reported to show a plasticization effect on epoxy matrix indicated by decrease in T_g [123]. In the present case, T_g first decreased at lowest loading of clay (combined platicization of effect of clay and large crystals), but as the clay % is increased (decreasing crystallinity, plasticization mainly due to clay instead of crsytals). The T_g as a function of clay weight% is shown in Figure 57.

Calculation of amount of nylon-6 reacted in the clay/nylon-6-epoxy composites using storage modulus in rubbery region (E'$_R$)

Storage modulus in rubbery region (E'$_R$ (Pa)) can be used to calculate moles of crosslinks in the given sample using the equation

$$E'_R = n_v RT \qquad [4]$$

Where n is moles of crosslinks per unit volume, R is universal gas constant (8.314 $m^3PaK^{-1}mol^{-1}$), and T is temperature in Kelvin. Moles of crosslinks per unit volume is shown in table 20

Table 20 – Moles of crosslinks per unit volume (n_v) calculated form Storage Modulus (E'_R) for each composition.

Composition	Storage Modulus (E'_R)	Moles of crosslinks per unit volume (n_v) (n/m^3)
EPNY10 (0 wt.% clay)	48000	15.47
EPNYCL0.5-10 (0.05 wt.% clay)	61000	19.66
EPNYCL1-10 (0.1 wt.% clay)	70000	22.56
EPNYCL5-10 (0.5 wt.% clay)	46000	14.83
EPNYCL10-10 (1 wt.% clay)	30000	9.67

The molecular weight of nylon-6 as a function of clay weight% (calculated by dilute solution viscometry) is discussed in section 3.3.4. Moreover, weight of nylon-6 added to the system was known in grams. Hence total moles of nylon-6 added to the clay/nylon-6-epoxy blend can be obtained by using equation:

$$no.\,of\ moles = \frac{wt.\,in\ grams\ of\ nylon-6}{molecular\ weight\ of\ nylon-6} \qquad [5]$$

The no. of moles of nylon-6 in the sample used for dynamic mechanical analysis can be obtained by equation

$$no.\,of\ moles\ of\ nylon\ 6\ in\ film = \frac{total\ no.\,of\ moles\ of\ nylon\ 6}{total\ volume\ of\ blend} \times volume\ of\ film \qquad [6]$$

Total no. of moles of nylon-6 in film used for dynamic mechanical analysis is shown in table 21.

Table 21- Total no. of moles of nylon-6 in film used for dynamic mechanical analysis

composition	weight of nylon-6 (grams)	Total moles of nylon-6 ($n_{nylon-6}$)	Total volume of blend (mm^3)	Volume of films (mm^3)	Moles of nylon-6 in film
EPNY10	1.33	0.000128343	30100	171.5	7.31256E-07
EPNYCL0.5-10 (0.05 wt.% clay)	1.37	0.00012853	30100	132.28	5.64847E-07
EPNYCL1-10 (0.1 wt.% clay)	1.36	0.000328479	30100	117.6	1.28336E-06
EPNYCL5-10 (0.5 wt.% clay)	1.31	0.000475938	30100	176.62	2.7927E-06
EPNYCL10-10 (1 wt.% clay)	1.23	0.001086736	30100	253.748	9.16136E-06

The moles in sample (film for DMA) per unit volume (m^3) can be calculated using equation:

$$moles\ per\ unit\ volume = \frac{moles\ in\ film}{total\ volume\ of\ film} \qquad [7]$$

The repeat unit of nylon-6 ($C_6H_{11}NO$) has molecular weight of 113, hence total number of repeat units in nylon-6 in clay/nylon-6 nanocomposites can be obtained.

The average moles of nylon-6 reacted in the composites per unit volume (N_{1v}) can be calculated by equation:

$$N_{1V} = \frac{moles\ of\ crosslinks\ of\ composites - moles\ of\ crosslinks\ in\ neat\ epoxy}{number\ of\ repeat\ units} \qquad [8]$$

The average moles of nylon-6 reacted in the epoxy/nylon-6 composite is shown in table 22.

Table 22 - The average moles of nylon-6 reacted in the epoxy/nylon-6 composite.

Composition	Total volume of film (m^3)	Moles of nyon-6 per unit volume (n/m^3)	Number of repeating units	Moles of nylon-6 reacted /m^3 (N_{1V})
Thermally cured neat epoxy	2.856E-07	NA	NA	NA
EPNY10 (0 wt.% clay)	1.715E-07	4.263881194	92	0.066781863
EPNYCL0.5-10 (0.05 wt.% clay)	1.3228E-07	4.270083691	94	0.109349618
EPNYCL1-10 (0.1 wt.% clay)	1.176E-07	10.91293708	37	0.360693298
EPNYCL5-10 (0.5 wt.% clay)	1.7662E-07	15.81188998	24	0.224963926
EPNYCL10-10 (1 wt.% clay)	2.53748E-07	36.1041741	10	0.032181314

The total weight of nylon-6 reacted per unit volume (g/m^3) can be calculated using equation:

$$reacted\ weight\ of\ nylon\ per\ unit\ volume\ \left(\frac{g}{m3}\right) = moles\ of\ nylon\ 6\ reacted\ per\ unit\ volume\ \times molecular\ weight \qquad [9]$$

Once, the weight of nylon-6 reacted per unit volume is knows, the total weight of nylon-6 reacted while curing can be obtained by using equation:

$$\text{total weight of nylon 6 reacted in composite} = \text{weight of nylon 6 reacted per unit volume} \times \text{total volume of blend} \quad [10]$$

Table 23 - The weight of nylon-6 reacted in the clay/nylon-6-epoxy composite.

Composition	Weight of nylon-6 reacted in composite sample film (g/m^3)	Total reaction volume (m^3)	Total weight of nylon-6 reacted in composite (g)
EPNY10	798.7694336	0.0000275	0.021966
EPNYCL0.5-10 (0.05 wt.% clay)	689.846329	0.0000301	0.020764
EPNYCL1-10 (0.1 wt.% clay)	399.3847168	0.000033	0.01318
EPNYCL5-10 (0.5 wt.% clay)	580.9232244	0.00003645	0.021175
EPNYCL10-10 (1 wt.% clay)	526.4616721	0.0000395	0.020795

Once, the total weight of nylon-6 reacted while curing is obtained, the total weight of unreacted nylon-6 in the composite can be calculated using equation:

$$\text{weight of unreacted nylon6 } (g) = \text{total weight of nylon 6 in blend } (g) - \text{weight of reacted nylon 6}(g) \quad [11]$$

Table 24 shows the fraction of reacted and unreacted nylon-6 in the composite

Table 24 – Total weight in grams of nylon-6 added to the clay/nylon-6-epoxy composite system along with fraction of reacted and unreacted nylon-6.

Composition	Weight of nylon-6 added to system (g)	Weight of nylon-6 reacted in composite (g)	Weight of nylon-6 unreacted in composite (g)	Weight fraction of nylon-6 reacted in composite (%)	Weight fraction of nylon-6 unreacted in composite (%)
EPNY10 (0 wt.% clay)	1.33	0.020830758	1.309169242	1.566222407	98.43377759
EPNYCL0.5-10 (0.05 wt.% clay)	1.37	0.035083382	1.334916618	2.560830797	97.4391692
EPNYCL1-10 (0.1 wt.% clay)	1.36	0.044950583	1.315049417	3.305189933	96.69481007
EPNYCL5-10 (0.5 wt.% clay)	1.31	0.018638047	1.291361953	1.422751652	98.57724835
EPNYCL10-10 (1 wt.% clay)	1.23	0.001096356	1.228903644	0.089134609	99.91086539

These results suggests that nanoclay facilitates the reaction of nylon-6 with epoxy at low concentration (0.05 wt.% and 0.1 wt.% with respect to solid content of epoxy), while at higher concentration of clay (0.5 wt.% and 1 wt.% with respect to solid content of epoxy), the reaction of nyon-6 is retarded, possibly due to hindrance pose of by high concentration of clay. The weight of nylon-6 reacted as a function of clay weight% is shown in Figure 64.

3.3.4 Effect of clay on morphology and anti-corrosion properties of clay/nylon-6-epoxy coatings

3.3.5.1 Direct Current Polarization

Potentiodynamic curves for nylon-6/epoxy coatings on Al 2024-T3 alloy substrate with and without clay at a weight ratio of 10/90, after 1 day and 2 months of exposure is shown in Figure 65. Different compositions including thermally cured neat epoxy, nylon-6/epoxy and nylon-6/epoxy containing clay with varied concentration were compared for corrosion performance. The presence of clay in nylon-6/epoxy coatings resulted in a significant reduction in the corrosion current. The corrosion current density decreased from 10^{-6} A/cm^{-2} to 10^{-10} A/cm^{-2} as the clay concentration was increased. The values of corrosion current and corrosion potential for all the systems are listed in table 7.

Figure 65a shows the DCP curves after 1 day of exposure. The thermally cured neat epoxy and nylon-6/epoxy (10/90) showed corrosion current (I_{corr}) almost in the same range of around 10^{-6} - 10^{-7} A/cm^{-2} but with increase in clay I_{corr} decreased by two orders of magnitude and showed a minimum of 10^{-9} A/cm^{-2}. These coatings were kept exposed for two months and potentiodynamic curves obtained after two months are shown in Figure 65(b). The least corrosion current was shown by composite coating containing 1 weight% clay at around 10^{-10} A/cm^{-2}. Moreover, an increase in corrosion potential from -1.2 V to -0.9 V was also observed. Beemat and Iroh [118] have reported that the decrease in corrosion current density and increase in corrosion potential simultaneously, indicates that protection from corrosion by coatings is provided by both diffusion-controlled and activation-controlled mechanism. After 2 months of exposure, Al alloy substrate coated with neat epoxy and nylon-6/epoxy containing 0.05 wt. %

and 0.5 wt. % clay began to show bending in anodic arms suggesting passivation behavior, which is shown by aluminum alloy due to formation of oxide layer.

Table 25 – Parameters obtained from direct current polarization for nylon-6/epoxy (10/90) on Al 2024-T3 alloy substrate

Compositions	**I_{corr} (Acm^{-2}) – after 1 day**	**E_{corr} (V) – after 1 day**	**Corrosion Rate (mpy) after 1 day**	**I_{corr} (Acm^{-2}) – after 2 months**	**E_{corr} (V) – after 2 months**	**Corrosion Rate (mpy) after 2 months**	**Morphology**
Neat Epoxy	3.7×10^{-7}	-0.66	576.8×10^{-3}	2.21×10^{-6}	-0.90	9.081	Large and sharp cracks
Nylon-6/Epoxy	4.0×10^{-6}	-0.79	422.4×10^{-3}	9.05×10^{-7}	-0.54	2.184	Cracks uniformly filled with crystals
0.05% clay	4.9×10^{-6}	-0.81	363.8×10^{-3}	4.73×10^{-8}	-0.86	998.4×10^{-3}	Large network of crystals with voids and cracks
0.1% clay	2.8×10^{-9}	-1.26	452.1×10^{-6}	9.49×10^{-9}	-0.93	156.3×10^{-3}	Relatively compact morphology with less cracks and small crystals
0.5% clay	6.4×10^{-9}	-0.86	$515.8\times$	$7.07\times$	-0.80	$941.7\times$	Large number of

			10^{-6}	10^{-8}		10^{-3}	clay particles with small crystals and lesser cracks
1% clay	1.6×10^{-9}	-1.20	242.8×10^{-6}	2.78×10^{-10}	-0.96	41.59×10^{-6}	Clay particles with small crystals, compact and crack-free morphology

3.3.5.2 Bode Plots

Figures 66 shows the Bode plots for thermally heated neat epoxy, nylon-6/epoxy with and without clay, coated on aluminum alloy substrate, cured with step-wise heating by 70°C for 3 hours followed by 100°C for 2 hours, 120°C for 2 hours and 150°C for 2 hours and exposed to 3.5% salt solution. Figure 66(a) shows the Bode plots for nylon-6/epoxy coatings at a weight ratio of 10/90 containing different concentration of clay. The impedance value for neat epoxy at 0.01 Hz was around 4×10^{4} Ω after 1 day of exposure, while nylon-6/epoxy coatings showed an impedance value increased by 2 orders of magnitude around 1×10^{6} Ω. On increasing clay concentration, impedance begin to increase, and at highest clay concentration of 1 weight % in the system, highest value of impedance was observed ($1\times10^{10}\Omega$). The Bode plots of coatings after exposure for two months are shown in Figure 66(b). The impedance for nylon-6/epoxy coating without clay was steady at 1×10^{6} Ω. Moreover, impedance value was substantially retained at 1×10^{9} Ω by coating containing 1 weight% clay. The impedance value as a function of exposure time is shown in Figure 60. It was observed that impedance value is retained by clay/nylon-6-epoxy coatings and drops slowly with exposure time, but at clay concentration of 1 weight %, the impedance value was highest at all times, while for coating without clay, impedance begin to decrease after 15 days of exposure.

A direct co-relation was found between the morphology and corresponding anti-corrosion performance. The coating containing 0.05 weight% clay, showed the minimum impedance value of around 1×10^6 ohms among clay coatings. The morphology of this coating is shown in Figure 67(a) which shows a large number of crystals on the surface. From molecular weight analysis, it is evident that at the smallest clay weight%, higher molecular weight nylon-6 was obtained, which resulted in larger size of crystals. These large crystals used nano clay particles as nucleating agents and formed a network of crystals with small pores. This porosity can allow slow passage of electrolytes through the coating which leads to degradation of coating over time thereby reducing effectiveness against corrosion. On the other hand, coating containing 1 weight% of nylon-6 showed highest impedance value. The morphology of this coating is shown in Figure 67(b), where non-porous and crack-free surface was observed. It was discussed that at higher concentration of clay, molecular weight of nylon-6 decreased. Hence, small crystals were formed which were uniformly distributed along with clay in the epoxy matrix which resulted in highly compact morphology. This highly improved the barrier properties of coating thereby showing best anti-corrosion performance with impedance value of $1\times10^{9.5}$ ohms.

3.4 Comparison of performance of nylon-6/epoxy and clay/nylon-6 epoxy with standard cured epoxy systems

The nylon-6/epoxy coatings and clay/nylon-6 epoxy coatings were obtained without use of any curing agent. This system was then compared with epoxy based coating cured with standard amine based curing agent, with and without clay. The 3 systems that were chosen for comparison are (1) Epikote 828 (DGEBA based epoxy resin) cured with aromatic amine 4,4-metylene dianiline cured at 100^O C for 8 hours and post-cured at 120^O C for 4 hours [62], (2) air curable epoxy ester hybrid blend with bisialne and polyurea containing clay [124], and (3) commonly used epoxy EPON 828 cured with amine based curing agent EPIKURE 8290-Y-60 [66]. The Bode plot for nylon-6/epoxy system showed an impedance value of $10^{8.2}$ ohms after 8 weeks of exposure to 3.5 weight% salt solution while impedance for epoxy amine system decreased to $10^{6.3}$ ohms after 7 days of exposure [62]. Then nylon-6/epoxy system containing clay was then compared with other standard epoxy systems containing clay. The nylon-6/epoxy system containing 1wt.% clay showed an impedance value of 10^{10} ohms before exposure and $10^{9.5}$oms after 8 weeks of exposure to 3.5 wt.% salt solution, in contrast with 10^7 ohms for epoxy ester/polysiloxane/polyurea hybrid coating containing 1wt.% of clay after 4 weeks and $10^{7.5}$ ohms after 14 weeks [124], and 10^{10} ohms for tradition epoxy/amine system before exposure [66]. The comparison has been summarized in table 9. The comparison indicates that the novel epoxy based system cured in presence of nyon-6 shows a better performance than traditional systems. Moreover, Clay further enhanced the anti-corrosion properties of coating and can be fruitfully utilized in practical applications for anti-corrosion applications.

Table 26 – *Comparison of |Z| (impedance) value at 0.01 Hz for nylon-6/epoxy and clay/nylon-6-epoxy composite system with tradition cured epoxy systems.*

	|Z|(ohms)
Epoxy/nylon system	**$10^{8.2}$ (8 weeks)**
Epoxy/Amine system	$10^{6.5}$ (7 day)
Epoxy/nylon-clay system	**10^{10} (1 day) $10^{9.5}$ (8 weeks)**
Epoxy/Amine-clay system	10^{10} (1 day), No info on time based study
EE/PU/Clay system	10^6 (1 day) 10^7(4 weeks) $10^{7.5}$ (14 weeks)

Summary

1. A novel and facile technique to synthesize nylon-6 and its composite with nano-clay has been discovered in solution via air terminated anionic polymerization.
2. The process of plasticizing epoxy resin by thermoplastics has been simplified by blending with solution polymerized nylon-6 and its nanocomposite leading to formation of 3 component system.
3. The synthesized nylon-6 assists in the curing of epoxy as indicated by FTIR and increase in the rubbery state storage modulus in dynamic mechanical analysis.
4. Nylon-6 effectively plasticizes epoxy indicated by reduction in T_g, studied by DSC and DMA. A multiphase morphology for epoxy/nylone-6 system was observed which was found changing considerably with changing composition.
5. The effect of organoclay on the thermal behavior and extent of crystallinity of nylon-6 composite films was studied by differential scanning calorimetry. The organoclay at lower concentrations increase the crystallinity of the nanocomposites, while decreases at higher concentration.
6. The dispersion and structure of the organoclay nylon-6 composites were studied by x-ray diffraction. The in-situ polymerization of nylon-6 lead to increase in the d-spacing of clay galleries leading to an intercalated composite system. Nylon-6 crystallized in γ-form in presence of clay which preferred to be in α-form in absence of clay.
7. The effect of clay on the properties of epoxy/nylon-6 system was studied for dynamic mechanical, thermal and morphological properties by blending epoxy with clay modified nylon-6. The T_g was decreased at lower concentration of clay but increased at higher concentration. At lower concentration of clay, melting point of nylon-6 in epoxy was increased.
8. A highly crystalline morphology was observed at lower loading of clay (properties were controlled by crystals) but mainly amorphous morphology was observed at higher level of clay along with clay stacks (properties were controlled by clay).
9. The epoxy coating filled with clay modified nylon showed better performance for corrosion protection on Al alloy. Water absorption by coatings decreased significantly, which also lead to decrease in corrosion current.

List of Figures

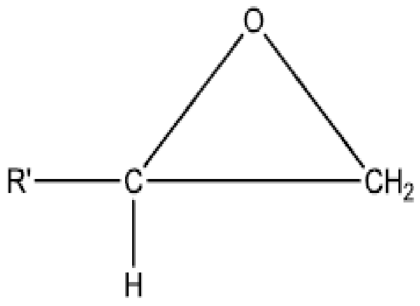

Figure 1 – Schematic representation of the structure of epoxide ring

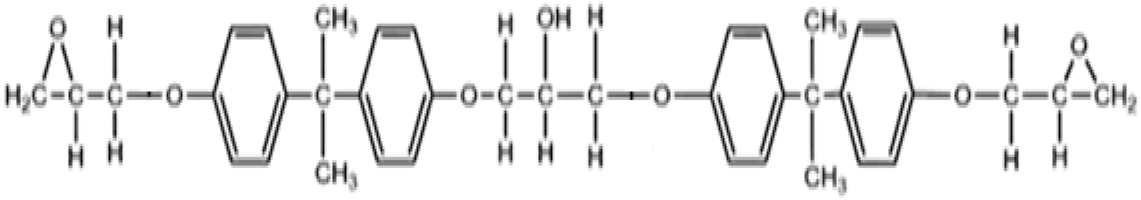

Figure 2(a) - Schematic representation of the structure of diglycidyl ether of bisphenol A

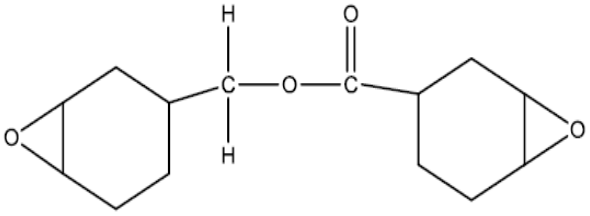

Figure 2(b) - Schematic representation of the structure of Cycloaliphatic epoxy

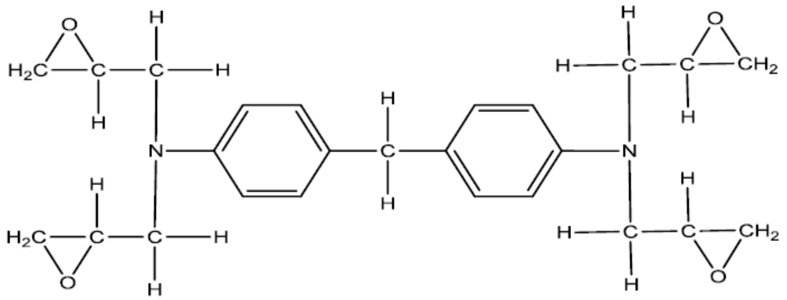

Figure 2(c) – Schematic of the structure of Tetra glycidyl methylene dianiline (TGMDA)

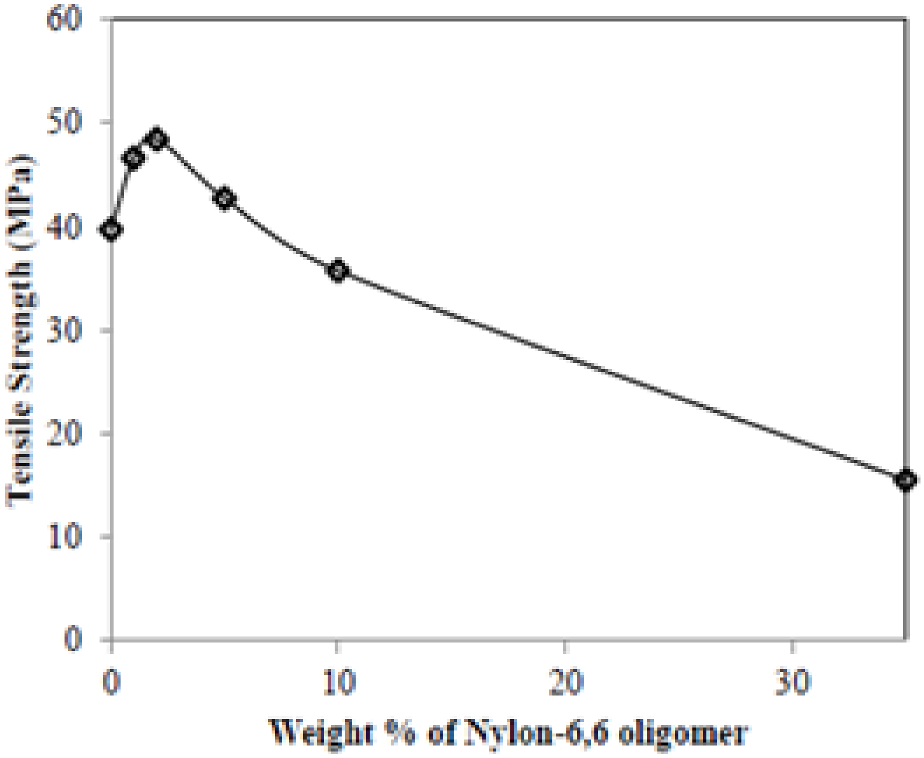

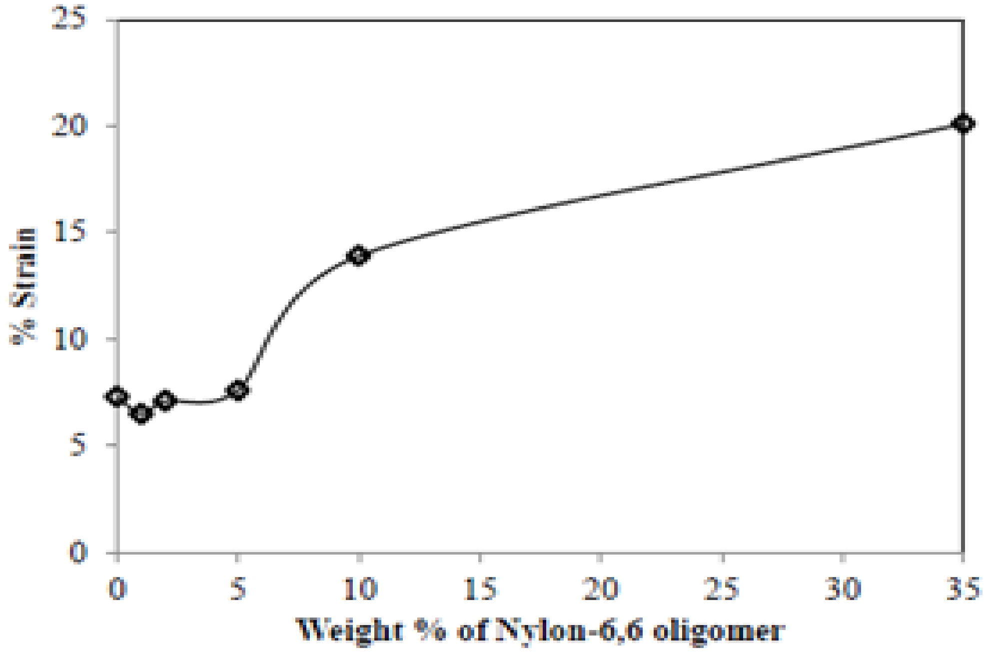

Figure 3 – Effect of Nylon-6,6 oligomer on tensile strength and strain of epoxy matrix [44]

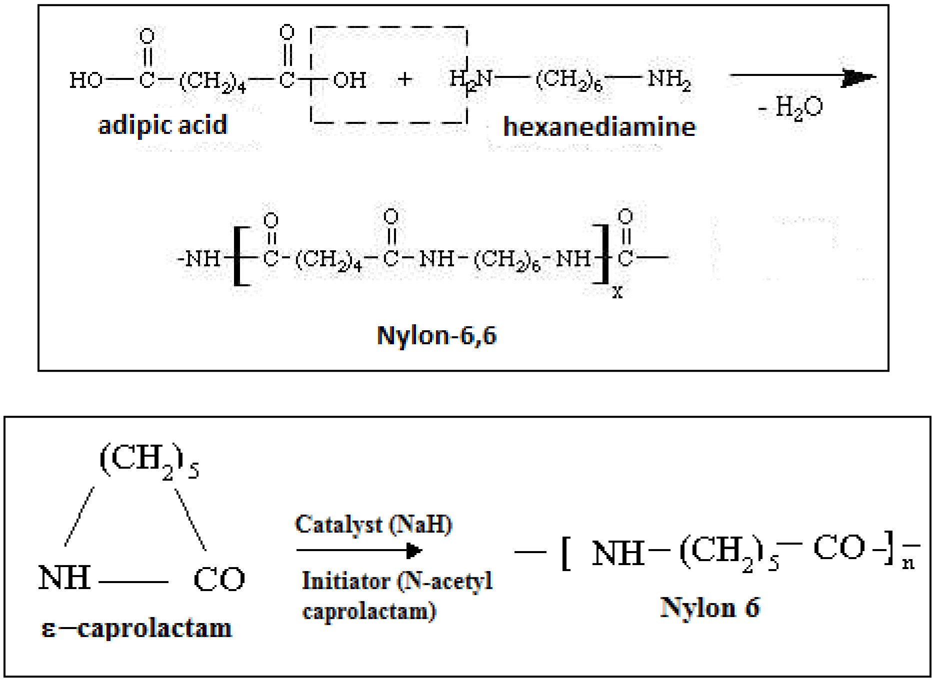

Figure 4 - Schematic representation of the synthesis and repeat unit of Nylon-6, 6 and nylon-6

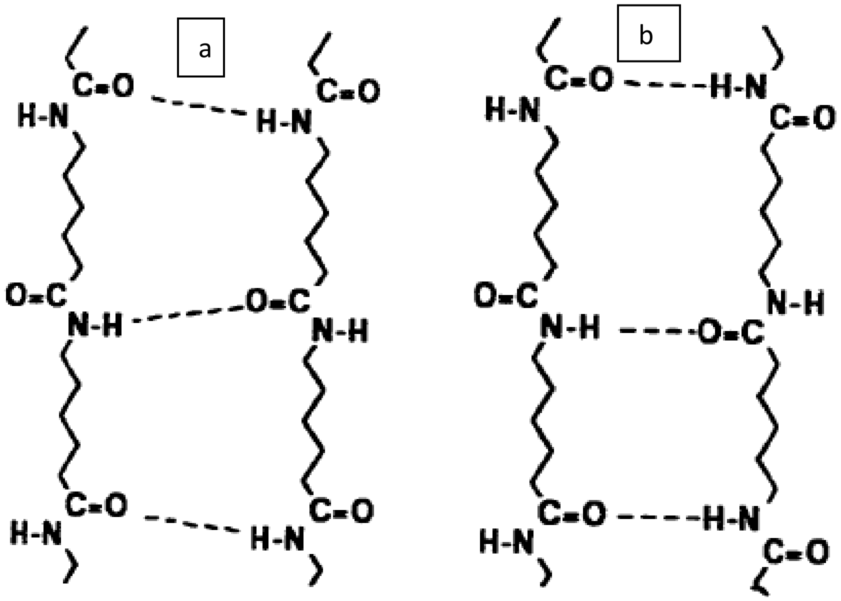

Figure 5- Nylon-6 (a) γ form and (b) α form.

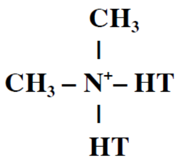

$$\begin{array}{c} CH_3 \\ | \\ CH_3-N^+-HT \\ | \\ HT \end{array}$$

Figure 6. Organic modifier for 15A Clay

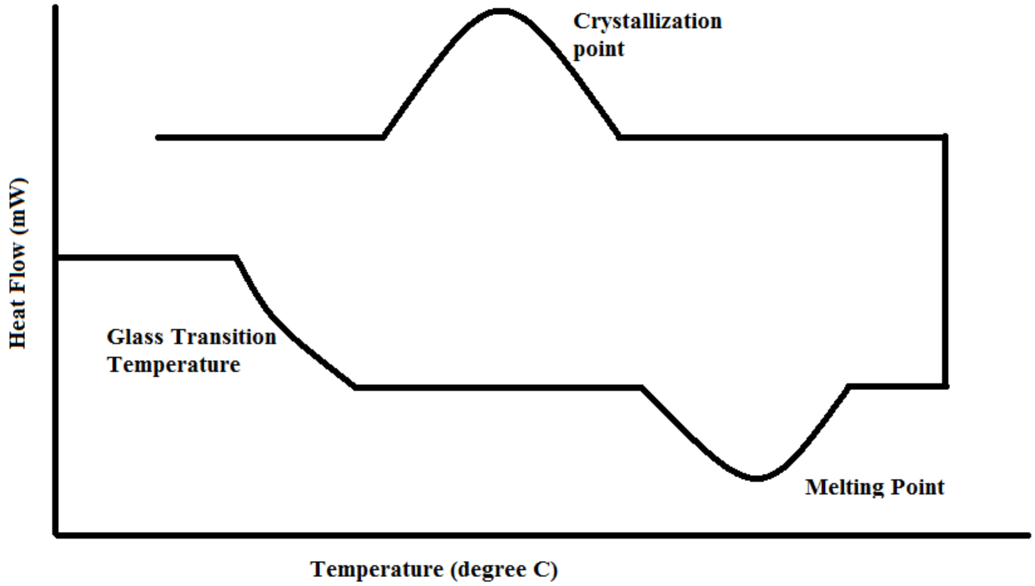

Figure 7 – Representation of a DSC Run [125]

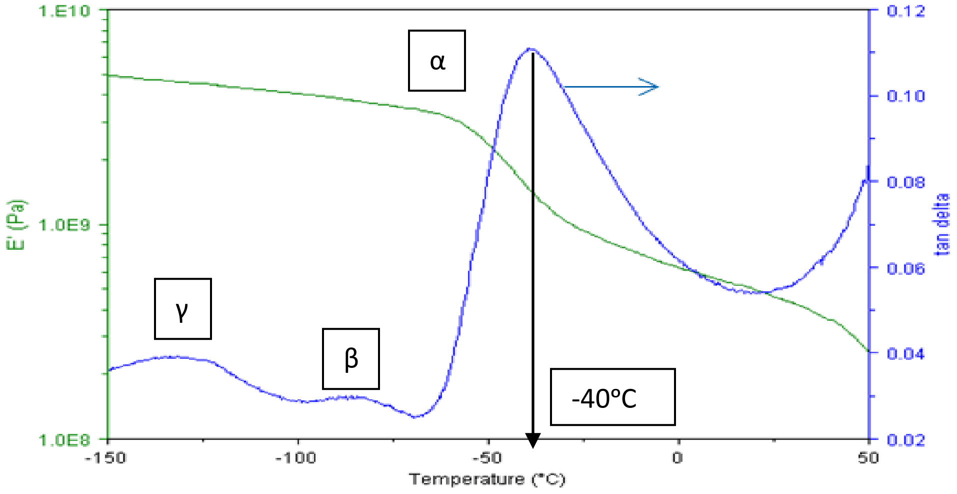

Figure 8 - Representation of plots of Storage Modulus and Tan delta as a function of temperature for polycaprolactone measured at 1Hz. [126]

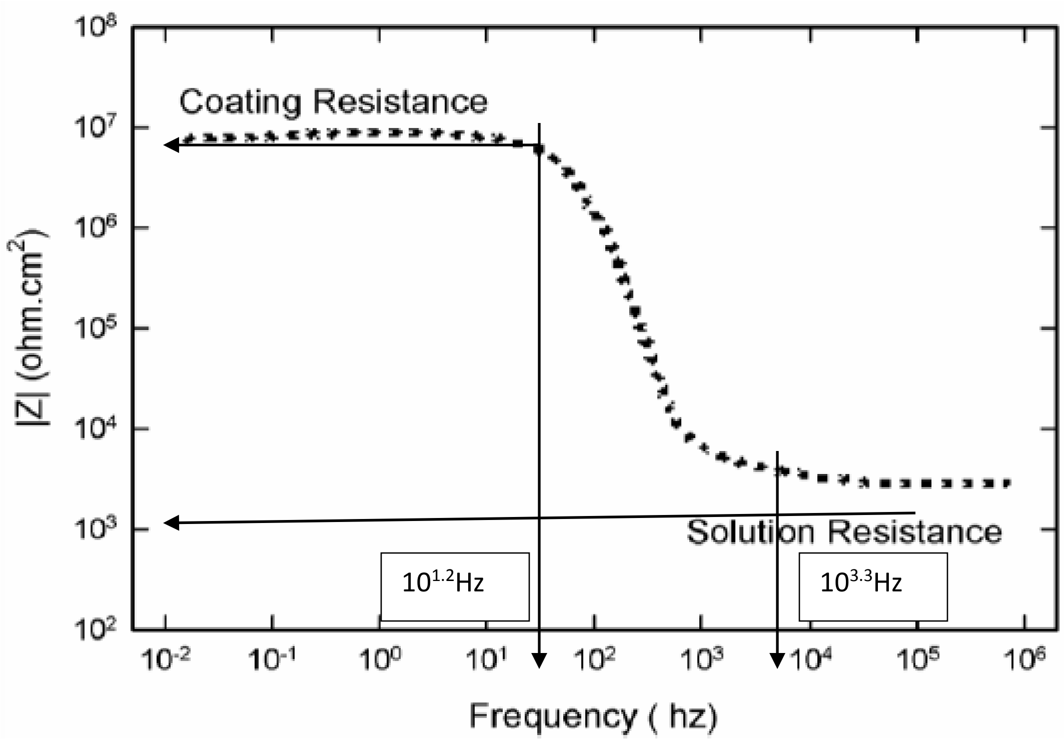

Figure 9 - Representation of a typical Bode plot for electrochemical impedance spectroscopy.

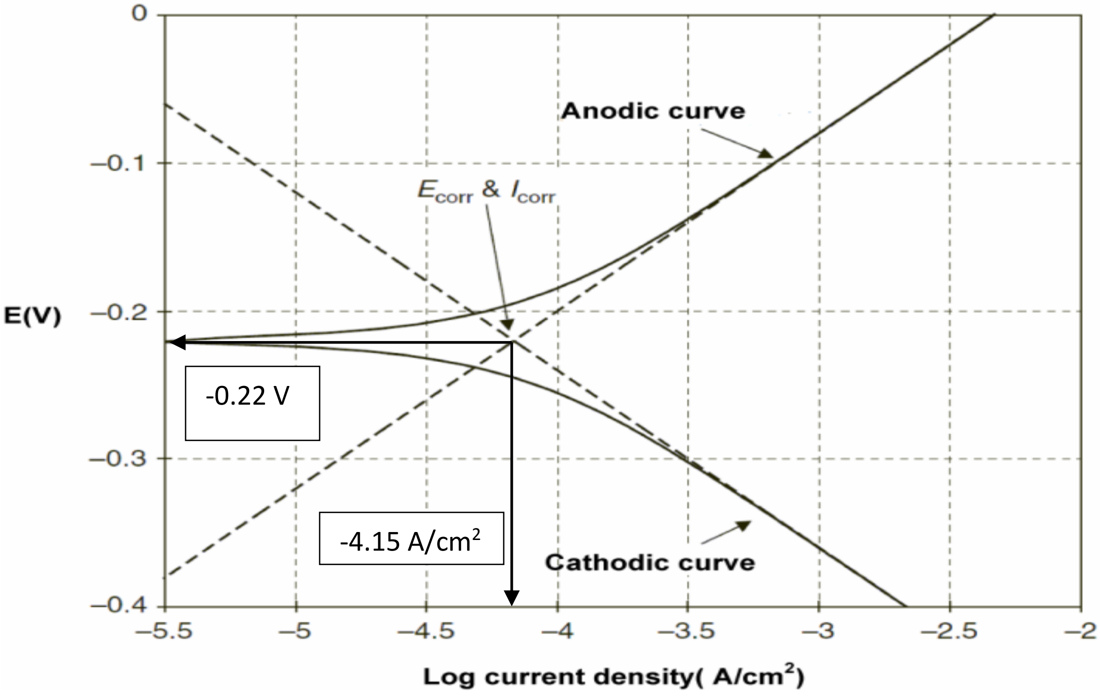

Figure 10 – Representation of a typical TAEFL Plots

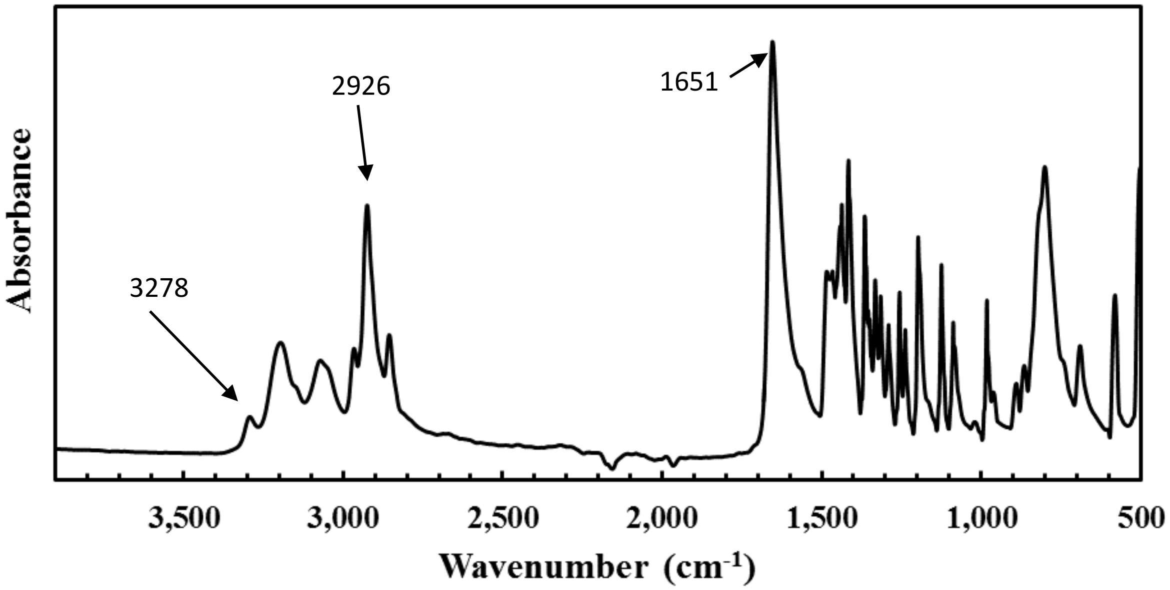

Figure 11 – FTIR spectrum of monomer (ε-caprolactam) used to synthesize nylon-6

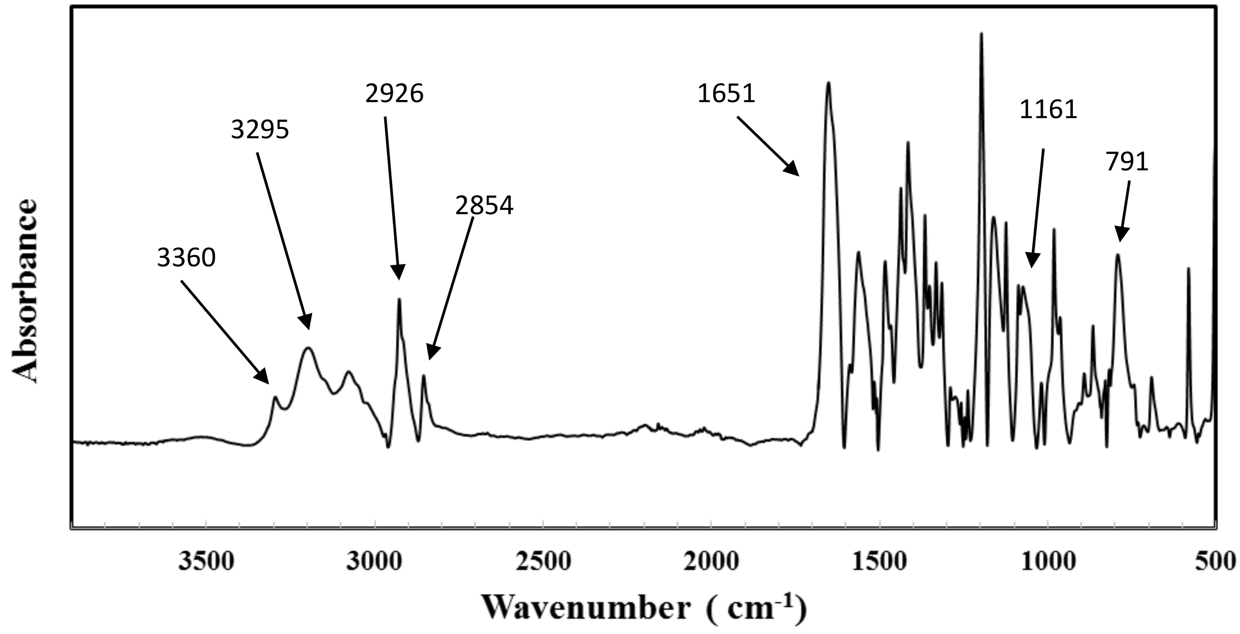

Figure 12 - FTIR Spectrum of neat nylon-6 precipitated from suspension in NMP by heating upto 200°C for 12 hours

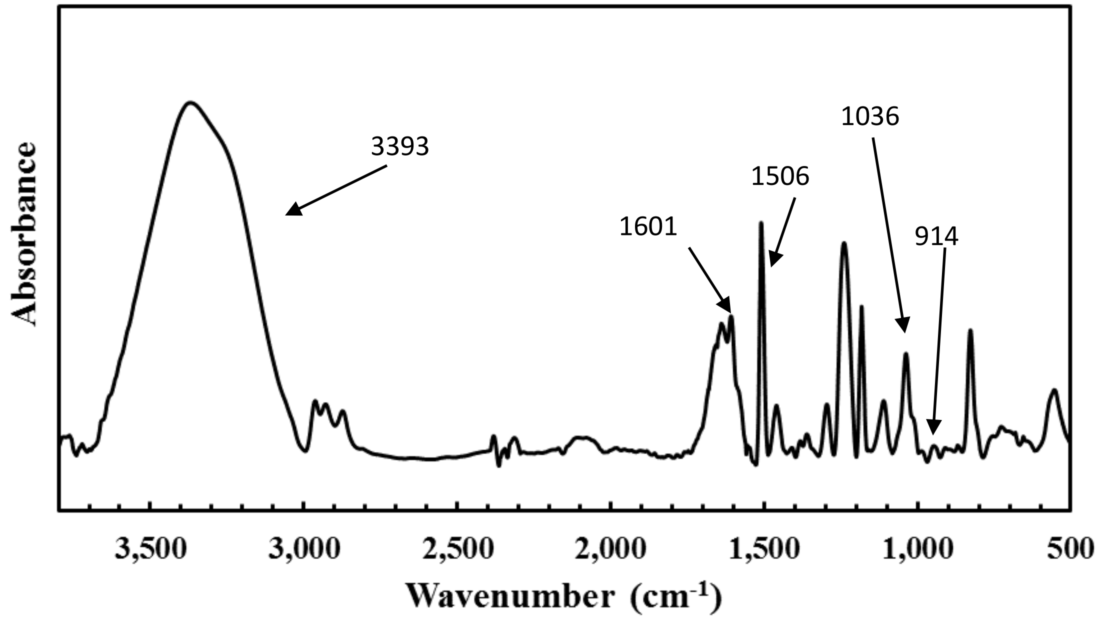

Figure 13 - FTIR Spectrum of uncured liquid epoxy emulsion (EPI-REZ 5522-WY-55)

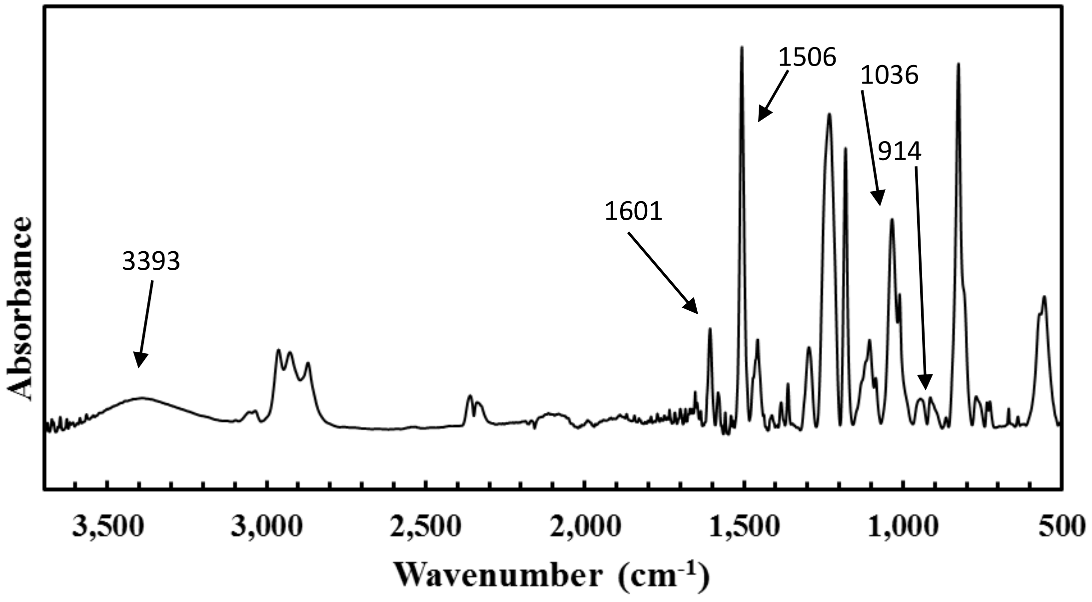

Figure 14 – FTIR Spectrum of thermally treated neat epoxy heated stepwise in oven for 9 hours (70° C -3h, 100°C -2h, 120°C -2h, 150°C – 2h)

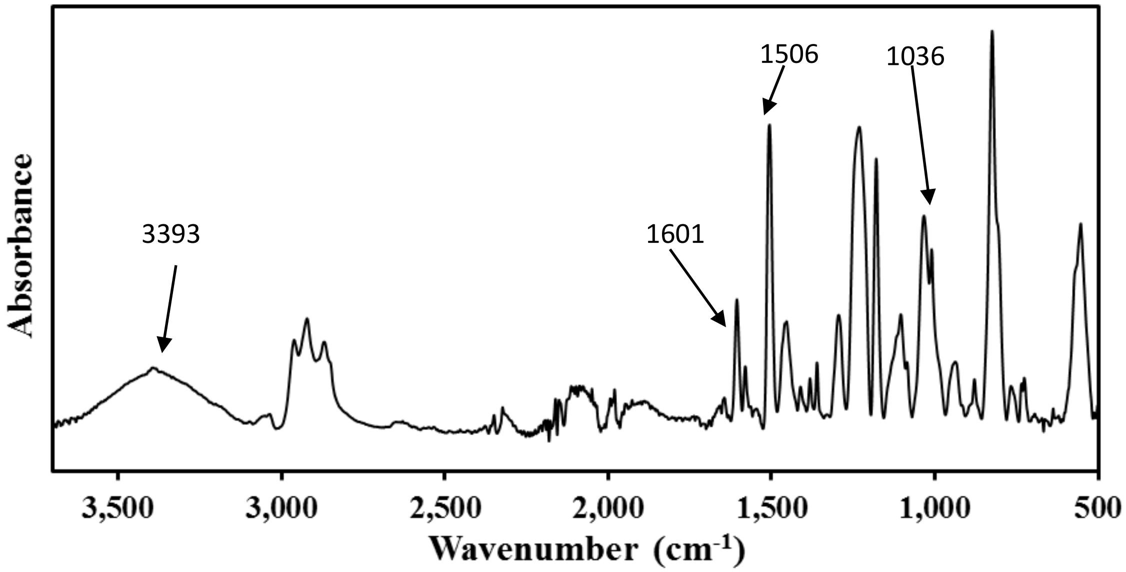

Figure 15 – FTIR spectrum of epoxy/nylon-6 (20 wt. %) heated stepwise in oven for 9 hours (70° C -3h, 100°C -2h, 120°C -2h, 150°C – 2h)

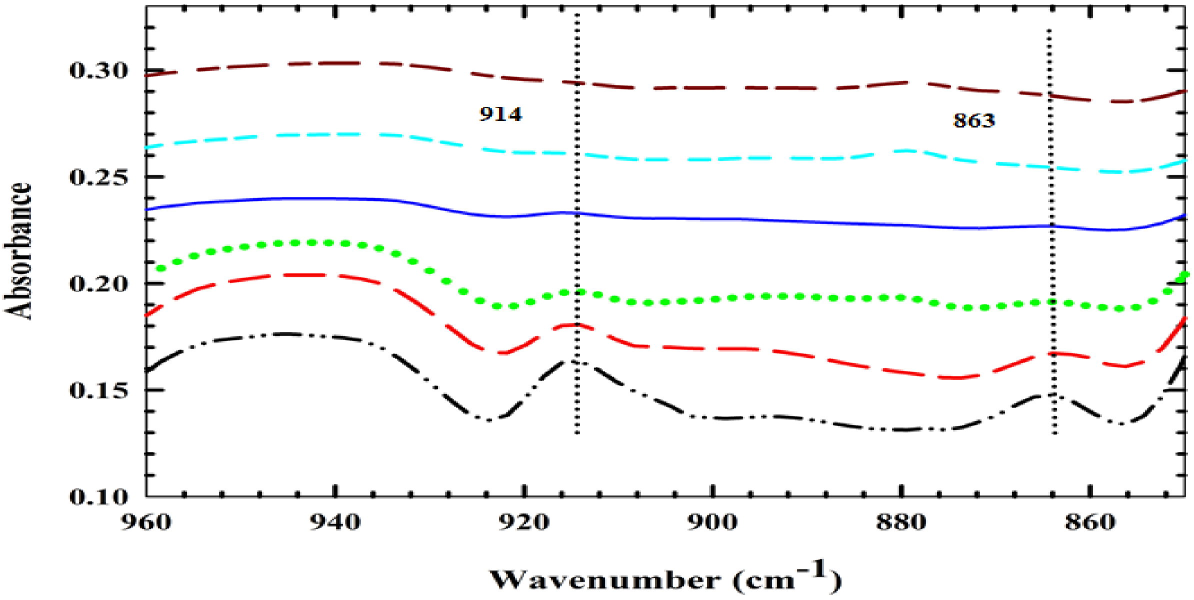

Figure 16 – FTIR spectra for thermally treated neat epoxy and nylon-6 filled epoxy (bottom – thermally treated epoxy, 5 wt. % PA-6, 10 wt. % PA-6, 15 wt. % PA-6, 20 wt. % PA-6, top – 30 wt. % PA-6) heated in oven for 9 hours (70° C -3h, 100°C -2h, 120°C -2h, 150°C – 2h)

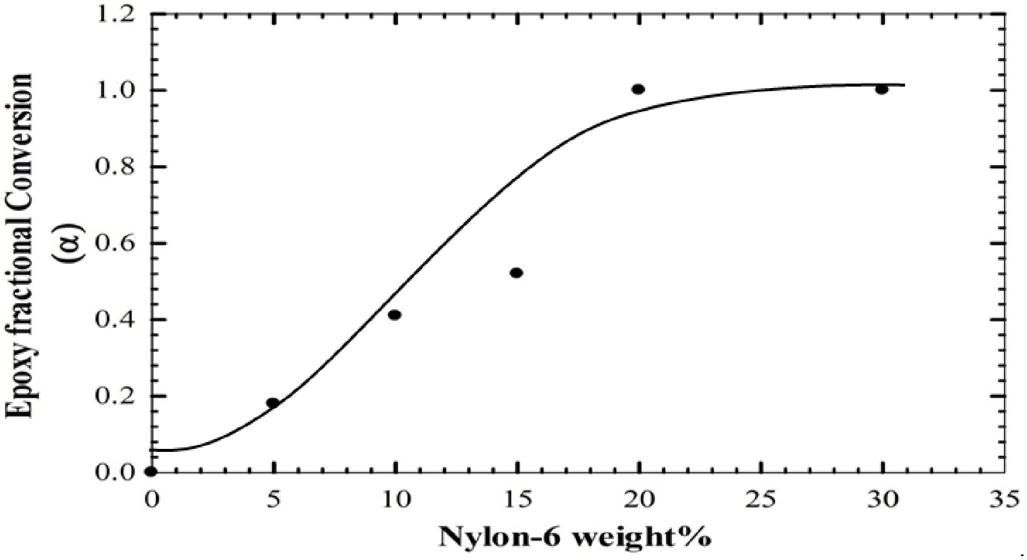

Figure 17 – Epoxy fractional Conversion as a function of nylon-6 wt. % all samples cured with stepwise heating for 9 hours upto 150°C

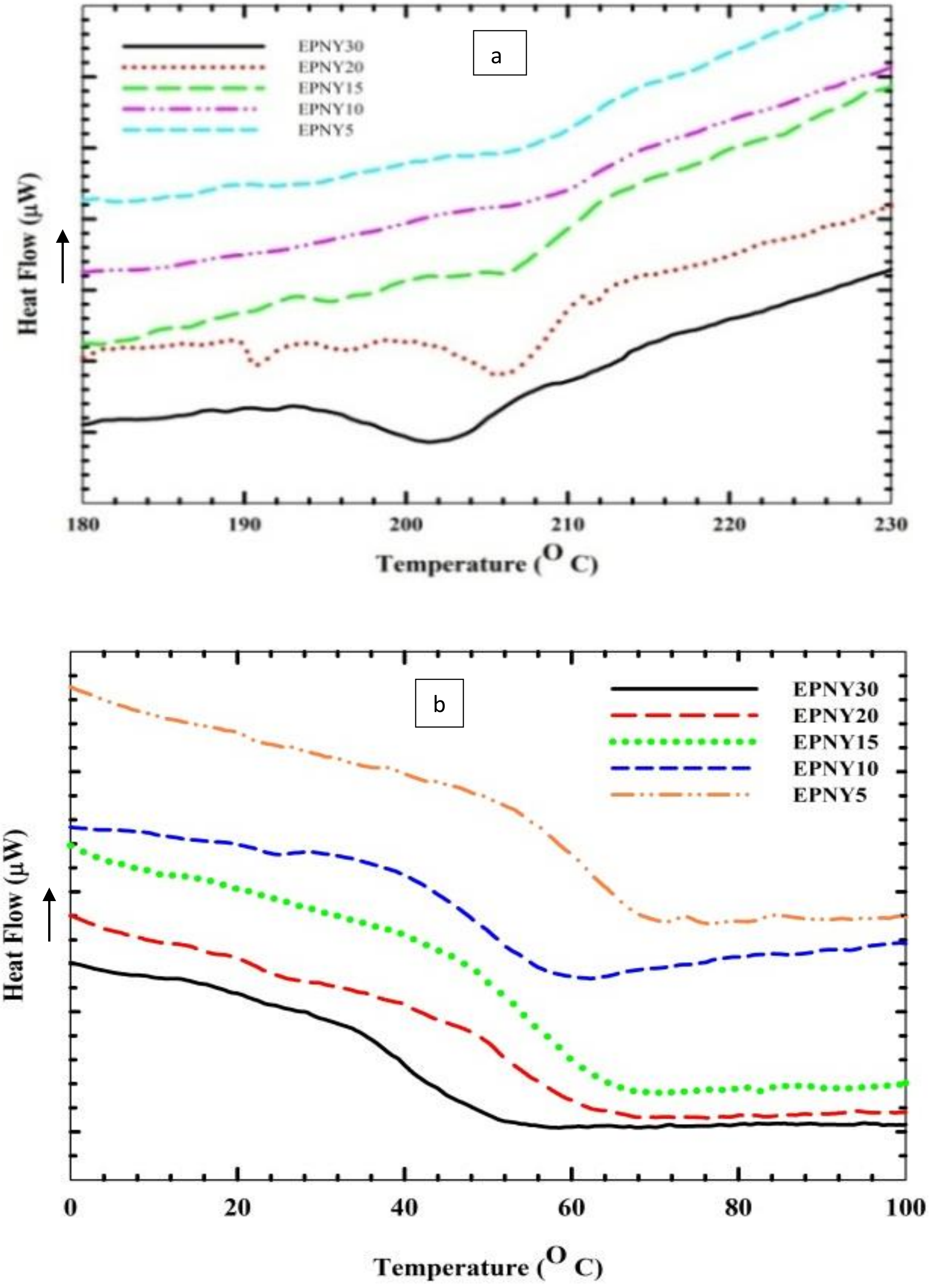

Figure 18 – DSC thermogram showing (a) Melting peaks, (b) Glass transitions Temperatures of epoxy/nylon-6 composites at heating rate of 5^{O}C/min

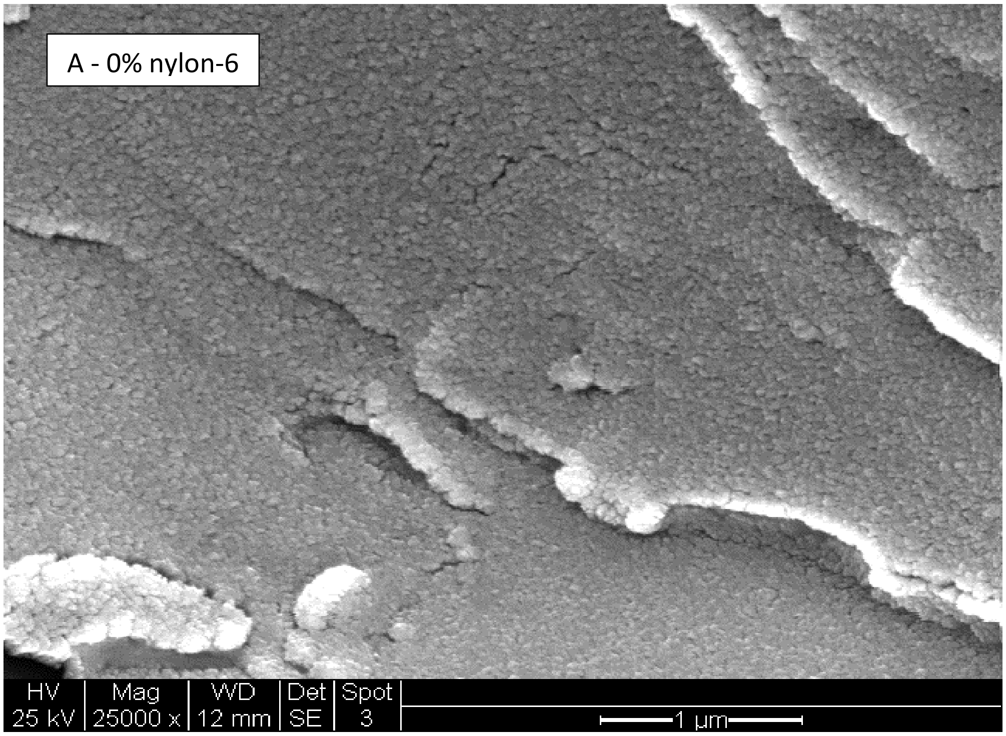

Figure 19a – SEM image of fractured surface of epoxy film

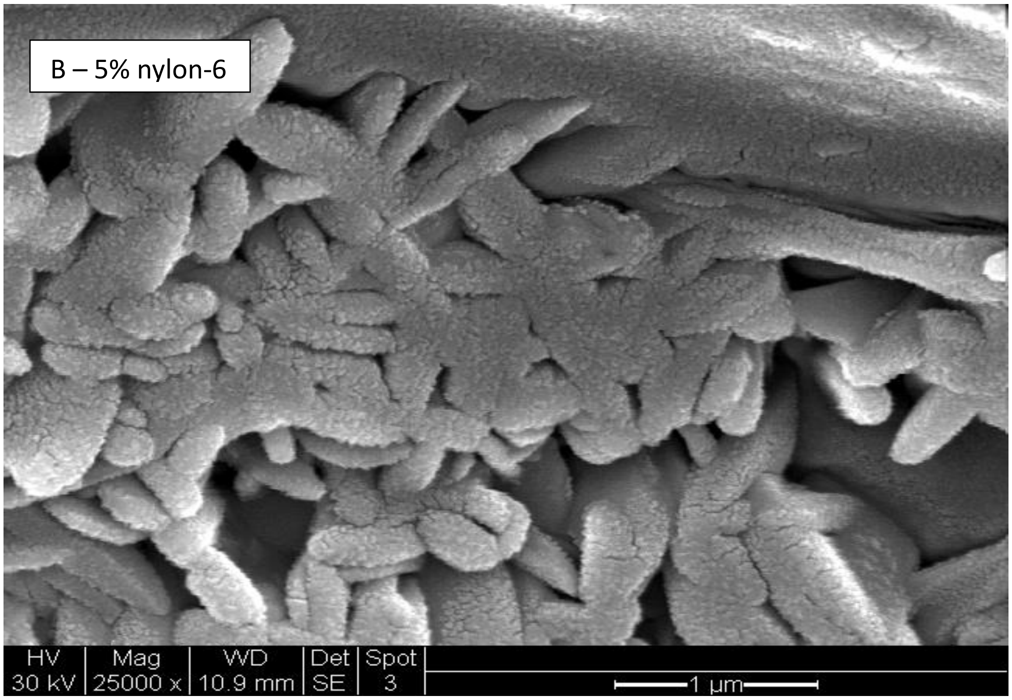

Figure 19b – SEM image of fractured surface of epoxy/nylon-6 (5 wt.%) film

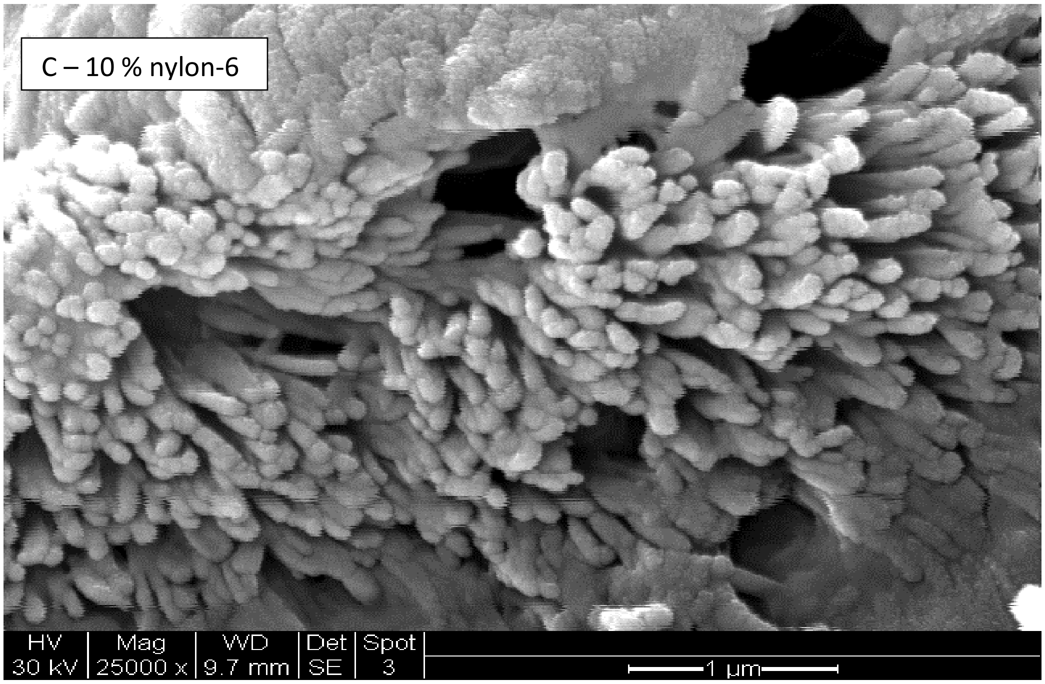

Figure 19c – SEM image of fractured surface of epoxy/nylon-6 (10 wt.%) film

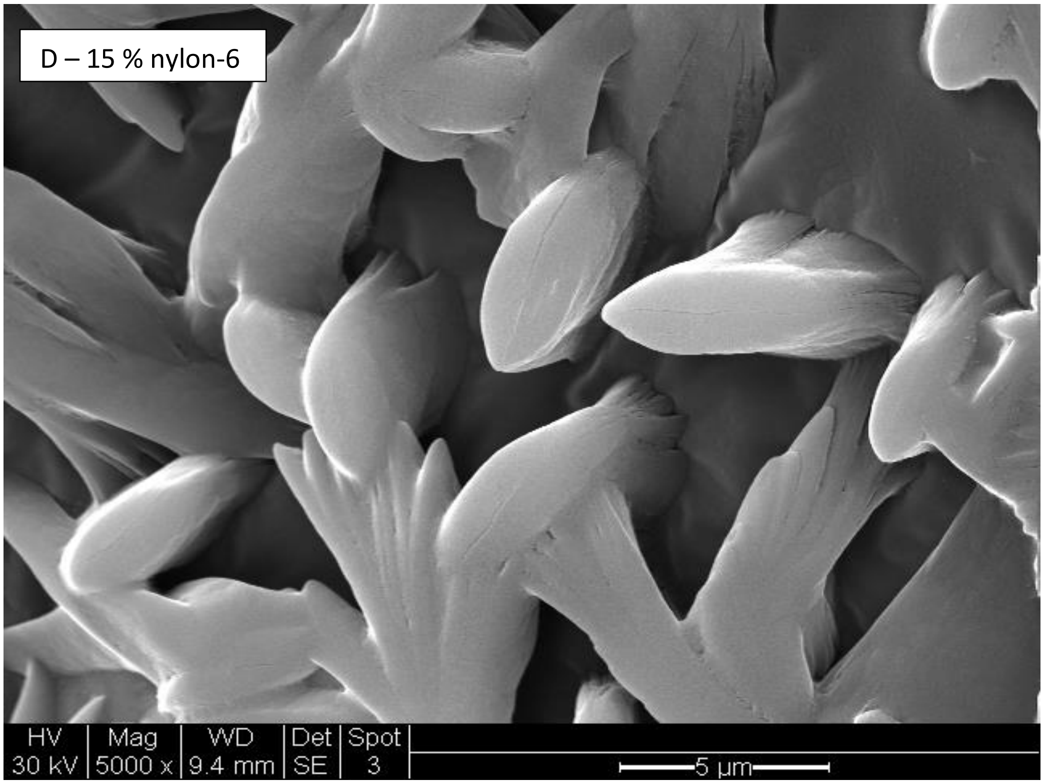

Figure 19d – SEM image of fractured surface of epoxy/nylon-6 (15 wt.%) film

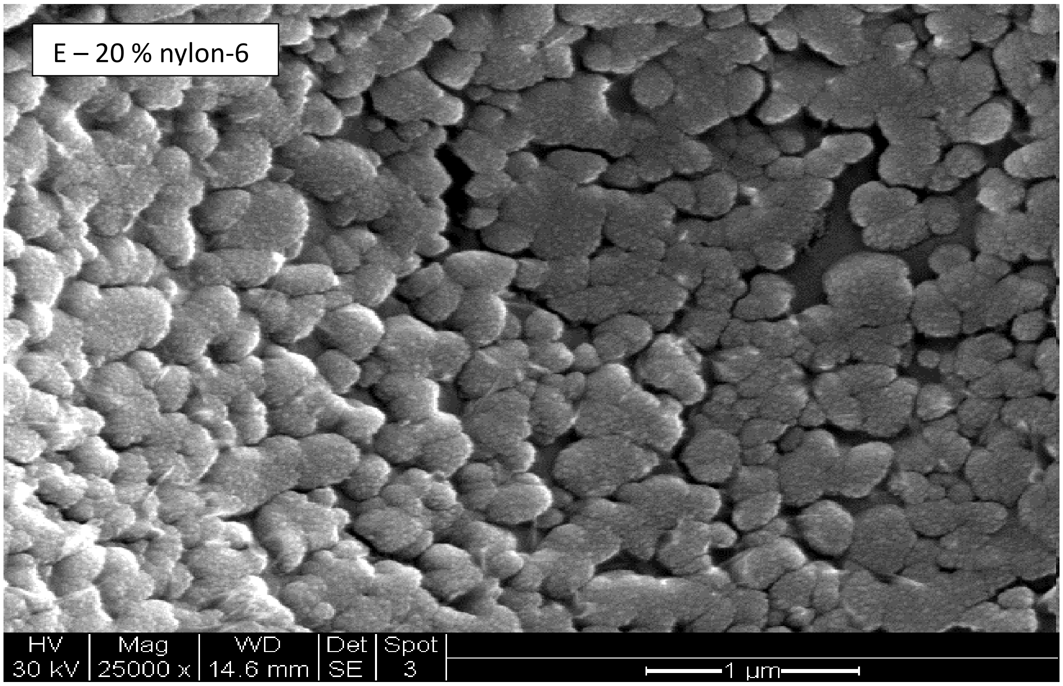

Figure 19e – SEM image of fractured surface of epoxy/nylon-6 (20 wt.%) film

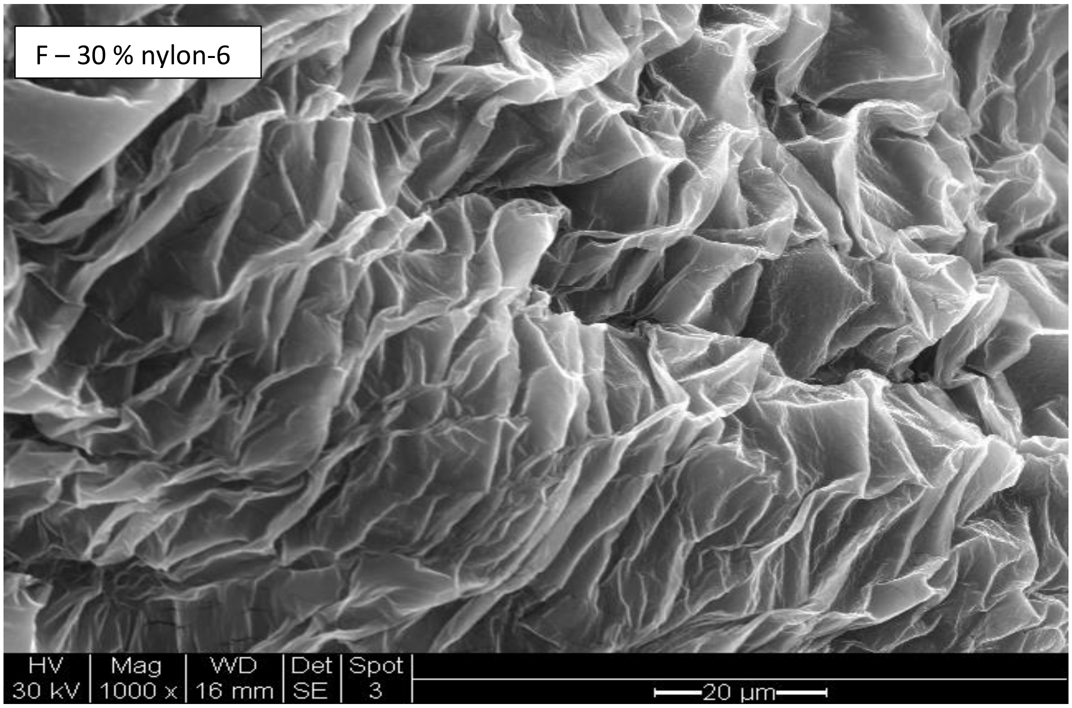

Figure 19f – SEM image of fractured surface of epoxy/nylon-6 (30 wt.%) film

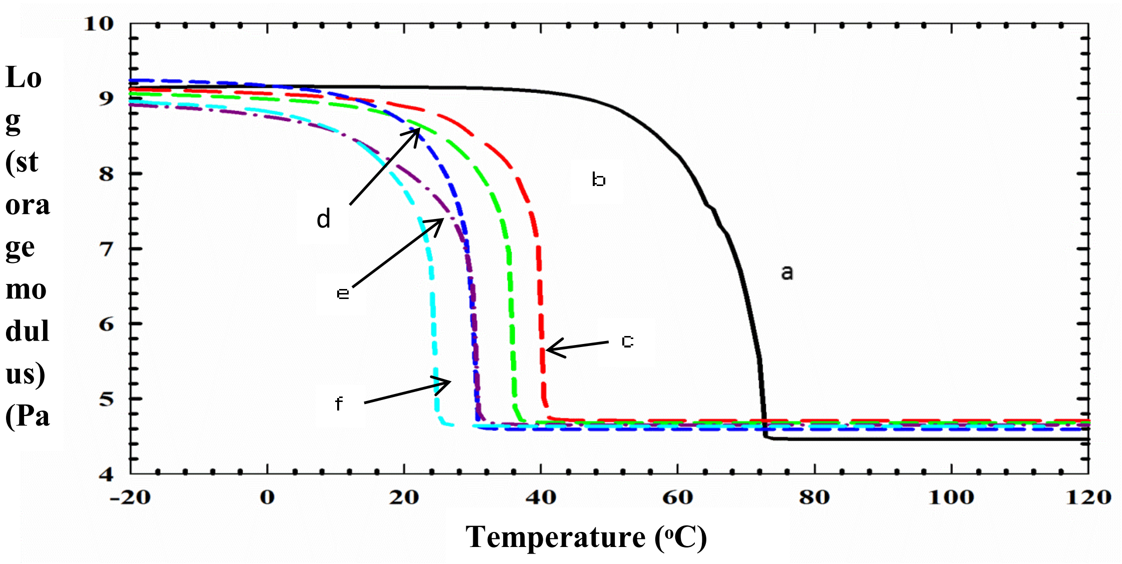

Figure 20 – Variation of storage modulus with temperature for various PA-6loading of composite films (a – neat epoxy, b – 5 wt. % PA-6, c – 10 wt. % PA-6, d – 15 wt. % PA-6, e – 20 wt. % PA-6, f – 30 wt. % PA-6)

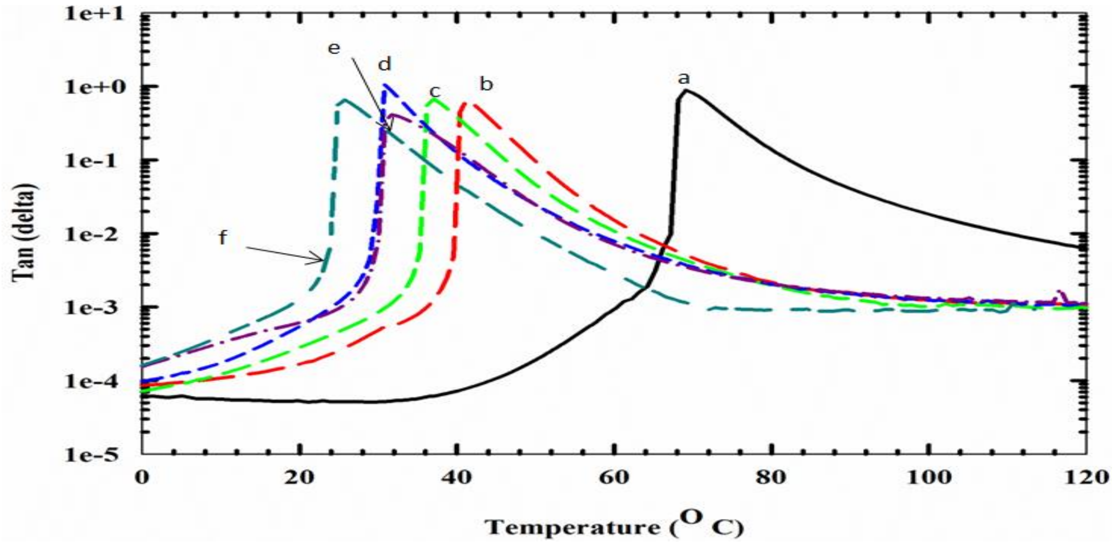

Figure 21 - Variation of tan delta with temperature for various nylon-6 loading of composite films (a – neat epoxy, b – 5 wt. % PA-6, c – 10 wt. % PA-6, d – 15 wt. % PA-6, e – 20 wt. % PA-6, f – 30 wt. % PA-6)

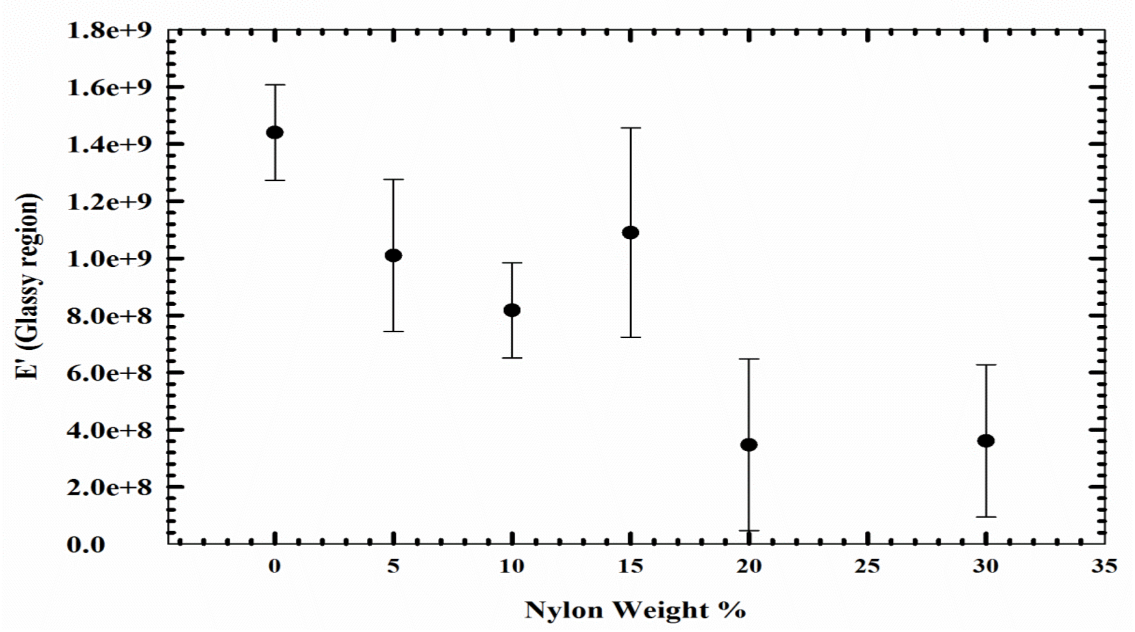

Figure 22 – Storage modulus in glassy region of nylon-6/epoxy films as a function of nylon-6 wt. % at $0^{O}C$

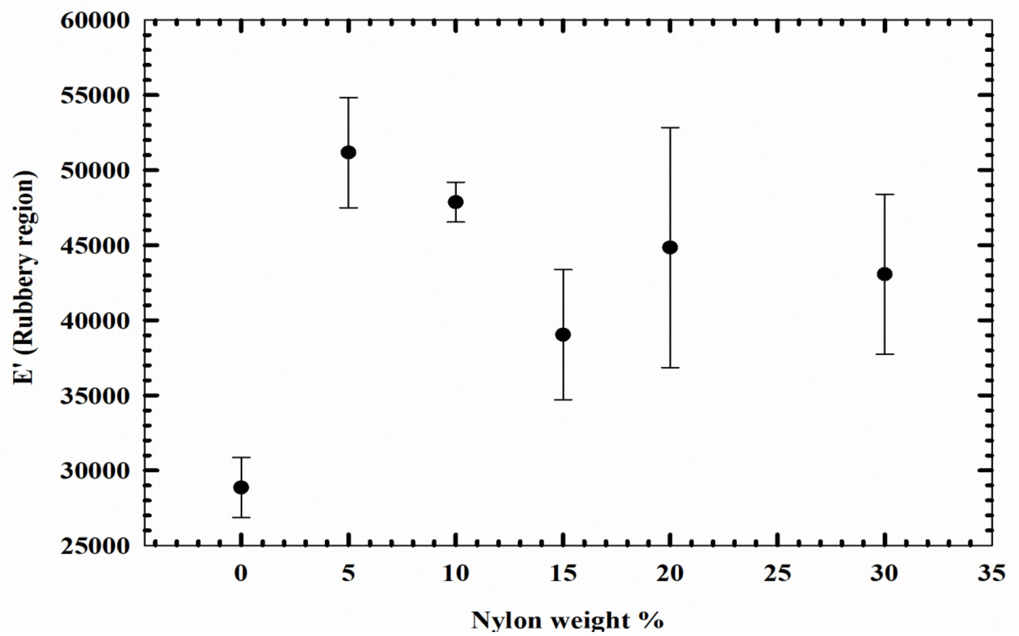

Figure 23 - Storage modulus of nylon-6/epoxy in rubbery region as a function of nylon-6 wt. % at $100^{O}C$

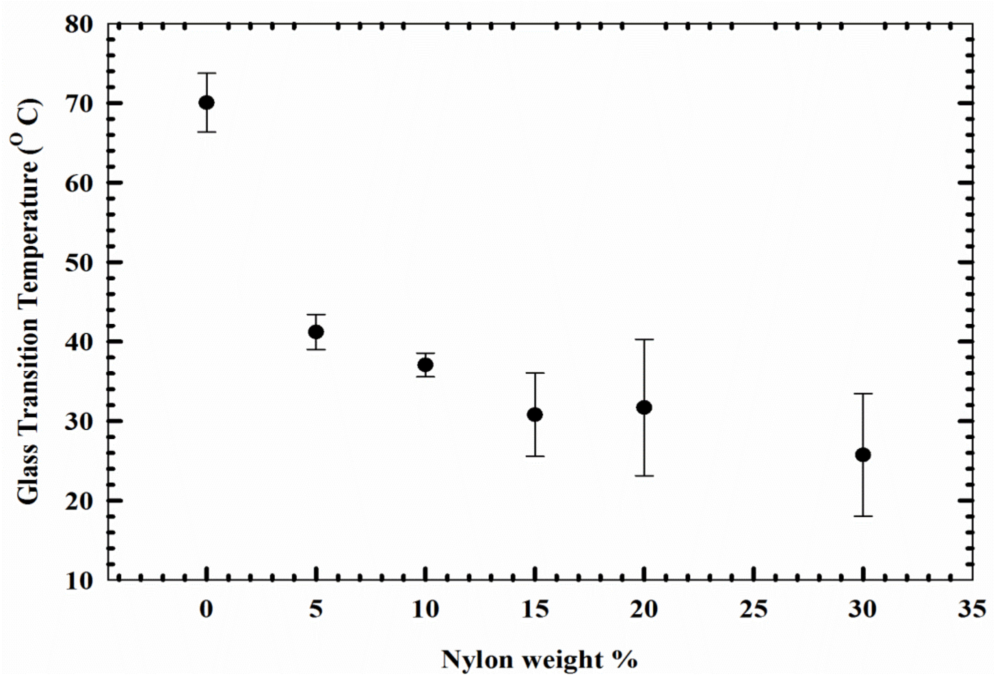

Figure 24 – Variation of T_g of the composite with increased loading of nylon-6 in epoxy

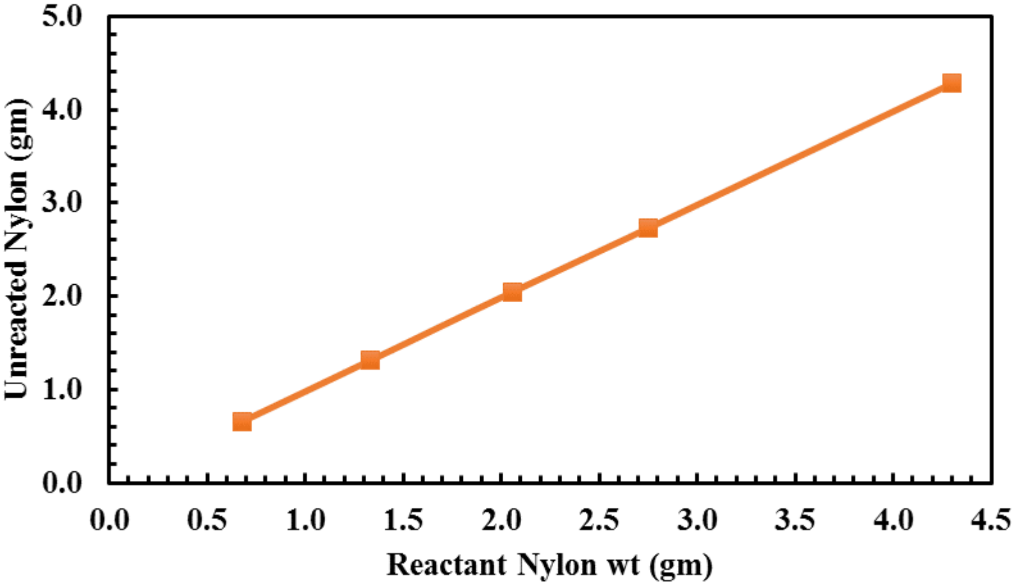

Figure 25 – Weight (g) of unreacted nylon-6 in nylon-6/epoxy composite as a function of total weight of nylon-6 added to the system.

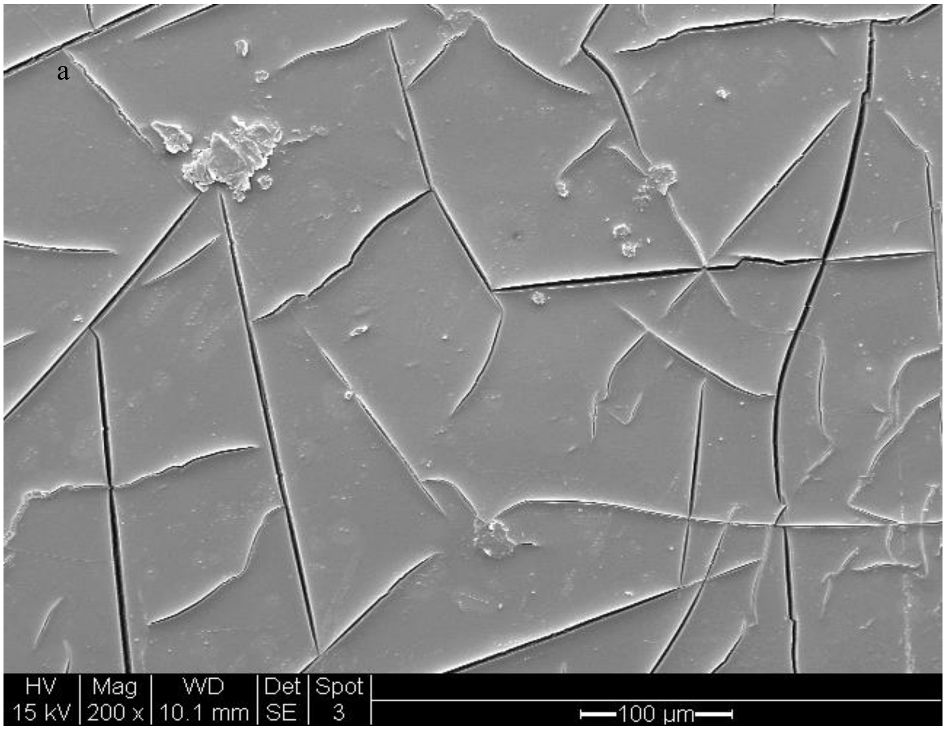

Figure 35a – SEM image of surface of thermally treated EPIREZ 5522-WY-55 epoxy coating on Al-2024 T3 aluminum alloy substrate

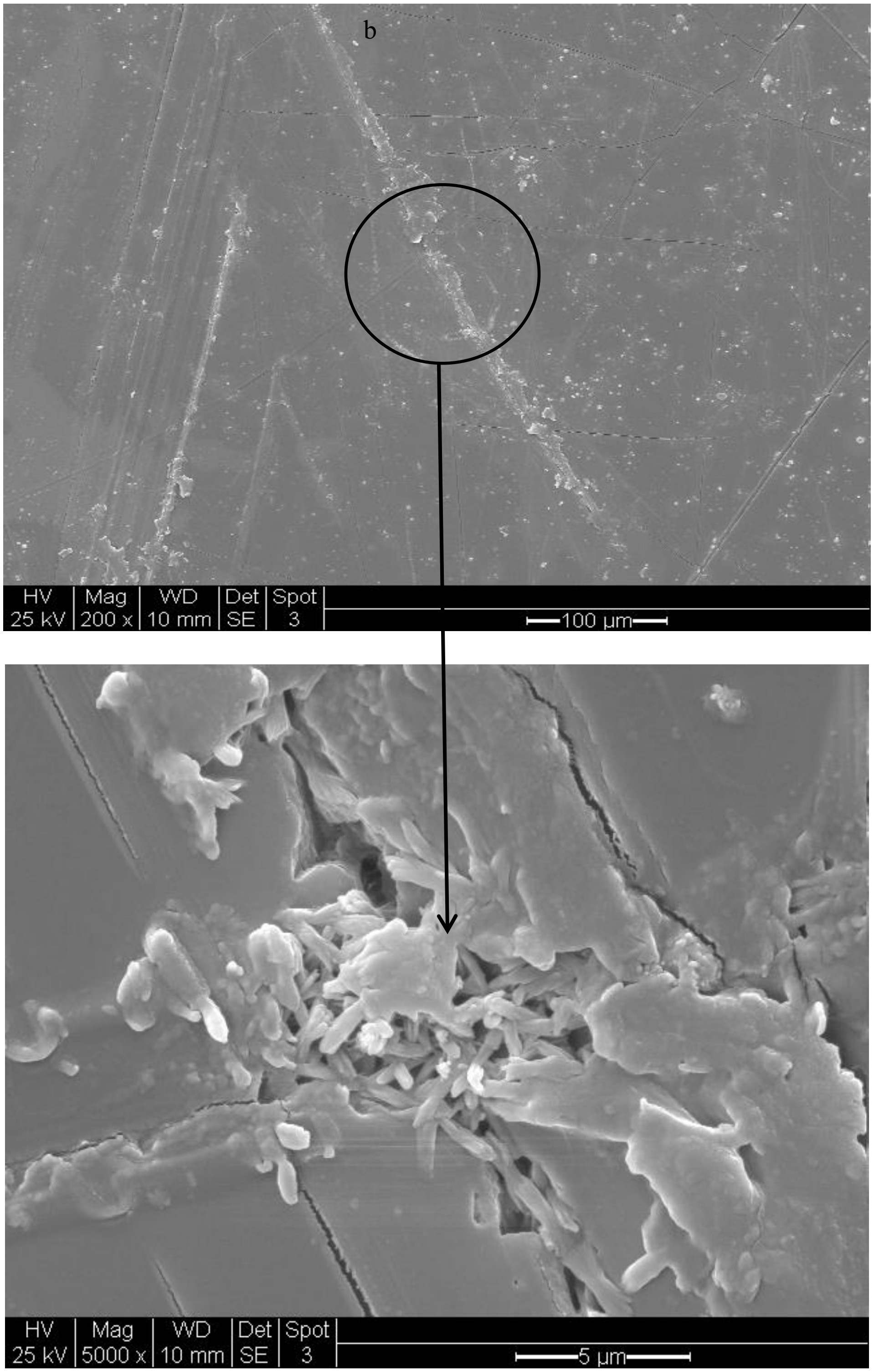

Figure 35b – SEM image of surface of epoxy/nylon-6 (10 wt.%) coating on Al-2024 T3 aluminum alloy substrate

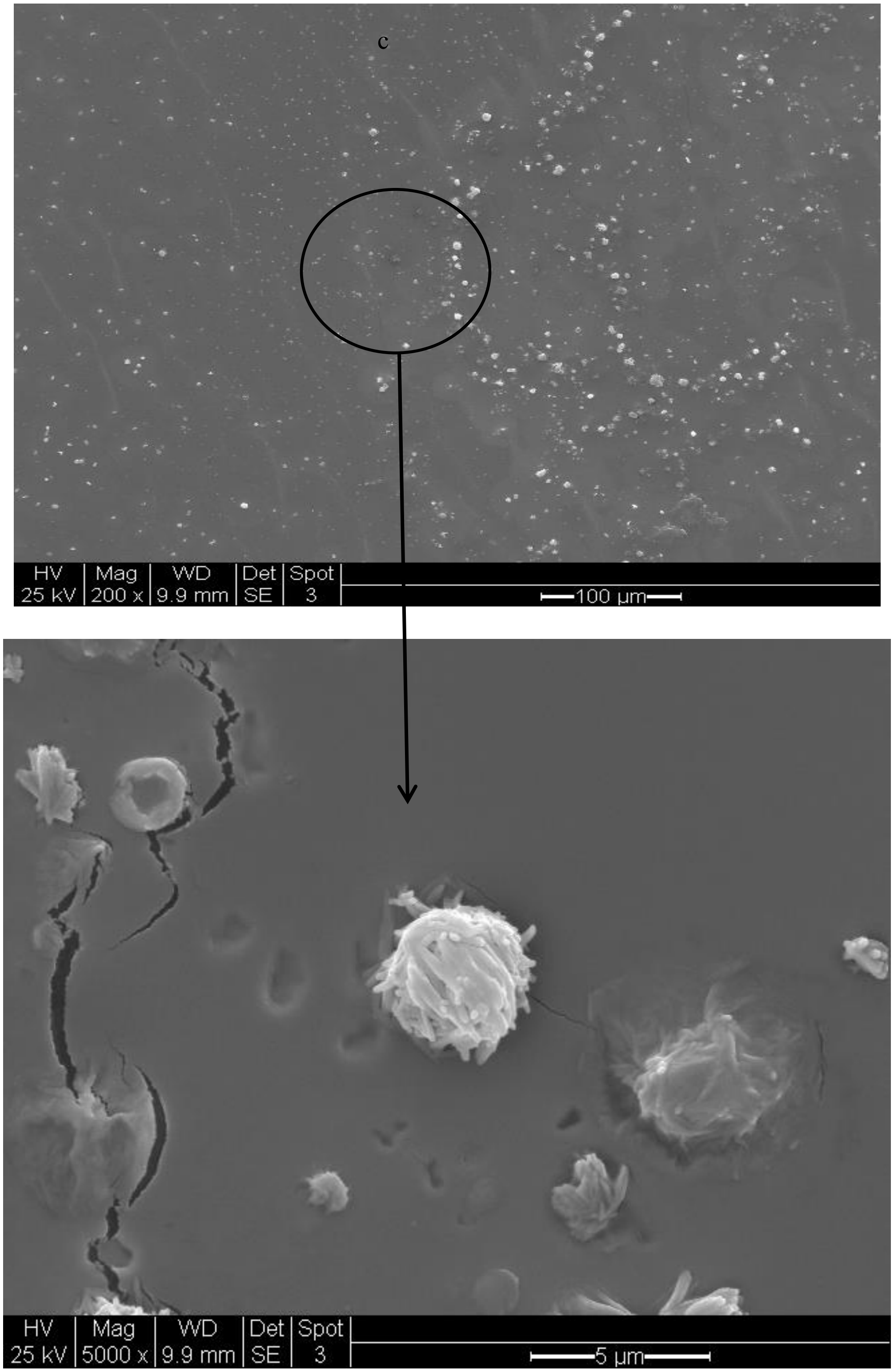

Figure 35c – SEM image of surface of epoxy/nylon-6 (10 wt.%) coating on Al-2024 T3 aluminum alloy substrate.

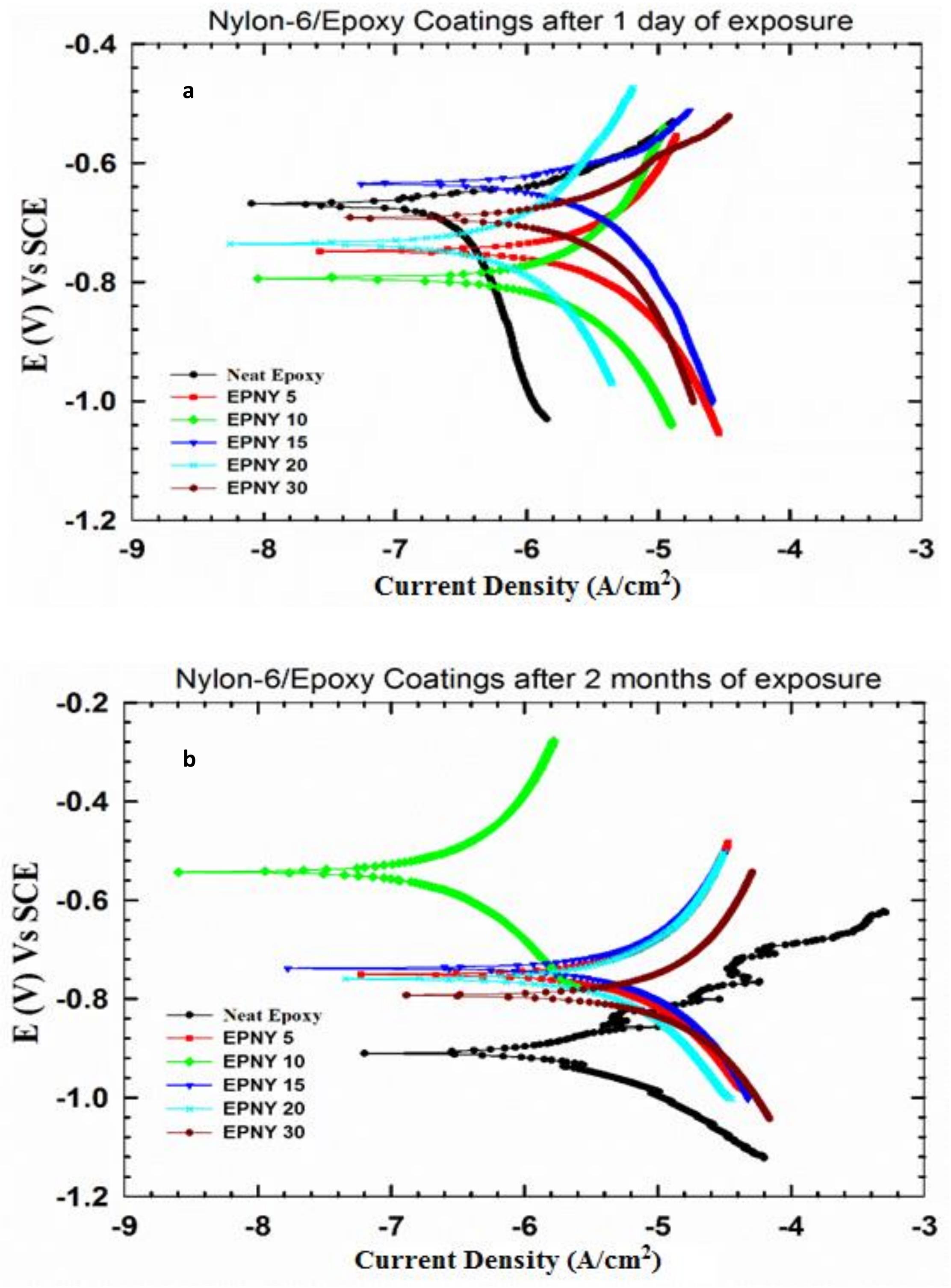

Figure 36 – DCP Plots for epoxy/nylon-6 coatings on Al 2024-T3 alloy substrate after (a) 1 day of exposure (b) after 2 months of exposure

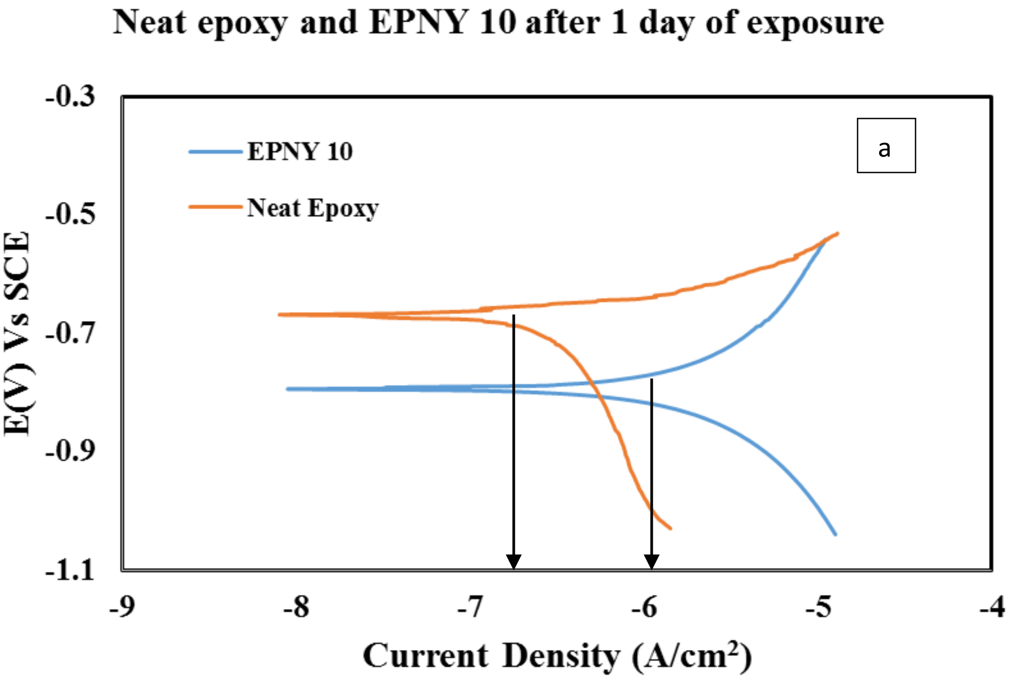

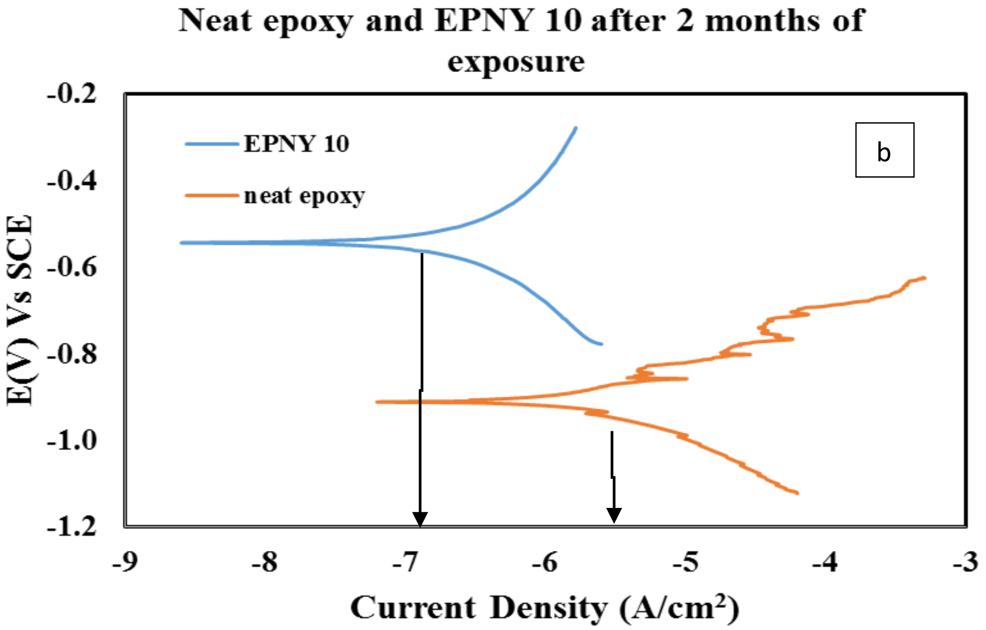

Figure 37 – DCP Plots for comparison of epoxy/nylon-6 (10% by weight) and thermally treated neat epoxy coatings on Al 2024-T3 alloy substrate after (a) 1 day of exposure (b) after 2 months of exposure

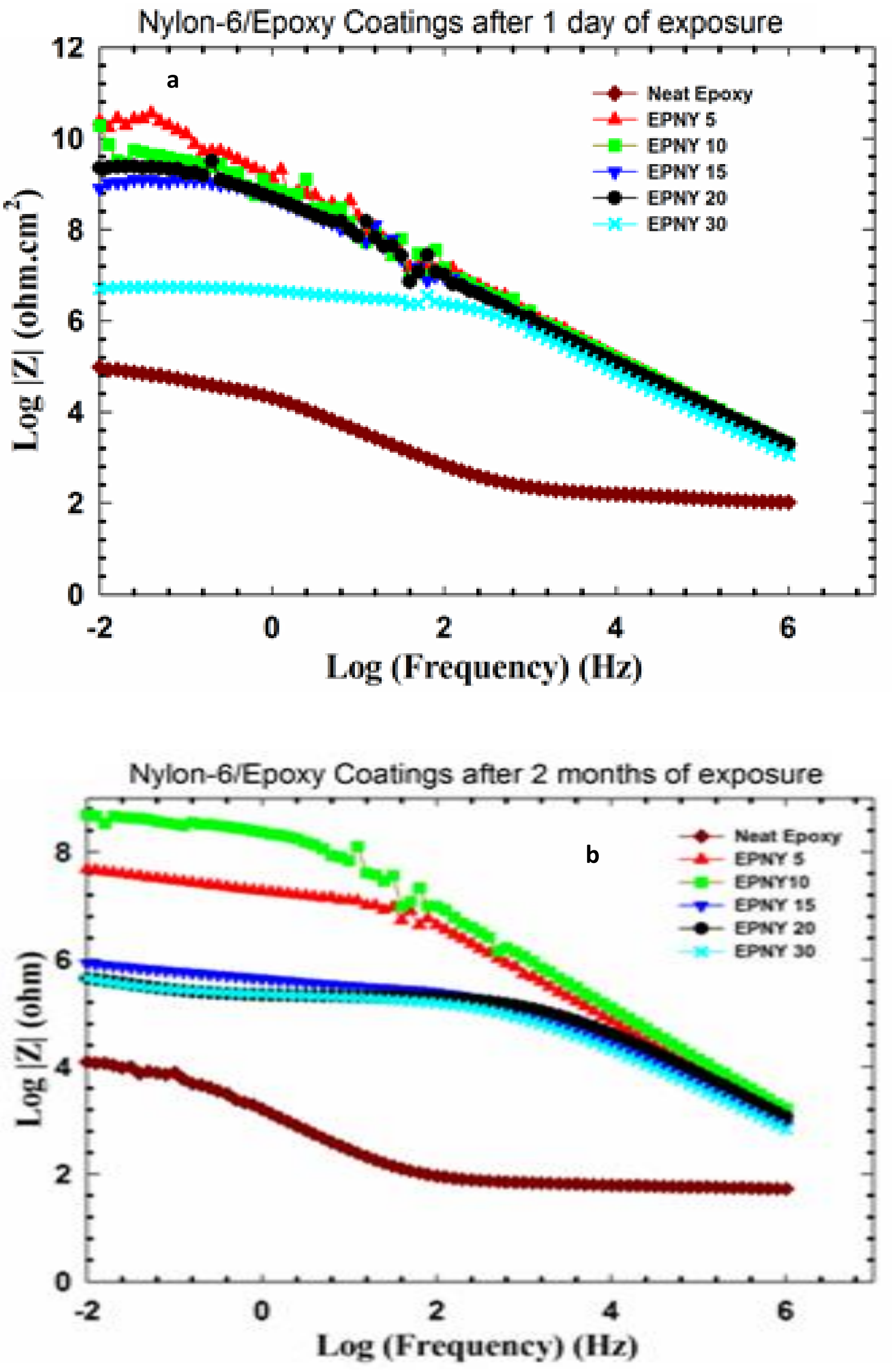

Figure 37 – Bode plots for epoxy/nylon-6 coatings on Al 2024-T3 alloy substrate after (a) 1 day of exposure (b) after 2 months of exposure.

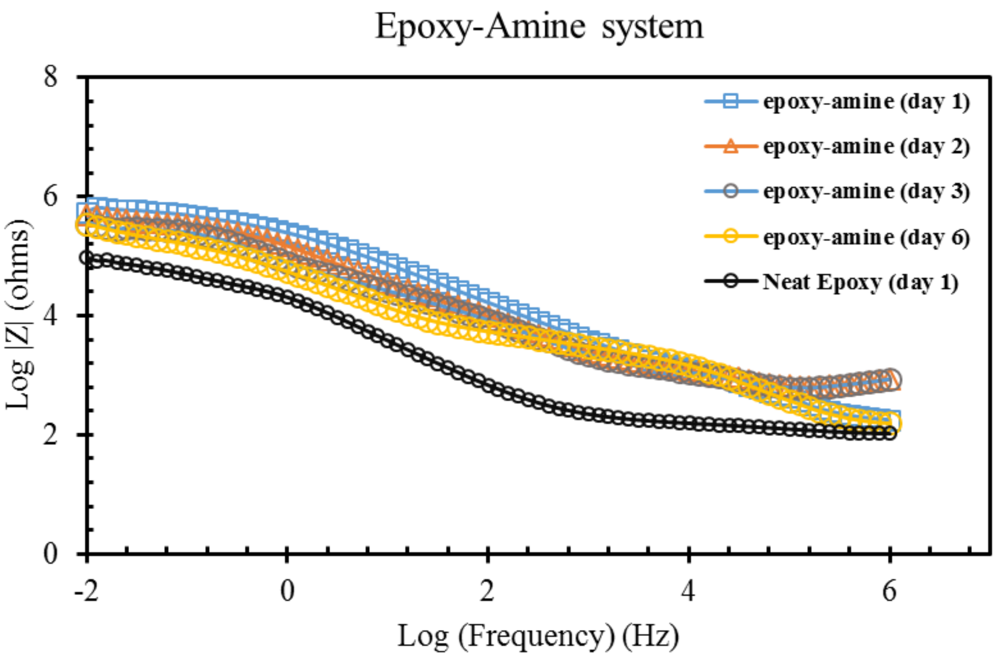

Figure 38 - Bode plots for epoxy coating cured with standard amine based curing agent on Al-2024 T3 alloy substrate

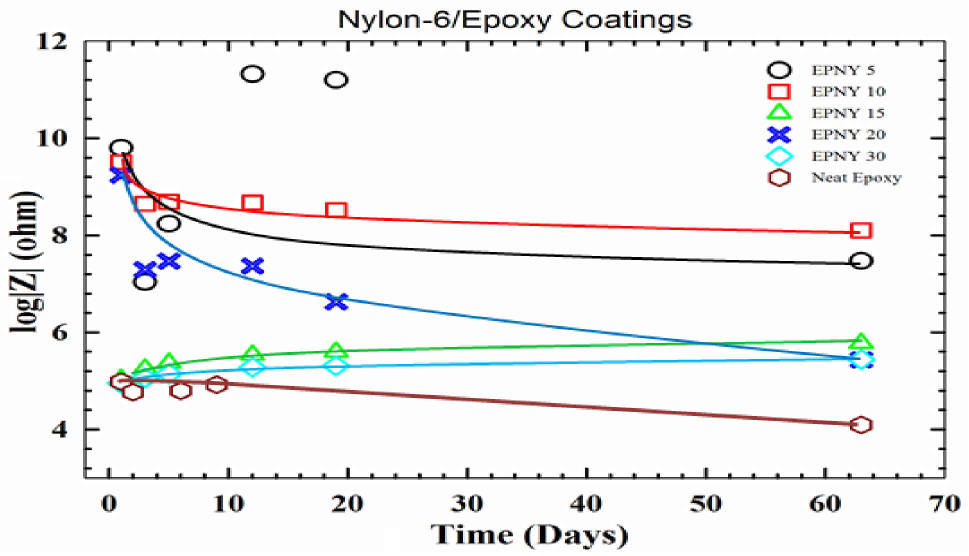

Figure 39 – Impedance as a function of exposure time of nylon-6/epoxy coatings on Al 2024-T3 alloy substrate

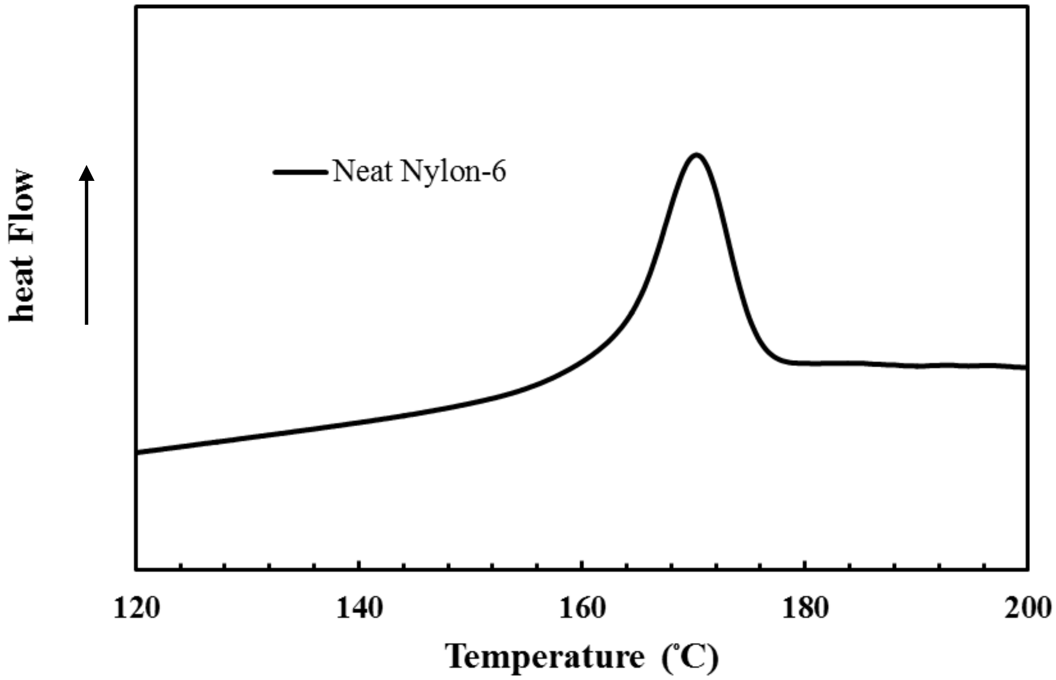

Figure 40a – DSC thermogram showing the crystallization peak for neat nylon-6

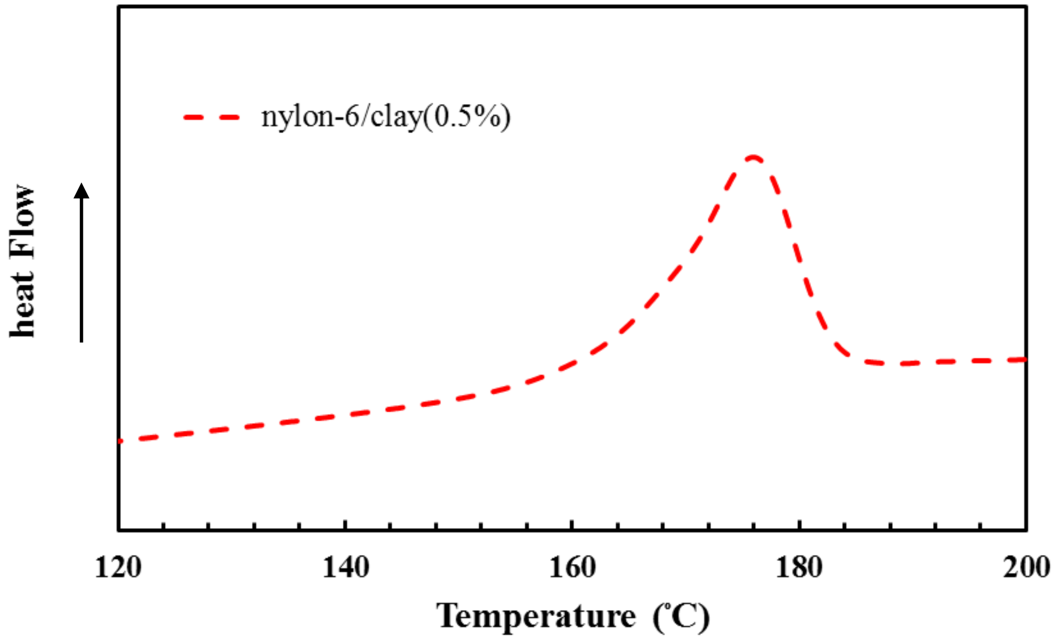

Figure 40b – DSC thermogram showing the crystallization peak for nylon-6/clay (0.5wt.%)

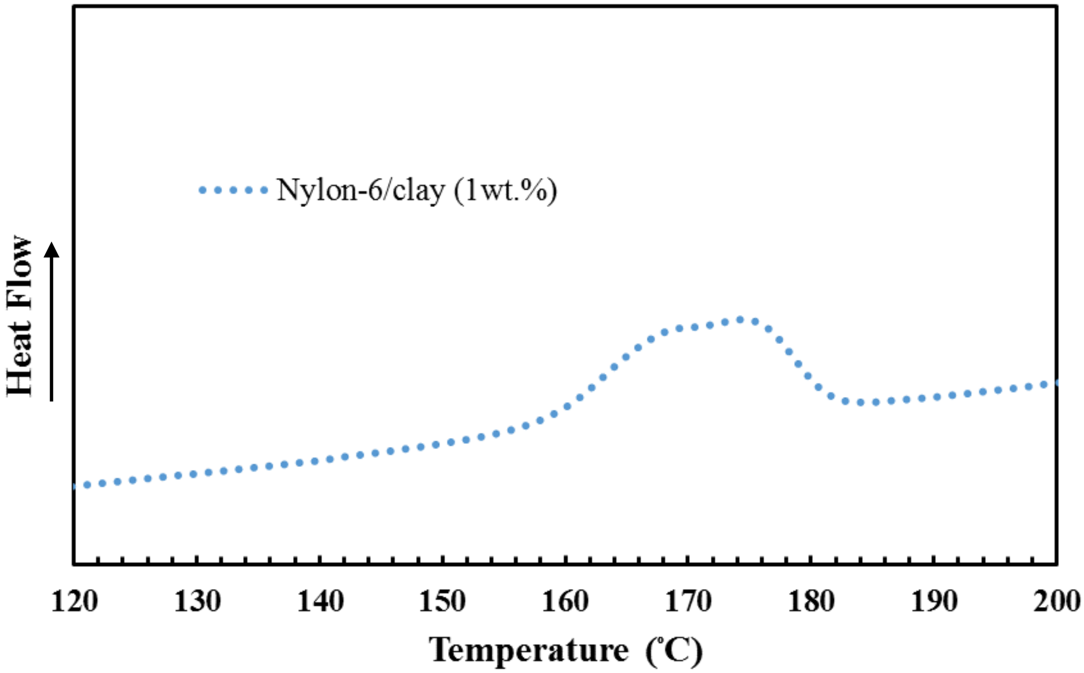

Figure 40c – DSC thermogram showing the crystallization peak for nylon-6/clay (1wt.%)

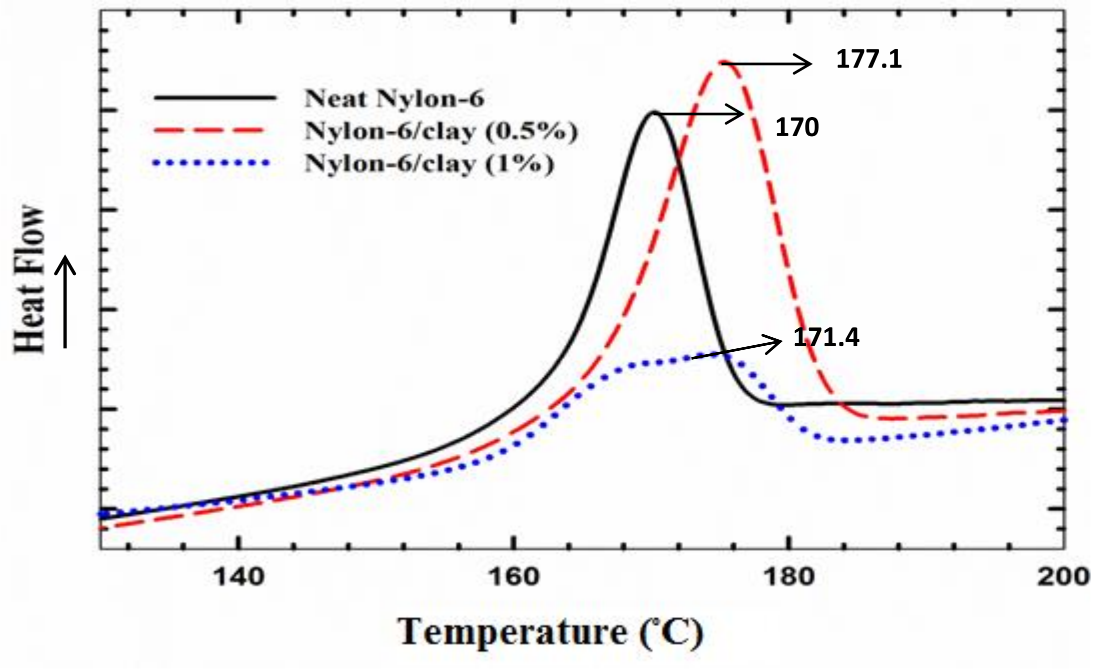

Figure 40 – DSC thermogram showing the crystallization peak for neat nylon-6 and its nanocomposites with clay at heating rate of 5°C/min

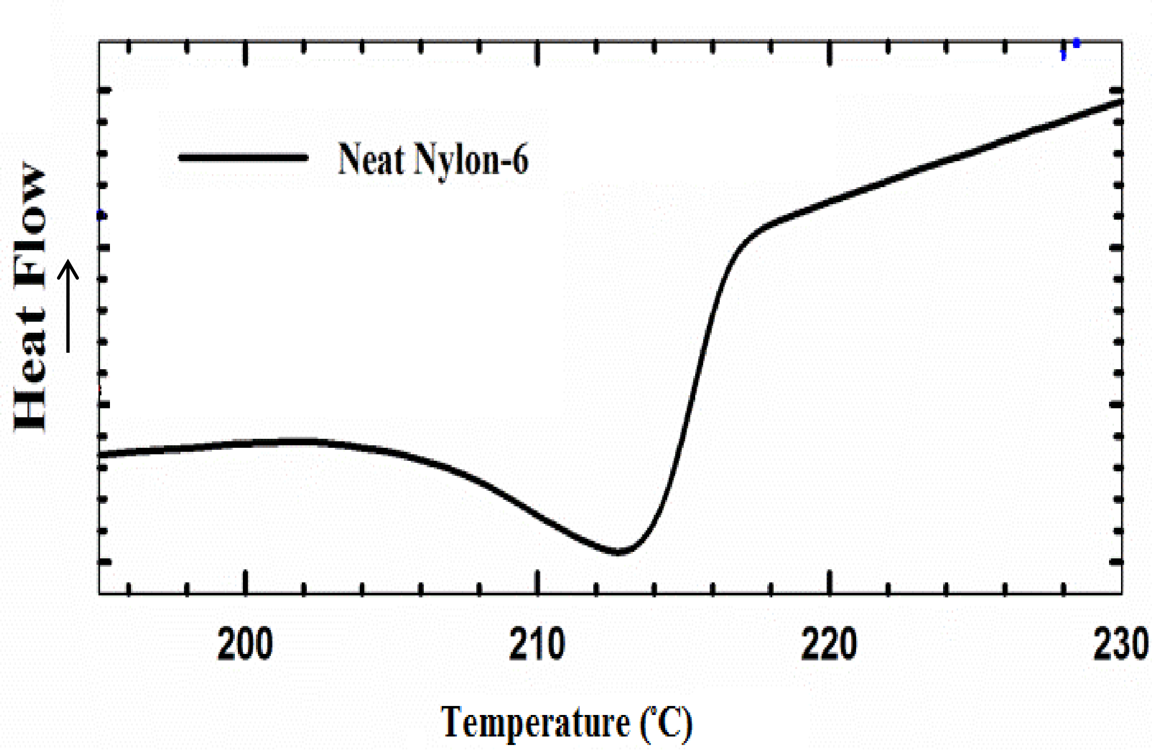
Heat Flow
Neat Nylon-6
200
210
220
230
Temperature (°C)

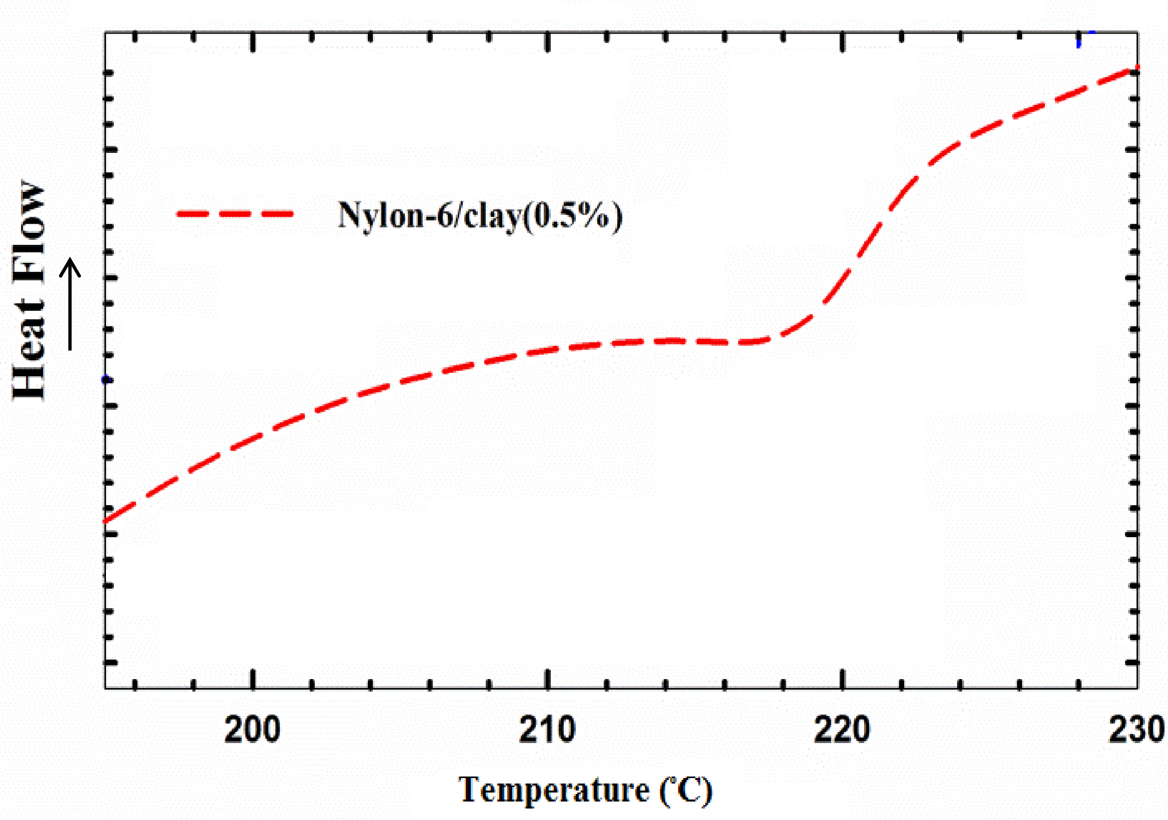
Heat Flow
Nylon-6/clay(0.5%)
200
210
220
230
Temperature (°C)

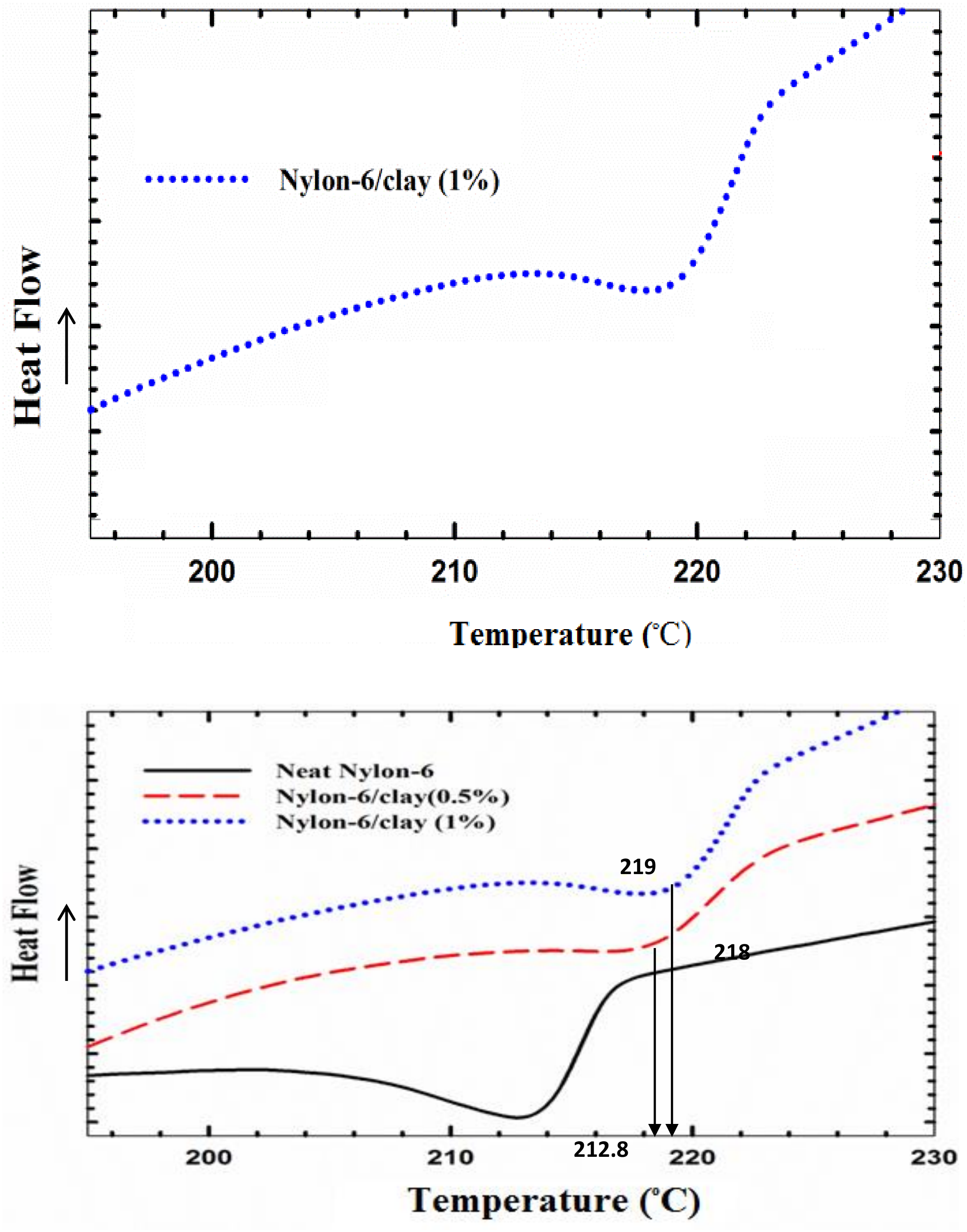

Figure 41 a – DSC Thermogram showing the melting peak of nylon-6 and its nanocomposites with clay after Second run

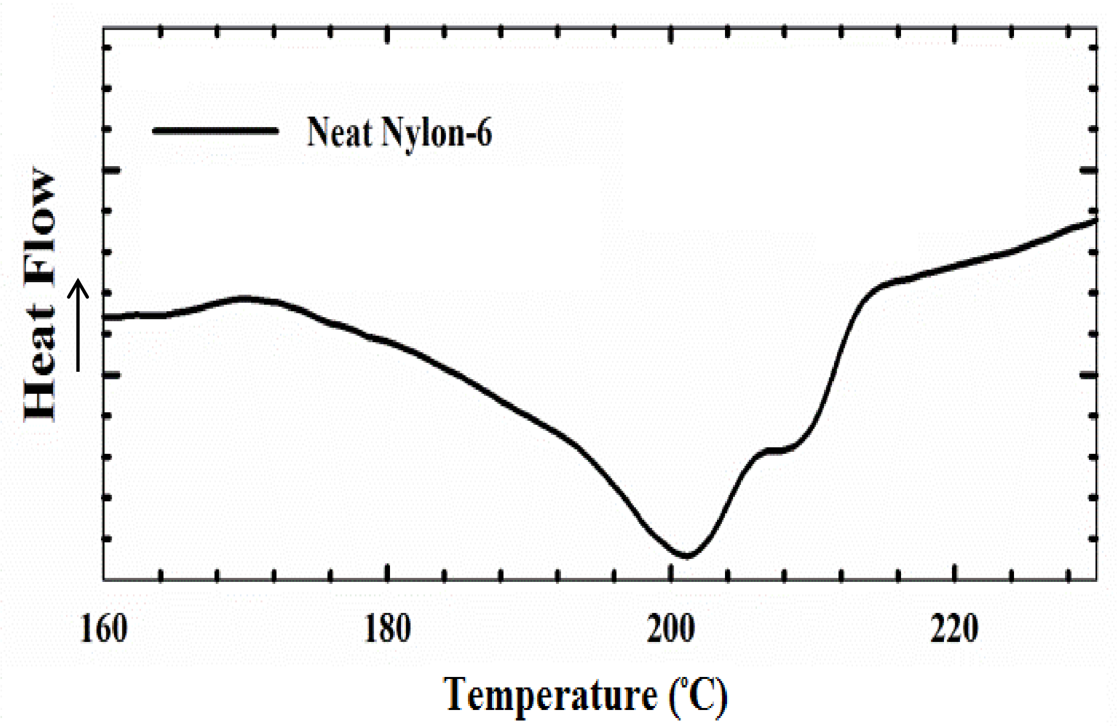
Neat Nylon-6
Heat Flow
160
180
200
220
Temperature (°C)

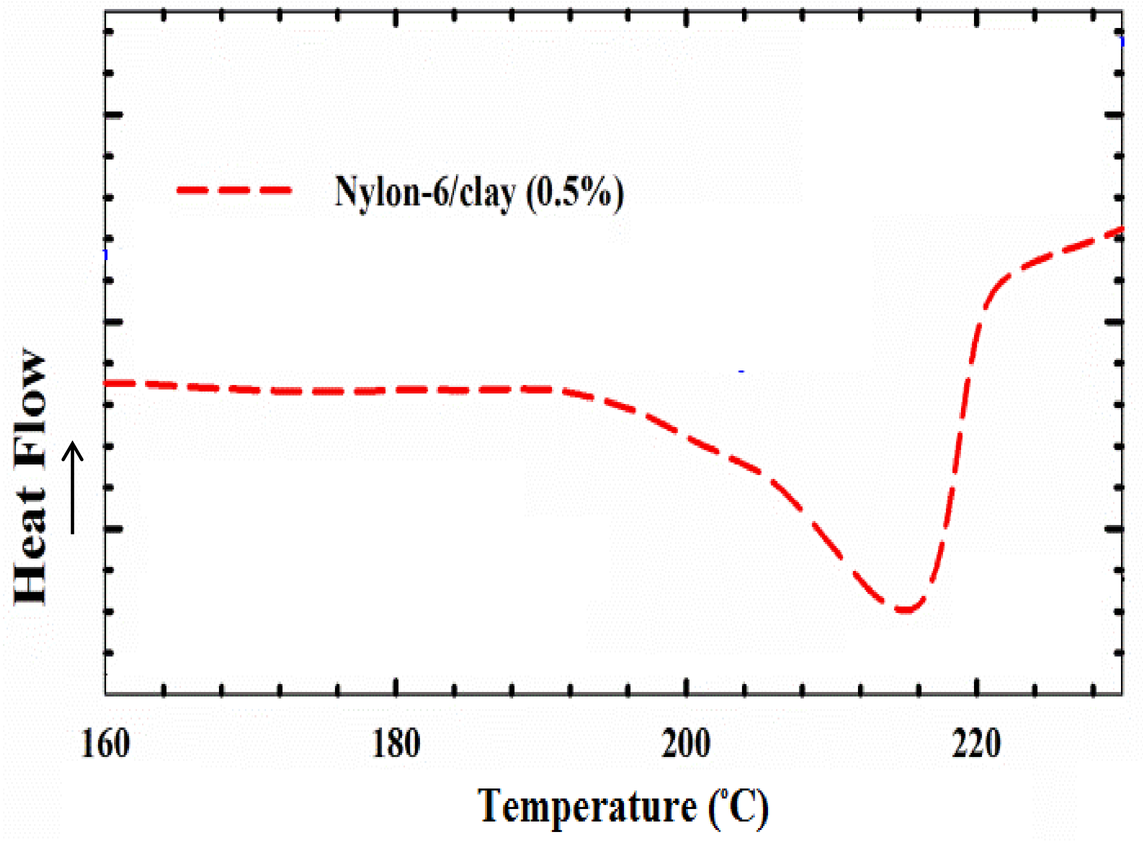
Nylon-6/clay (0.5%)
Heat Flow
160
180
200
220
Temperature (°C)

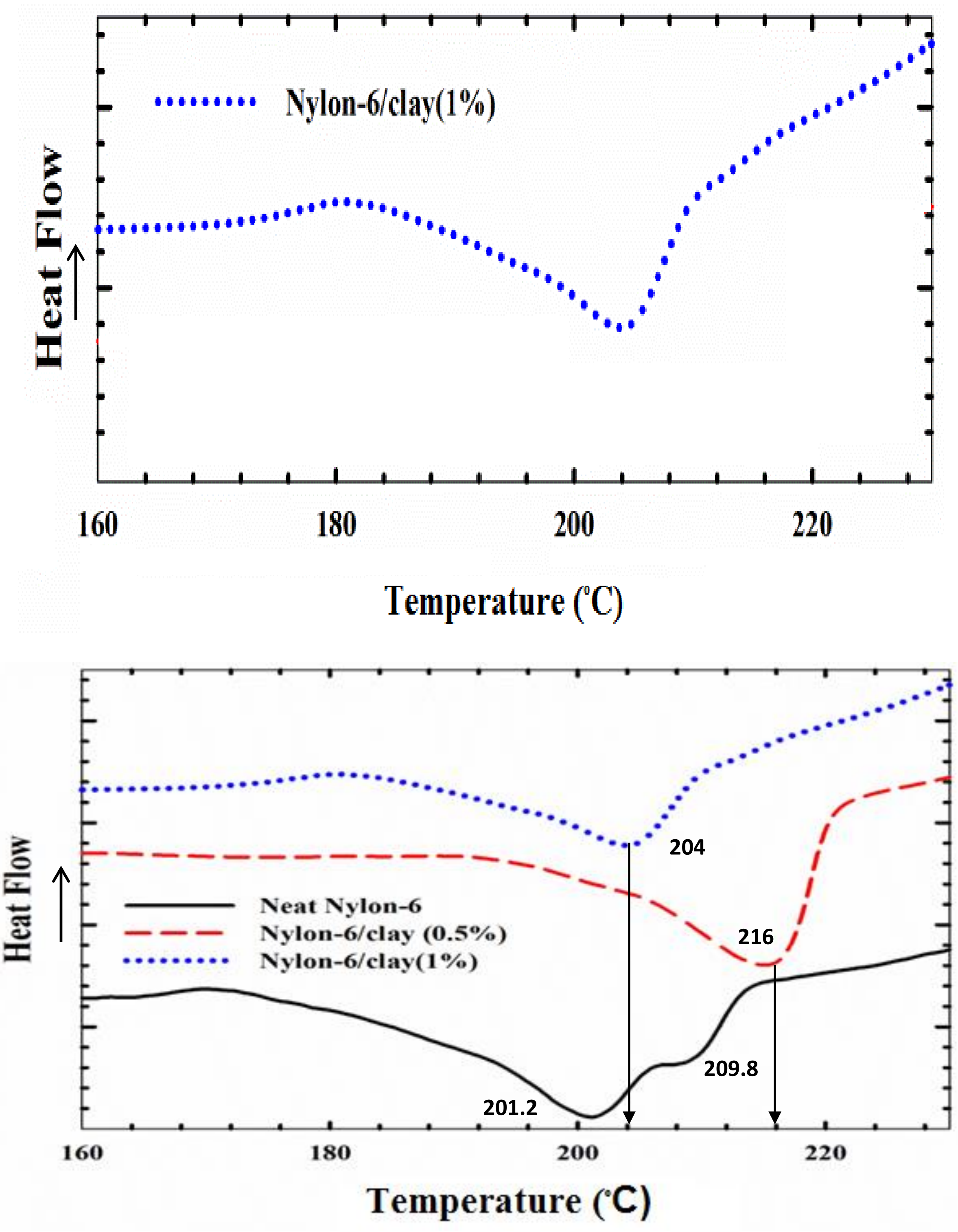

Figure 41 b – DSC Thermogram showing the melting peak of nylon-6 and its nanocomposites with clay after third run

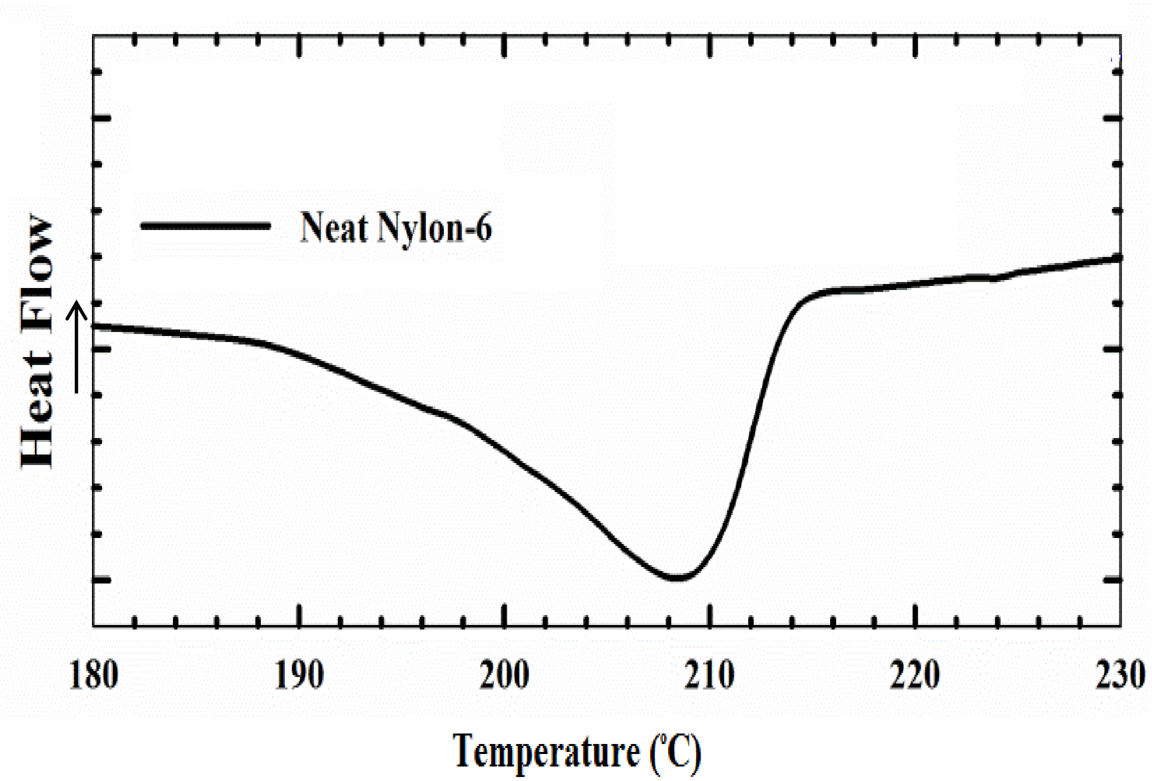
Neat Nylon-6
Heat Flow
180
190
200
210
220
230
Temperature (°C)

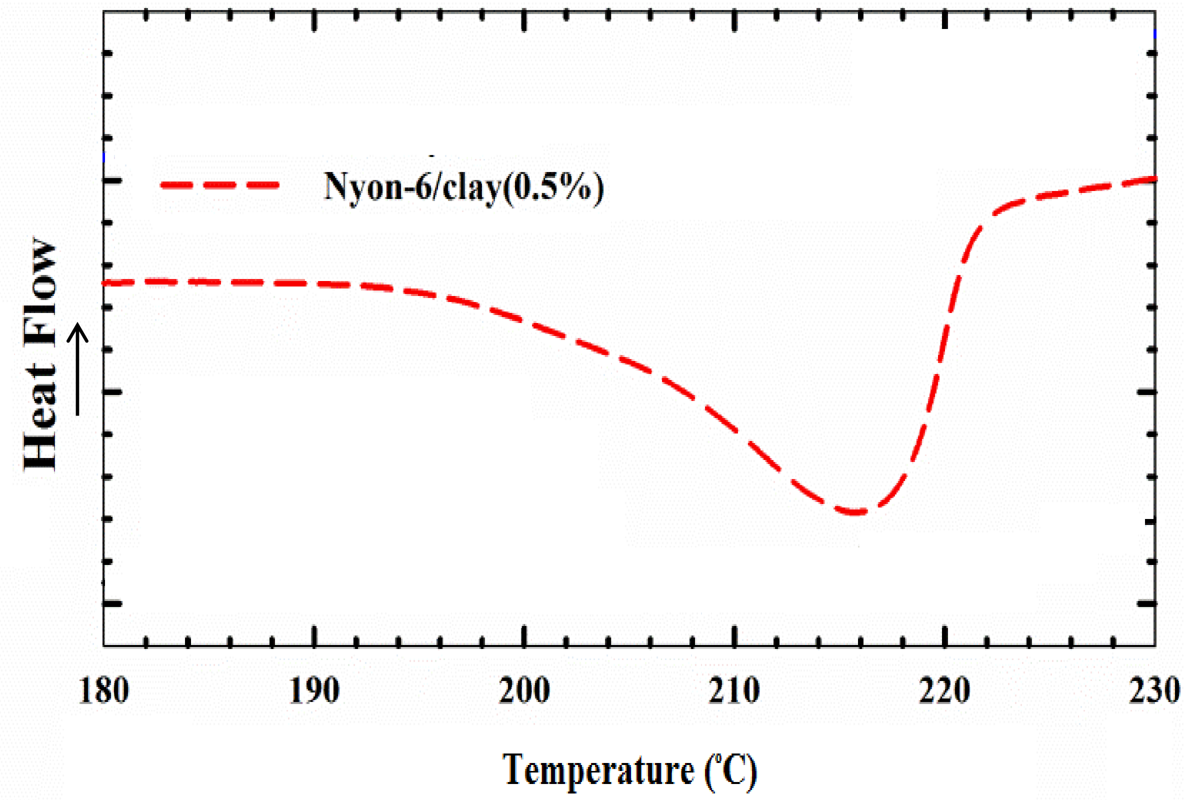
Nyon-6/clay(0.5%)
Heat Flow
180
190
200
210
220
230
Temperature (°C)

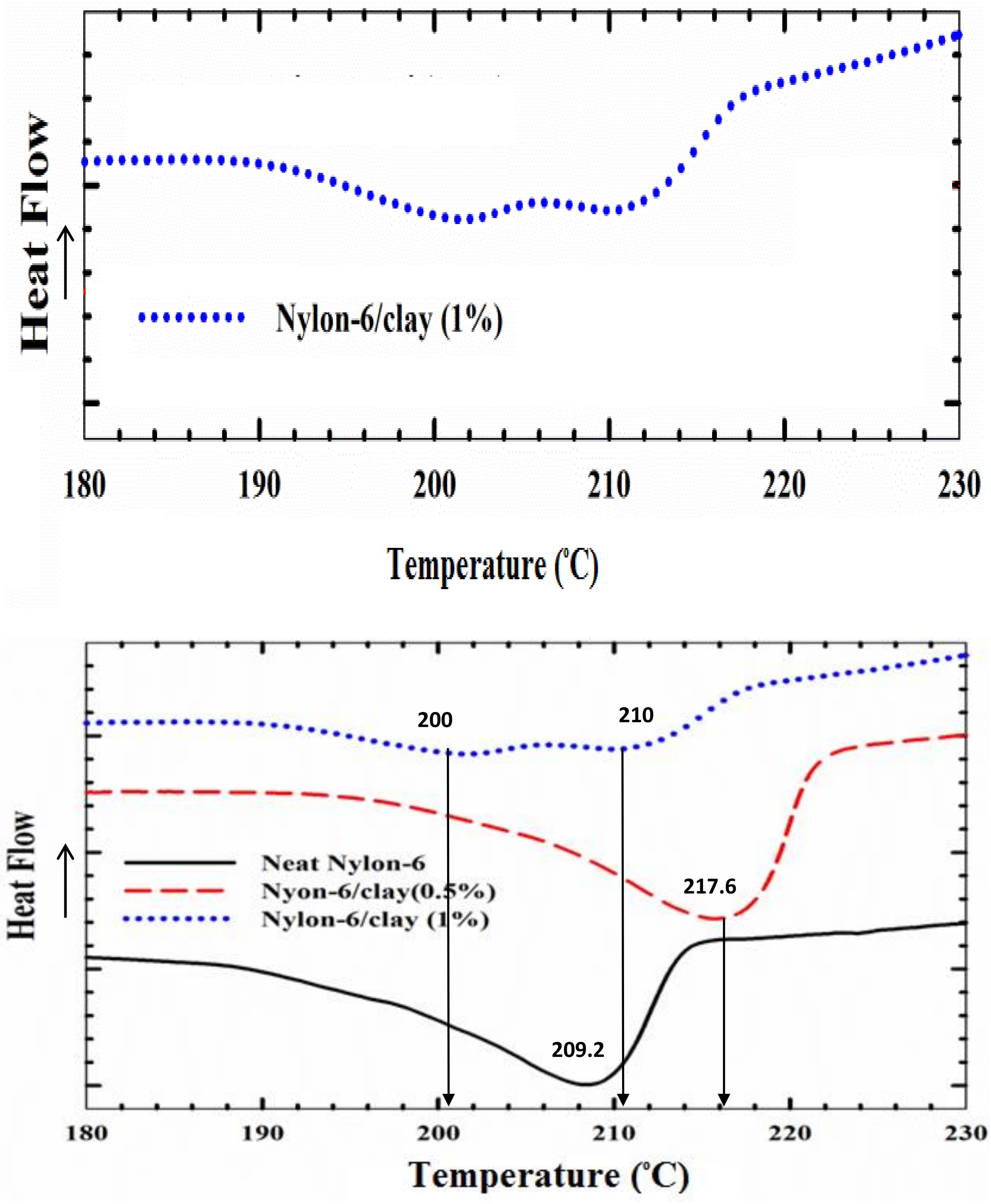

Figure 41 c – DSC Thermogram showing the melting peak of nylon-6 and its nanocomposites with clay after fourth run

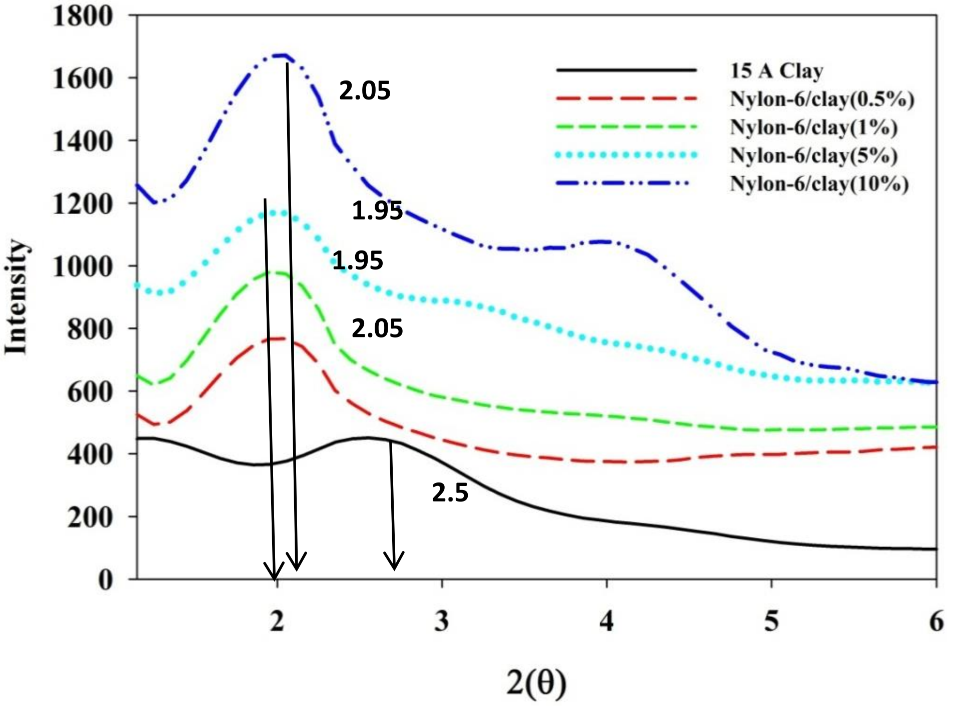

Figure 43 – X-ray diffraction pattern for nylon-6/clay composite at lower angle.

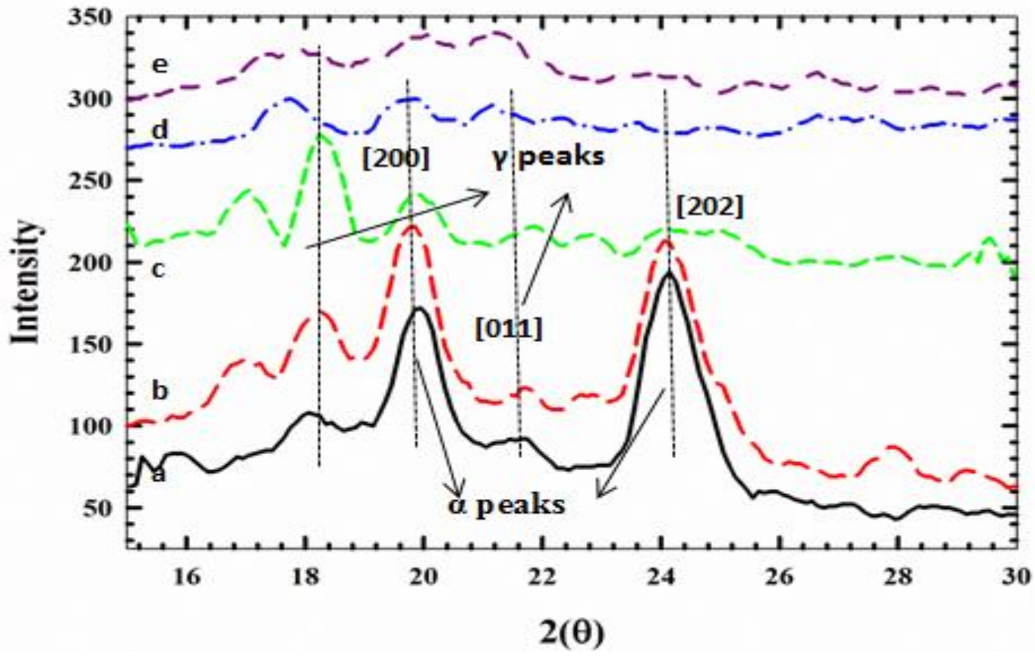

Figure 44 – X-ray diffraction pattern for nylon-6/clay composite at higher angle (a- neat nylon-6, b- nylon-6/clay(0.5%), c- nylon-6/clay(1%), d- nylon-6/clay(5%), e- nylon-6/clay(10%))

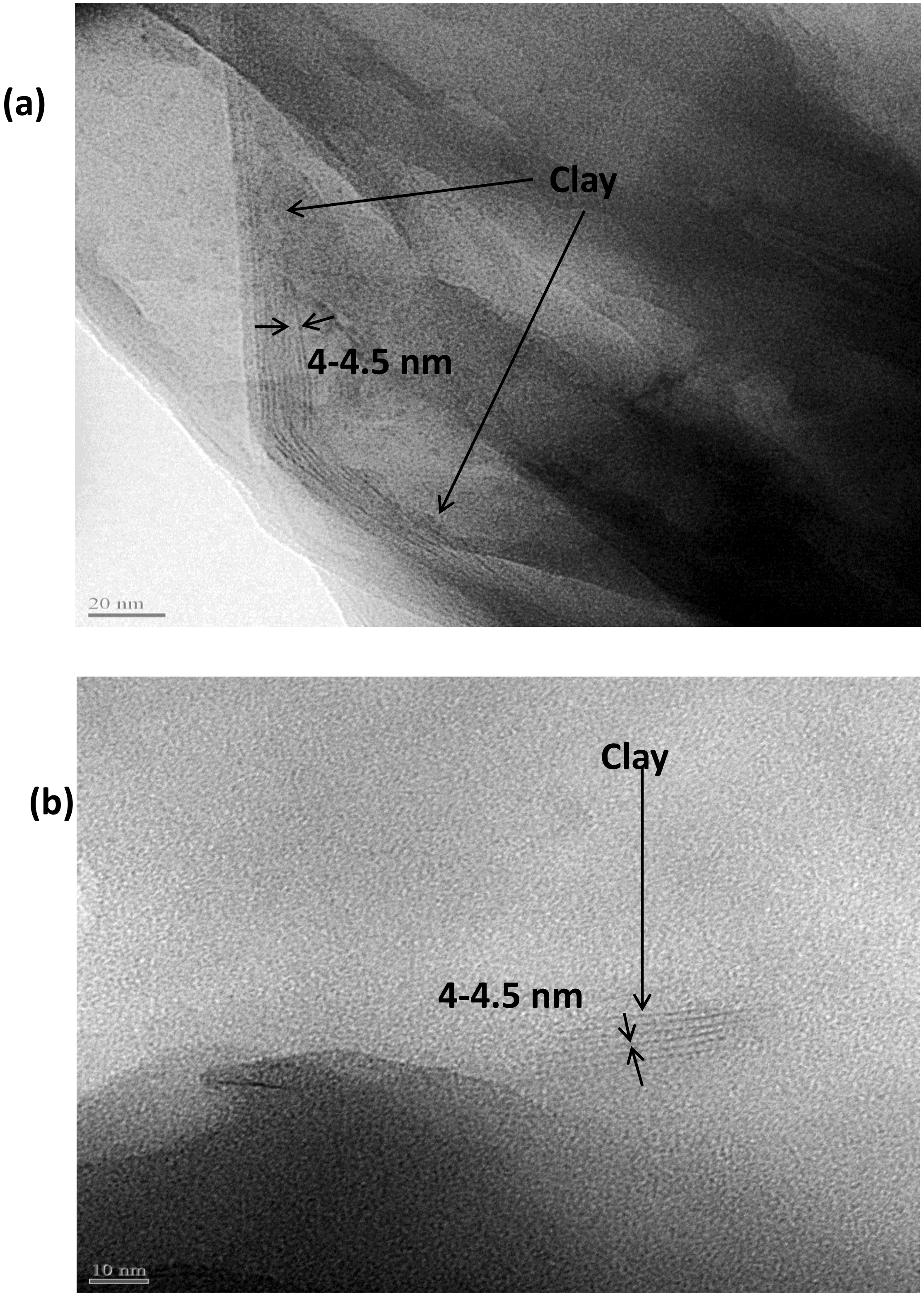

Figure 45 – TEM images for nylon-6/clay (a-5% and b-10%)

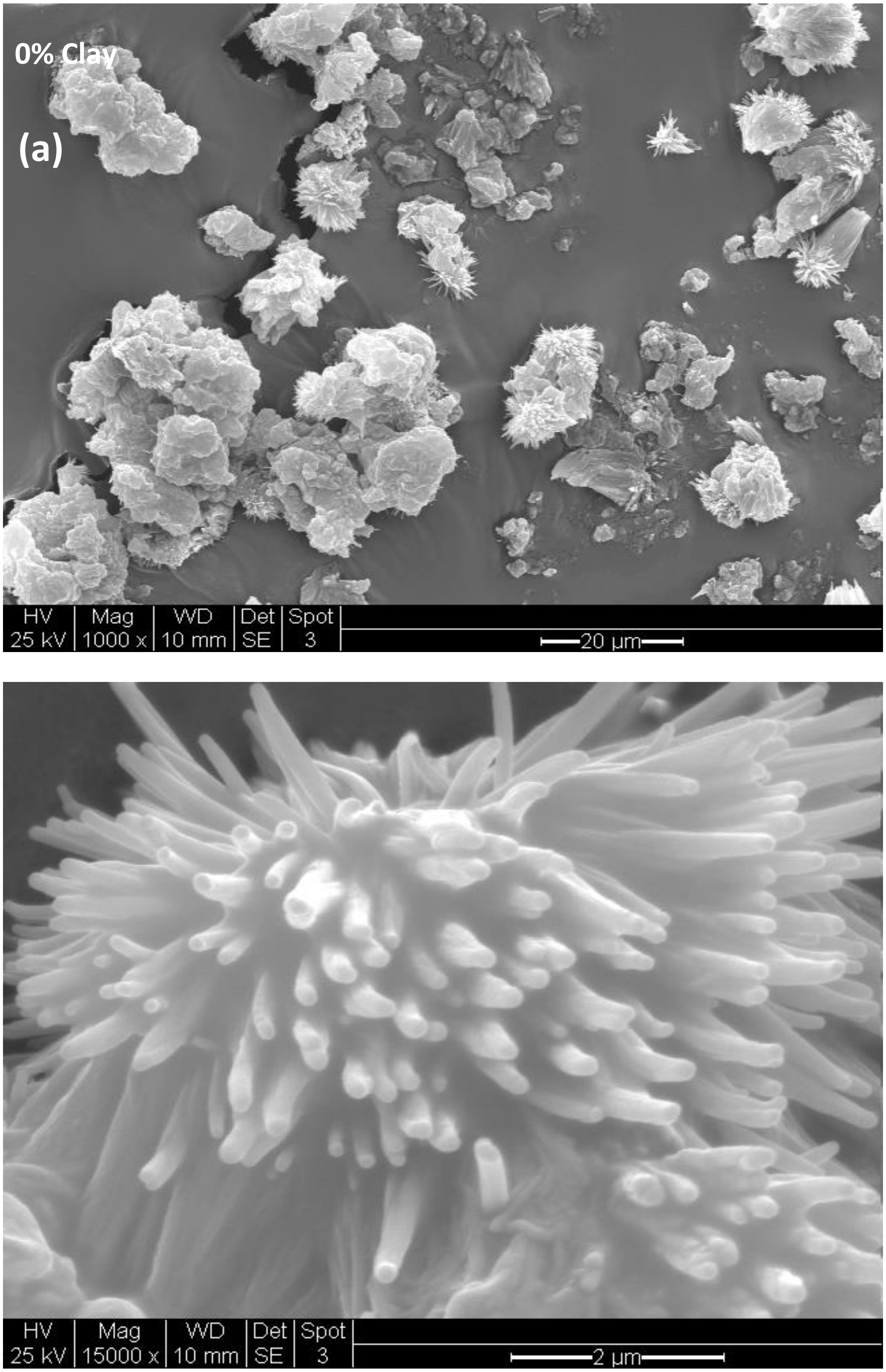

Figure 46 a – SEM images of neat nylon-6

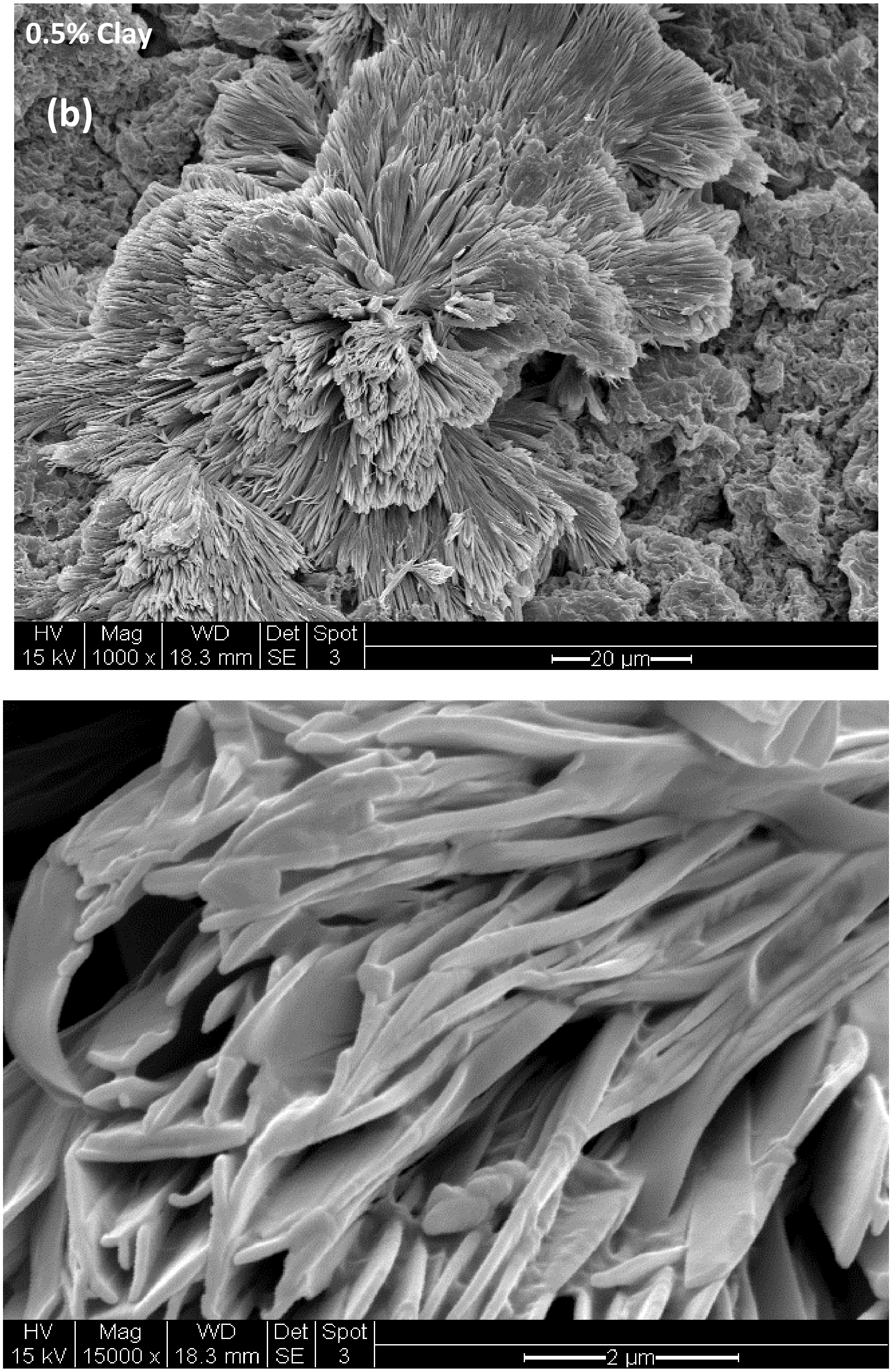

Figure 46 b – SEM images of neat nylon-6/clay (0.5 wt%)

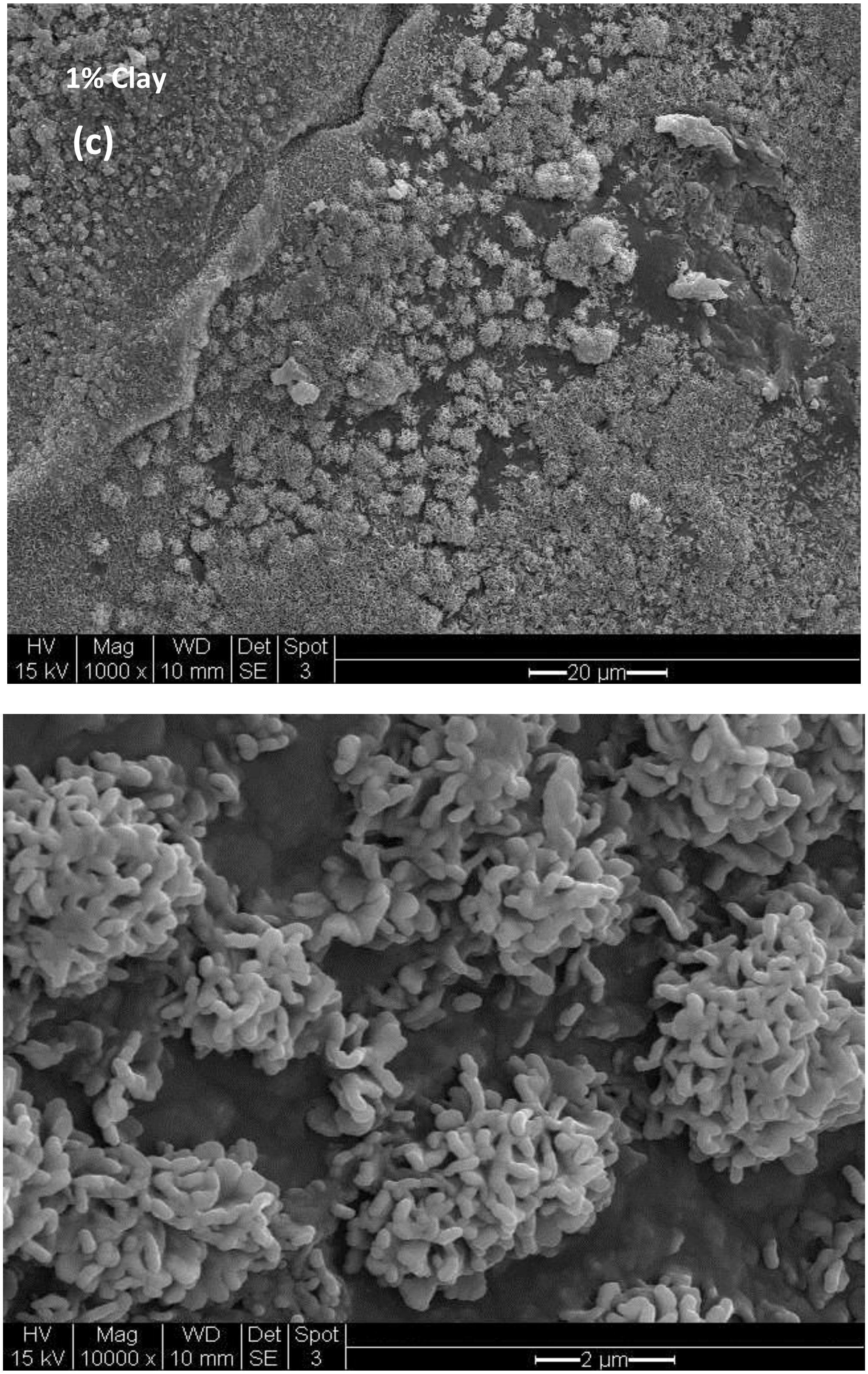

Figure 46 c – SEM images of neat nylon-6/clay (1 wt.%)

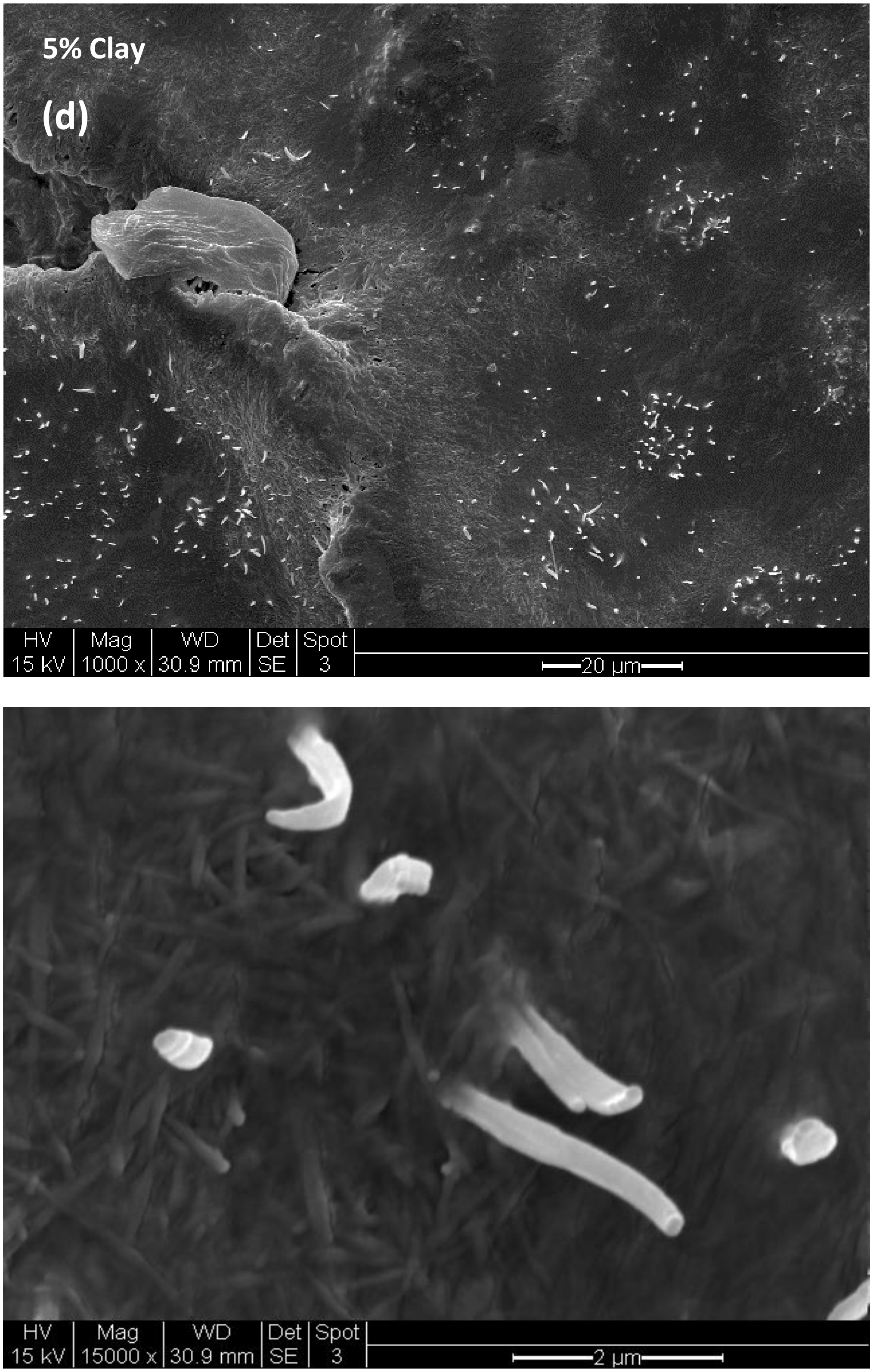

Figure 46 d – SEM images of neat nylon-6/clay (5 wt%)

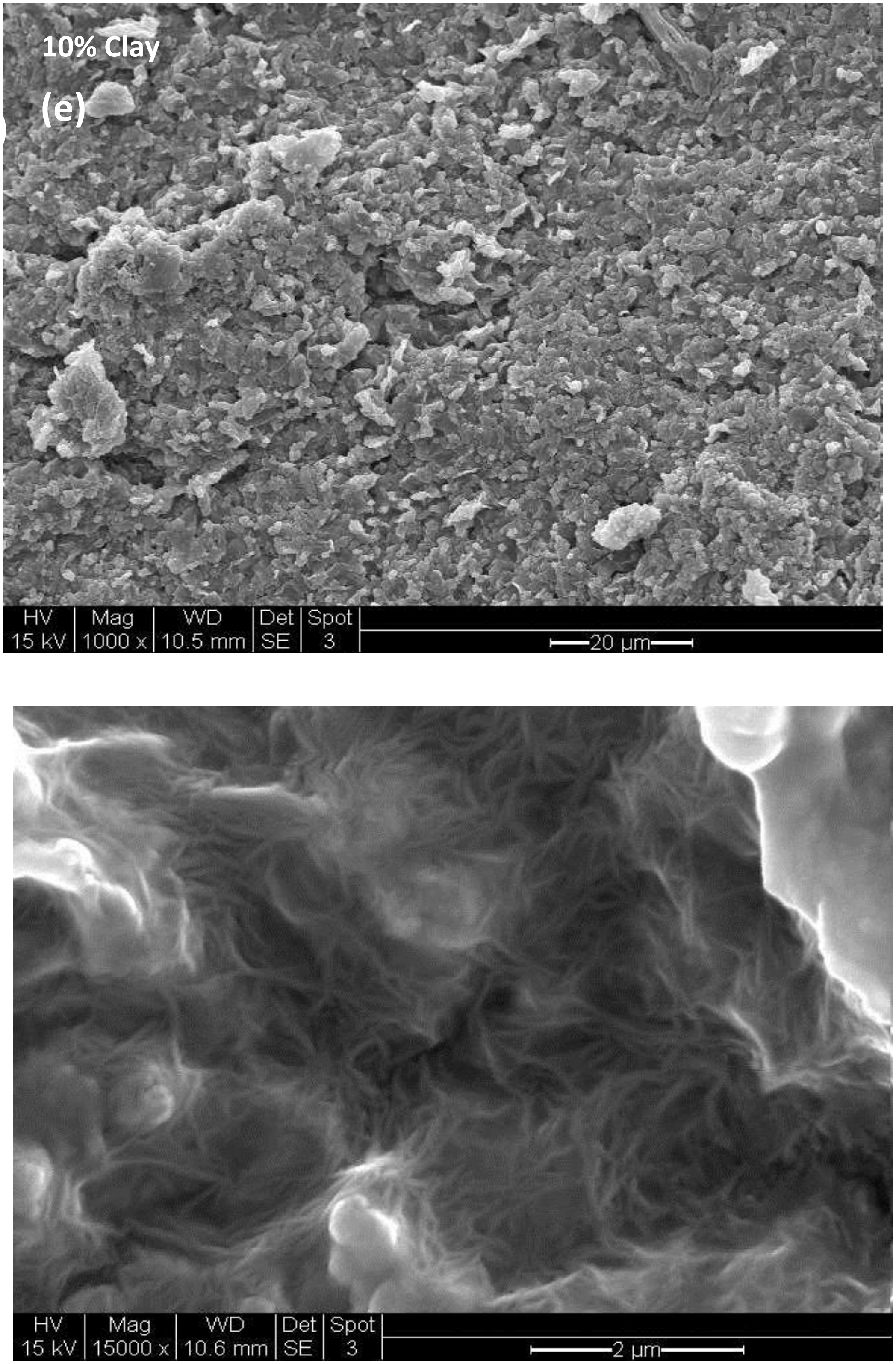

Figure 46 e – SEM images of neat nylon-6/clay (10 wt.%)

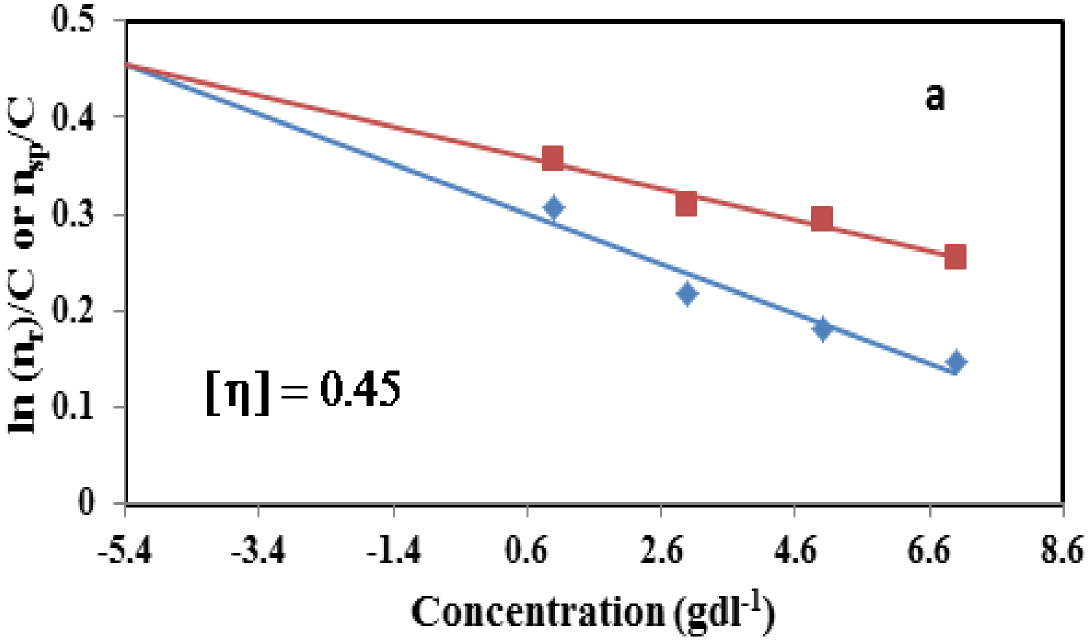

Figure 47a – Dilute solution viscosity plots of neat nylon-6

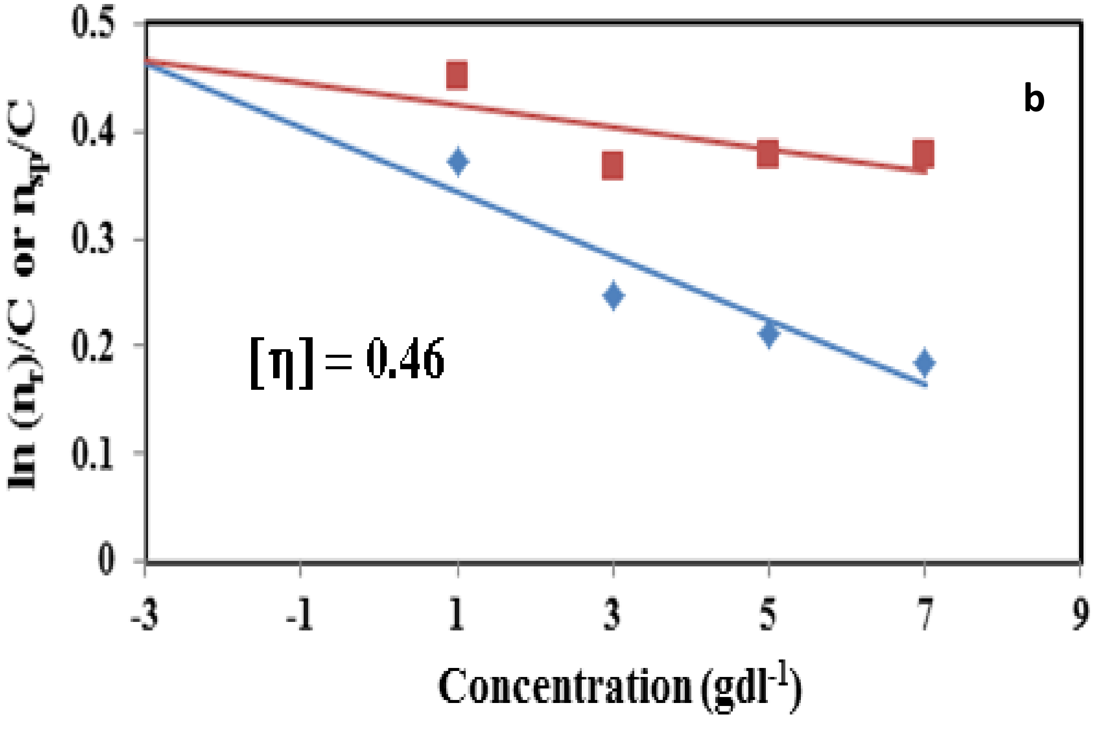

Figure 47b – Dilute solution viscosity plots of nylon-6/clay (0.5%)

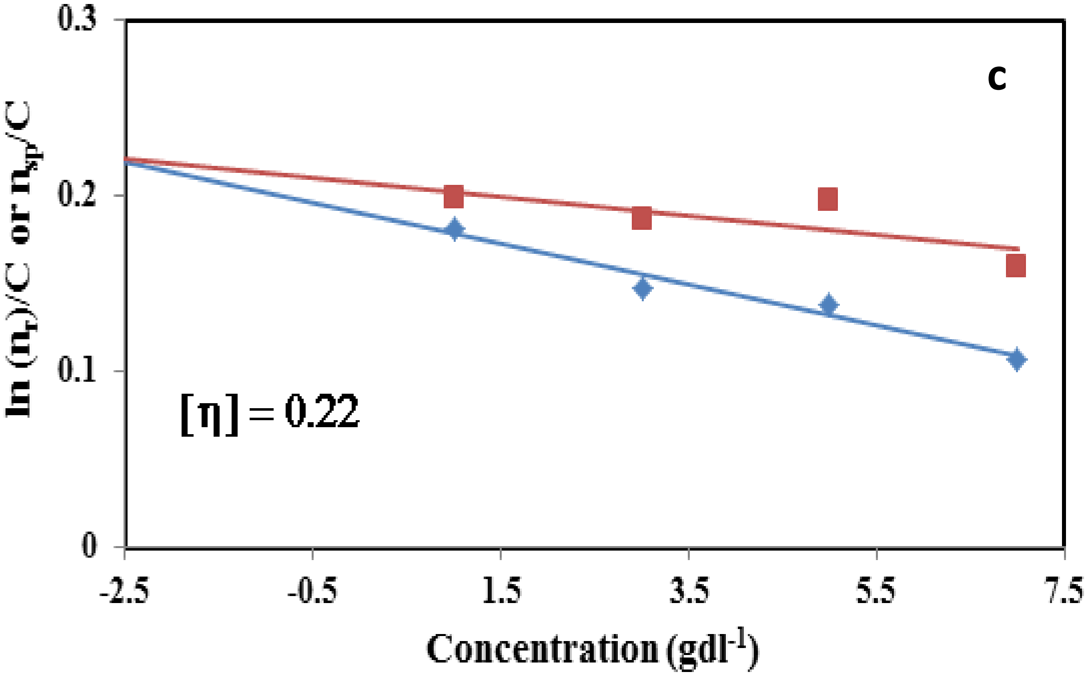

Figure 47c – Dilute solution viscosity plots of nylon-6/clay (1%)

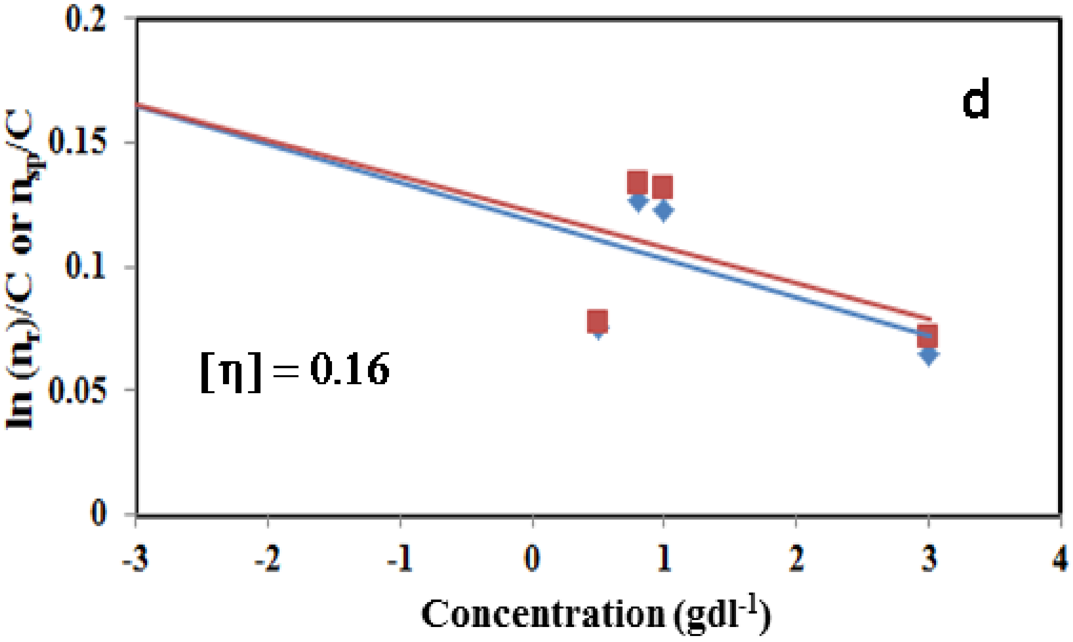

Figure 47d – Dilute solution viscosity plots of nylon-6/clay (5%)

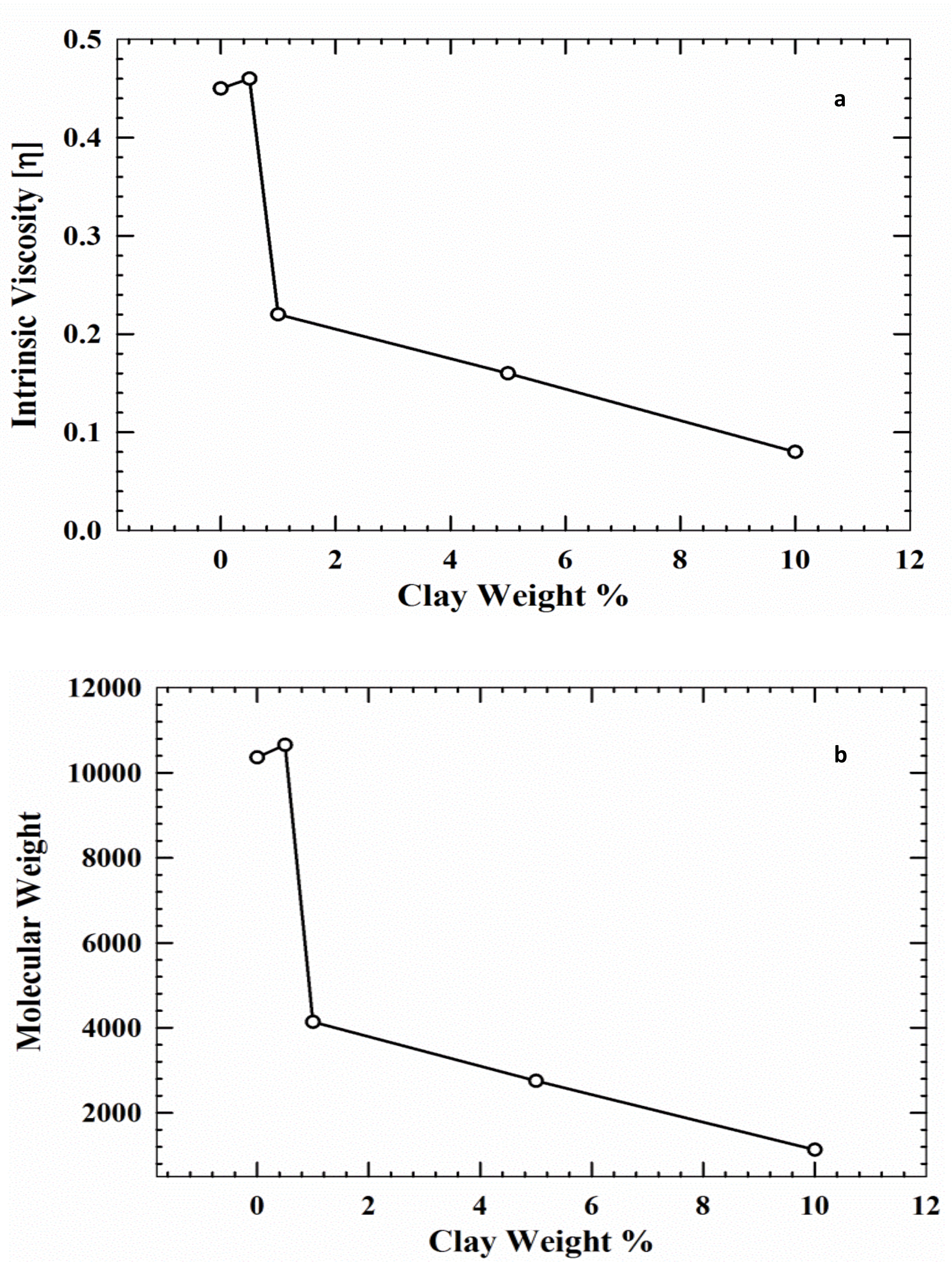

Figure 48- (a) Intrinsic Viscosity and (b) Molecular weight of clay/nylon-6 composite as a function of clay concentration.

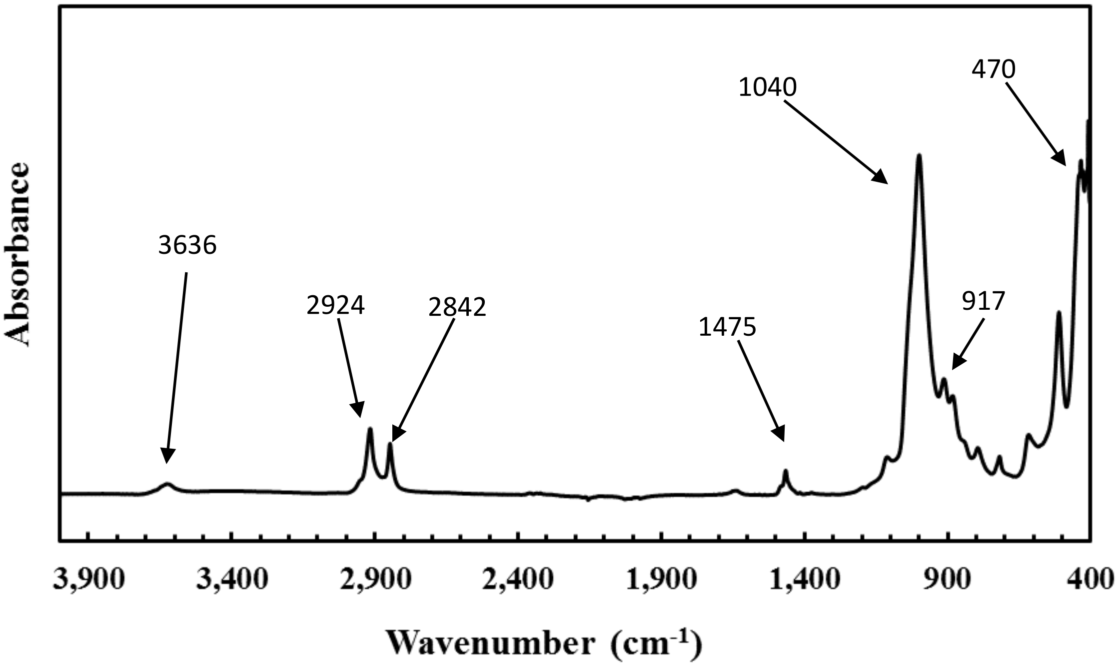

Figure 49 – FTIR spectrum of Cloisite 15A clay

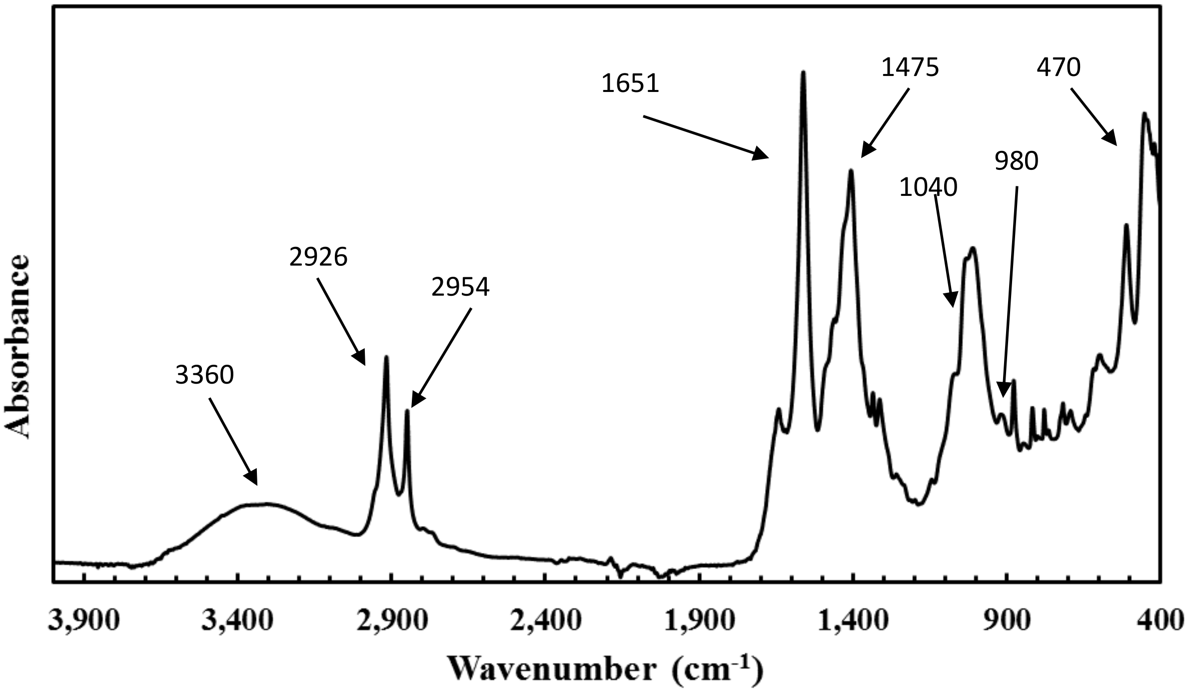

Figure 50 – FTIR spectrum of clay/nylon-6 (10 wt.%) nanocomposite

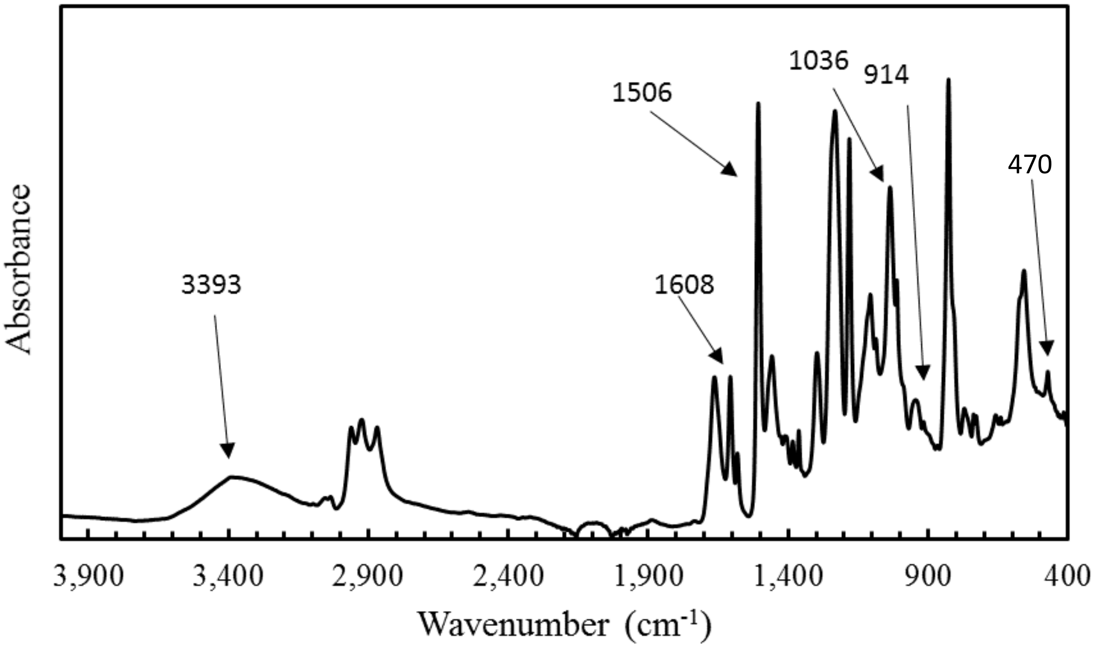

Figure 51 – FTIR spectrum of epoxy/nylon-6 (10wt.%) coating containing 0.1 wt.% of clay.

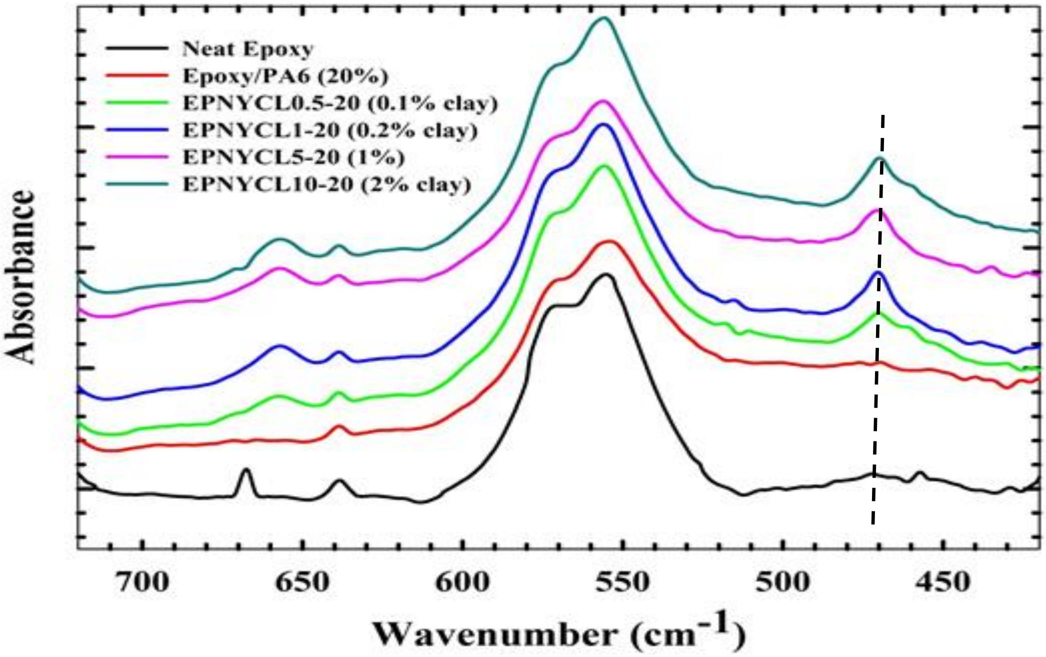

Figure 52 – FTIR spectrum for neat epoxy, nlyon-6/epoxy and clay/nylon-6-epoxy systems showing peak at 470 cm^{-1}

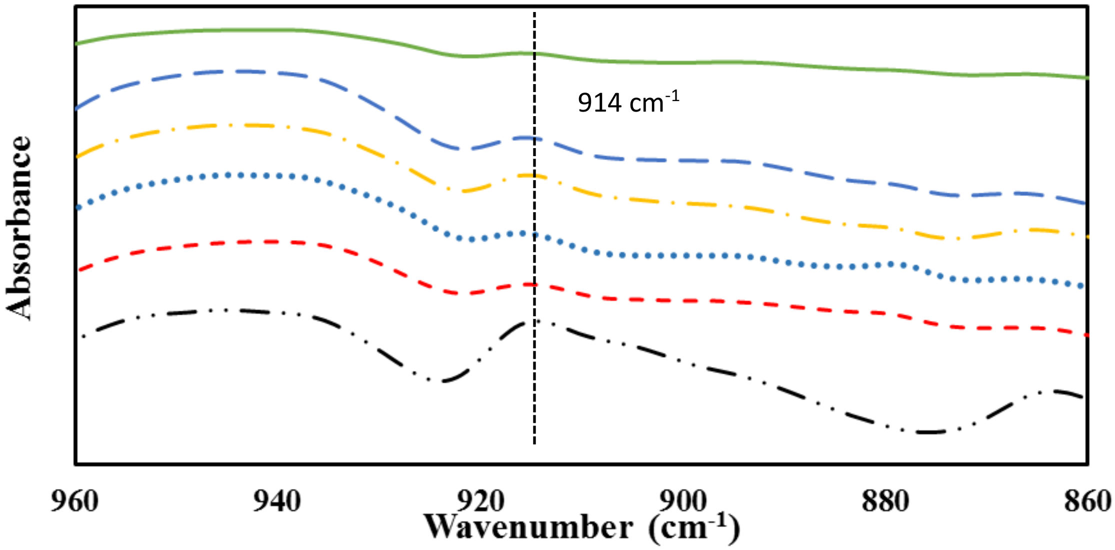

Figure 53– FTIR spectra for thermally treated neat epoxy and nylon-6/clay filled epoxy ((a) thermally treated epoxy, (b) 10 wt. % nylon-6 (0wt.% clay), (c) 0.05 wt.% clay, (d) 0.1wt.% clay, (e) 0.5 wt.% clay and (f) 0.1 wt.% clay in nylon-6/epoxy) heated in oven for 9 hours (70° C -3h, 100°C -2h, 120°C -2h, 150°C – 2h)

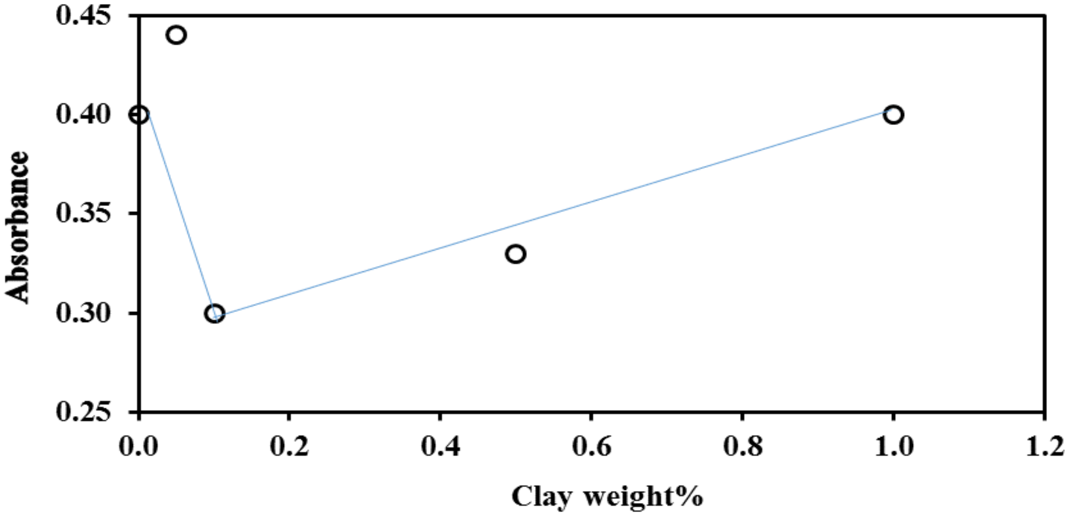

Figure 54 – Epoxy fractional Conversion as a function of nylon-6 wt. % all samples cured with stepwise heating for 9 hours upto 150°C

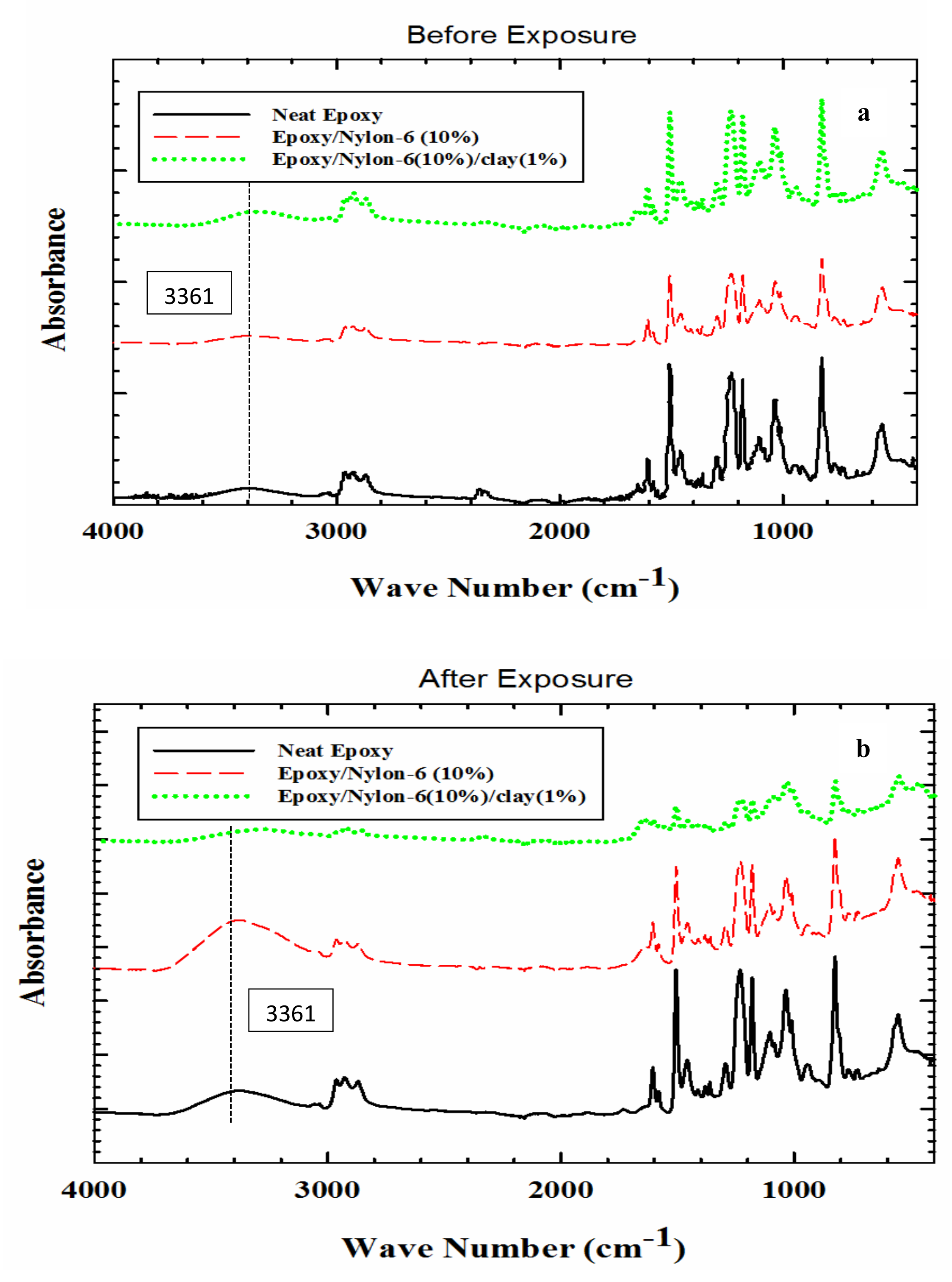

Figure 55 – FTIR spectrum of homo-polymerized neat epoxy, epoxy/nylon-6 and epoxy/nylon-6/clay (a) before exposure (b) after 2 months of exposure to 3.5 weight% salt solution

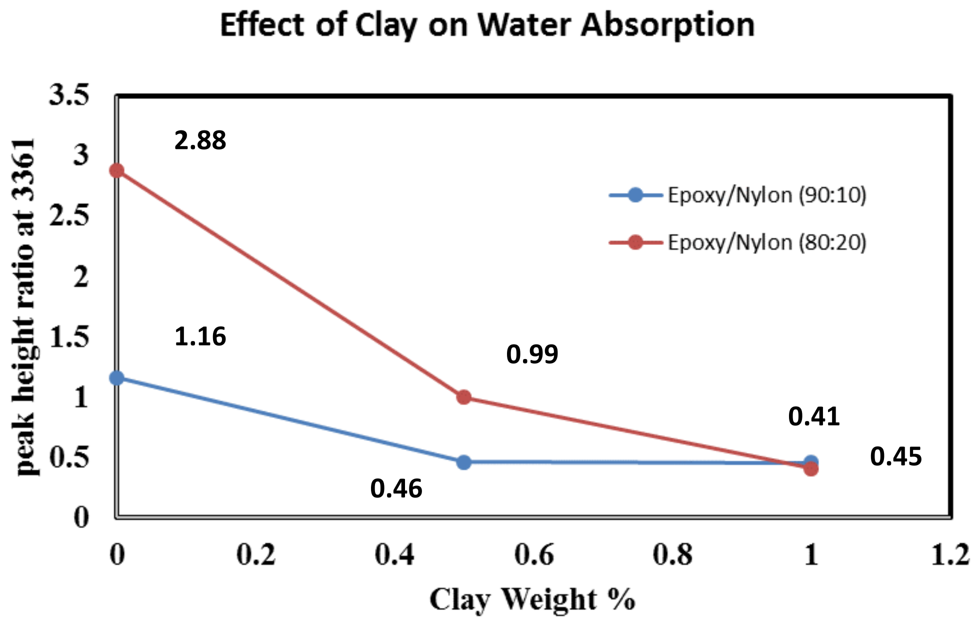

Figure 56 – Ratio of water absorption peak height at 3361 in FTIR after exposure to 3.5 weight% salt solution for 2 months to that of fresh sample.

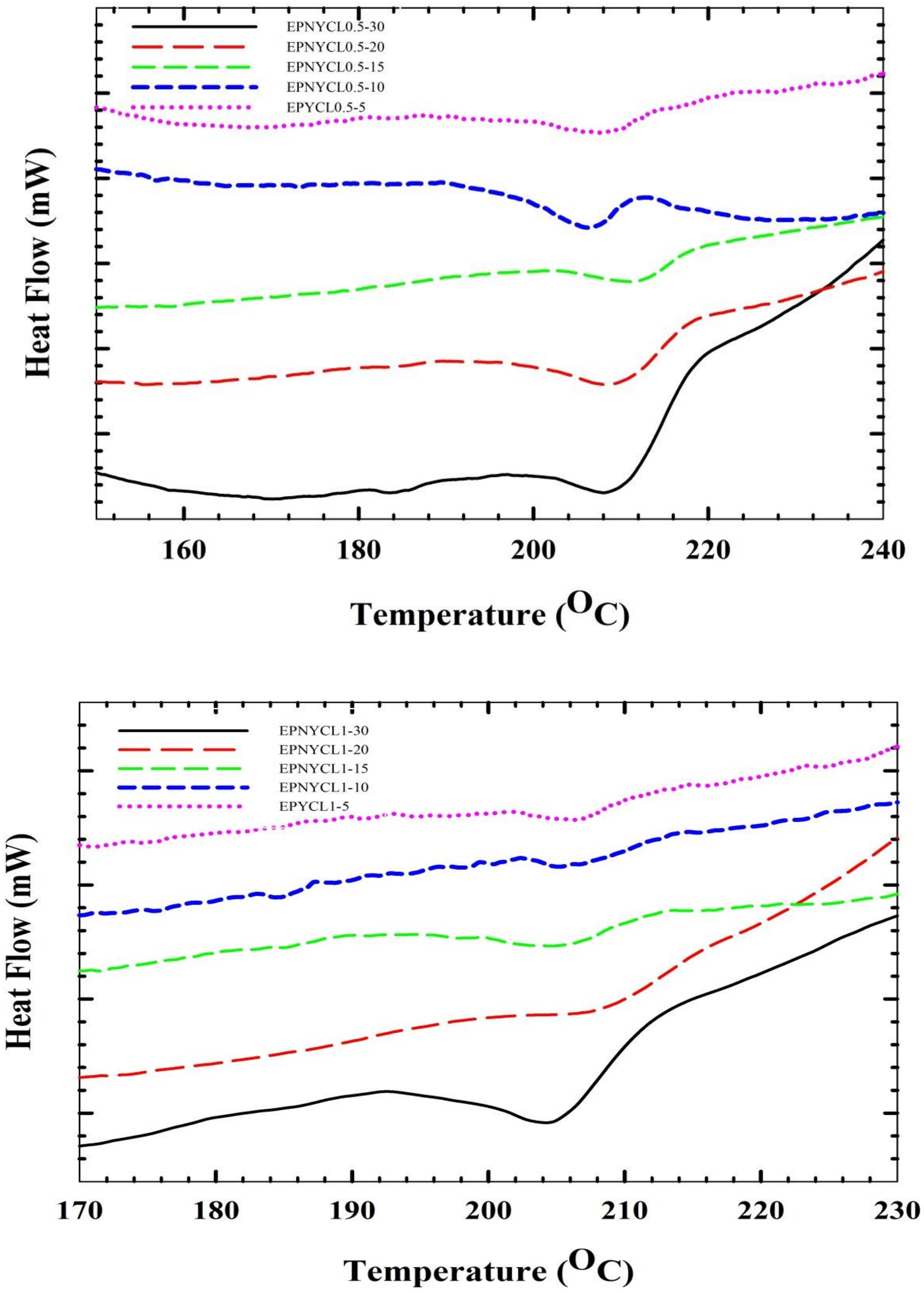

Figure 57 – DSC Melting peak for (a) EPNYCL0.5 and (b) EPNYCL1 at heating rate of 5^{O}C/min

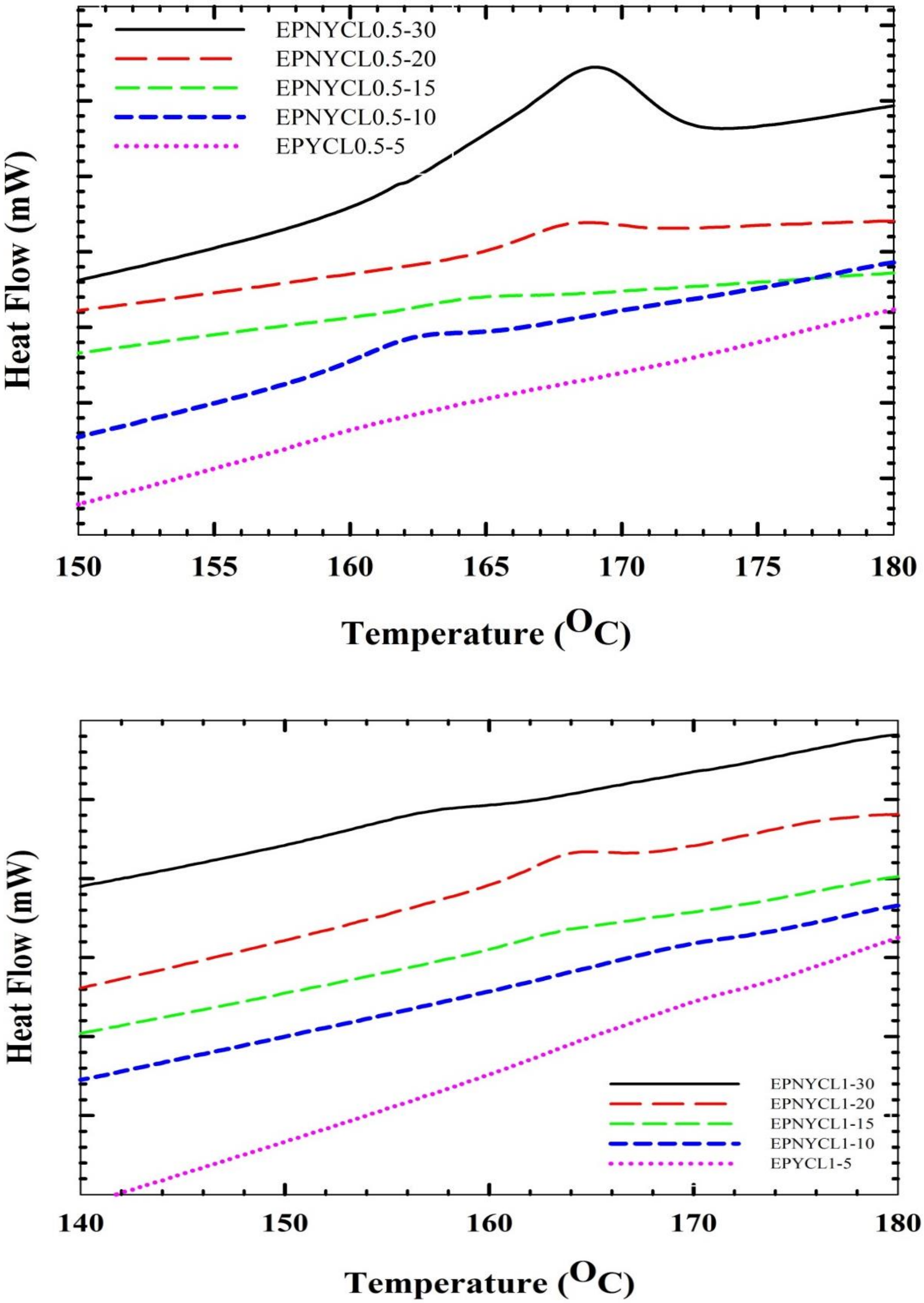

Figure 58 – DSC Crystallization peak for (a) EPNYCL0.5 and (b) EPNYCL1 at heating rate of

5^{O}C/min

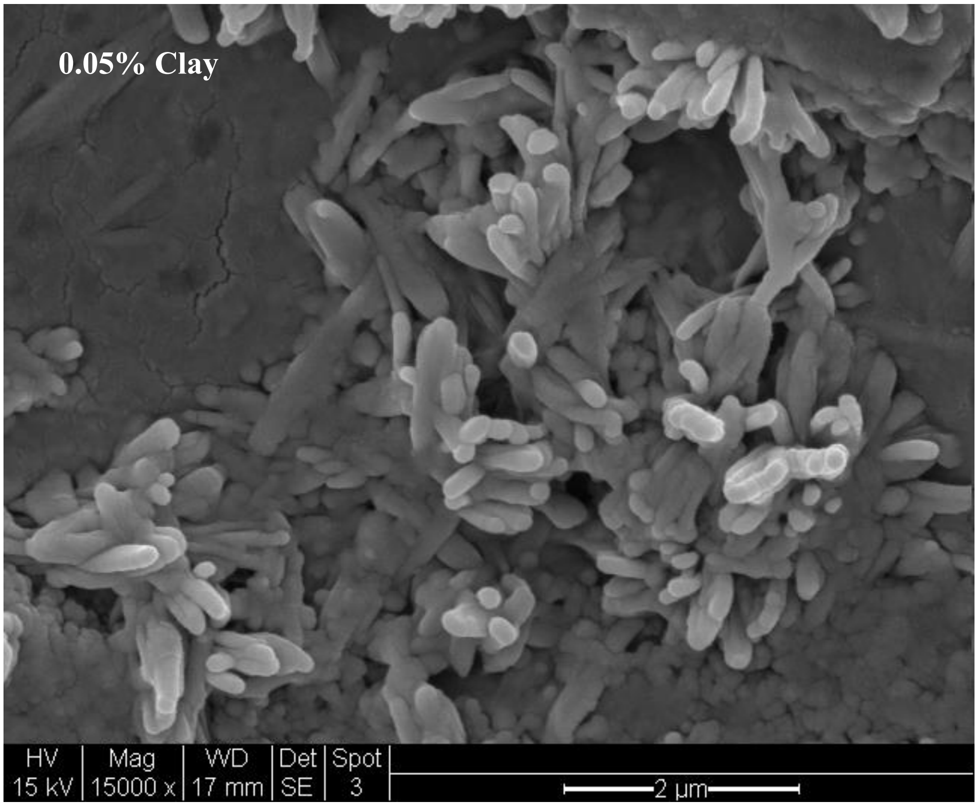
0.05% Clay
HV 15 kV
Mag 15000 x
WD 17 mm
Det SE
Spot 3
2 µm

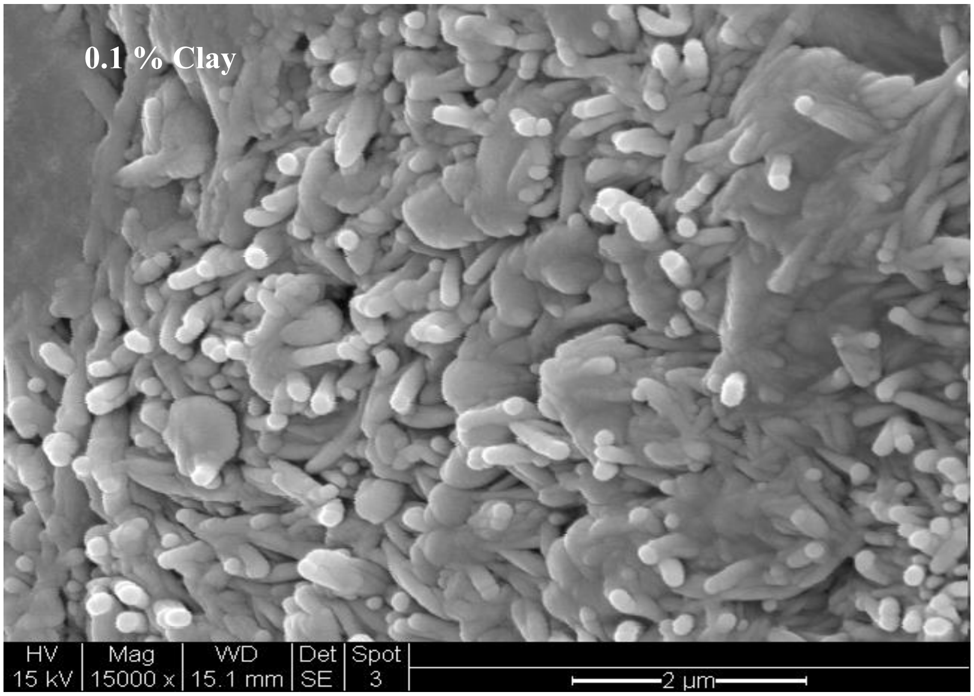
0.1 % Clay
HV 15 kV
Mag 15000 x
WD 15.1 mm
Det SE
Spot 3
2 µm

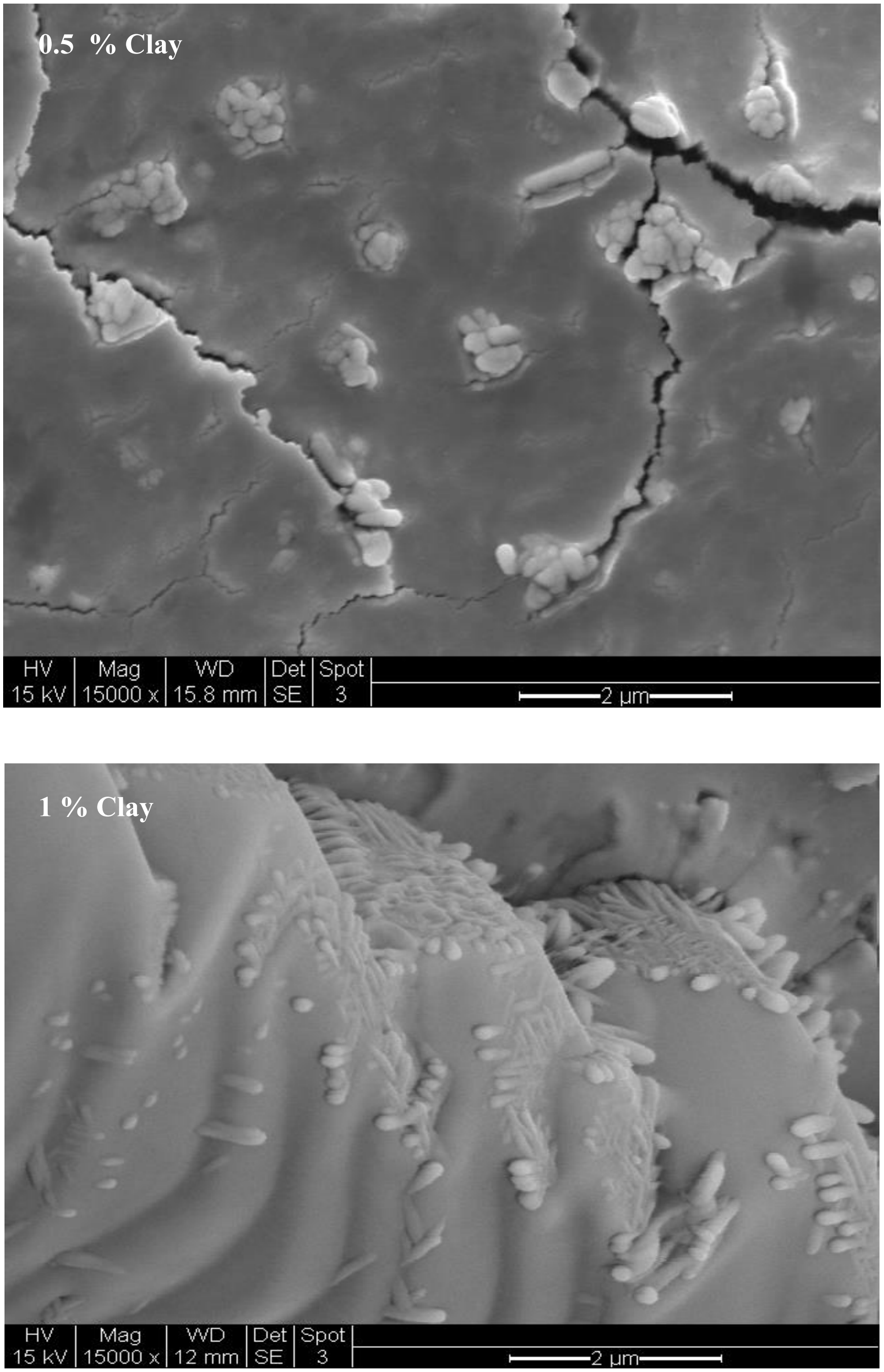

Figure 59 – SEM images of cross-section of fractured surface of clay/nylon-6-epoxy system at constant epoxy:nylon 6 ratio of 90 : 10

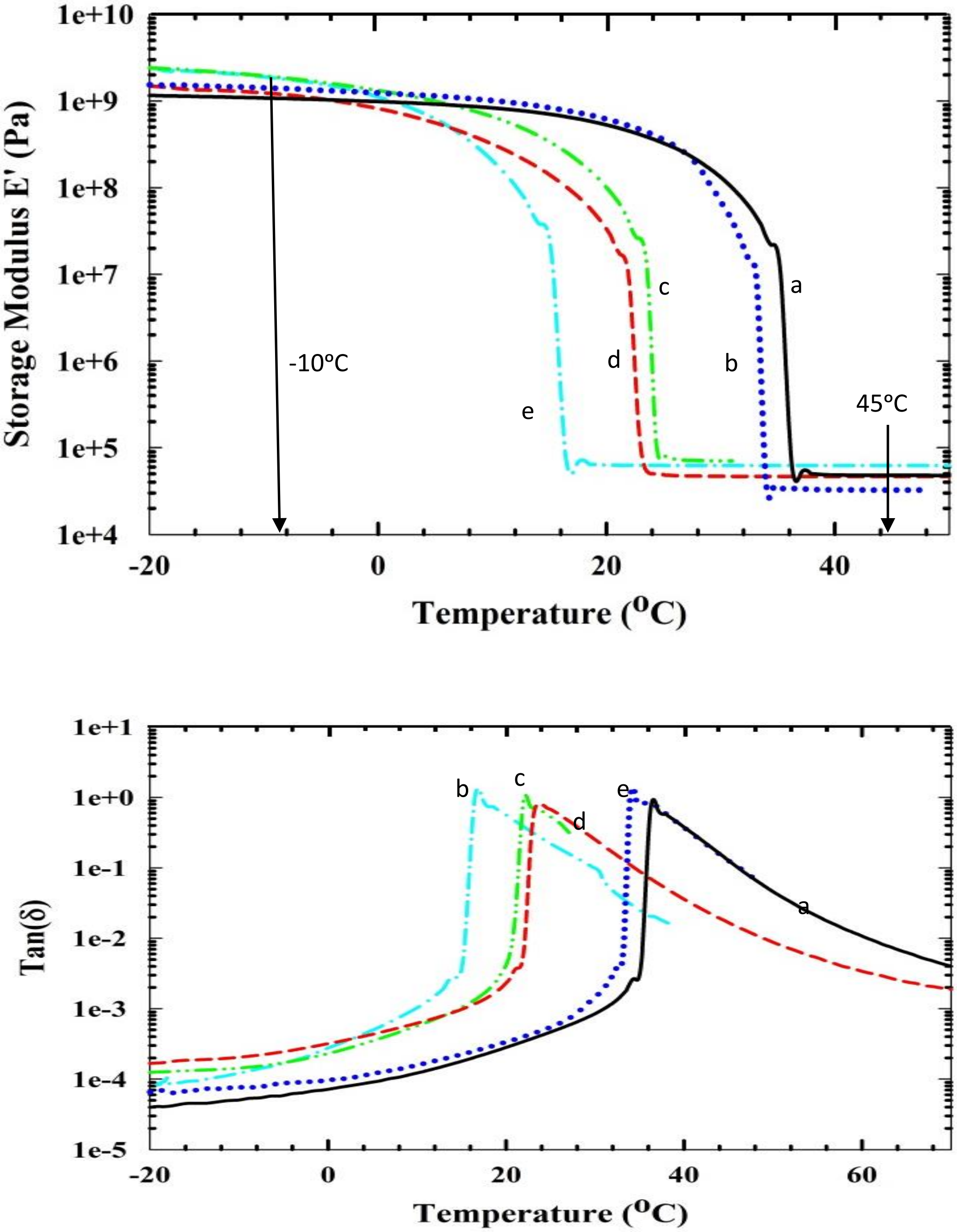

Figure 60 – Dynamic Mechanical Properties (storage modulus and tan(δ) as a function of temperature) of Clay-nylon-6/epoxy componensts at epoxy: nylon ratio of 90:10 by weight (a-0 wt.% clay, b- 0.05 wt.% clay, c- 0.1 wt.% clay, d- 0.5 wt.% clay and 1wt.% clay with respect to solid content of epoxy)

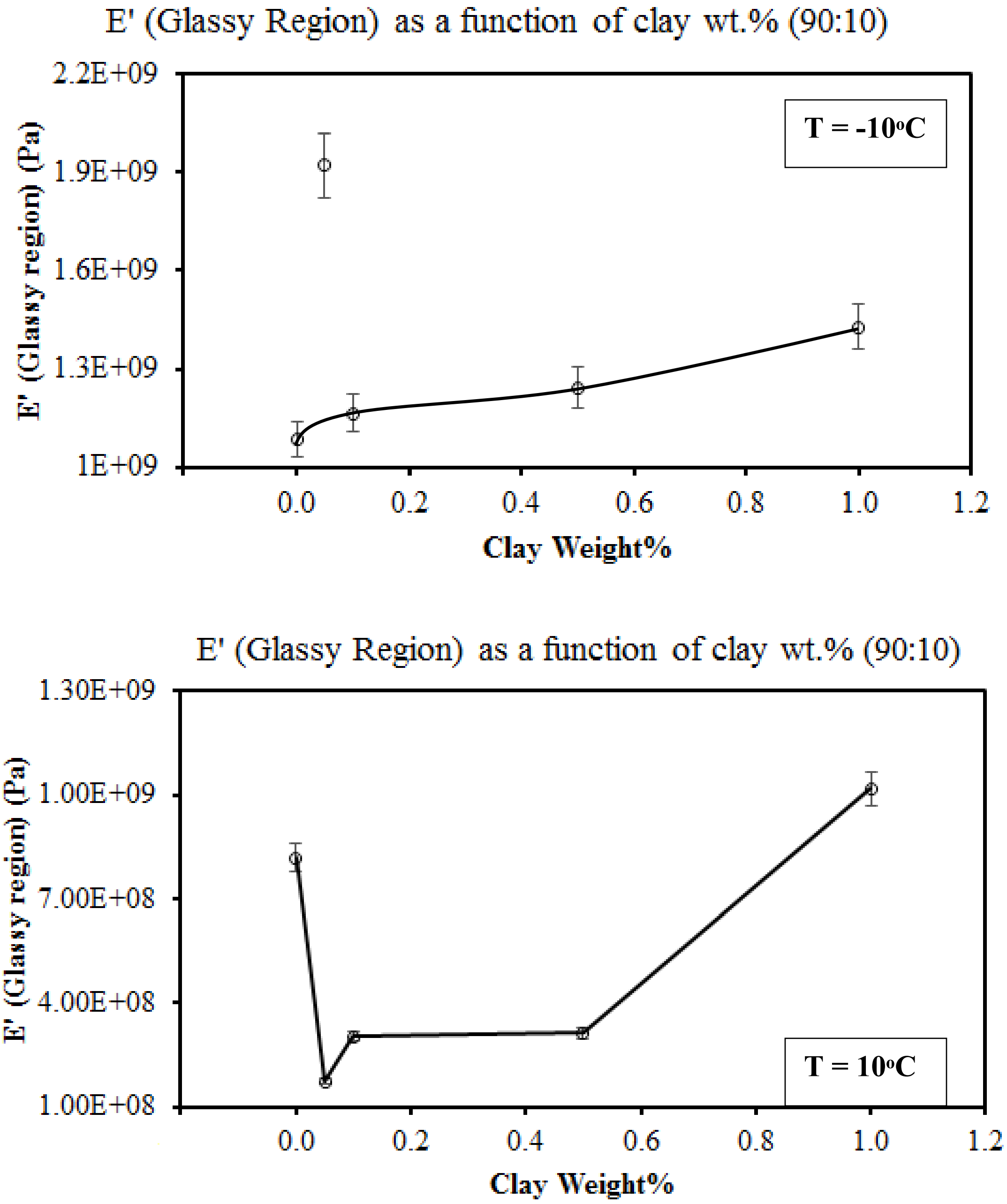

Figure 61 –Storage Modulus of clay/nylon 6-epoxy nanocomposite films as a function of clay weight% (a) in glassy region at T=-10^{O}C (b) in transition region at T=10^{O}C

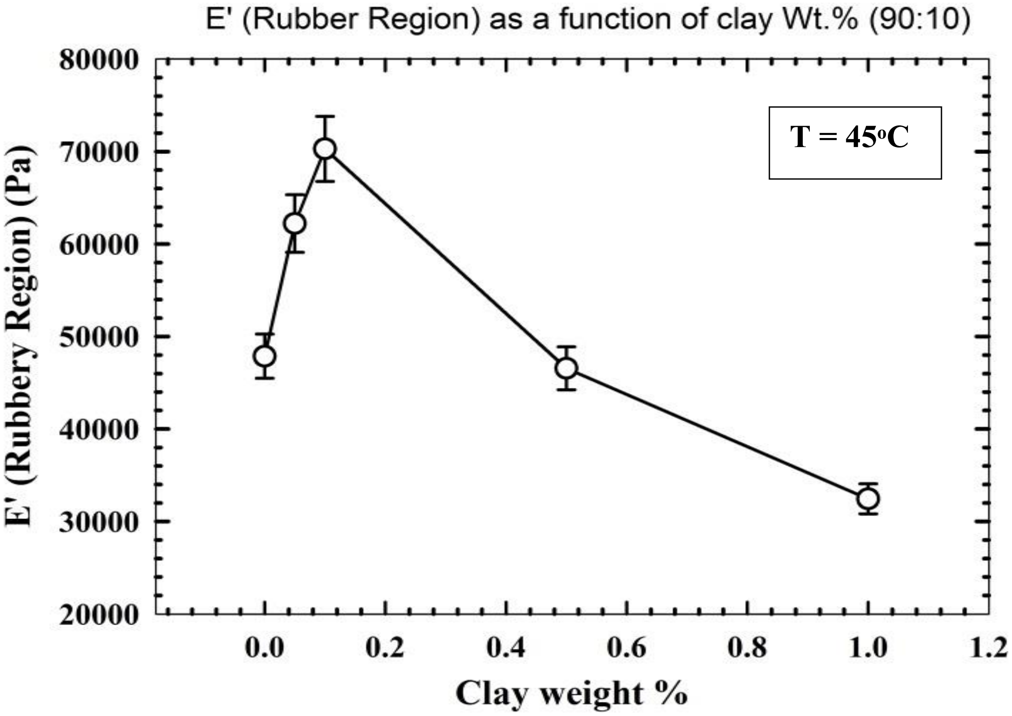

Figure 62 –Storage Modulus of clay/nylon 6-epoxy nanocomposite films as a function of clay weight% in rubbery region at T=45^{O}C

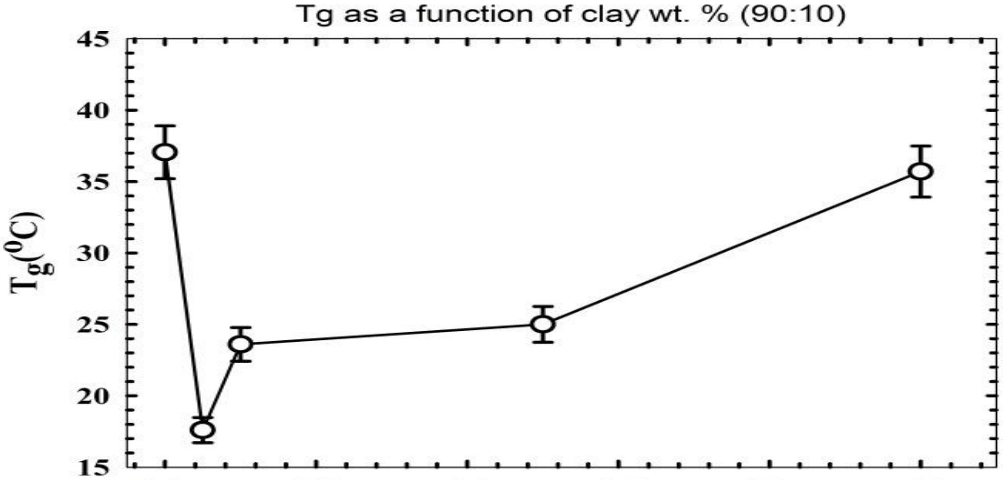

Figure 63 –Glass transition temperature of clay/nylon 6-epoxy nanocomposite films as a function of clay weight% for epoxy: nylon-6 ratio of 90:10.

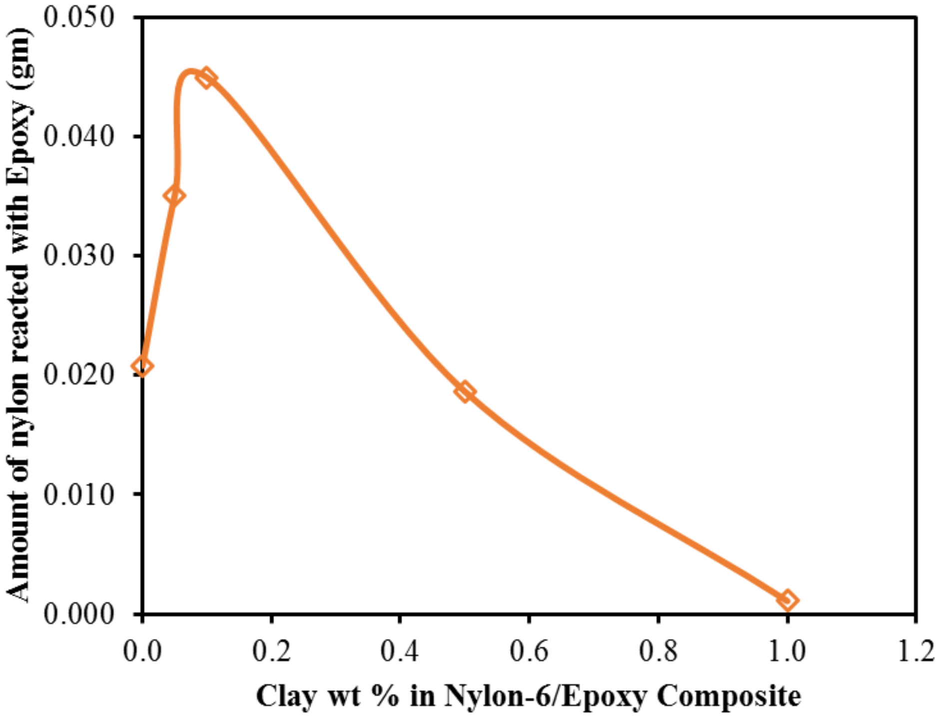

Figure 64 – Weight of nylon-6 reacted with epoxy as a function of clay weight%.

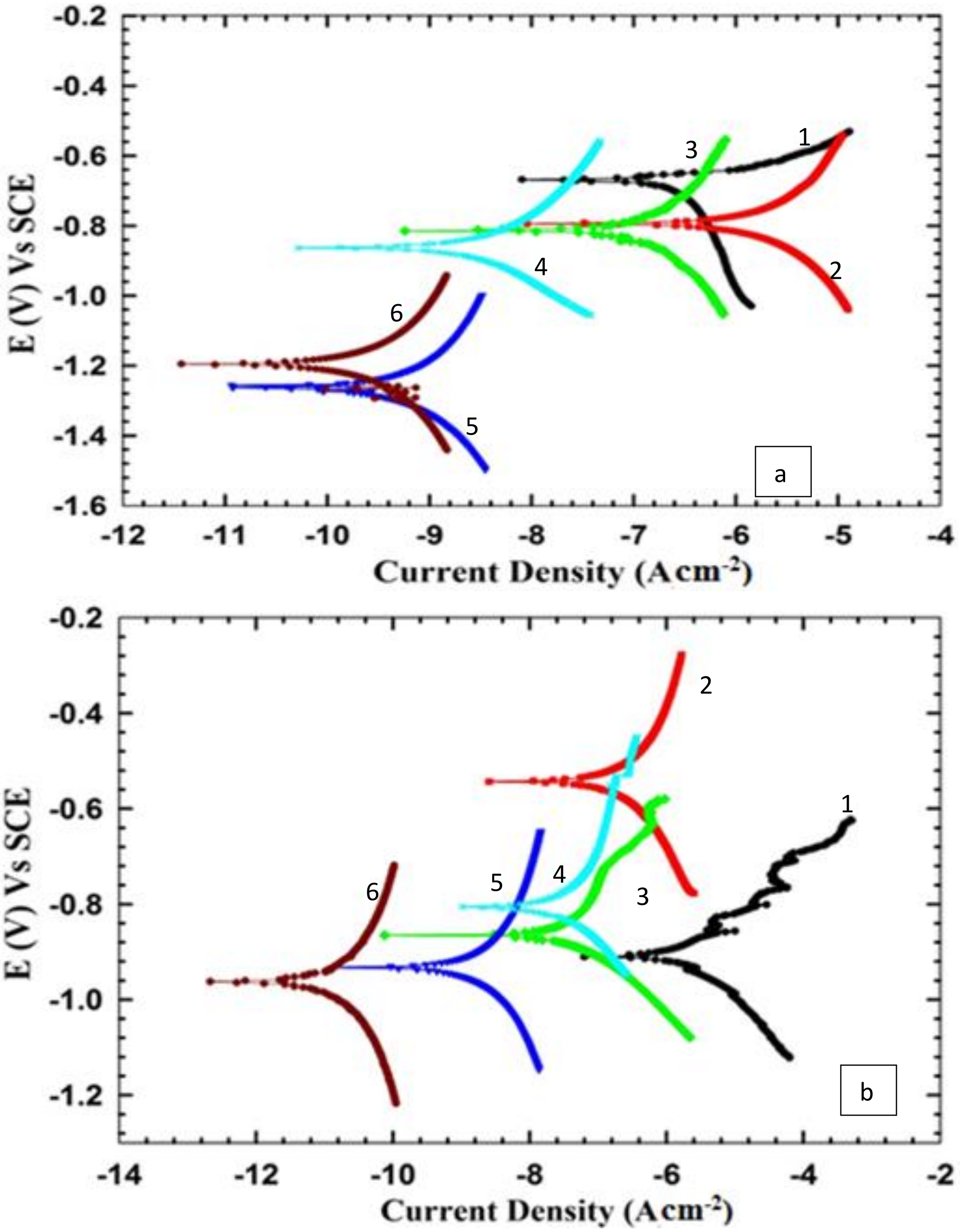

Figure 65 - DCP Plots for epoxy/nylon-6 (90:10) coatings on Al 2024-T3 alloy substrate filled with clay after (a) 1 day of exposure (b) after 2 months of exposure to 3.5 weight% salt solution (1- thermally cured neat epoxy, 2- epoxy/nylon-6(10wt.%), 3 - 0.05wt.% clay, 4 – 0.1 wt.% clay, 5- 0.5 wt.% clay, 6- 1 wt.% clay with respect to solid content in epoxy).

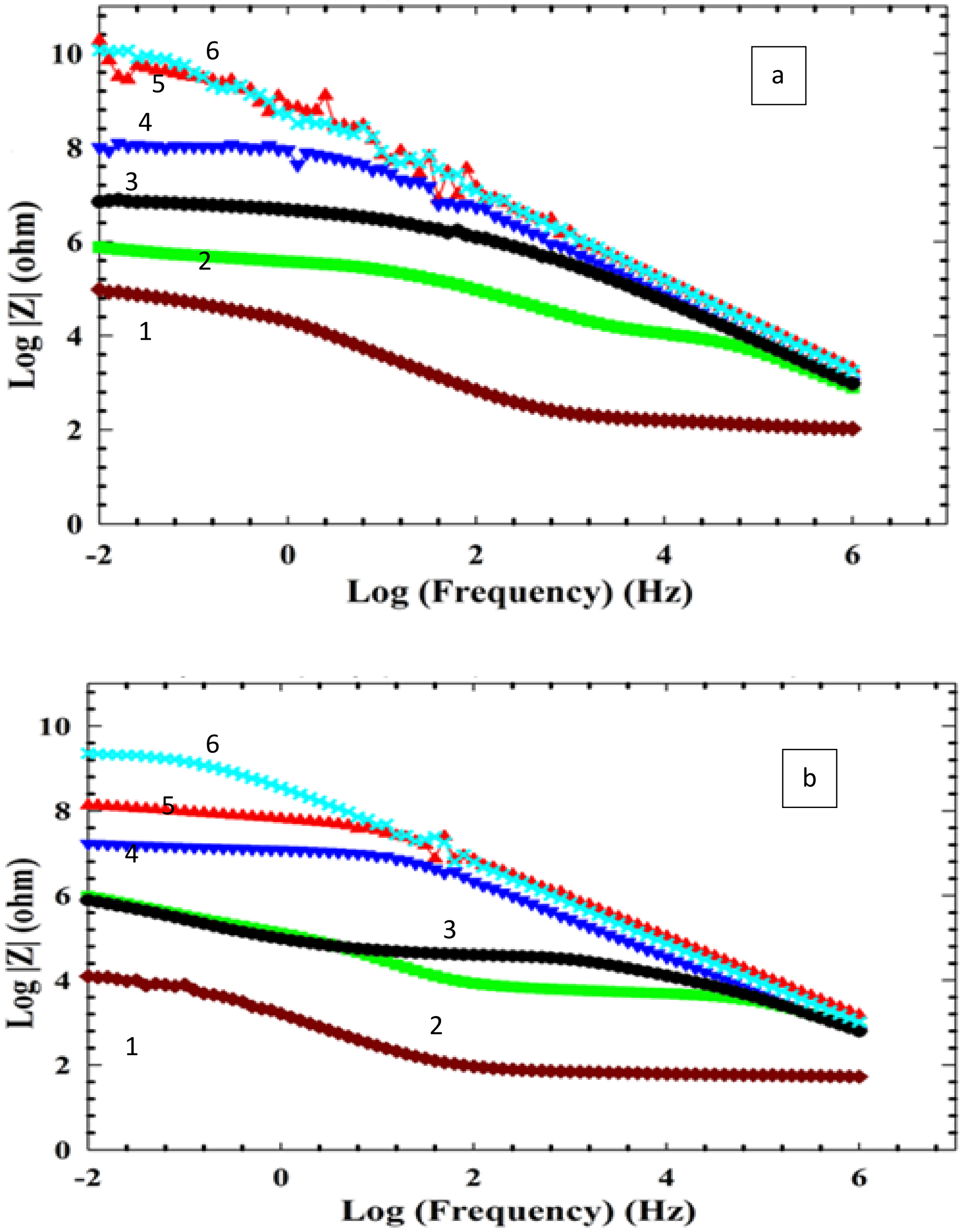

Figure 66 - Bode Plots for clay modified nylon-6 filled epoxy coatings on Al 2024-T3 alloy substrate after exposure to 3.5% salt solution for 2 months at epoxy: nylon-6 ratio of 90:10 (a) after 1 day of exposure (b) after 2 months of exposure to 3.5 weight% salt solution. (1- thermally cured neat epoxy, 2- epoxy/nylon-6(10wt.%), 3 - 0.05wt.% clay, 4 – 0.1 wt.% clay, 5- 0.5 wt.% clay, 6- 1 wt.% clay with respect to solid content in epoxy)

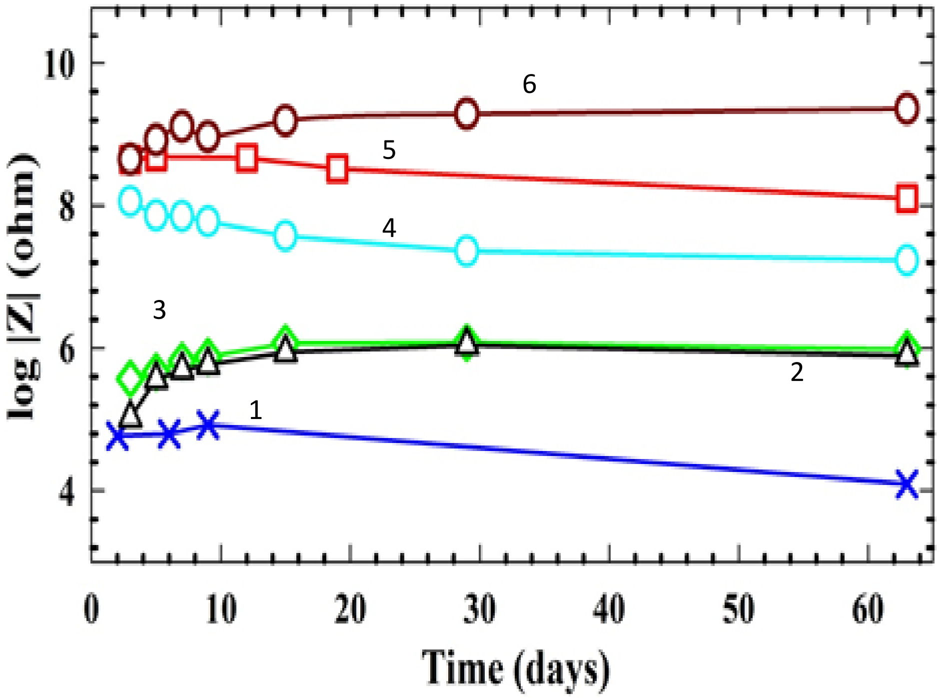

Figure 67 – Impedance |Z| at frequency of 0.1 Hz for clay modified nylon-6/epoxy coatings on Al 2024-T3 alloy substrate as a function of exposure time for epoxy: nylon-6 ratio of 90: 10 (1- thermally cured neat epoxy, 2- epoxy/nylon-6(10wt.%), 3 - 0.05wt.% clay, 4 – 0.1 wt.% clay, 5- 0.5 wt.% clay, 6- 1 wt.% clay with respect to solid content in epoxy)

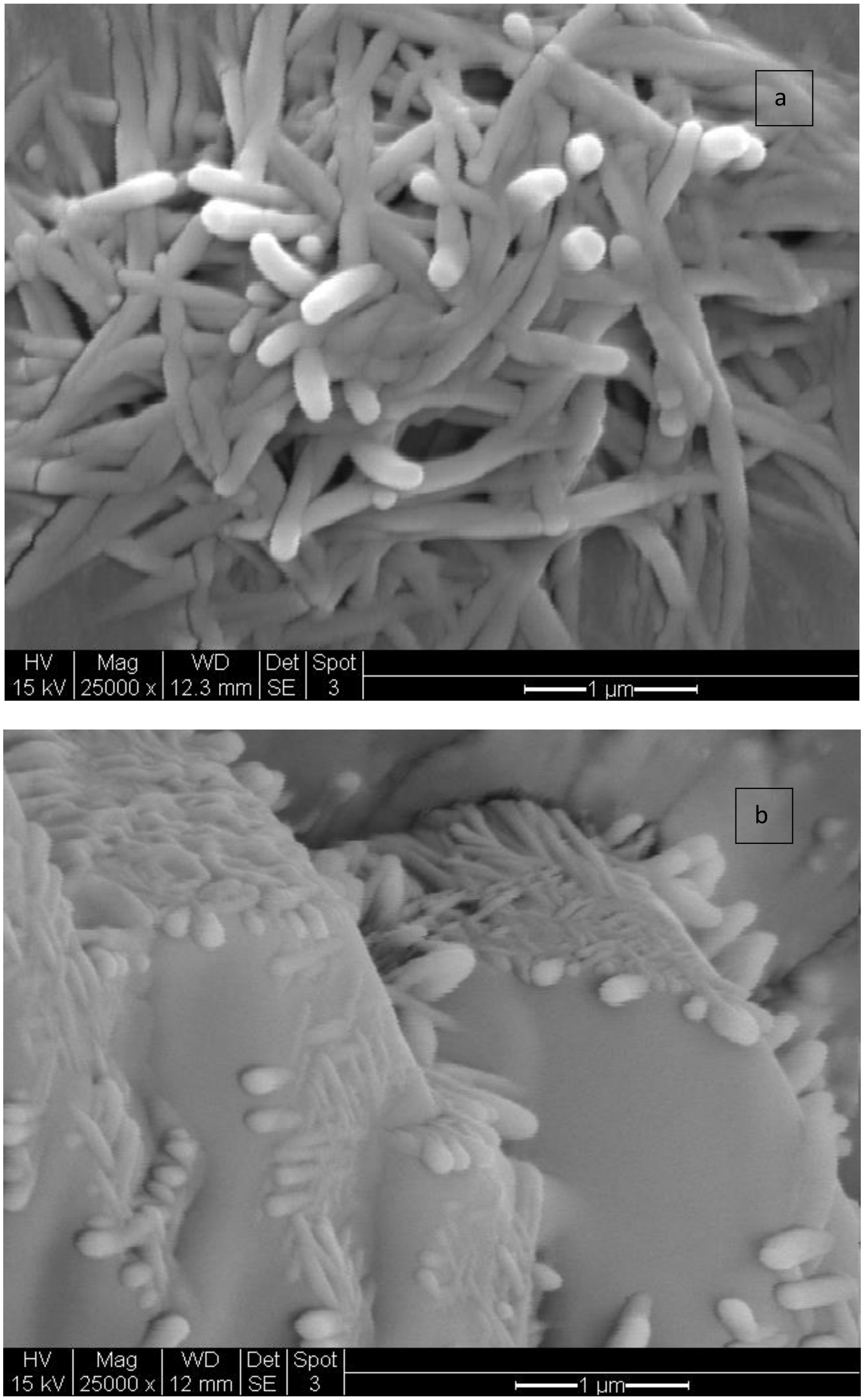

Figure 68 – SEM image of epoxy coating (a) containing 10 weight% of nylon and 0.05 weight% of clay, (c) containing 10 weight% of nylon and 1 weight% of clay

References

[1] C.A. May, Epoxy Resins: Chemistry and Technology, M. Dekker, 1988.

[2] L. Barone, S. Carciotto, G. Cicala, A. Recca, Thermomechanical properties of epoxy/poly(ε-caprolactone) blends, Polymer Engineering & Science, 46 (2006) 1576-1582.

[3] J.H. Luft, IMPROVEMENTS IN EPOXY RESIN EMBEDDING METHODS, The Journal of Biophysical and Biochemical Cytology, 9 (1961) 409-414.

[4] C.-S. Wang, J.R. Berman, L.L. Walker, A. Mendoza, Meta-bromobiphenol epoxy resins: Applications in electronic packaging and printed circuit board, Journal of Applied Polymer Science, 43 (1991) 1315-1321.

[5] S. Kim, J. Kim, S.H. Lim, W.H. Jo, C.R. Choe, Effects of mixing temperatures on the morphology and toughness of epoxy/polyamide blends, Journal of Applied Polymer Science, 72 (1999) 1055-1063.

[6] H. Lee, K. Neville, Handbook of epoxy resins, (1967).

[7] P.F. Bruins, P.I.o. Brooklyn, Epoxy resin technology, Interscience Publishers, 1968.

[8] E.N. Jacobsen, Asymmetric Catalysis of Epoxide Ring-Opening Reactions, Accounts of Chemical Research, 33 (2000) 421-431.

[9] F.H. Walker, Acid catalyzed polymerization of aqueous epoxy resin emulsions and uses thereof, in, Google Patents, 2001.

[10] P.K. Mallick, Fiber-Reinforced Composites: Materials, Manufacturing, and Design, Second Edition, Marcel Dekker, 1993.

[11] E. Oleinik, Epoxy-aromatic amine networks in the glassy state structure and properties, in: K. Dušek (Ed.) Epoxy Resins and Composites IV, Springer Berlin Heidelberg, 1986, pp. 49-99.

[12] H. Dodiuk, S. Kenig, Low temperature curing epoxies for structural repair, Progress in Polymer Science, 19 (1994) 439-467.

[13] J.M. Ready, E.N. Jacobsen, Highly Active Oligomeric (salen)Co Catalysts for Asymmetric Epoxide Ring-Opening Reactions, Journal of the American Chemical Society, 123 (2001) 2687-2688.

[14] X.M. Chen, B. Ellis, Coatings and other applications of epoxy resins, in: B. Ellis (Ed.) Chemistry and Technology of Epoxy Resins, Springer Netherlands, 1993, pp. 303-325.

[15] J. Comyn, C.C. Horley, D.P. Oxley, R.G. Pritchard, J.L. Tegg, The Application of Inelastic Electron Tunnelling Spectroscopy to Epoxide Adhesives, The Journal of Adhesion, 12 (1981) 171-188.

[16] Z. Wang, M. Xie, Y. Zhao, Y. Yu, S. Fang, Synthesis and properties of novel liquid ester-free reworkable cycloaliphatic diepoxides for electronic packaging application, Polymer, 44 (2003) 923-929.

[17] C. Beisele, B. Kultzow, Experiences with new hydrophobic cycloaliphatic epoxy outdoor insulation systems, Electrical Insulation Magazine, IEEE, 17 (2001) 33-39.

[18] R. Mezzenga, L. Boogh, J.-A.E. Månson, A review of dendritic hyperbranched polymer as modifiers in epoxy composites, Composites Science and Technology, 61 (2001) 787-795.

[19] S. Sourour, M.R. Kamal, Differential scanning calorimetry of epoxy cure: isothermal cure kinetics, Thermochimica Acta, 14 (1976) 41-59.

[20] A. Groβ, H. Kollek, A. Schormann, H. Brockmann, Spectroscopical contributions to the regioselectivity of nucleophilic curing reactions in epoxy resins, International Journal of Adhesion and Adhesives, 8 (1988) 147-158.

[21] L. Xu, J.H. Fu, J.R. Schlup, In situ Near-Infrared Spectroscopic Investigation of Epoxy Resin-Aromatic Amine Cure Mechanisms, Journal of the American Chemical Society, 116 (1994) 2821-2826.

[22] S.A. Gedur, Comparative characteristics of epoxy polymer-based optical materials, J. Opt. Technol., 66 (1999) 129.

[23] C. Zilg, R. Mülhaupt, J. Finter, Morphology and toughness/stiffness balance of nanocomposites based upon anhydride-cured epoxy resins and layered silicates, Macromolecular Chemistry and Physics, 200 (1999) 661-670.

[24] W.S. Johnson, A.C.D.-o.H.M. Fibers, T. Composites, A.C.E.-o.F. Testing, Delamination and Debonding of Materials: A Symposium Sponsored by ASTM Committees D-30 on High Modulus Fibers and Their Composites and E-24 on Fracture Testing, Pittsburgh, Pa., 8-10 Nov. 1983, ASTM, 1985.

[25] L. Li, Y. Yu, Q. Wu, G. Zhan, S. Li, Effect of chemical structure on the water sorption of amine-cured epoxy resins, Corrosion Science, 51 (2009) 3000-3006.

[26] J.R. Vinson, Advanced Composite Materials, Environmental Effects: A Symposium, Dayton, Ohio, 29 - 30 Sept. 1977, ASTM, 1978.

[27] Adhesive Technology Formulations Hand Book, Engineers India Research Institute, 2005.

[28] G. Levita, S. Petris, A. Marchetti, A. Lazzeri, Crosslink density and fracture toughness of epoxy resins, J Mater Sci, 26 (1991) 2348-2352.

[29] R. Thomas, A. Boudenne, L. Ibos, Y. Candau, S. Thomas, Thermophysical properties of CTBN and HTPB liquid rubber modified epoxy blends, Journal of Applied Polymer Science, 116 (2010) 3232-3241.

[30] C.B. Bucknall, A.H. Gilbert, Toughening tetrafunctional epoxy resins using polyetherimide, Polymer, 30 (1989) 213-217.

[31] S.K. Siddhamalli, Toughening of epoxy/polycaprolactone composites via reaction induced phase separation, Polymer Composites, 21 (2000) 846-855.

[32] I. Blanco, G. Cicala, O. Motta, A. Recca, Influence of a selected hardener on the phase separation in epoxy/thermoplastic polymer blends, Journal of Applied Polymer Science, 94 (2004) 361-371.

[33] A.F. Yee, R.A. Pearson, Toughening mechanisms in elastomer-modified epoxies, Journal of Materials Science, 21 (1986) 2462-2474.

[34] D.S. Parker, A.F. Yee, Factors Influencing the Mode I Interlaminar Fracture Toughness of a Rubber Toughened Thermoplastic Matrix Composite, Journal of Thermoplastic Composite Materials, 2 (1989) 2-18.

[35] C.B. Bucknall, A. Karpodinis, X.C. Zhang, A model for particle cavitation in rubber-toughened plastics, Journal of Materials Science, 29 (1994) 3377-3383.

[36] N. Chikhi, S. Fellahi, M. Bakar, Modification of epoxy resin using reactive liquid (ATBN) rubber, European Polymer Journal, 38 (2002) 251-264.

[37] Y. Okamoto, Thermal aging study of carboxyl-terminated polybutadiene and poly(butadiene-acrylonitrile)-reactive liquid polymers, Polymer Engineering & Science, 23 (1983) 222-225.

[38] D. Ratna, Phase separation in liquid rubber modified epoxy mixture. Relationship between curing conditions, morphology and ultimate behavior, Polymer, 42 (2001) 4209-4218.

[39] R. Thomas, D. Yumei, H. Yuelong, Y. Le, P. Moldenaers, Y. Weimin, T. Czigany, S. Thomas, Miscibility, morphology, thermal, and mechanical properties of a DGEBA based epoxy resin toughened with a liquid rubber, Polymer, 49 (2008) 278-294.

[40] J. Kim, R. Robertson, Toughening of thermoset polymers by rigid crystalline particles, Journal of Materials Science, 27 (1992) 161-174.

[41] Z. Zhong, Q. Guo, Miscibility and cure kinetics of nylon/epoxy resin reactive blends, Polymer, 39 (1998) 3451-3458.

[42] R.A. Pearson, A.F. Yee, Influence of particle size and particle size distribution on toughening mechanisms in rubber-modified epoxies, J Mater Sci, 26 (1991) 3828-3844.

[43] R.A. Pearson, A.F. Yee, Toughening mechanisms in thermoplastic-modified epoxies: 1. Modification using poly(phenylene oxide), Polymer, 34 (1993) 3658-3670.

[44] A.A.C. J. Bragg, M. T. Duran and V. Castano, Chemistry and Chemical technology, 2009, 3, 111, Preparation and Properties of (epoxy resin)/(Nylon 6,6 oligomer) blends, Chemistry and Chemical Technology, 3 (2009) 5.

[45] B.S. Gorton, Interaction of nylon polymers with epoxy resins in adhesive blends, Journal of Applied Polymer Science, 8 (1964) 1287-1295.

[46] L. Sun, G.L. Warren, D. Davis, H.J. Sue, Nylon toughened epoxy/SWCNT composites, J Mater Sci, 46 (2011) 207-214.

[47] A. Vyas, J.O. Iroh, In situ growth of multilayered crystals in amorphous matrix: Thermal, dynamic mechanical, and morphological analysis of nylon-6/epoxy composites, Journal of Applied Polymer Science, 130 (2013) 3319-3327.

[48] A. Vyas, J.O. Iroh, Morphology and structure of nylon-6 crystallized in epoxy resin matrix, Polymer Engineering & Science, 54 (2014) 858-866.

[49] D.R. Holmes, C.W. Bunn, D.J. Smith, The crystal structure of polycaproamide: Nylon 6, Journal of Polymer Science, 17 (1955) 159-177.

[50] J.P. Parker, P.H. Lindenmeyer, On the crystal structure of nylon 6, Journal of Applied Polymer Science, 21 (1977) 821-837.

[51] A. Okada, M. Kawasumi, I. Tajima, T. Kurauchi, O. Kamigaito, A solid state NMR study on crystalline forms of nylon 6, Journal of Applied Polymer Science, 37 (1989) 1363-1371.

[52] R.F. Stepaniak, A. Garton, D.J. Carlsson, D.M. Wiles, The characterization of nylon 6 filaments by x-ray diffraction, Journal of Applied Polymer Science, 23 (1979) 1747-1757.

[53] D.C. Vogelsong, Crystal structure studies on the polymorphic forms of nylons 6 and 8 and other even nylons, Journal of Polymer Science Part A: General Papers, 1 (1963) 1055-1068.

[54] H.J. Ploehn, C. Liu, Quantitative Analysis of Montmorillonite Platelet Size by Atomic Force Microscopy, Industrial & Engineering Chemistry Research, 45 (2006) 7025-7034.

[55] D. Yebassa, S. Balakrishnan, E. Feresenbet, D. Raghavan, P.R. Start, S.D. Hudson, Chemically functionalized clay vinyl ester nanocomposites: Effect of processing parameters, Journal of Polymer Science Part A: Polymer Chemistry, 42 (2004) 1310-1321.

[56] J. Singh-Beemat, J.O. Iroh, Effect of clay on the corrosion inhibition and dynamic mechanical properties of epoxy ester–polyurea–polysiloxane hybrid coatings, Polymer Engineering & Science, (2012) n/a-n/a.

[57] W. Lertwimolnun, B. Vergnes, Influence of compatibilizer and processing conditions on the dispersion of nanoclay in a polypropylene matrix, Polymer, 46 (2005) 3462-3471.

[58] B.M. Caruta, Nanomaterials: New Research, Nova Science, 2005.

[59] S.C. Products, (cloisite/product bulletin).

[60] P.A. Sørensen, S. Kiil, K. Dam-Johansen, C.E. Weinell, Anticorrosive coatings: a review, J Coat Technol Res, 6 (2009) 135-176.

[61] M.R. Bagherzadeh, F. Mahdavi, Preparation of epoxy–clay nanocomposite and investigation on its anti-corrosive behavior in epoxy coating, Progress in Organic Coatings, 60 (2007) 117-120.

[62] A. Foyet, T.H. Wu, L. van der Ven, A. Kodentsov, G. de With, R. van Benthem, Influence of mixing ratio on the permeability of water and the corrosion performance of epoxy/amine coated un-pretreated Al-2024 evaluated by impedance spectroscopy, Progress in Organic Coatings, 64 (2009) 138-141.

[63] T. Thi Xuan Hang, T.A. Truc, T.H. Nam, V.K. Oanh, J.-B. Jorcin, N. Pébère, Corrosion protection of carbon steel by an epoxy resin containing organically modified clay, Surface and Coatings Technology, 201 (2007) 7408-7415.

[64] J. Singh-Beemat, J.O. Iroh, L. Feng, Mechanism of corrosion protection of aluminum alloy substrate by hybrid polymer nanocomposite coatings, Progress in Organic Coatings, 76 (2013) 1576-1580.

[65] W.-G. Ji, J.-M. Hu, L. Liu, J.-Q. Zhang, C.-N. Cao, Improving the corrosion performance of epoxy coatings by chemical modification with silane monomers, Surface and Coatings Technology, 201 (2007) 4789-4795.

[66] C. Chen, M. Khobaib, D. Curliss, Epoxy layered-silicate nanocomposites, Progress in Organic Coatings, 47 (2003) 376-383.

[67] X. Shi, T.A. Nguyen, Z. Suo, Y. Liu, R. Avci, Effect of nanoparticles on the anticorrosion and mechanical properties of epoxy coating, Surface and Coatings Technology, 204 (2009) 237-245.

[68] D. Chemicals, Dow Epoxy - Polyamide Curing Agents, in, 2014.

[69] S.J. Wu, T.K. Lin, S.S. Shyu, Cure behavior, morphology, and mechanical properties of the melt blends of epoxy with polyphenylene oxide, Journal of Applied Polymer Science, 75 (2000) 26-34.

[70] H. Kishi, K. Uesawa, S. Matsuda, A. Murakami, Adhesive strength and mechanisms of epoxy resins toughened with pre-formed thermoplastic polymer particles, Journal of Adhesion Science and Technology, 19 (2005) 1277-1290.

[71] L. Wang, K. Wang, L. Chen, Y. Zhang, C. He, Preparation, morphology and thermal/mechanical properties of epoxy/nanoclay composite, Composites Part A: Applied Science and Manufacturing, 37 (2006) 1890-1896.

[72] S. Palraj, M. Selvaraj, P. Jayakrishnan, Effect of phosphate coatings on the performance of epoxy polyamide red oxide primer on galvanized steel, Progress in Organic Coatings, 54 (2005) 5-9.

[73] J. Singh-Beemat, J.O. Iroh, The effect of morphology on the corrosion inhibition and mechanical properties of hybrid polymer coatings, Journal of Applied Polymer Science, 128 (2013) 1616-1624.

[74] M.E. Orazem, B. Tribollet, Electrochemical Impedance Spectroscopy, Wiley, 2011.

[75] E. McCafferty, Introduction to Corrosion Science, Springer, 2010.

[76] H. Arimoto, α–γ Transition of nylon 6, Journal of Polymer Science Part A: General Papers, 2 (1964) 2283-2295.

[77] R.E. Smith, F.N. Larsen, C.L. Long, Epoxy resin cure. II. FTIR analysis, Journal of Applied Polymer Science, 29 (1984) 3713-3726.

[78] A. Cherdoud-Chihani, M. Mouzali, M.J.M. Abadie, Study of crosslinking AMS/DGEBA system by FTIR, Journal of Applied Polymer Science, 69 (1998) 1167-1178.

[79] I. dell'Erba, R. Williams, Epoxy networks modified by multifunctional polyhedral oligomeric silsesquioxanes (POSS) containing amine groups, Journal of Thermal Analysis and Calorimetry, 93 (2008) 95-100.

[80] C. Ramírez, M. Rico, A. Torres, L. Barral, J. López, B. Montero, Epoxy/POSS organic–inorganic hybrids: ATR-FTIR and DSC studies, European Polymer Journal, 44 (2008) 3035-3045.

[81] Y.P. Khanna, W.P. Kuhn, Measurement of crystalline index in nylons by DSC: Complexities and recommendations, Journal of Polymer Science Part B: Polymer Physics, 35 (1997) 2219-2231.

[82] D.R.H. Jones, M.F. Ashby, Engineering Materials 2: An Introduction to Microstructures, Processing and Design, Elsevier Science, 2005.

[83] P.J. Flory, Theory of crystallization in copolymers, Transactions of the Faraday Society, 51 (1955) 848-857.

[84] Y.-K. Choi, K.-i. Sugimoto, S.-M. Song, Y. Gotoh, Y. Ohkoshi, M. Endo, Mechanical and physical properties of epoxy composites reinforced by vapor grown carbon nanofibers, Carbon, 43 (2005) 2199-2208.

[85] H. Hama, K. Tashiro, Structural changes in non-isothermal crystallization process of melt-cooled polyoxymethylene. [I] Detection of infrared bands characteristic of folded and extended chain crystal morphologies and extraction of a lamellar stacking model, Polymer, 44 (2003) 3107-3116.

[86] K.P. Menard, Dynamic Mechanical Analysis: A Practical Introduction, Second Edition, Taylor & Francis, 2008.

[87] H. Ishida, D.J. Allen, Mechanical characterization of copolymers based on benzoxazine and epoxy, Polymer, 37 (1996) 4487-4495.

[88] P. Sollich, F. Lequeux, P. Hébraud, M.E. Cates, Rheology of Soft Glassy Materials, Physical Review Letters, 78 (1997) 2020-2023.

[89] L. Sun, G. Warren, D. Davis, H.J. Sue, Nylon toughened epoxy/SWCNT composites, Journal of Materials Science, 46 (2011) 207-214.

[90] A. Vyas, J. Iroh, Thermal behavior and structure of clay/nylon-6 nanocomposite synthesized by in situ solution polymerization, J Therm Anal Calorim, (2014) 1-14.

[91] W.J. Lorenz, F. Mansfeld, Determination of corrosion rates by electrochemical DC and AC methods, Corrosion Science, 21 (1981) 647-672.

[92] G. Höhne, W. Hemminger, H.J. Flammersheim, Differential Scanning Calorimetry, Springer, 2003.

[93] Y. Kojima, A. Usuki, M. Kawasumi, A. Okada, T. Kurauchi, O. Kamigaito, Synthesis of nylon 6–clay hybrid by montmorillonite intercalated with ϵ-caprolactam, Journal of Polymer Science Part A: Polymer Chemistry, 31 (1993) 983-986.

[94] P.C. Painter, M.M. Coleman, Fundamentals of Polymer Science: An Introductory Text, Technomic Publishing Company, 1997.

[95] T.D. Fornes, D.R. Paul, Crystallization behavior of nylon 6 nanocomposites, Polymer, 44 (2003) 3945-3961.

[96] D.R. Paul, L.M. Robeson, Polymer nanotechnology: Nanocomposites, Polymer, 49 (2008) 3187-3204.

[97] J.W. Cho, D.R. Paul, Nylon 6 nanocomposites by melt compounding, Polymer, 42 (2001) 1083-1094.

[98] H. Arimoto, M. Ishibashi, M. Hirai, Y. Chatani, Crystal structure of the γ-form of nylon 6, Journal of Polymer Science Part A: General Papers, 3 (1965) 317-326.

[99] Z. Zhao, W. Yu, Y. Liu, J. Zhang, Z. Shao, Isothermal crystallization behaviors of nylon-6 and nylon-6/montmorillonite nanocomposite, Materials Letters, 58 (2004) 802-806.

[100] X. Liu, Q. Wu, Phase transition in nylon 6/clay nanocomposites on annealing, Polymer, 43 (2002) 1933-1936.

[101] D.L. VanderHart, A. Asano, J.W. Gilman, NMR Measurements Related to Clay-Dispersion Quality and Organic-Modifier Stability in Nylon-6/Clay Nanocomposites, Macromolecules, 34 (2001) 3819-3822.

[102] R.R. Hegde, G.S. Bhat, B. Deshpande, Morphology and Properties of Nylon 6 Blown Films Reinforced with Different Weight Percentage of Nanoclay Additives, International Journal of Polymer Science, 2012 (2012) 14.

[103] Y. Zhang, J.H. Yang, T.S. Ellis, J. Shi, Crystal structures and their effects on the properties of polyamide 12/clay and polyamide 6–polyamide 66/clay nanocomposites, Journal of Applied Polymer Science, 100 (2006) 4782-4794.

[104] S.K. Swain, A.I. Isayev, PA6/clay nanocomposites by continuous sonication process, Journal of Applied Polymer Science, 114 (2009) 2378-2387.

[105] L. Liu, Z. Qi, X. Zhu, Studies on nylon 6/clay nanocomposites by melt-intercalation process, Journal of Applied Polymer Science, 71 (1999) 1133-1138.

[106] L.J. Mathias, R.D. Davis, W.L. Jarrett, Observation of α and γ Crystal Forms and Amorphous Regions of Nylon 6−Clay Nanocomposites Using Solid-State 15N Nuclear Magnetic Resonance, Macromolecules, 32 (1999) 7958-7960.

[107] L. Li, L.M. Bellan, H.G. Craighead, M.W. Frey, Formation and properties of nylon-6 and nylon-6/montmorillonite composite nanofibers, Polymer, 47 (2006) 6208-6217.

[108] D.M. Lincoln, R.A. Vaia, Z.G. Wang, B.S. Hsiao, Secondary structure and elevated temperature crystallite morphology of nylon-6/layered silicate nanocomposites, Polymer, 42 (2001) 1621-1631.

[109] H. Li, Y. Wu, H. Sato, L. Kong, C. Zhang, K. Huang, D. Tao, J. Chen, X. Liu, Y. Zhao, Y. Xu, J. Wu, Y. Ozaki, A New Facile Method for Preparation of Nylon-6 with High Crystallinity and Special Morphology, Macromolecules, 42 (2009) 1175-1179.

[110] N.S. Murthy, H. Minor, M.K. Akkapeddi, B.V. Buskirk, Characterization of polymer blends and alloys by constrained profile-analysis of X-ray diffraction scans, Journal of Applied Polymer Science, 41 (1990) 2265-2272.

[111] J. Longun, B. Buschle, N. Nguyen, M. Lo, J.O. Iroh, Comparison of poly(o-anisidine) and poly(o-anisidine-co-aniline) copolymer synthesized by chemical oxidative method, Journal of Applied Polymer Science, 118 (2010) 3123-3130.

[112] J.E. Mark, Physical Properties of Polymers Handbook, Springer, 2007.

[113] S.M. Aharoni, n-Nylons, their synthesis, structure, and properties, J. Wiley & Sons, 1997.

[114] T.D. Fornes, P.J. Yoon, H. Keskkula, D.R. Paul, Nylon 6 nanocomposites: the effect of matrix molecular weight, Polymer, 42 (2001) 09929-09940.

[115] A. Usuki, Y. Kojima, M. Kawasumi, A. Okada, Y. Fukushima, T. Kurauchi, O. Kamigaito, Synthesis of nylon 6-clay hybrid, Journal of Materials Research, 8 (1993) 1179-1184.

[116] T.M. Theophanides, Infrared Spectroscopy - Materials Science, Engineering and Technology, InTech, 2012.

[117] B. Ramezanzadeh, M.M. Attar, M. Farzam, A study on the anticorrosion performance of the epoxy–polyamide nanocomposites containing ZnO nanoparticles, Progress in Organic Coatings, 72 (2011) 410-422.

[118] J. Singh-Beemat, J.O. Iroh, Characterization of corrosion resistant clay/epoxy ester composite coatings and thin films, Progress in Organic Coatings, 74 (2012) 173-180.

[119] H. Luo, Y.C. Guan, K.N. Han, Corrosion Inhibition of a Mild Steel by Aniline and Alkylamines in Acidic Solutions, Corrosion, 54 (1998) 721-731.

[120] L. Philippe, C. Sammon, S.B. Lyon, J. Yarwood, An FTIR/ATR in situ study of sorption and transport in corrosion protective organic coatings: 1. Water sorption and the role of inhibitor anions, Progress in Organic Coatings, 49 (2004) 302-314.

[121] L.J. Fetters, D.J. Lohse, D. Richter, T.A. Witten, A. Zirkel, Connection between Polymer Molecular Weight, Density, Chain Dimensions, and Melt Viscoelastic Properties, Macromolecules, 27 (1994) 4639-4647.

[122] W.K. Goertzen, M.R. Kessler, Dynamic mechanical analysis of carbon/epoxy composites for structural pipeline repair, Composites Part B: Engineering, 38 (2007) 1-9.

[123] K. Wang, L. Chen, J. Wu, M.L. Toh, C. He, A.F. Yee, Epoxy Nanocomposites with Highly Exfoliated Clay: Mechanical Properties and Fracture Mechanisms, Macromolecules, 38 (2005) 788-800.

[124] J.S. Beemat, Processing and Properties of Hybrid Silane-Epoxy Nanocomposite Coatings, in, University of Cincinnati, 2012.

[125] P.t.a.C. Fleming, Differential Scanning Calorimetry, webpage.

[126] A. Instruments, Dynamic Mechanical Analysis, Information Webpage.

Publications

Peer Reviewed Journal Papers

1. Aniket Vyas, Jude Iroh "In-situ Growth of Multilayered Crystals in Amorphous Matrix: Thermal, Dynamic Mechanical and Morphological Analysis of Nylon-6/Epoxy Composites ", **Journal of Applied Polymer Science**, Vol. 130, Issue 5, Pg 3319-3327, 2013
2. Aniket Vyas, Jude Iroh "Morphology and Structure of Nylon-6 Crystallized in Epoxy Resin Matrix", **Polymer Science and Engineering**, Vol. 54, Issue 4, Pg 858-866, 2014
3. Aniket Vyas, Jude Iroh "Thermal Behavior and Structure of Clay/Nylon-6 Nanocomposite Synthesized by In-Situ Solution Polymerization ", **Journal of Thermal Analysis and Calorimetry**, DOI 10.1007/s10973-014-3681-y, 2014
4. Aniket Vyas, Jude Iroh "Clay Induced Thermoplastic Crystals in Thermoset Matrix: Thermal, Dynamic Mechanical and Morphological Analysis of Clay/Nylon-6-Epoxy Nanocomposites", **Polymer Composites** (under review)
5. Aniket Vyas, Jude Iroh "Novel Semi-Crystalline Hybrid Coatings: Corrosion Inhibition and Morphological Analysis of Clay/Nylon 6-Epoxy Nanocomposites", **Progress in Organic Coatings** (under preparation)

Conference Proceedings

1. Aniket Vyas, Jude Iroh "Thermo-mechaincal and Morphological properties of Clay/Nylon 6-Epoxy Nanocomposites", Section – Engineering Properties and Structure, **Society of Plastic Engineering (SPE)** ANTEC, Las Vegas, Nevada, USA April 2014.
2. Aniket Vyas, Jude Iroh "Development of Large Volume Continuously Processable Epoxy-Polyamide Resin with Remarkable Thermoplastic Properties", **SAMPE University**

Research Symposium, Long Beach, California, May 2013

3. Aniket Vyas, Jude Iroh “Morphology and Properties of Nylon-6/Epoxy Composites”, Section - Polymer alloys, **Society of Plastic Engineering (SPE)** ANTEC, Cincinnati, April 2013
4. Aniket Vyas, Jude Iroh “Morphology and Thermal Behavior of Clay/Nylon-6 Nanocomposites Synthesized by In-Situ Solution Polymerization of ε-Caprolactam”, **Society of Plastic Engineering (SPE)** ANTEC, Cincinnati, 2013

Invention Disclosure and Patent

1. **Aniket Vyas**, Jude Iroh, Brad Ruff “Novel Cost-Effective Eco-Friendly Heat Sensitive 3D Printer Print Bed Coating for Fused Filament Fabrication” (Provisional Patent USPTO S No. 61/971759)
2. **Aniket Vyas**, Jude Iroh “A novel method for producing large volume continuously processable epoxy-polyamide resin with remarkable thermoplastic properties” (2012) UC 112-085 (Invention Disclosure filed as co-inventor).

Polymer Engineering and Science, Vol. 54, Issue 4, Pg 858-866, 2014

MORPHOLOGY AND STRUCTURE OF NYLON-6 CRYSTALLIZED IN EPOXY RESIN MATRIX

Aniket Vyas, Jude O Iroh, Material Science and Engineering Program, College of Engineering & Applied Science, University of Cincinnati, Cincinnati, OH 45221-0012, USA

1. Introduction

Epoxy is a thermoset polymers which is extensively used as coatings and adhesives in automotive, construction, and aerospace industries primarily because of its excellent physical, chemical and mechanical properties [1, 2]. The outstanding stiffness and strength of epoxy resin make it a useful matrix material in advanced structural composites [3]. In spite of the desirable properties of epoxy resin such as good adhesion, and excellent chemical and thermal stability, there are notable shortcomings which prevent their widespread use in aerospace and automobile industries.

Epoxy resins are inherently brittle in nature due to their high cross-link density and glassy nature. They are stiff and brittle especially in the presence of sharp cracks. Hence, an improvement in the toughness of epoxy resin is greatly desired for increased durability. Toughening of epoxy resin has often been successfully done by incorporation of a rubber or thermoplastic polymer. Yee et al.[4, 5] has thoroughly investigated the mechanism behind toughening of epoxy in presence of thermoplastics as second phase. The second phase precipitates during the curing process and produces a two phase microstructure consisting of small rubber or thermoplastic particles dispersed in a matrix of epoxy.

Various ductile engineering thermoplastics has been used as modifying agent such as polysulfone, polyester [6], poly(ether-imides), poly(ϵ-caprolactone) [2] and polyamides [3, 7]. These thermoplastics are found to be promising since they do not decrease the inherent properties of epoxy matrix as in case of rubbers [5, 8]. Thermoplastics provide a wider variety of toughening mechanisms such as (1) crack pinning, (2) particle bridging, (3) crack path deflection, (4) particle yielding, (5) particle-yielding induced shear banding, and (6) micro cracking [3, 4, 9, 10].

Among different thermoplastics used to modify epoxy, a special attention has been paid on use of polyamides or nylons. They are known to increase the toughness of brittle epoxy not just by physical interaction and creation of multiphase morphology but also by forming chemical bonds [11-13]. Kim et al [3] studied the effect of mixing temperature on morphology of blends and reported that morphology plays an important role in deciding the fracture toughness of composites, based on the size of crystalline nylon phase in amorphous epoxy matrix. Cardwell and yee [7] reported that presence of nylon particles triggers crack bridging mechanism and toughens epoxy matrix due to large plastic deformation of nylon rich phase. Zhong et al [12] studied the kinetics of curing of epoxy by nylon and identified that greater chemical interaction reduces the crystallinity of nylon in epoxy matrix. Wang et al [13] studied the thermo-mechanical properties of epoxy/nylon blends but no direct correlation was explained on basis of structure and morphology. Hence, it can be inferred that morphology plays an important role in deciding the ultimate mechanical and thermal properties.

The morphology on other hand directly depends upon the processing method. Nylon/epoxy composites have been fabricated successfully by previous researcher, however the processing methods reported are limited to tedious techniques which make them difficult to be used in practical applications or commercialization. For example, nylon is first dissolved in hot alcohol or acid and then blended with epoxy resin [11-13] or solid nylon powder is dispersed in epoxy resin and then heated above melting point [3].

Alcohol is a low boiling solvent and acid is corrosive in nature thus these composites cannot be used in surface coating applications. Moreover, heating nylon to high temperature for processing of composite is not a cost-effective method. Thus, in order to make the processing of epoxy polyamide more efficient and practically suitable; versatile, cost effective and a greener method is desired.

In this article, a morphological study has been discussed obtained by a novel method to formulate nylon-6/epoxy composites. The idea of growth of thermoplastic crystals from solution has been successfully implemented for nylon-6 crystals to grow on epoxy as substrate material for nucleation. The blend on curing leads to growth of crystals in amorphous matrix and gives rise to a unique and remarkable morphology.

2. Experimental

2.1. Materials

Polyfunctional Water Dispersible DGEBA based Epoxy resin (EPIREZ 5522-WY-55) was purchased from Hexion Chemicals, Houston, USA. ϵ -caprolactam, 95% pure-Dry Sodiam Hydride, N-acetylcaprolactam & NMP solvent were purchased from Sigma-Aldrich, USA for solution Polymerization ε-caprolactam. The Al-2024-T3 was purchased from Q-labs, Cleveland, Ohio.

2.2. Procedure

2.2.1. Synthesis of Nylon-6 in N-Methylpyrollidone

Polymerization was carried out in an oil bath assembly. 100 ml of NMP was taken in a 3 neck flask and 30 g of monomer (ϵ -caprolactam) was added to it and stirred till it formed a colorless solution. Nitrogen supply was turned on & temperature was raised to 80 ^{O} C. 0.72 g of NaH (catalyst) was then added to the solution & stirred till it dissolved completely. This process of dissolution was accompanied by a series of color changes from colorless to dark blue which eventually turned black on complete dissolution. Temperature was then gradually raised to 160 ^{o} C and 0.396 g of N-acetyl Caprolactam (Initiator) was added to the solution while maintaining the stirring. The color of solution then turned to dark blue. After addition of initiator solution was stirred for 30 minutes and the nitrogen supply was turned off. The black solution gently turned to a dark orange viscous solution. Nylon 6 existed as a homogeneous solution at higher temperature but while transferring to a glass jar at room temperature it began to phase separate and existed in a suspension form.

2.2.2. Preparation of Nylon-6 / Epoxy blends

Epoxy was taken in a glass jar, Nylon 6 suspension was added in various amounts to it & NMP was further added to dilute the solution to reduce the viscosity for ease of processing in order to have defect free films and coatings. Nylon 6 was added as 0, 5, 10, 15, 20 & 30 weight % with respect to solid content of Epoxy resin. The mixture was then stirred using mechanical stirrer for 1 hour at room temperature to obtain homogeneous solution and then ultra-sonicated for 5 minutes.

2.2.3. Preparation of solid Nylon-6, coatings and free standing Films of Epoxy/Nylon-6 blends

5 ml of nylon-6 suspension was taken in a teflon mold and gradually heated up to 200 ^{O} C for 24 hours in vacuum oven to fully evaporate the solvent & likewise Nylon 6 granules were obtained from the solution.

Composite coatings were formed via solution casting method. 2 ml of blend was dropped on Al alloy panel and the coating was cured in a stepwise manner, heating initially at 70^{O}C for 3 hours, 100 ^{O}C for 2 hours, 120 ^{O}C for 2 hours and 150 ^{O}C for 2 hours.

8 ml of blend was taken and casted in 1.5'' * 1.5'' * 1/4 '' Teflon molds to form free standing films. The films were cured in vacuum oven in a stepwise manner, heating initially at 50 ^{O} C for 13 hours, 100 ^{O} C for 4 hours, 120 ^{O} C for 2 hours and finally 150 ^{O} C for 2 hours.

The free standing films were quenched in liquid nitrogen and broken to see the cross-section of fractured surface under Scanning Electron Microscopy.

2.2.4. Characterization

Scanning Electron Microscope was a Philips model FEI XL 30 ESEM-FEG. The software used to capture images was Scandium. Aluminum stubs with carbon tape were used as sample holders and the sample was coated with Au-Pd before subjecting to SEM.

Wide angle X-ray diffraction (WAXD) was carried out using Philip X-Ray diffractometer. X-Ray diffraction tests were performed using Cu-K radiation source at a wavelength of 1.54 A^{O} between 2θ angles of 15 to 30^{O}.

A Keyence digital microscope was used to capture image at low magnification, model no. VHX-600ES0.

3. Results and Discussion

3.1 Growth of nylon-6 crystals from suspension in NMP

The polymerization process for synthesis of nylon-6 was carried out in NMP as solvent. This plays an important role in crystal formation. As proposed by vasiliu-oprea[14], the polymerization begins in a homogeneous liquid phase. As the reaction proceeds, chain grows which causes change in composition of medium and leads to decreased solubility of growing macromolecules. Hence polymer precipitates rapidly to form nuclei. These primary particles aggregate to form colloidal suspension. The chain growth with diffusion of monomer from solution to colloid takes place inside droplets and leads to increase in viscosity and dimension of macromolecule. Hence after reaction is complete, the nylon-6 crystals exist in NMP as a suspension with swollen chains at room temperature. When NMP is removed by heating, the chain folding begins to occur in a compact manner giving rise to distinct nylon-6 granules with extremely high crystallinity. The SEM images at lower and higher magnification of such granules are shown in figure 1. The size of crystal lamellae ranged from 2 – 20 µm. Each lamella was found to have fiber like crystals emerging radially outwards.

At higher magnification, layers connected to a common center in a complex manner were observed. They can be considered as spherulites uniformly distributed to fill the space made up of smaller crystalline substructures [15]. As the Spherultic growth is nucleated at center, followed by radiating growth and branch often to occupy outwardly increasing volume.

Hence it was confirmed that this novel route of synthesis via anionic polymerization leads to formation of nylon-6 crystals suspended in NMP. The crystallinity further increases when solvent is removed as the growth spiral begins to propagate. This technique was then utilized to make nylon-6/epoxy composites. As the thermoplastic polymer was in a suspension form and highly crystalline, it was anticipated that on blending with epoxy resins, spherulitic crystals will grow in the epoxy matrix on removal of solvent (curing). The nylon-6 suspension was thus blended with water dispersible epoxy resin followed by curing. The study of resulting multiphase morphology was analyzed in two separate aspects: a) at the surface of epoxy; b) in the bulk of epoxy. The heterogeneous morphology is discussed in section 3.3 and 3.4.

3.2 X-Ray Diffraction Analysis for Nylon-6

Nylon-6 is known to have two major polymorphs or crystalline forms. The difference in crystal structure results from different packing of nylon-6 chains by hydrogen bonding. It may occur in an anti-parallel or parallel way. The anti-parallel arrangement is termed as α form, while parallel arrangement results in γ form. When nylon-6 is subjected to X-Ray diffraction, the polymers chains arranged in an orderly fashion in form of a crystal leads to a peak in diffraction pattern. The location of peak at a particular angle gives information about nature of crystalline form, length of crystals and stability of crystals.

Nylon-6 was synthesized in NMP and crystallized by removing solvent. To analyze the crystal structure of nylon-6, it was subjected to Wide angle X-Ray diffraction in two runs. The X-Ray diffraction pattern is shown in figure 2 (a and b). In both runs, the location of major peaks remained unchanged and on basis of both runs all peaks essential to determine the structure of nylon-6 were decided. The location of major peaks, d-spacing, crystallite length and crystal planes along with type of polymorph are shown in table 1. The major peaks were observed at 19.91^{O} and 24.04^{O} which represents α form of crystals [16, 17] but small peaks at about 21^{O} and 18^{O} were also observed which represents γ form of crystals [18]. Hence it can be inferred that nylon-6 synthesized by solution polymerization exist as mixture of α and γ type of crystals with a majority of α polymorph.

The crystallite length and corresponding d-spacing can be calculated using Scherrer equation and bragg's law respectively [18, 19]. The scherrer equation used is as follows:

$$D(hkl) = \frac{K\lambda}{\beta(hkl)\ cos\theta} \qquad [1]$$

Where D(hkl) is the mean crystallite size along [hkl] direction, K is the shape factor (scherrer constant, value of 0.94 is used in this case), β(hkl) is the half width of the crystalline peak in radians and θ is the half scattering angle.

According to braggs law d-spacing was calculated by the following equation:

$$n\lambda = 2dsin\theta \qquad [2]$$

Where n is a constant integer (1 in our case), λ is wavelength, d is d spacing and θ is diffraction angle in degrees.

Hence, it can be inferred that during crystallization process crystals grows primarily in 200 and 002 planes with chains arranged in an anti-parallel fashion (α phase). In both the runs of XRD, the peak at 24.8 was prominent. It has been reported in literature that peak at 24^{O} is actually composed of strong peak at 24^{O} for [002] reflection and a weak peak for 24.8^{O} for [202] reflection [17]. The experimental results followed the same trend with a prominent weak peak at 24.8^{O}. During crystal growth, chain folding takes place in such a way that polymer chains assumes most stable configuration [20]. The α polymorph is more stable than γ polymorph at room temperature [21]. Hence it is apparent that majority of crystals grow in anti-parallel fashion (α form).

In the present experiment, Nylon-6 was polymerized in NMP and after completion of reaction nylon-6 existed as suspension in NMP. Polymerization and crystallization occurs simultaneously in the solution and further crystallization in nylon-6 granules takes place on removal of solvent.

This leads to creation of morphology with very sharp features along with a wide distribution of crystals ranging from 12 nm to 94 nm crystallite lengths in various planes. The existence of nylon-6 as a mixture of α and γ form with a dominance of α over γ has been reported previously for caprolactam polymerized in ethyl benzene with Sodium bis (2-methoxyethoxy) aluminum hydride/isophorone diisocyanate catalytic system [14].

Nylon-6 usually assumes monoclinic lattice structure with unit cell dimensions of a = 0.956 nm, b = 1.724 nm, c = 0.801 nm for α form with unit cell angle of 67.5^O and a = 0.933 nm, b = 1.688 nm, c = 0.478 nm for γ form with unit cell angle of 121^O [18]. The representation of lattice structure is shown in figure 3 for α and γ crystal form of nylon-6.

In Summary, WAXD results show that for nylon-6 synthesized in NMP and crystallized from it, crystals exist majorly as α polymorph and marginal γ type crystals with high crystallinity, along with a wide distribution of crystals growing radially outwards in different planes.

3.3 Morphology of nylon-6/epoxy coating (surface)

Nylon-6/epoxy blend was first spread on an Al alloy substrate followed by curing. The surface of the polymer composite coating was then observed under Optical microscope and Scanning electron microscope to analyze the surface morphology.

3.3.1 Optical Microscopy

Initially, the surface of polymer composite coated on Al alloy as a substrate was observed under optical microscope. Conventional optical microscope is useful only when structures to be investigated are at least 1μm [22]. When ordinary microscopes are used to observe crystalline features, nothing is seen as there is no significant contrast between light absorbed by crystalline and non-crystalline zone. In practice, polarized light is used in order to introduce contrast.

But in the present study, coated sample with different epoxy/nylon-6 composition were subjected to regular optical microscope (non-polarized). For the sample coated with neat epoxy, a clear amorphous surface was observed with no distinct features or variation in contrast as shown in figure 4(a). When, nylon-6 was introduced as 5 weight % in epoxy resin, a distinct crystalline feature was observed at the highest resolution (1000x) possible as shown in figure 4(b). The feature appeared to be dendritic in nature with branched crystals forming a tree like shape. This was the first indication of growth of large crystals of nylon-6 in epoxy matrix. The dendrite was about 100-120 μm in length with different branches protruding out. The dendrite in of nylon-6 was grown not only by removal of solvent but also in presence of epoxy as diluent. Although the dendritic nature is not the prerequisite for spherulitic growth, but many of the solution grown dendrites are described in literature as spherulites [15]. The spherulites of nylon 6 grown from formic acid solution reported by eppe et al. [23] were very similar to the dendrite of polyethylene floating in solution reported by wunderlich [24]. This suggests that the ease of formation of multilayered crystals and dendrite formation are at the root of spherulitic formation of polymer crystals.

The 3rd sample containing 10% by weight of nylon-6 in epoxy also showed presence of distinct crystalline feature taking a shape of a star or a flat based pyramid as shown in figure 4(c). In the samples containing nylon-6, along with the presence of distinct crystalline feature, a significant variation in the brightness of the color can also be observed. This again indicates the presence of crystals in epoxy matrix as brightness in color varies only due to variation in refractive index of crystalline and amorphous zones. The image of crystal obtained at 10 weight % of nylon-6 in composition was very similar to multilayer polyethylene crystal reported by mitsuhashi and kellar [25], but they observed the crystal while it was floating in the solution. They considered it to be a helicoidal ribbon which is tight at the center then edges rather than a solid spiral pyramid while existing in solution. But in present case, as solution is removed growth spiral propagates up and down; on sedimentation, however, the growth spiral collapses giving appearance of flat based pyramid.

When nylon-6 % in blend was further increased to 20%, no distinct noticeable features were observed but a variation in brightness of color was clearly visible (figure 4(d)). This suggests that increasing nylon-6 in composition begin to dominate in composite and behaving as a bulk material small crystals begin to grow all over matrix. The dendrite and pyramid shaped morphology of nylon-6 was observed on the surface of epoxy. To verify the preliminary findings by optical microscopy and to further investigate the nature of crystallization, small coated sample were prepared using same blend solution to be analyzed under SEM at higher magnification for better understanding and clarity.

3.3.2 Scanning electron Microscopy

Figure 5(a) shows the SEM micrograph of neat epoxy coated surface. The surface appears to be remarkably glassy and amorphous with very sharp and long cracks. The brittle nature of neat epoxy can be clearly observed with this kind of morphology. The epoxy resin was then blended with nylon-6 suspension followed by curing to form a coating on Al alloy coupon as a substrate. Morphology of the surface of composite coating 10% of nylon-6 in composition by weight can be seen in figure 5(b).

As discussed earlier, multilayered crystals with spherulites have tendency to grow radially outwards along with high level of branching to occupy free volume. Following the same manner, crystals of nylon-6 were found to be growing within the cracks and crevices of epoxy matrix. The sharp brittle cracks were filled with ductile nylon-6 crystals. This phenomenon of growth of crystals to fill the voids and crack leads to plasticization of epoxy along with increase in toughness and reduction in brittleness. On closely spotting a crack filled with nylon-6 crystals at higher magnification, long fibril crystals were observed with length ranging from 0.5-2 µm.

On further increasing nylon-6 concentration to 20%, a significant variation in surface morphology was observed as shown in figure 5(c). The number of cracks was found to be reduced and the cracks that were present were also very small in size. The nylon-6 crystals reduced in size but increased in number and were found to be dispersed on the surface. On closely observing the morphology at higher magnification, each nylon crystal was seen to be followed by one tail or crack. This indicates crack path altering or bridging mechanism due to presence of crystals in the way of crack propagation [3].

Since nylon-6 and epoxy resin are thoroughly mixed in the blend when curing of epoxy is carried out, growth of crystals can be visualized in two conducts: firstly on the surface of epoxy and secondly within the bulk of epoxy resin beneath the surface as the epoxy serves as heterogeneous nucleus. Crystallization on such a surface is enhanced due to reduction in interfacial energy. Further, nucleation is enhanced on a heterogeneous surface because when a sample is cooled to crystallization temperature, the surface is usually cooler [26].After surface morphology, the multiphase morphology in the bulk of film was investigated for variation along with composition, as discussed in next section.

3.4 Morphology of fractured Nylon-6/epoxy composite film (bulk)

The morphology within the bulk of composite free standing film was investigated by fracturing the film in liquid nitrogen. The effect of composition on nature of crystals was noticeable at the fractured surface. Figure 6(a) is the fractured surface of neat epoxy which is clearly amorphous in nature with no thermoplastic crystals in it. As the concentration of nylon-6 was increased to 5% by weight, various crystalline zones were observed. Figure 6(b) shows one of the crystalline zones with large number of small crystals. Few crystals were protruding out of the amorphous matrix and few were embedded in the matrix. Presence of crystals was also observed in all the cracks developed during the fracture of film. This indicates that nylon-6 crystals growing in epoxy matrix were isotropic in distribution. Effect of further increasing the concentration of nylon-6 up to 15% can be seen in figure 6(c). Large crystals grown inside the epoxy matrix were seen coming out of the fractured surface. This suggests that nylon crystals after growing, begins to form network overlapped by amorphous zone. On brittle fracture in liquid nitrogen, these networks were broken which can be easily seen in SEM image. On further increasing the concentration of nylon-6, the crystals began to play an important role by acting as bulk material in composite by dominating epoxy as matrix material. As a result at 30% nylon-6 weight, a complete different morphology was observed where only one phase was present as shown in figure 6(d).

It is well known that crystallization behavior of polymer becomes modified in a blend due to presence of other component [27]. The nature of crystals in present study was different for neat nylon-6 and that in epoxy matrix although spherulites were observed in both the cases. Furthermore, the nature of crystals was also found to be dependent on the composition of blend. When nylon-6 was crystallized during the process of curing of epoxy resin, the non-crystalline impurity is excluded from crystalline zone. The degree of exclusion depends upon the relative rates of diffusion rate of non-crystalline component (D) and growth rate of crystalline component (G) [28, 29].

In the present study, crystals can be seen to be overlapped or encapsulated by amorphous epoxy in the bulk. This suggests that since epoxy (non-crystalline impurity) is in high amount, its excess is excluded from inter-lamellar region to the outside of lamellar stacks. Hence, it can be inferred that D is small for the epoxy/nylon-6 system and the non-crystalline impurity is excluded only at length scale of lamellar bundle.

4. Conclusion

A novel process was explored to prepare nylon-6/epoxy composite with multiphase morphology. As a part of process, nylon-6 was successfully synthesized in solution via anionic polymerization. This method leads to formation of nlon-6 with high crystallinity. A crystalline morphology containing spherulites was observed which was found to grow radially outwards with branching to occupy free volume. Nylon-6 existed as a mixture of α and γ type of crystals with a wide distribution. This aspect of crystal growth was utilized and applied to modify epoxy. Epoxy served as a heterogeneous substrate to enhance the crystallization by providing various sites for effective nucleation. During the crystallization process, crystals began to grow radially outwards in form of spherulites and fulfilled the gaps and cracks developed in epoxy matrix during the process of curing. A multiphase morphology was also obtained in the bulk of free standing film consisting of nylon-6 crystals encapsulated by amorphous phase of epoxy. Hence it can be inferred from morphology that this novel route to modify epoxy is a versatile, environmental friendly and cost-effective technique to toughen and plasticize brittle epoxy.

Acknowledgment

This study was funded by grants from office of naval research (ONR) # N00014-09-1-0980 and National Science Foundation (NSF) # CMMI-0758656. We would also like to thank *Soumyarwit Manna* at Advanced Material Characterization Center (AMCC), University of Cincinnati who assisted in capturing the SEM images.

References

1. CA May, *Epoxy Resins: Chemistry and Technology*: M. Dekker, (1988).
2. L. Barone,S. Carciotto,G. Cicala and A. Recca, *Polymer Engineering & Science* **46,** 1576 (2006)
3. S. Kim,J. Kim,S.H. Lim, W.H. Jo andC.R. Choe, *Journal of Applied Polymer Science* , **72**, 1055 (1999).
4. A.F. Yee and R.A. Pearson. *Journal of Materials Science*, **21,** 2462 (1986).
5. D.S. Parker and A.F. Yee. *Journal of Thermoplastic Composite Materials*, **2,** 2(1989).
6. J. Kim and R.E. Robertson. *Journal of Materials Science*, **27,** 3000 (1992).

7. B.J. Cardwell and A.F. Yee. *Journal of Materials Science*, **33,** 5473 (1998).

8. C.B. Bucknall, A. Karpodinis and X.C. Zhang. *Journal of Materials Science*, **29**, 3377 (1994)

9. R.A. Pearson, *Sources Of Toughness In Modified Epoxies,* Ph.D. thesis University Of Michigan, (1990).

10. R.A. Pearson and A.F. Yee, *Polymer* , **34,** 3658 (1993).

11. B.S. Gorton. *Journal of Applied Polymer Science*, **8**, 1287 (1964)

12. Z. Zhong and Q. Guo, *Polymer*, **39**, 3451 (1998)

13. Y.Y. Wang and S.A. Chen. *Polymer Engineering & Science*, **20**, 823 (1980)

14. C. Vasiliu-Oprea and F. Dan, *Journal of Applied Polymer Science*, **62**, 1517 (1996)

15. B. Wunderlich, *Macromolecular physics*: Academic Press (1973).

16. D.R. Holmes, C.W. Bunn and D.J. Smith, Journal of Polymer Science, **17**, 159 (1955).

17. H. Li, Y. Wu, H. Sato, L. Kong, C. Zhang, K. Huang, D. Tao,J. Chen, X. Liu, Y. Zhao, Y. Xu, J. Wu and Y. Ozaki, *Macromolecules*, **42**, 1175 (2009).

18. H. Arimoto, M. Ishibashi, M. Hirai and Y. Chatani. *Journal of Polymer Science Part A: General Papers*, **3**, 317 (1965)

19. Z Zhao, W. Yu, Y. Liu, J. Zhang and Z. Shao, *Materials Letters*, **58**, 802, (2004).

20. P.C. Painter and M.M. Coleman, *Fundamentals of Polymer Science: An Introductory Text*, Second Edition: Taylor & Francis, (1998).

21. S.M. Aharoni, *n-Nylons, their synthesis, structure, and properties*: J. Wiley & Sons, (1997).

22. D.I. Bower, *An Introduction to Polymer Physics*: Cambridge University Press, (2002).

23. R Eppe, E.W. Fischer and H.A. Stuart, *Journal of Polymer Science*, **34**, 721, (1959).

24. B. Wunderlich and P. Sullivan, *Journal of Polymer Science*, **61**, 195, (1962).

25. S. Mitsuhashi and A. Keller, *Polymer*, **2**, 109, (1961).

26. H. Schonhorn, *Macromolecules*, **1**, 145, (1968).

27. V.M. Nadkarni, V.L. Shingankuli and J.P. Jog. *Journal of Applied Polymer Science,* **46**, 339, (1992).

28. H.D. Keith and J.F.J. Padden . *Journal of Applied Physics*, **35**, 1270, (1964).

29. L.A. Utracki, *Polymer Blends Handbook*: Kluwer Academic Publishers, (2002).

Tables

Table - 1 X-ray Diffraction Pattern for Nylon-6

Major Peaks (α – polymorph)

2(θ)	**d-spacing (A^O)**	**Crystallite Length (nm)**	**Crystal Planes**	**Polymorph type**
19.91	4.45	12.578	$[200]_\alpha$	α
24.04	3.69	31.433	[002]	α
24.8	3.58	94.437	[202]	α

Minor Peaks (γ polymorph)

2(θ)	**d-spacing (A^O)**	**Crystallite Length**	**Crystal Planes**	**Polymorph type**
18.03	4.91	93.385		γ
21	4.22	42.212	$[002]_\gamma$	γ

Figure captions

Figure 1 – SEM image of nylon-6 granules precipitated from NMP (a-lower magnification, b-higher magnification)

Figure 2 – X-Ray diffraction pattern for nylon-6

Figure 3 – X-ray diffraction of Nylon-6 along with fitted curve

Figure 4 – Optical microscopy image of surface of epoxy/nylon-6 coating (a-0%, b-5%, c-10% and d-20%)

Figure 5 – SEM image of surface of epoxy/nylon-6 (a-0 wt. %, b-10 wt. %, c-20 wt. %) coating

Figure 6 – SEM image of fractured surface of epoxy/nylon-6 film (a-0%, b-5%, c-15% and d-30% by weight)

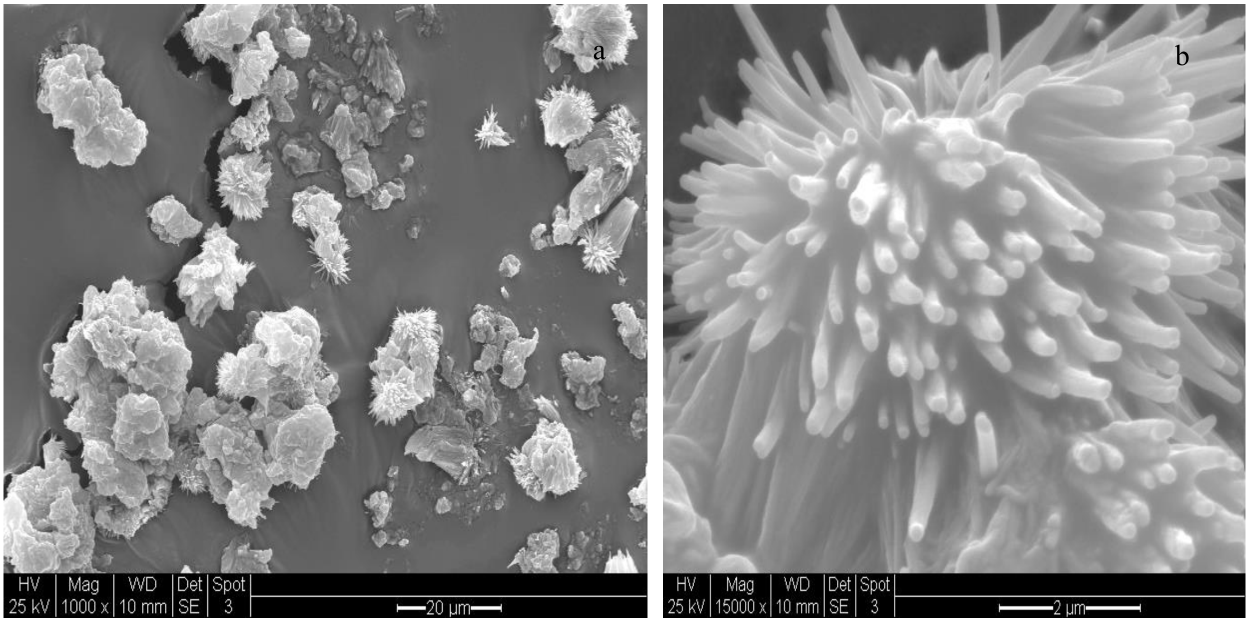

Figure 1 – SEM image of nylon-6 granules precipitated from NMP (a-lower magnification, b-higher magnification)

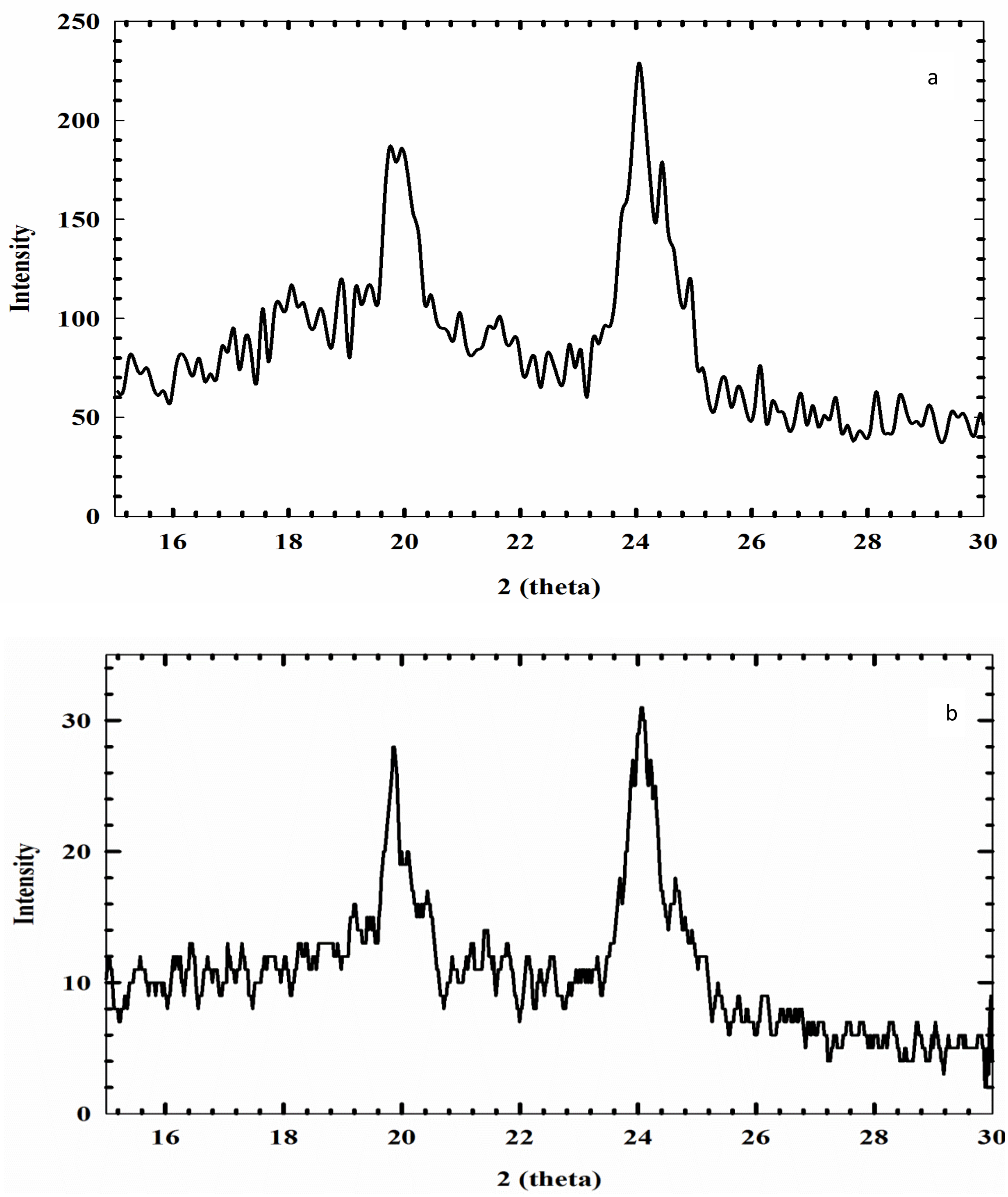

Figure 2 – X-Ray diffraction pattern for nylon-6 (a) 1st run (b) 2nd run

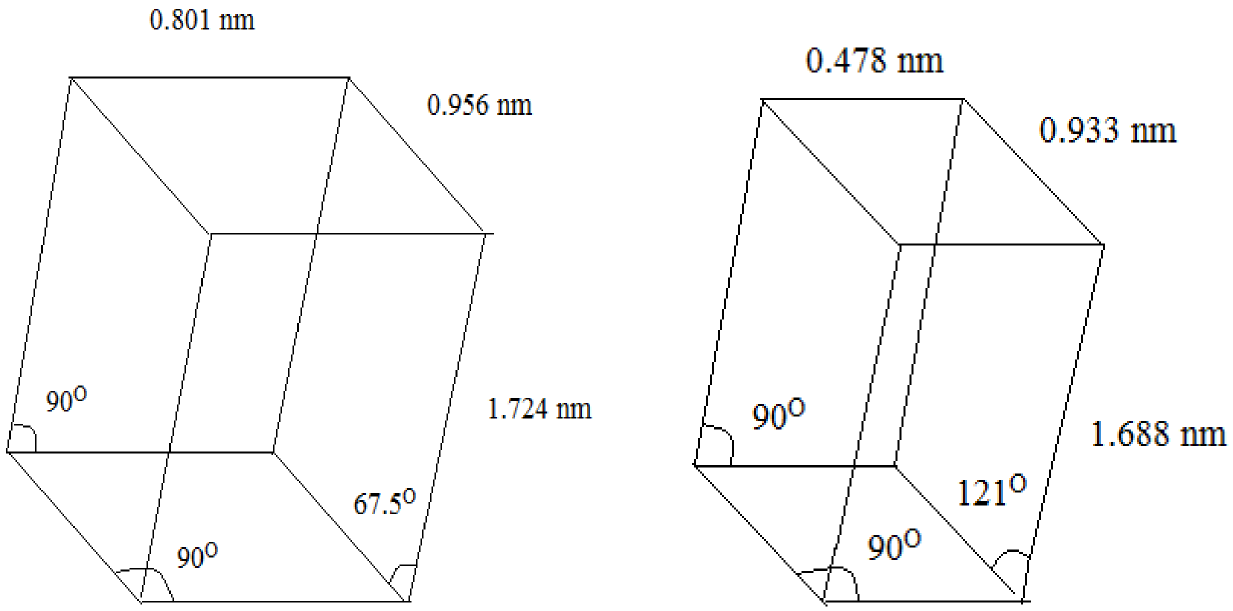

(a) (b)

Figure 3 – representation of Crystal lattice for (a) α and (b) γ polymorphs of nylon-6.

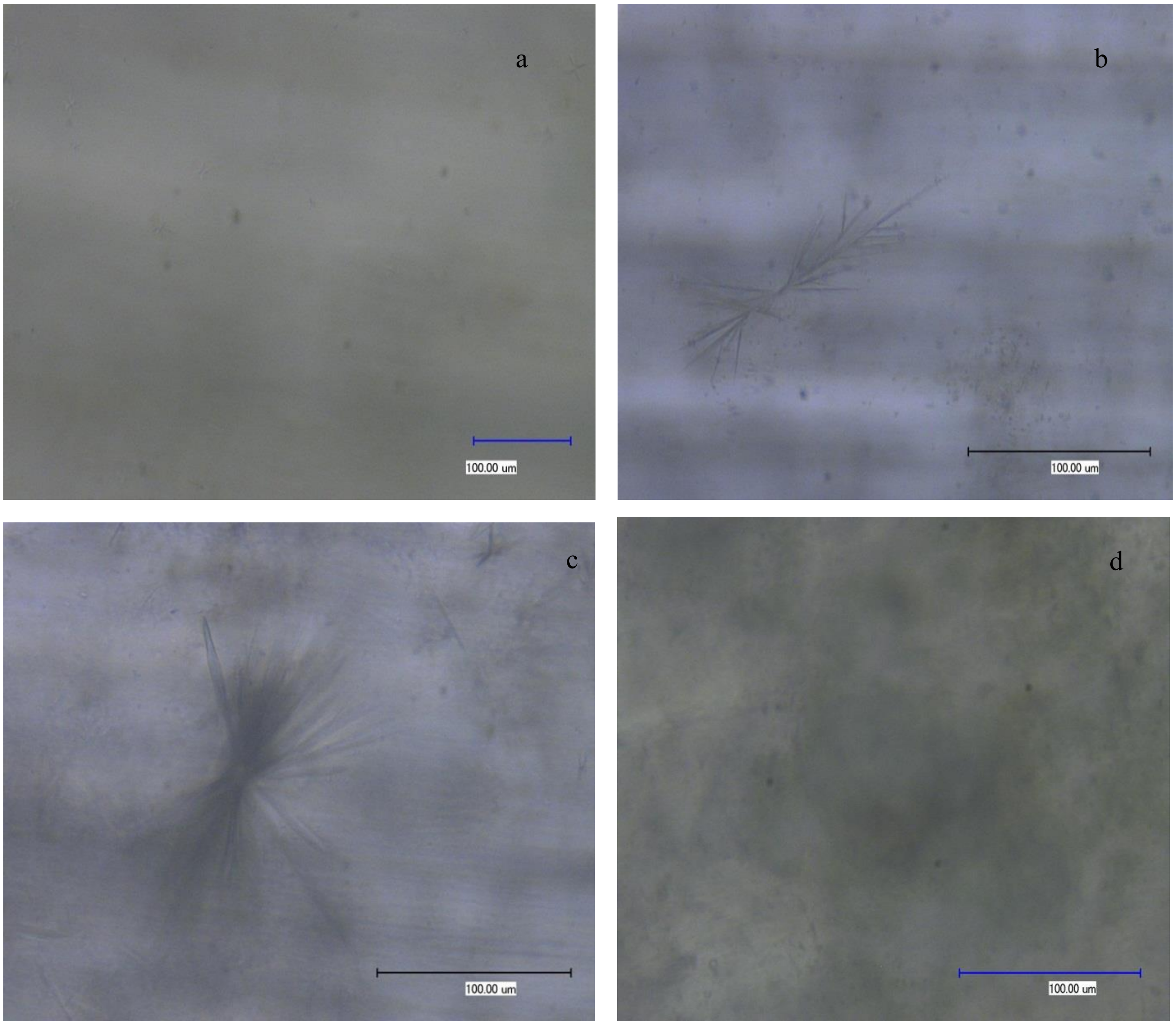

Figure 4 – Optical microscopy image of surface of epoxy/nylon-6 coating (a-0%, b-5%, c-10% and d-20%)

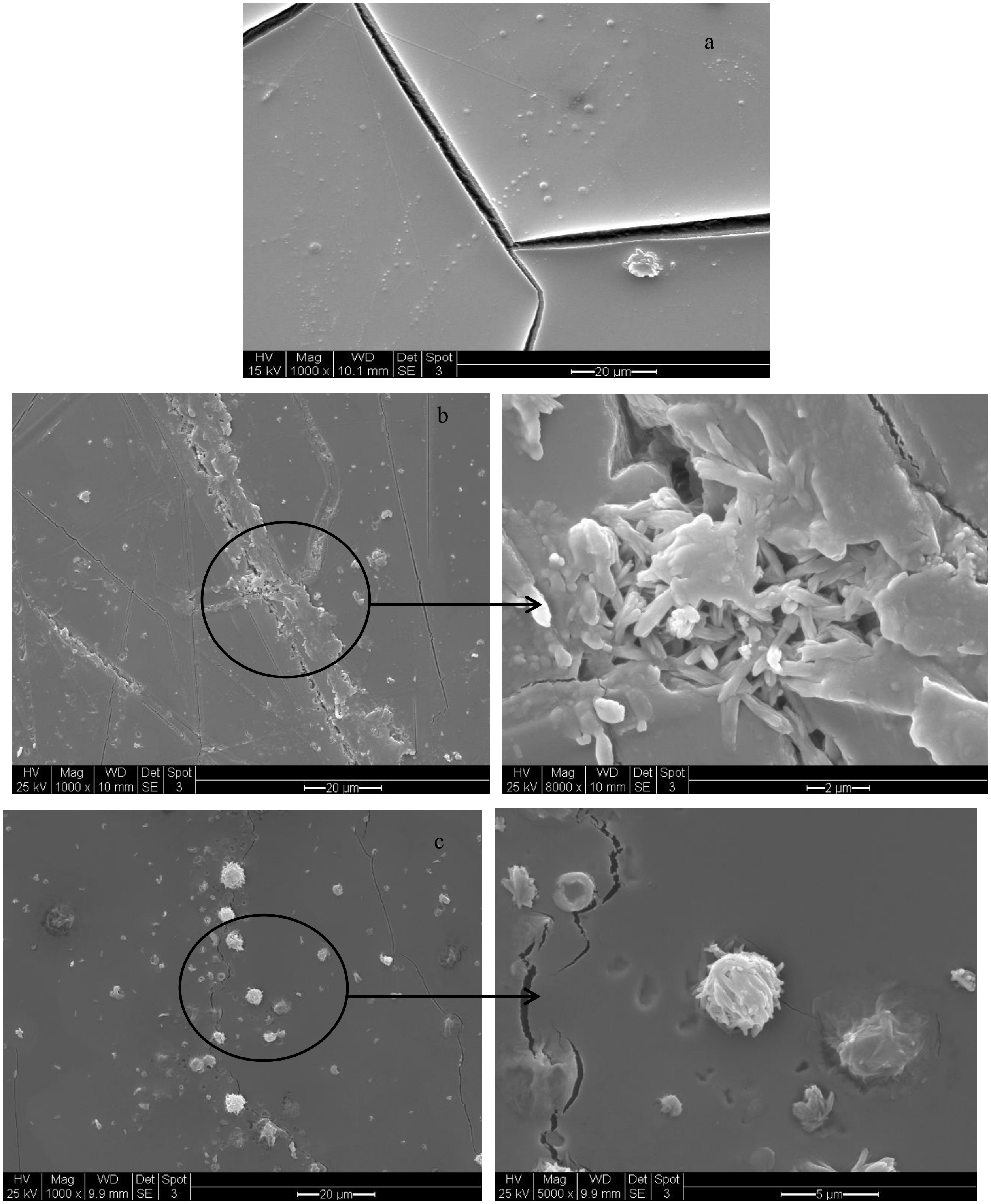

Figure 5 – SEM image of surface of epoxy/nylon-6 (a-0 wt. %, b-10 wt. %, c-20 wt. %) coating

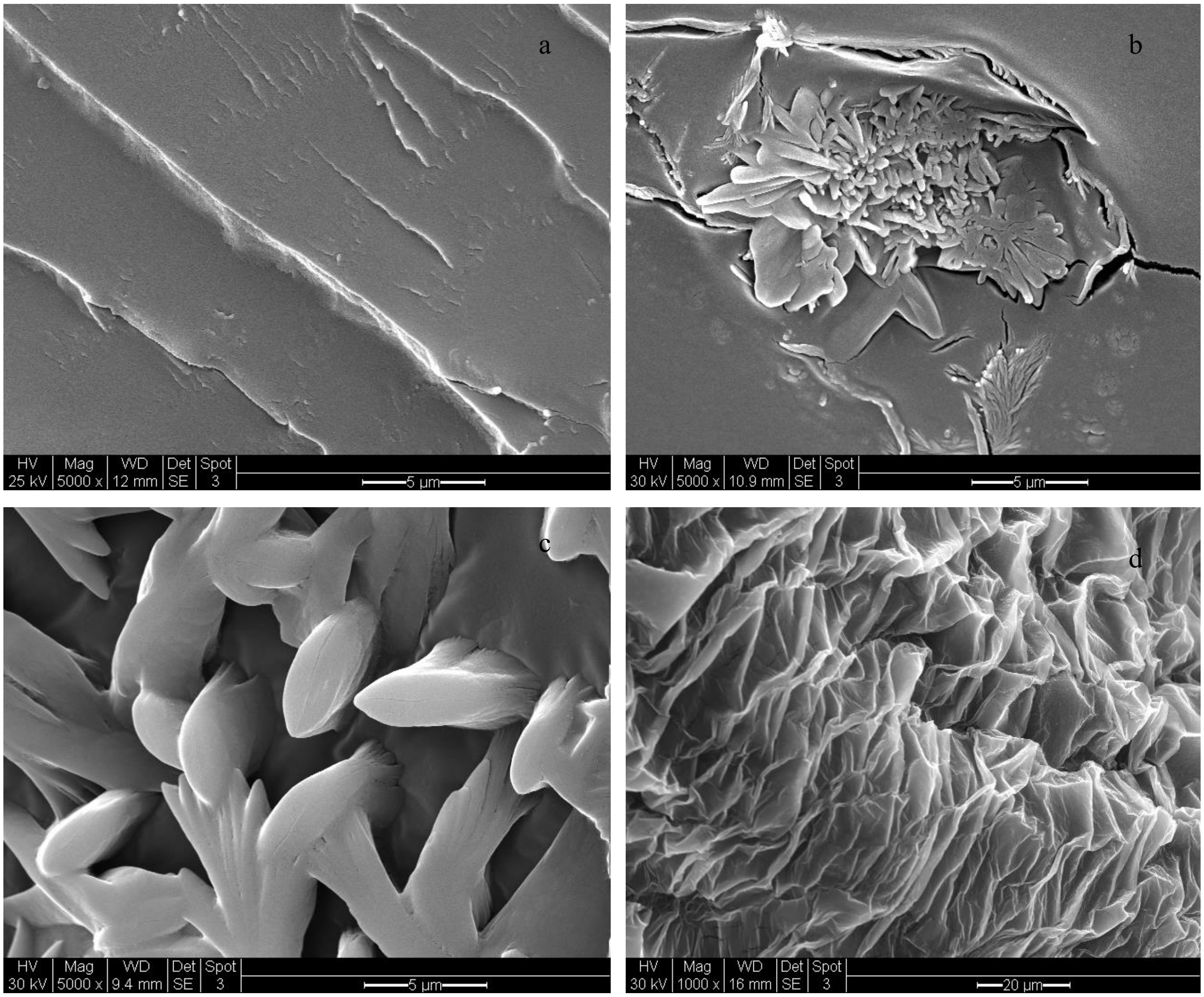

Figure 6 – SEM image of fractured surface of epoxy/nylon-6 film (a-0%, b-5%, c-15% and d-30% by weight)

Journal of Applied Polymer Science, Vol. 130, Issue 5, Pg 3319-3327, 2013

IN-SITU GROWTH OF MULTILAYERED CRYSTALS IN AMORPHOUS MATRIX: THERMAL, DYNAMIC MECHANICAL AND MORPHOLOGICAL ANALYSIS OF NYLON-6/EPOXY COMPOSITES

Aniket Vyas, Jude Iroh, Material Science and Engineering Program, College of Engineering & Applied Science, University of Cincinnati, Cincinnati, OH 45221-0012, USA

INTRODUCTION

Epoxy resins are extensively used as coatings and adhesives in automotive, construction, and aerospace industries, primarily because of their excellent thermal and mechanical properties, such as high stiffness, high strength, chemical resistance and dimensional stability with excellent adhesion to a variety of surfaces. In spite of outstanding properties, there are few drawbacks associated with epoxy, like inherit brittleness, low toughness, presence of micro-cracks and poor fracture resistance. To overcome these drawbacks, incorporation of second phase, such as rubber or thermoplastic polymers, has often been successful to enhance the toughness and lower the brittleness of epoxy. The epoxy–thermoplastic composites have been studied since the 1980s with considerable progress in property improvement[1-3].

The modification of epoxy with rubber particles has shown significant increase in fracture toughness of brittle epoxy but at the expense of elastic modulus and glass transition temperature. Another major problem associated with rubbers such as polybutadiene is the presence of a high level of unsaturation, which provides sites for thermal and oxidative degradation. Moreover, the presence of double bonds in chain can cause further cross-linking which may result in a loss of elastomeric properties and ductility of precipitated particles[4,5].

In order to overcome the drawbacks in the use of rubber as a modifying agent, ductile engineering thermoplastics like polysulfone, polyester, poly(ether-imides), poly(ϵ-caprolactone) and polyamides have been studied as alternate modifiers. These thermoplastics are found to be promising since they do not decrease the inherent properties of the epoxy matrix[1,2].

Nylon-6 is a type of polyamide thermoplastic which has been known to toughen epoxy not only by physical mixing but also by chemical interactions [6,7]. Most of the previous research in the area of epoxy-nylon blends has been focused on mechanical properties but very little attention has been paid to prevailing chemical interactions. Gorton[6] reported that the amide functional group in nylon backbone reacts with the epoxide functional group on the basis of swelling tests. Zhong et al [7] studied the chemical reaction, cure kinetics and phase behavior of epoxy-nylon system using FTIR and DSC. They found that curing reaction depends on composition and that curing decreases the crystallinity of nylon. This suggests that the chemical reaction has a profound effect on resulting multiphase structure which controls the thermal and mechanical properties, but there was no clear understanding of this phenomenon.

In a study by Sangcheol Kim et al [3] premade Nylon-6 powder was mixed with epoxy by heating the mixture above 200°C followed by cooling to room temperature. They found that the existence of multiphase structure, and hence ultimate properties of composite, depended on the mixing method. In another study by Jun Kyung Kim et al. [8], Nylon-6 powder was dispersed in epoxy resin mixed with the curing agent. They found that the inclusion of nylon-6 increase the fracture toughness without any loss of young's modulus or yield strength. Nylon-6, 6 [9], nylon-4, 6 [10] and nylon-12 [11] have also been used as reinforcing agents with epoxy in order to modify epoxy resin properties.

For proper mixing of nylon-6 with epoxy, nylon-6 is desired in solution form. The known solvents for Nylon 6 are formic acid, hexafluoroisopropanol (HFIP) and m-cresol but acid may lead to corrosion in surface coating application while m-cresol is highly toxic and HFIP is very costly.

In this work, a novel nylon-6/epoxy resin reactive mixing process based on solution polymerization of Nylon 6 in NMP, a low volatility solvent, is explored. Nylon-6 was obtained in suspension form after polymerization and was then blended with water-based epoxy resin at room temperature at low shear with mechanical stirring. The obtained nylon-6 was found to react easily with epoxy resin. The morphology of the films was observed by using Scanning Electron Microscope (SEM) while the transition temperature and mechanical property were determined by DSC and DMA.

The aim of this work is to develop a greater understanding of the processing-morphology-property relationship for nylon-6/epoxy resin composites. The effect of composition on the morphology and properties of the composites is presented in this paper.

EXPERIMENTAL

Materials

Polyfunctional Water Dispersible DGEBA based Epoxy resin (EPIREZ 5522-WY-55) was purchased from Hexion Chemicals, Houston, USA. ϵ -caprolactam, 95% pure-Dry Sodiam Hydride, N-acetylcaprolactam & NMP solvent were purchased from Sigma-Aldrich, USA for solution Polymerization ε-caprolactam.

Procedure

Synthesis of Nylon-6 in N-Methylpyrollidone

Polymerization was carried out in an oil bath assembly. 100 ml of NMP was taken in a 3 neck flask and 30 g of monomer (ϵ -caprolactam) was added and stirred until it formed a colorless solution. Nitrogen supply was turned on and temperature was raised to 80^{O}C. 0.72 g of NaH (catalyst) was then added to the solution and stirred till it dissolved completely. This process of dissolution was accompanied by a series of color changes from colorless to dark blue which eventually turned black upon complete dissolution. Temperature was then gradually raised to 160^{o}C and 0.396 g of N-acetyl Caprolactam (Initiator) was added to the solution while maintaining the stirring. After addition of initiator, solution was stirred for 30 minutes, then nitrogen supply was turned off, and the black solution was observed to gently turning into a dark orange viscous solution. Nylon 6 existed as a homogeneous solution at higher temperature but while transferring to a glass jar at room temperature it began to phase separate and existed in a suspension form.

Preparation of Nylon-6/Epoxy Blends

Epoxy was transferred to a glass jar, nylon-6 suspension was added in various amounts and NMP was further added to dilute the solution to reduce the viscosity for ease of processing in order to have defect-free films and coatings. Nylon 6 was added as 0, 5, 10, 15, 20 & 30 weight % with respect to solid content of epoxy resin. The mixture was then stirred using mechanical stirrer for 1 hour at room temperature to obtain homogeneous solution and then ultra-sonicated for 5 minutes.

Preparation of Solid Nylon- 6 and Free Standing Films of Epoxy/Nylon-6 Blends

5 ml of nylon-6 suspension was taken in a Teflon mold and gradually heated up to 200^{O}C for 24 hours in vacuum oven to fully evaporate the solvent and likewise nylon-6 granules were precipitated from the solution.

8 ml of blend was taken and casted in 1.5'' × 1.5'' × 1/4 '' teflon molds. The films were cured in vacuum oven in a stepwise manner, heating initially at 50^{O}C for 13 hours, 100^{O}C for 4 hours, 120 ^{O} C for 2 hours, and finally 150^{O}C for 2 hours and were then cut with a sharp razor blade to obtain rectangular films for Dynamic Mechanical Testing.

The free-standing films were quenched in liquid nitrogen and broken to see the cross-section of fractured surface under Scanning Electron Microscopy.

The films and coatings were prepared from the solution with different amounts of NMP. At low amount of NMP (high Viscosity), defects like pinholes, cracks & bubbles were observed, thus solution was diluted (viscosity was reduced) until defect free films were obtained and that system was considered for further study, but the amount of NMP in all systems was kept constant.

Characterization

The viscosity of blend was measured by shear viscometry using the Brookfield Viscometer. The Viscometer spindle speed was varied from 0.5 to 100 rpm and temperature was maintained at 25^{O}C.

Nicolet 6700 FT-IR instrument, equipped with a smart orbit ATR accessory with diamond crystal, was used to determine the chemical composition of the samples. ATR was performed over a wave number range between 4000 cm^{-1} and 400 cm^{-1}.

Dynamic Mechanical Spectroscopy (DMS) was used to study the variation of storage modulus and tan δ of neat epoxy and epoxy/Nylon 6 composite films with respect to temperature. Dynamic Mechanical Analysis was performed between -20^{O}C to 140^{O}C by using DMS6000, Seiko Instruments Inc. The test was performed under tensile loading at a heating rate of $5^{O}C$/min and a frequency of 1 Hz.

Differential scanning Calorimeter (DSC) was used to measure thermal properties of Nylon 6 and modified epoxy. DSC was performed at the heating rate of $5^{O}C$/min using DSC6200, Seiko Instruments Inc.

Scanning Electron Microscope was a Philips model FEI XL 30 ESEM-FEG. The software used to capture images was Scandium. Aluminum stubs with carbon tape were used as sample holders, and the sample was coated with Au-Pd before subjecting to SEM.

RESULTS AND DISCUSSION

Rheological Behavior

Figure 1 shows the dependency of shear viscosity of epoxy/nylon-6 blend on shear rate with varying nylon-6 amount. The solution with greater amount of nylon-6 showed higher value of viscosity at all spindle speeds. The viscosity for all of the solutions increased with spindle speed indicating shear thickening. At low spindle speed there was a sharp increase in the viscosity with nylon-6 loading, while at high speed the increase was gradual as shown in Figure 2.

This kind of flow behavior suggests that an increase in Nylon-6 wt. % in solution, results in more deviation from Newton's law of viscosity and the solution behaves more as a dilatant. The possible reason for this can be shear-induced particle migration or in other words, under stress nylon-6 tends to crystallize and behave more like a solid then solution [12,13].

There are two possible mechanisms for shear-induced particle migration during shear flow, heterogenity of the stress field and strong inter-particle interactions. In first case, the particles tend to migrate to lower shear stress regions while in second case; the situation becomes more complex involving a coupled relationship between the thermodynamics and hydrodynamic forces [14].

At low shear rate, inter-particle force is more dominant in solution with low nylon-6 and shear force is dominant in solution with high nylon-6 loading. Hence, in the former case, suspended particles tends to remain in ordered layers compared to solution with high nylon-6 loading, where particles tend to enter a state of flocculation and behaves more like a solid. This leads to a sharp increase in the viscosity of solutions at low shear rate. Whereas, at high shear rate, shear force is more dominant then inter-particle force in all the solutions and thus there is a gradual increase in the viscosity.

Fourier Transform Infrared Spectroscopy

Figure 3 shows the FTIR spectra for the synthesized nylon-6. As expected, the characteristic amide peak was observed at 1651.6 (primarily due to carbonyl stretching vibration). CH_2 asymmetric and symmetric stretching was observed at 2926.6 and 2854.3 respectively. A small peak was observed at 3295 which can be attributed to hydrogen-bonded N-H stretching and peak at 1161.3 can be attributed to CONH skeletal motion [15]. Peak at 791.3 belongs to N-H wagging and peak at 1351.6 corresponds to C-N stretch of amide linkage. This confirms that ε-caprolactam was successfully polymerized to form nylon-6 in NMP.

Figures 4 and 5 show the FTIR spectra for neat epoxy and epoxy/nylon-6 (20wt. %) composite respectively. The characteristic peak of epoxide ring is observed at 914 cm^{-1} and 863 cm^{-1} [16]. On closely observing these two peaks in Figure 6, nylon-6 prepared in suspension form was found to be assisting in the curing of epoxy. All of the samples were cured under same conditions of time and temperature, but with the increase in nylon-6 wt. % the peak corresponding to epoxide group gradually lowered, and at higher loading of nylon-6 (20 and 30 wt. %) the peak completely vanished indicating complete curing. The broad peak corresponding to –OH stretching at 3393.5 in neat epoxy was found to be narrowed with a relatively sharp peak at 3392.5 in epoxy/nylon-6 blend indicating the presence of amine group in the system which indicates hydrogen bonding.

Previously, many authors have done a time based study for curing of epoxy using FTIR, maintaining the same composition[17,18]. Following the similar guidelines, a composition based study was carried out for the curing of epoxy as a function of wt. % of Nylon 6.

All the samples were cured for same period of time and epoxy fractional conversion was calculated based on the peak area variation of epoxy group's absorption at 914 cm^{-1}. The internal standard was chosen as stretching vibration of C=C at 1506 cm^{-1} characteristic peak of benzene to quantify the variation. The epoxy fractional conversion is calculated as:

$$\alpha = 1 - \left(\frac{\left(\frac{Aepoxy}{Abenzene}\right)with\ nylon}{\left(\frac{Aepoxy}{Abenzene}\right)without\ nylon}\right) \qquad [1]$$

where A is the area under absorption peak.

Figure 7 gives the variation of epoxy fractional conversion as a function of weight % of nylon-6 in epoxy resin and was found to be increasing with the loading of nylon-6. The conversion is found to be low at low loading (5%) which increases sharply at 10 and 15% and then reaches a plateau at 20%, after which the conversion becomes almost constant.

Dynamic Mechanical Analysis

Figures 8 and 9 shows the dynamic mechanical properties for the neat and nylon-6-loaded epoxy films. The storage modulus and tangent-to-loss modulus are studied as a function of temperature beginning in the glassy state, through the T_g, and ending as a rubbery plateau.

The storage modulus, which provides a measure of material stiffness under tensile deformation of a solid sample at room temperature, was highest for the neat epoxy, whereas the systems with nylon-6 showed lowering of storage modulus in glassy region. The variation of storage modulus with different nylon-6 loading in glassy region is shown in Figure 10. The fall of storage modulus in this region confirms the plasticizing effect of nylon-6 with an increase in flexibility of epoxy which is inherently brittle by nature. As can be seen Figure, the storage moduli of composite decreased almost linearly with addition of nylon-6. In glassy state, stiffness is related to changes in the stored elastic energy upon small deformation as the molecular segments resist motion [19]. The composites with nylon-6 appear less able to resist segmental motion and thus are not able to store elastic energy, resulting in lower glassy modulus.

An increase in storage modulus in rubbery region was observed from neat epoxy to epoxy/nylon-6 blend. In composite systems, storage modulus was highest for 5% but decreased gradually with increase in nylon-6 weight % though it was greater than neat epoxy for all blends as shown in Figure 11. This phenomenon can be attributed to reaction between epoxy and nylon-6 which causes increase in crosslink density evident by the rise in elastic modulus. The presence of unreacted nylon-6 for higher amounts acts as plasticizer [20] which causes fall in T_g, with increase in fraction of nylon-6. The curve for T_g as a function of composition is shown in Figure 12. The T_g drops sharply from neat epoxy (70^0C) to 5% (41.2^0C), then decreases gradually from 5 to 30 % (25.7^0C).

The reason for drop of T_g has been cited as under-curing of epoxy due to partial miscibility of second phase in epoxy [20]; another reason can be flexible aliphatic nature of thermoplastic backbone [2]. In the present case increase in nylon-6 loading leads to increase in cross-link density as indicated by increase in storage modulus in rubbery region. Moreover FTIR results also suggest increased curing of epoxy. Hence, a possible reason for lowering of T_g by addition of nylon-6 should be its plasticizing effect, i.e. it reduces the intermolecular forces among chain of epoxy and essentially lubricates the macromolecular chains.

Furthermore in the given temperature range, presence of single peak for tan (delta) indicates the existence of a single amorphous phase in cured epoxy/nylon-6 blend. If the two starting materials had different phases in amorphous region and prevented reaction, then two T_g peaks would be expected, one for each amorphous phase which is observed for immiscible or partially miscible thermoplastic blends.

The observed T_g from DMA was compared with the theoretical linear model given by Fox equation which predicts the dependency of T_g on composition. The Fox equation is a simple additive law which does not account for any kind of interaction between two polymers in the systems. The comparison can be seen in Figure 13. A negative deviation was observed from the ideality which suggests the presence of strong hydrogen bonds and chemical interaction between two participating polymer entities.

Differential Scanning Calorimeter

Thermal transitions in nylons have been widely studied by previous researchers using DSC [21]. Nylon-6 and its blends with epoxy were subjected to DSC to investigate thermal transitions. Figure 14 is the DSC thermogram for nylon-6 which shows glass transition temperature (T_g), Melting point (T_m) and crystallization temperature (T_c). The nylon-6 and composite samples were first heated to 60^0C from room temperature followed by quenching with liquid nitrogen and the second run was started from -20^0C to 250^0C. They were then cooled rapidly to room temperature and were reheated from – 20^0C to 250^0C and then cooled to monitor the crystallization peak.

A sharp fall in the baseline was observed for neat nylon-6 from 9^0C to 32^0C suggesting T_g to be around 25-28^0C. The onset temperature for melting of nylon-6 was 188^0C, the peak was observed at 209^0C and the offset temperature was around 215^0C. The crystallization begins to occur at 177^{0}C, reached a peak at 170^{0}C and the peak dropped at 160^{0}C. The % crystallinity was calculated on basis of the following formula:

$$\%Crystallinity = \frac{\Delta Hf}{\Delta Hf0} \times 100 \qquad [2]$$

Where ΔH_f is measured heat of fusion from DSC and ΔH_{f0} is heat of fusion of equilibrium crystals (totally crystalline polymer). A commonly accepted average value of 230 (+/- 20) J/g for nylon-6 was used as ΔH_{f0} for calculating crystallinity [21]. The approximate value of ΔH_f calculated from melting peak of nylon-6 was 89.71 J/g.

The calculated crystallinity was around 35-42%.

For the composites with loading of nylon-6, associated melting peak was well observed, but with the reduction in nylon-6, the melting peak began to broaden and no clear and distinct peak was observed at lower loading of nylon-6 (5 and 10%) suggesting significantly low crystallinity. Figure 15 is the DSC thermogram showing the melting peak of epoxy/nylon-6 composites and Figures 16 is a comparison between glass transition temperatures. Table 1 shows the onset melting point, peak melting point, offset melting point and T_g of neat nylon-6 and its blends with epoxy.

The T_g shown in Figure 16 was calculated in the third run of DSC, where solvent was evaporated and curing was complete. Hence, T_g observed by DSC was higher than that of DMA. In few compositions of epoxy/nylon-6, distinct multiple peaks over a broad range were observed. This suggests a wide distribution of nylon crystals in epoxy matrix.

As nylon-6 was crystallized in a solution of epoxy and NMP, epoxy can be considered as a diluent in present case. The results on melting were in accordance with Flory's Theory of Depression of Melting Point in presence of diluent. The T_m for neat nylon-6 was 215^{O}C, which was more than T_m of nylon-6 in epoxy for all compositions. But when T_m was analyzed only for composites, it was found to decrease with increase in nylon-6 concentration (decrease in epoxy as diluent) which is in opposition to Flory's Theory, where T_m is expected to decrease with increase in diluent. Figure 17 shows a variation in onset, peak and offset melting points. All of them showed a decrease with increase in composition. This phenomenon can be explained on the basis of thermodynamics. The equilibrium melting point is given by following equation[12]

$$Tm = \frac{\Delta Hf}{\Delta Sf} \qquad [3]$$

The addition of nylon-6 in epoxy can be viewed as increase of nylon-6 chains in epoxy. During processing of composites, two phenomena take place: reaction (curing) and crystallization. At higher concentration, more chains of nylon-6 react with epoxy and reacted chains of nylon-6 exist in amorphous state [7]. Molecular weight of epoxy resin increases, i.e. at higher composition epoxy acts as more effective diluent. Secondly, melting point depends on change in enthalpy and entropy of the system according to equation 3. The melting point depends upon the ratio of ΔH_f to ΔS_f. Once melting initiates, there are more number of crystalline chains going through transition to liquid state at higher composition. The more are chains, the more is number of conformations, which will lead to increase in entropy of system according to Boltzman's equation:

$$S = K \ln \omega \qquad [4]$$

Melting temperature is inversely dependent on entropy, hence at higher composition, more number of chains lead to increased entropy which results in lowering of melting point.

Morphology

The structure of crystals grown from solution has been reported for higher density polyethylene, slightly branched polyethylene, polypropylene, poly(4-methylpentene-1), polyoxymethylene. In all above mentioned polyolefins and polyoxymethylene, only weak secondary forces exist between neighboring chain segments, but polyamides have relatively stronger hydrogen bonds which greatly influences the nature of crystal growth. Previous studies were limited to precipitation of polyamides from formic acid near room temperature, where spherulitic structures were obtained composed of lathlike lamellae. Later, growth of single crystals of alcohol soluble nylon from solution was thoroughly investigated by P.H. Geil [22]. The crystal structure of nylon-6 crystals has been demonstrated as dendrite or febrile with the appearance of being a bundle as ribbon twisted together in the middle while some of them being a radial array by previous authors [22,23].

The crystalline morphology of neat nylon-6 obtained by solution polymerization and then precipitated from suspension in NMP was observed under SEM (Figure 18). A unique morphology was observed with fiber like crystals; hence it was vital to see the growth and nature of crystals in Epoxy matrix.

It was observed that crystals grow in distinct crystalline zones within the amorphous epoxy matrix. As the nylon in composition increases, the number of crystalline zones increases and after certain composition phase inversion takes place. Three distinct SEM images have been shown for comparison in Figure 19. The first one is of neat epoxy which represents only amorphous phase. The second image is of epoxy/nylon-6 (10%) which shows nylon-6 crystals growing within the amorphous matrix and protruding out of the fractured surface. In this case, epoxy can be considered as diluent which dilutes nylon-6, causing growth of large crystals during the process of curing. The third SEM image is of epoxy/nlon-6 (20%) which shows various crystals distributed uniformly among the amorphous matrix. This can be considered as composition where phase inversion initiates.

The process of crystal growth in epoxy matrix can be visualized as a series of events that occurs during the process of curing. All the epoxy/nylon-6 blends initially exists as a miscible solution. In the state of solution, polymer chains are free to move in any direction i.e. chains are in their random state. As the heat is supplied to initiate the curing process, the solvent begins to evaporate. Due to lack of solvent and dilution, polymer chains realign themselves to acquire the most stable state. Epoxy being the amorphous polymer forms a cross-linked network, but nylon-6 is able to crystalize due to presence of amide group which tends to hold up the chain in an orderly fashion via hydrogen bonding. Hence, surface of epoxy chain acts as an impurity or nucleating agent for crystals of nylon-6 and the thermoplastic chains begins to fold over the surface leading to formation crystal lamellae. Their radical growth leads to formation of spherulites. Hence, the cured film of homogenous blend exists in two phases: a crystalline nylon-6 phase with febrile crystals and an amorphous epoxy and reacted nylon-6/epoxy phase. The nylon-6 chains which were able to crystallize represent the part of nylon-6 that could not take part in the reaction with epoxy. It has been reported that the reaction of nylon with epoxy leads to decrease in its crystallinity. The amorphous part of nylon-6 reacts with epoxy leading to a single amorphous phase indicated by presence of one T_g.

Infrared Spectroscopy suggests the presence of chemical linkages between two entities, on the other hand DSC and Morphology suggests the presence of nylon-6 crystals in product formed.

Hence, the novel product can be considered as a copolymer of epoxy and nylon-6 which contains crystallite domains in the long chain. The resultant product can either be semi-crystalline network structure or semi-crystalline branched structure or non-interacting network structure. The schematic of proposed modified epoxy is shown in Figure 20.

CONCLUSIONS

A non-conventional method to synthesize nylon-6 was successfully explored via ring-opening polymerization of ε-caprolactam in N-methylpyrollidone solvent leading to a very simple and efficient blending of nylon-6 with water-based epoxy. The increase in concentration of nylon-6 in epoxy leads to lowering of Tg with increase in flexibility indicating the plasticizing effect on epoxy. Nylon-6 was found to be assisting in the curing of epoxy as confirmed by FTIR studies and an increase in storage modulus in rubbery region. All the prepared systems exhibit heterogeneity and the morphology changes considerably with variation in thermoplastic component. The thermal transitions studied using DSC revealed that nylon-6 prepared by this method attains a high crystallinity. During the processing of composite, curing of epoxy and crystallization of nylon-6 occurs simultaneously leading to formation of crystalline zones in amorphous matrix.

ACKNOWLEDGEMENTS

This study was funded by grants from office of naval research (ONR) # N00014-09-1-0980 and National Science Foundation (NSF) # CMMI-0758656. We would also like to thank Soumyarwit Manna at Advanced Material Characterization Center (AMCC), university of Cincinnati who assisted in capturing the SEM images.

REFERENCES

1. Hodgkin, J. H.; Simon, G. P.; Varley, R. J. Polymers for Advanced Technologies 1998, 9, 3-10.

2. Barone, L.; Carciotto, S.; Cicala, G.; Recca, A. Polymer Engineering & Science 2006, 46, 1576-1582.

3. Kim, S.; Kim, J.; Lim, S. H.; Jo, W. H.; Choe, C. R. Journal of Applied Polymer Science 1999, 72, 1055-1063.

4. Okamoto, Y. Polymer Engineering & Science 1983, 23, 222-225.
5. Ratna, D. Polymer 2001, 42, 4209-4218.
6. Gorton, B. S. Journal of Applied Polymer Science 1964, 8, 1287-1295.
7. Zhong, Z.; Guo, Q. Polymer 1998, 39, 3451-3458.
8. Kim, J.; Robertson, R. Journal of Materials Science 1992, 27, 161-174.
9. J. Bragg, A. A. C., M. T. Duran and V. Castano, Chemistry and Chemical technology, 2009, 3, 111. Chemistry and Chemical Technology 2009, 3, 5.
10. Bergshoef, M. M.; Vancso, G. J. Advanced Materials 1999, 11, 1362-1365.
11. Cardwell, B. J.; Yee, A. F. Journal of Materials Science 1998, 33, 5473-5484.
12. Painter, P. C.; Coleman, M. M. Fundamentals of Polymer Science: An Introductory Text, Second Edition; Taylor & Francis, 1998.
13. Galindo-Rosales, F.; Rubio-Hernández, F.; Velázquez-Navarro, J. Rheologica Acta 2009, 48, 699-708.
14. Utracki, L. A. Polymer Blends Handbook; Kluwer Academic Publishers, 2002.
15. Lee, K.-H.; Kim, K.-W.; Pesapane, A.; Kim, H.-Y.; Rabolt, J. F. Macromolecules 2008, 41, 1494-1498.
16. dell'Erba, I.; Williams, R. Journal of Thermal Analysis and Calorimetry 2008, 93, 95-100.
17. Smith, R. E.; Larsen, F. N.; Long, C. L. Journal of Applied Polymer Science 1984, 29, 3713-3726.
18. Cherdoud-Chihani, A.; Mouzali, M.; Abadie, M. J. M. Journal of Applied Polymer Science 1998, 69, 1167-1178.
19. Ishida, H.; Allen, D. J. Polymer 1996, 37, 4487-4495.
20. Sun, L.; Warren, G.; Davis, D.; Sue, H. J. Journal of Materials Science 2011, 46, 207-214.
21. Khanna, Y. P.; Kuhn, W. P. Journal of Polymer Science Part B: Polymer Physics 1997, 35, 2219-2231.
22. Geil, P. H. Journal of Polymer Science 1960, 44, 449-458.
23. Ramesh, C.; Keller, A.; Eltink, S. J. E. A. Polymer 1994, 35, 5293-5299.

List of Figures

Figure 1 – Variation of viscosity with shear rate for different nylon-6 wt. % in epoxy solution

Figure 2 - Viscosity at various nylon-6 wt. % at spindle speed of 20 and 100 rpm

Figure 3 – FTIR spectrum of nylon-6 precipitated from suspension in NMP

Figure 4 – FTIR Spectrum of neat epoxy heated in oven for 9 hours

Figure 5 – FTIR spectrum of epoxy/nylon-6 (20 wt. %) heated in oven for 9 hours

Figure 6 – FTIR spectra of neat and nylon-6 filled epoxy (bottom - neat epoxy, 5 wt. % nylon, 10 wt. % nylon, 15 wt. % nylon, 20 wt. % nylon, top – 30 wt. % nylon)

Figure 7 – Epoxy fractional Conversion as a function of nylon-6 wt %.

Figure 8 – variation of storage modulus with temperature for various nylon-6 loading of composite films (a – neat epoxy, b – 5 wt. % nylon, c – 10 wt. % nylon, d – 15 wt. % nylon, e – 20 wt. % nylon, f – 30 wt. % nylon)

Figure 9 - Variation of tan delta with temperature for various Nylon-6 loading of composite films (a – neat epoxy, b – 5 wt. % nylon, c – 10 wt. % nylon, d – 15 wt. % nylon, e – 20 wt. % nylon, f – 30 wt. % nylon)

Figure 10 – storage Modulus in glassy region as a function of nylon-6 wt. %

Figure 11 - storage Modulus in Rubbery region as a function of nylon-6 wt. %

Figure 12 – variation of Tg of the composite with increased loading of nylon-6 in epoxy

Figure 13 – comparison of experimental dependency of T_g on composition with fox equation

Figure 14 –DSC thermogram for nylon-6 showing glass transition temperature, melting temperature and crystallization temperature

Figure 15 – DSC curve for epoxy – nylon composites films showing T_m

Figure 16 – DSC curve for epoxy – nylon composites films showing T_g

Figure 17- Comparison of onset, peak and offset melting temperature of nylon-6 in epoxy

Figure 18 – SEM image of nylon-6 crystallized from nylon-6-NMP solution

Figure 19 - SEM Images of cross-section of fractured Surface for neat epoxy, epoxy/nylon-6 (10 and 20%)

Figure 20 – Schematic of possible structures of modified epoxy

Table:

Table 1 – The peak value of melting depression for different composition.

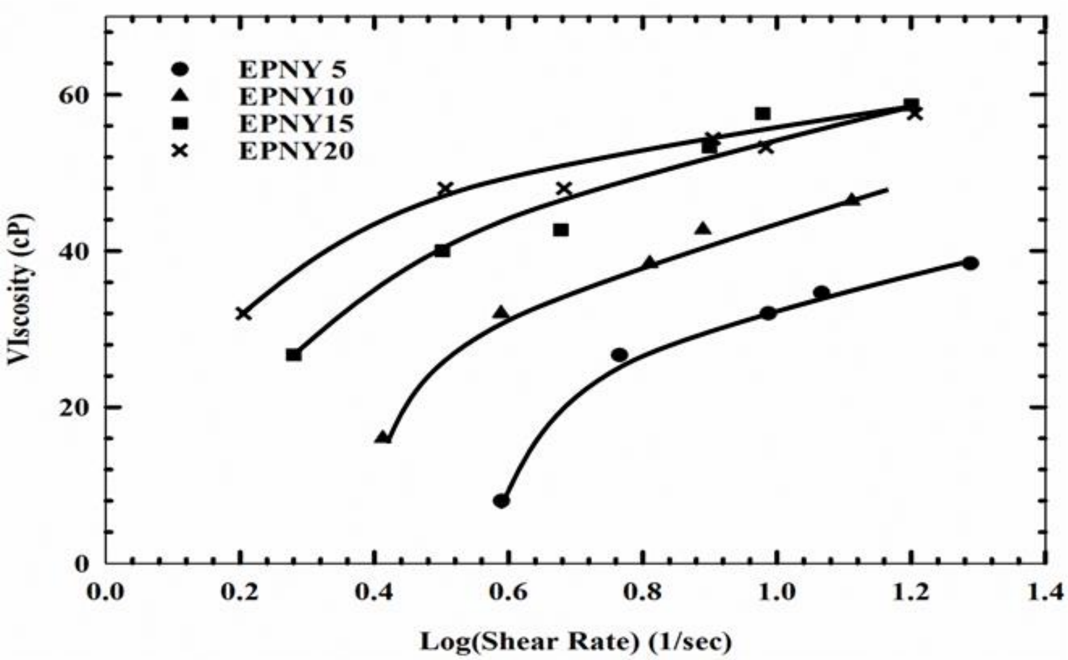

Figure 1 – Variation of Viscosity with shear rate for different nylon-6 wt. % in epoxy solution

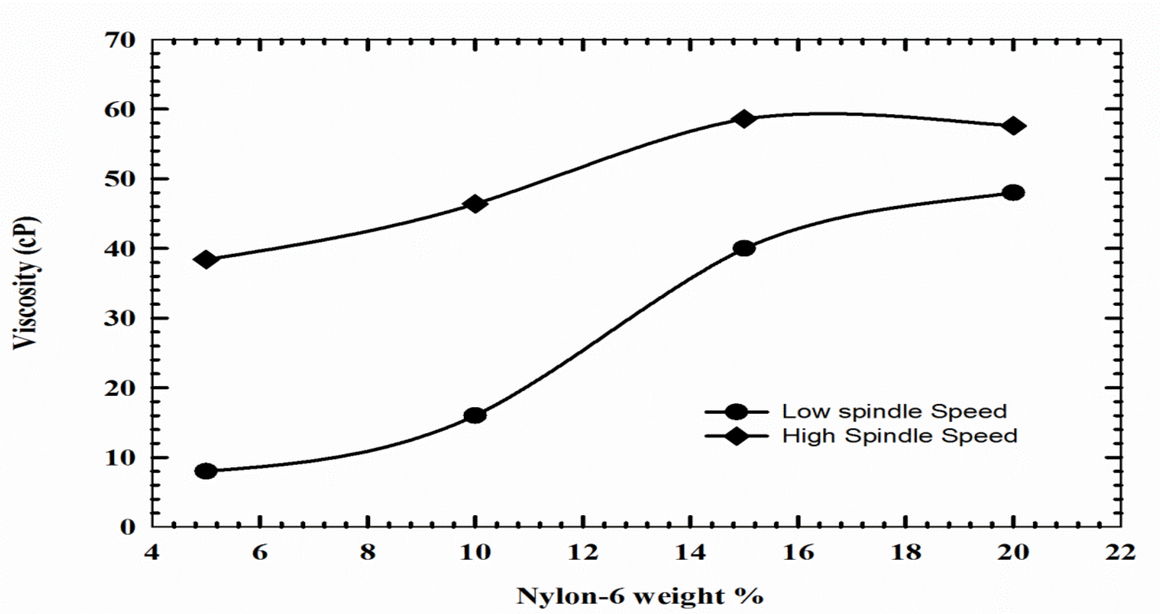

Figure 2 - Viscosity at various nylon-6 wt. % at spindle speed of 20 and 100 rpm.

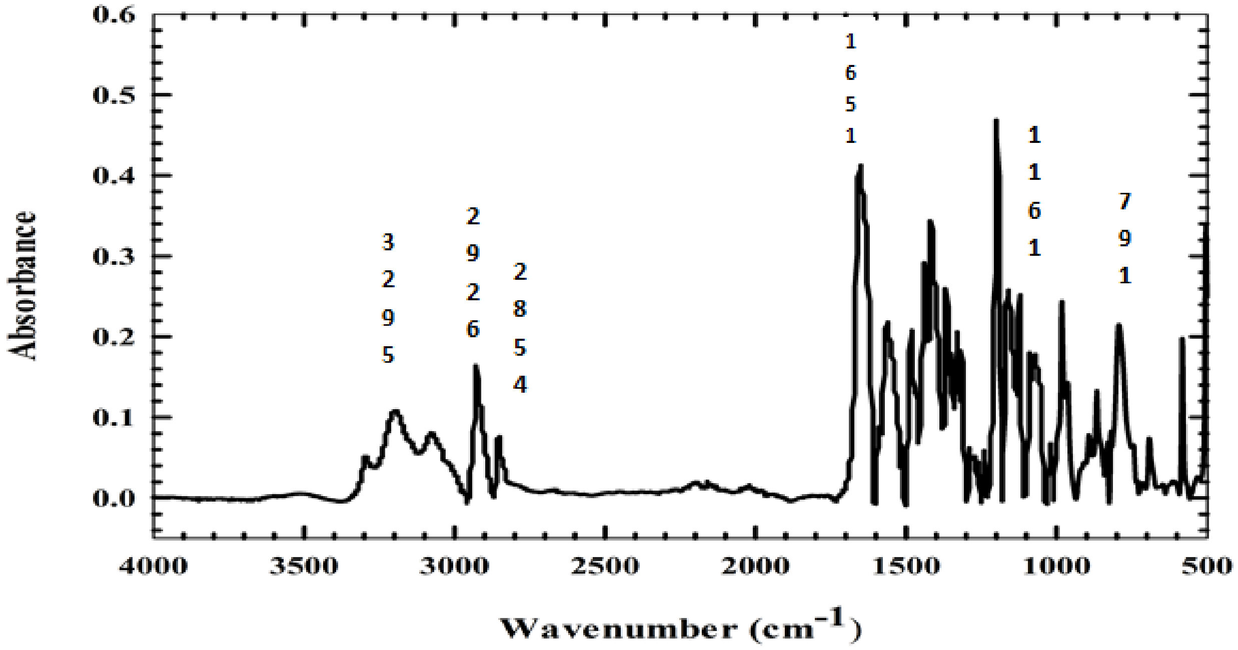

Figure 3 – FTIR spectrum of nylon-6 precipitated from suspension in NMP

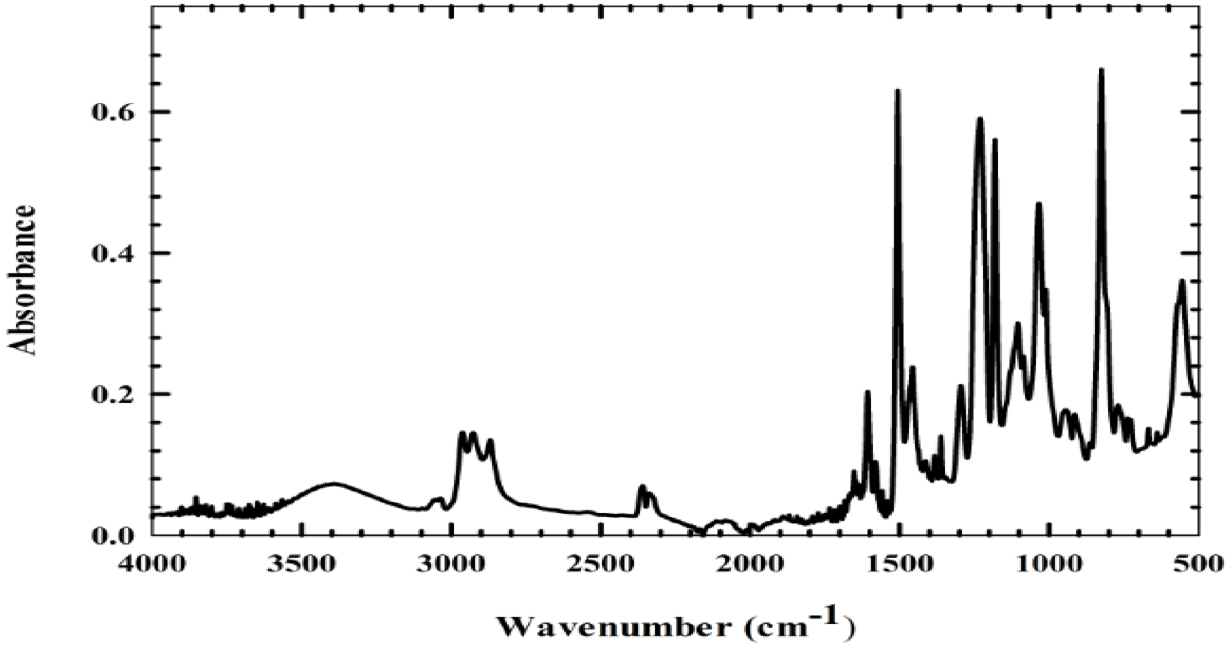

Figure 4 – FTIR Spectrum of neat epoxy heated in oven for 9 hours

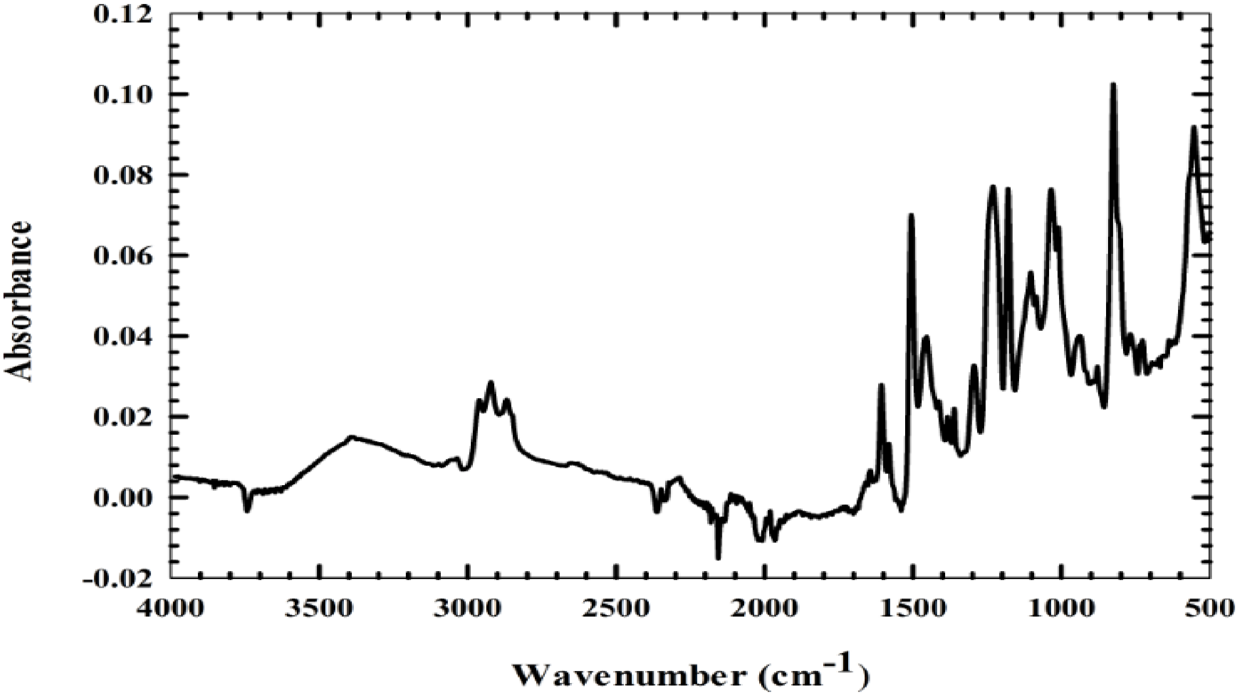

Figure 5 – FTIR spectrum of epoxy/nylon-6 (20 wt. %) heated in oven for 9 hours

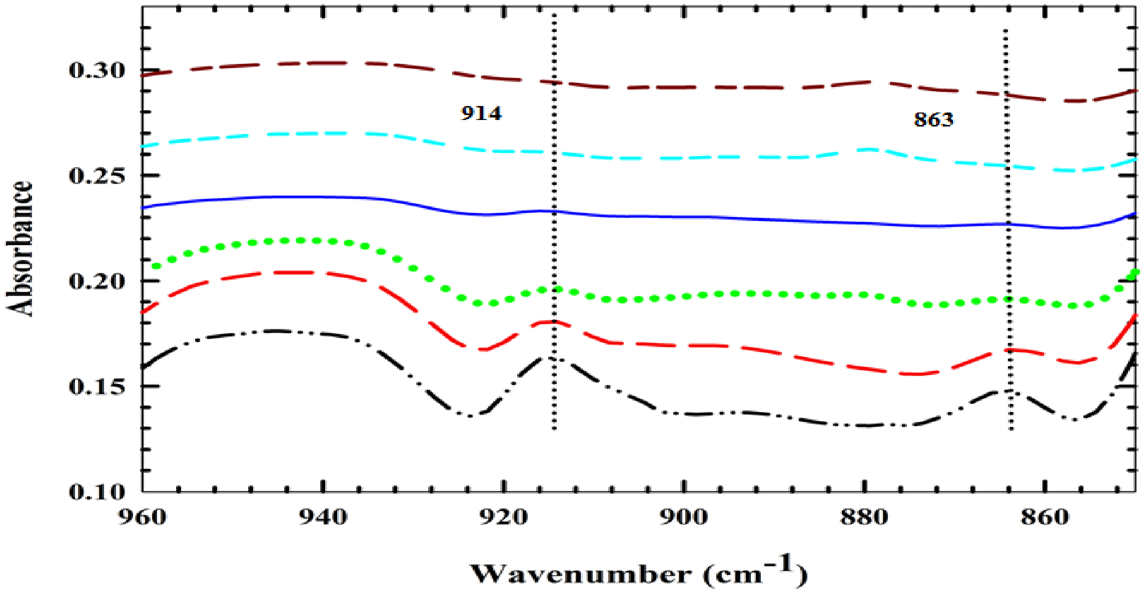

Figure 6 – FTIR spectra of neat and nylon-6 filled epoxy (bottom - neat epoxy, 5 wt. % nylon, 10 wt. % nylon, 15 wt. % nylon, 20 wt. % nylon, top – 30 wt. % nylon)

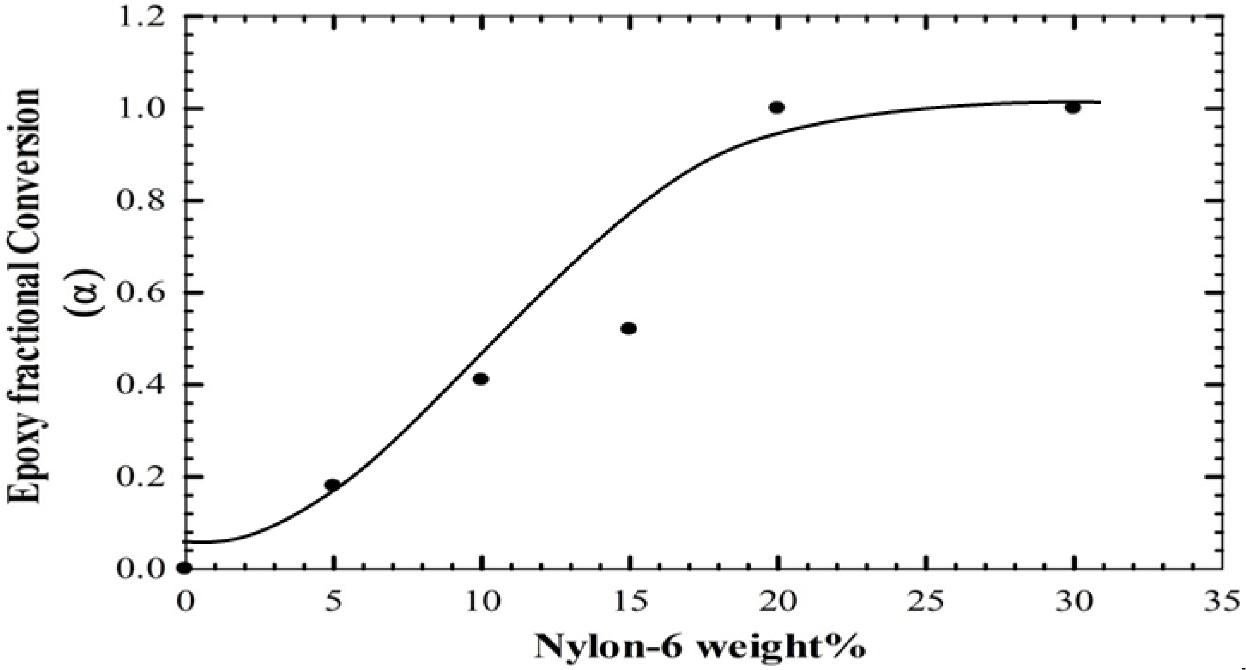

Figure 7 – Epoxy fractional Conversion as a function of nylon-6 wt %.

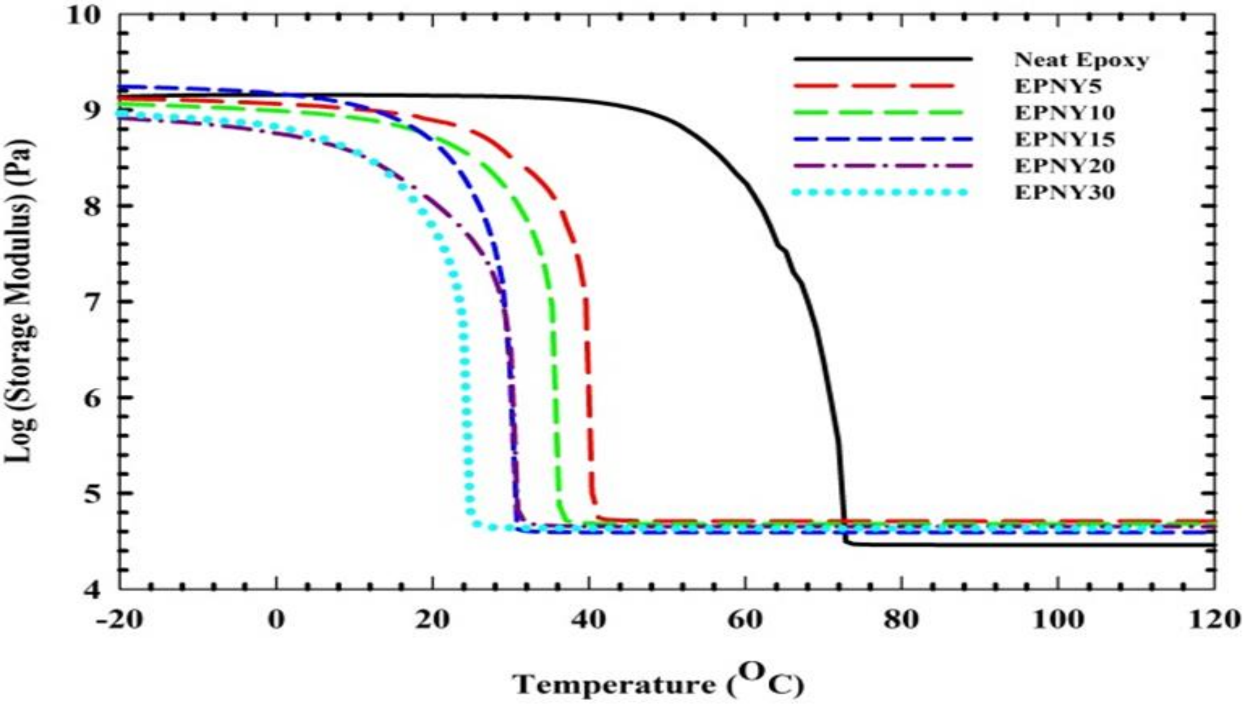

Figure 8 – variation of storage modulus with temperature for various nylon-6 loading

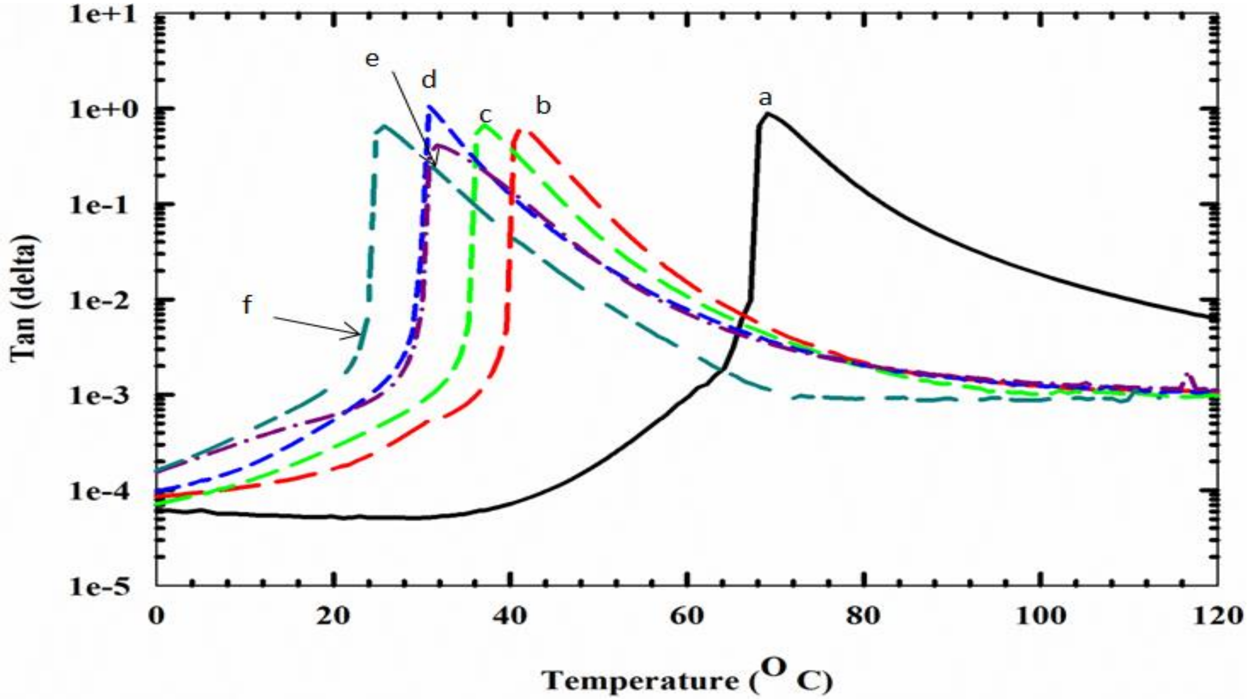

Figure 9 - Variation of tan delta with temperature for various nylon-6 loading of composite films

(a – neat epoxy, b – 5 wt. % nylon, c – 10 wt. % nylon, d – 15 wt. % nylon, e – 20 wt. % nylon, f – 30 wt. % nylon)

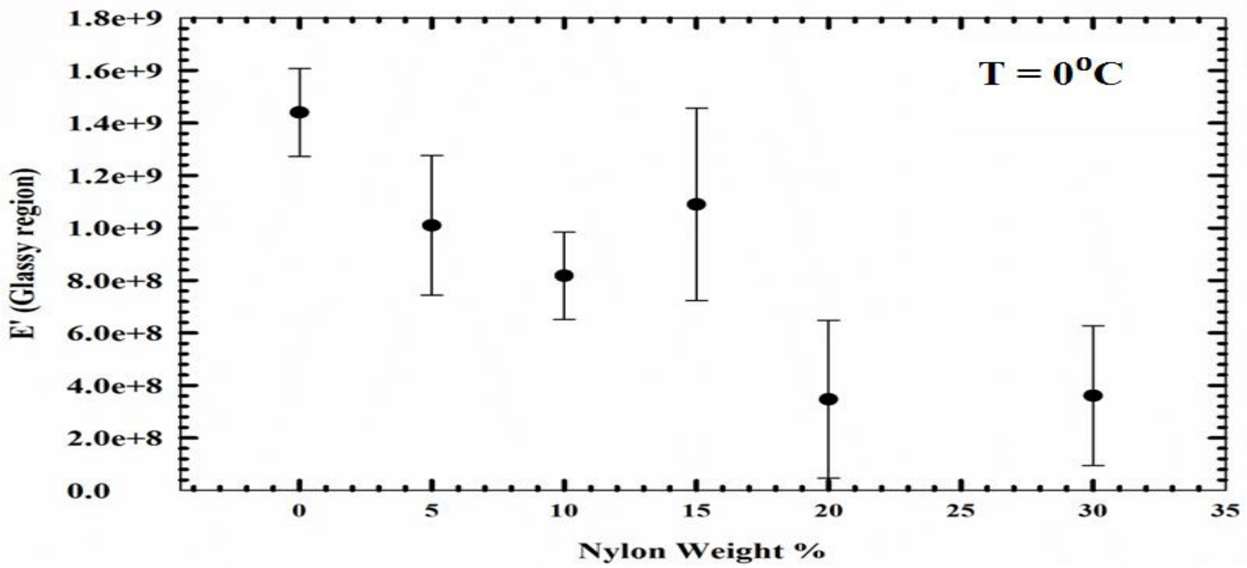

Figure 10 – Storage modulus in glassy region as a function of nylon-6 wt. %

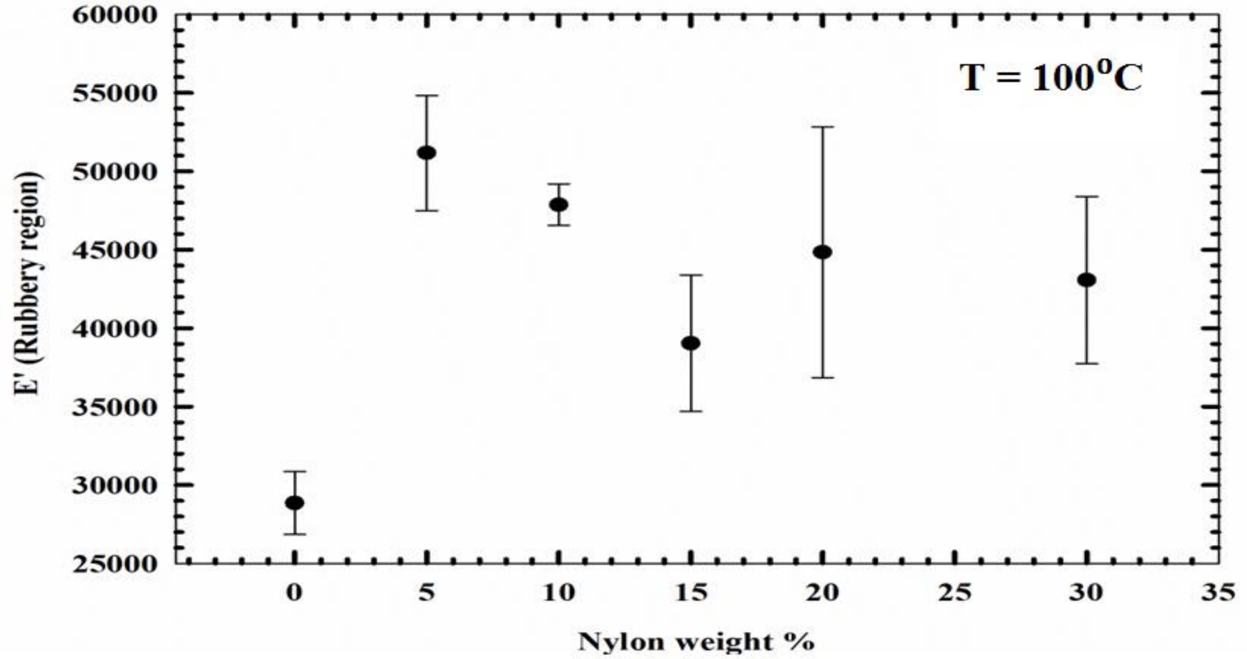

Figure 11 - Storage modulus in rubbery region as a function of nylon-6 wt. %

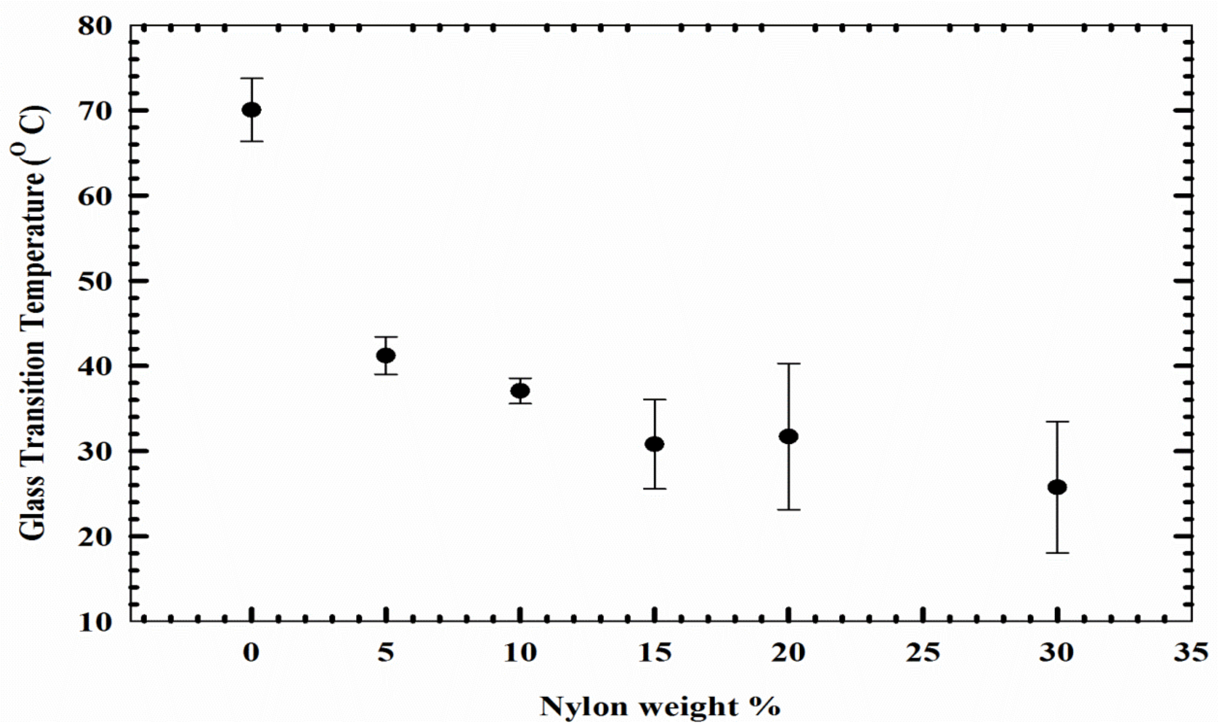

Figure 12 – variation of T_g of the composite with increased loading of nylon-6 in epoxy

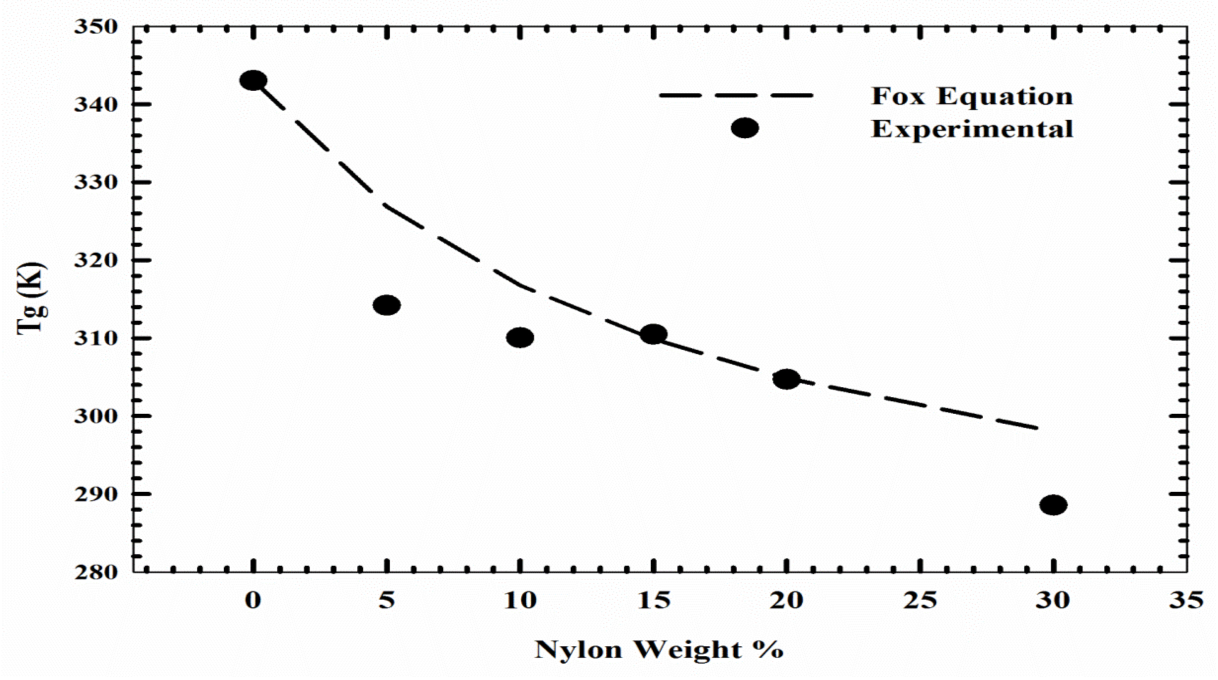

Figure 13 – comparison of experimental dependency of T_g on composition with fox equation

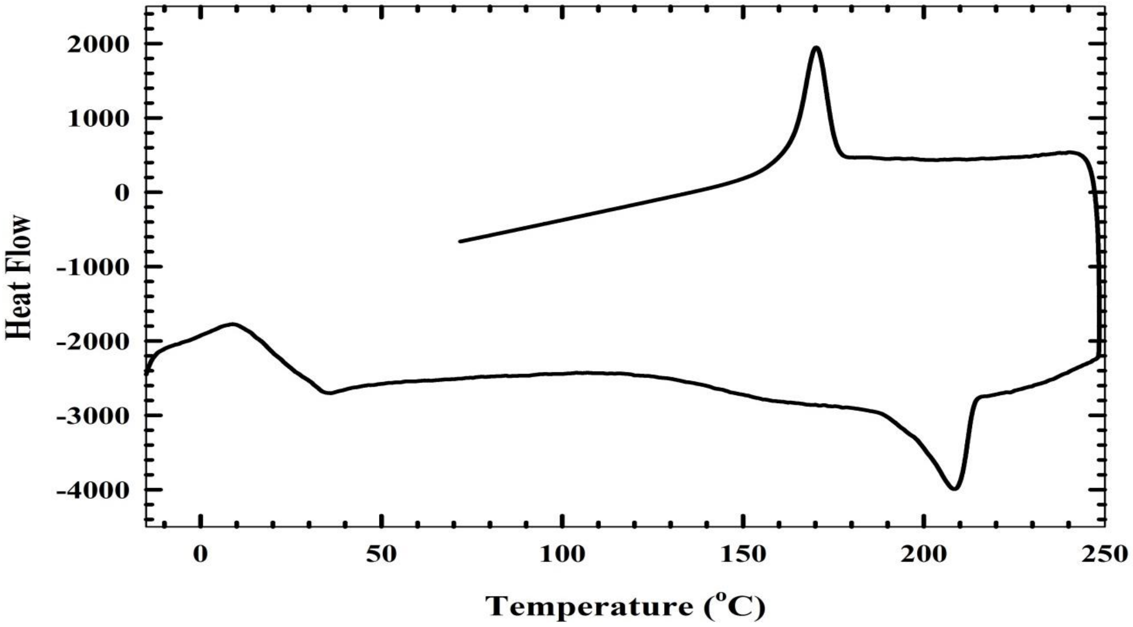

Figure 14 –DSC thermogram for nylon-6 showing glass transition temperature, melting temperature and crystallization temperature

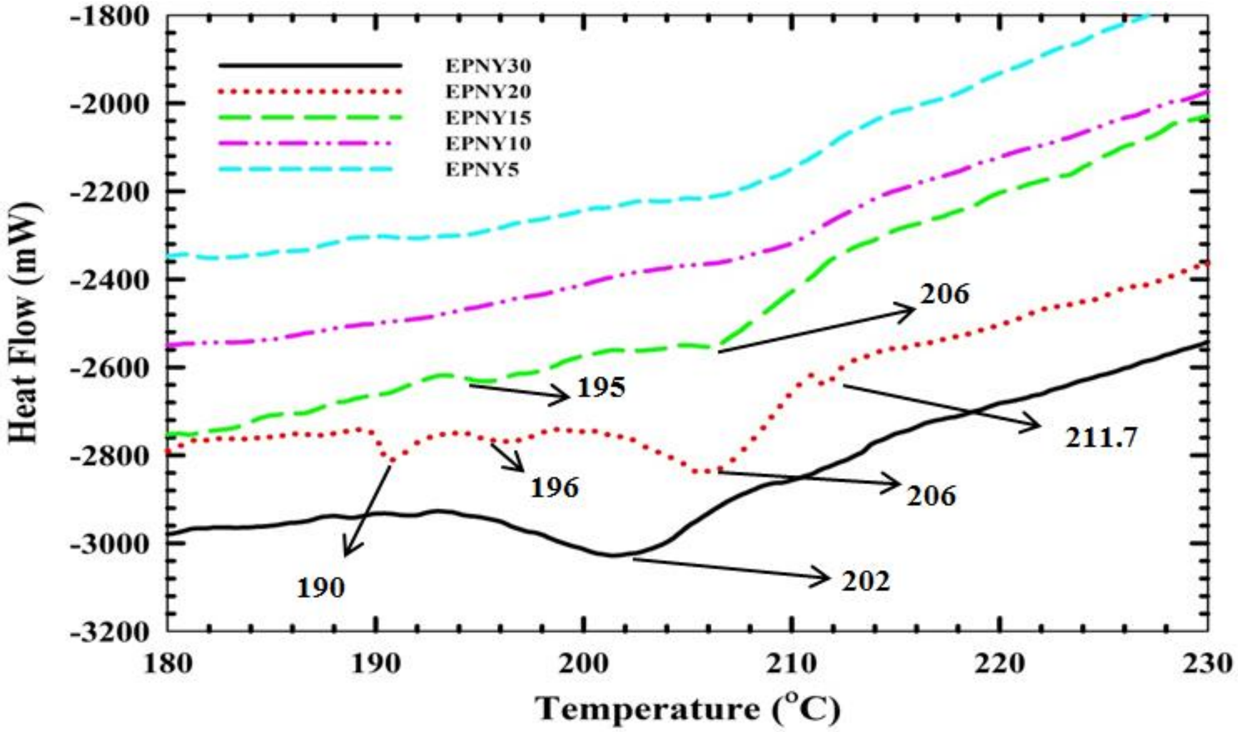

Figure 15 – DSC curve for epoxy – nylon composites films showing T_m

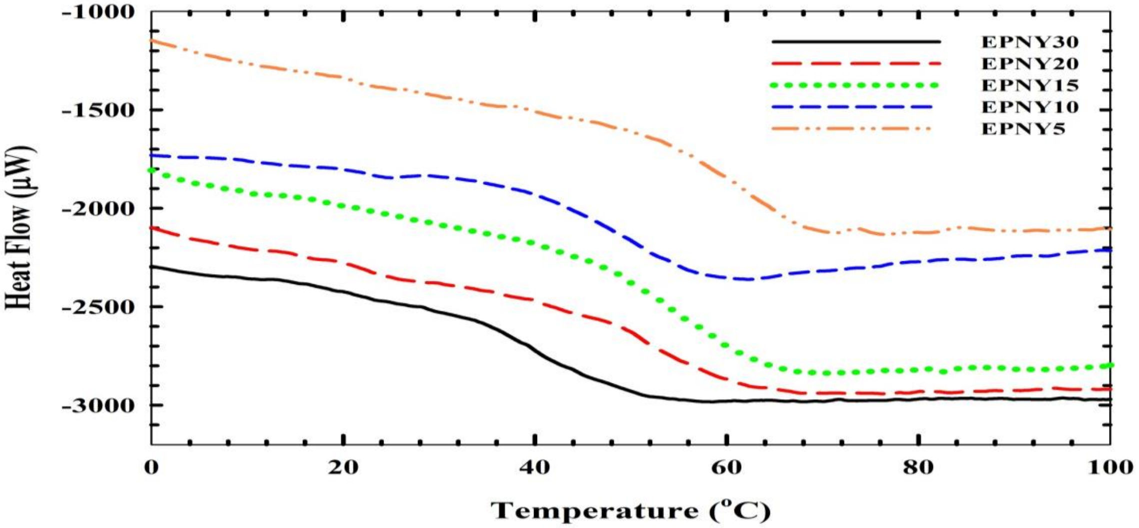

Figure 16 – DSC curve for epoxy – nylon composites films showing T_g

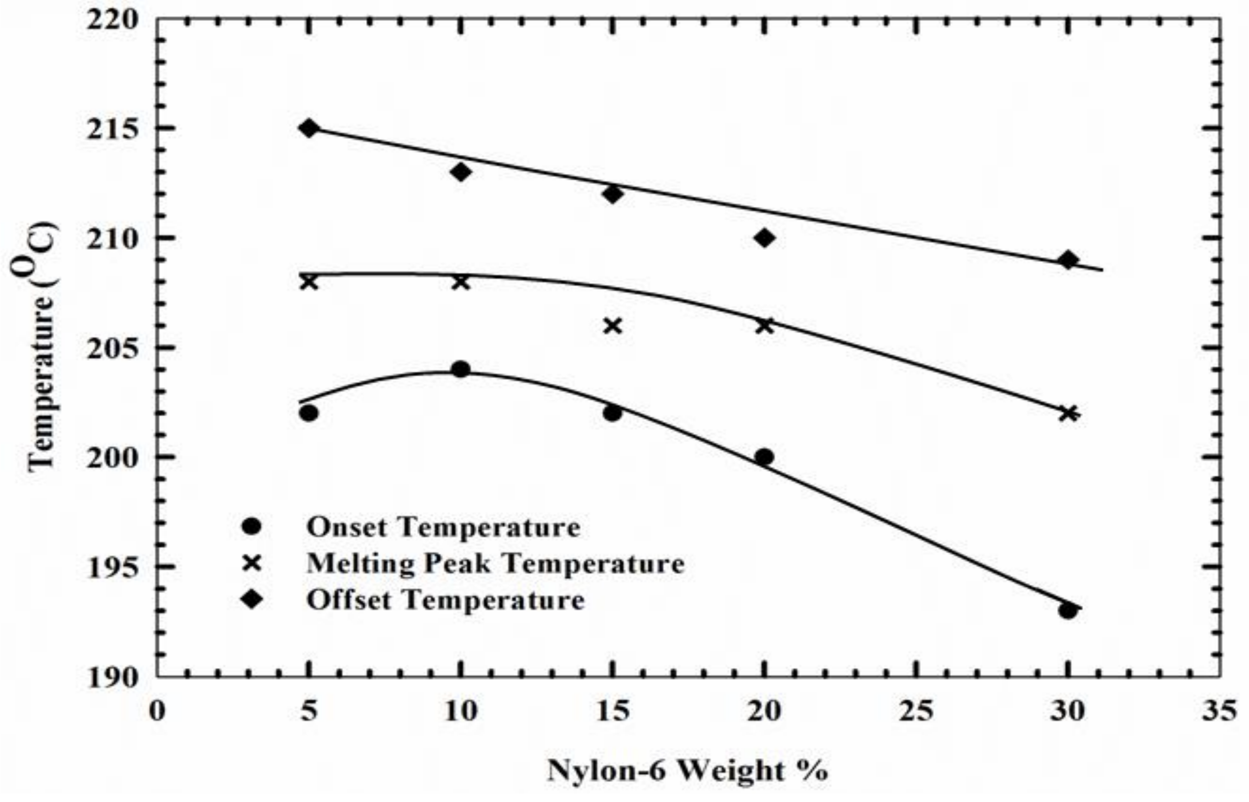

Figure 17- Comparison of Onset, peak and offset melting temperature of nylon-6 in epoxy

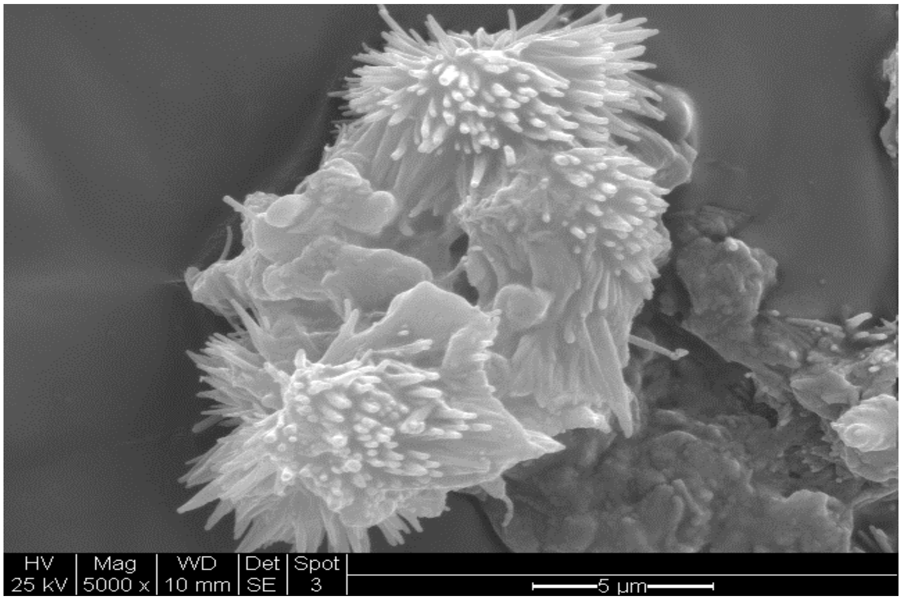

Figure 18 – SEM image of nylon-6 crystallized from nylon-6-NMP solution

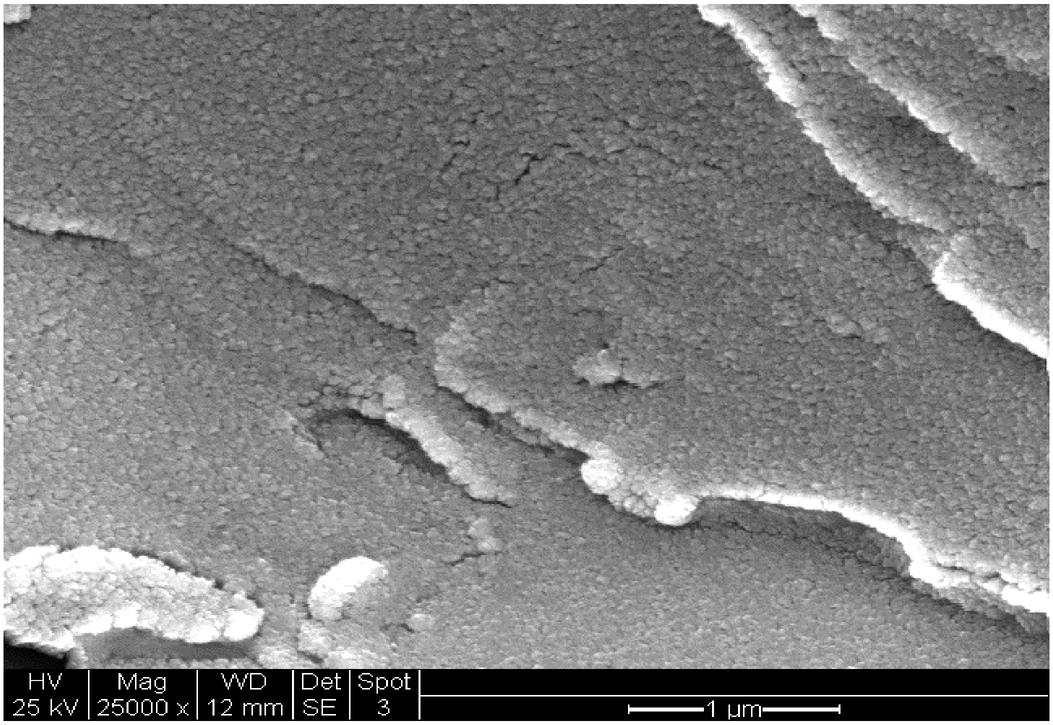

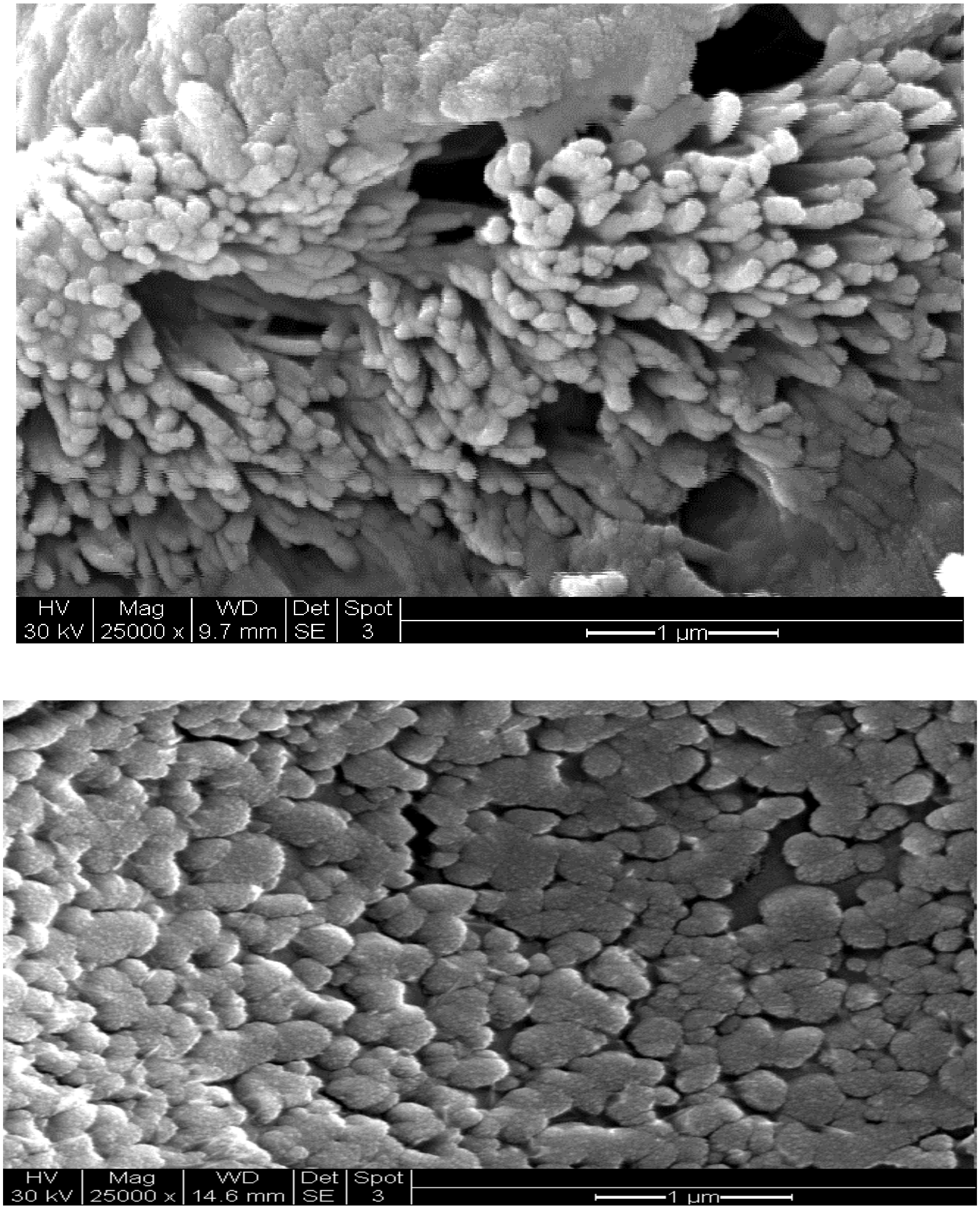

Figure 19 - SEM Images of cross-section of fractured Surface for neat epoxy, epoxy/nylon-6 (10 and 20%)

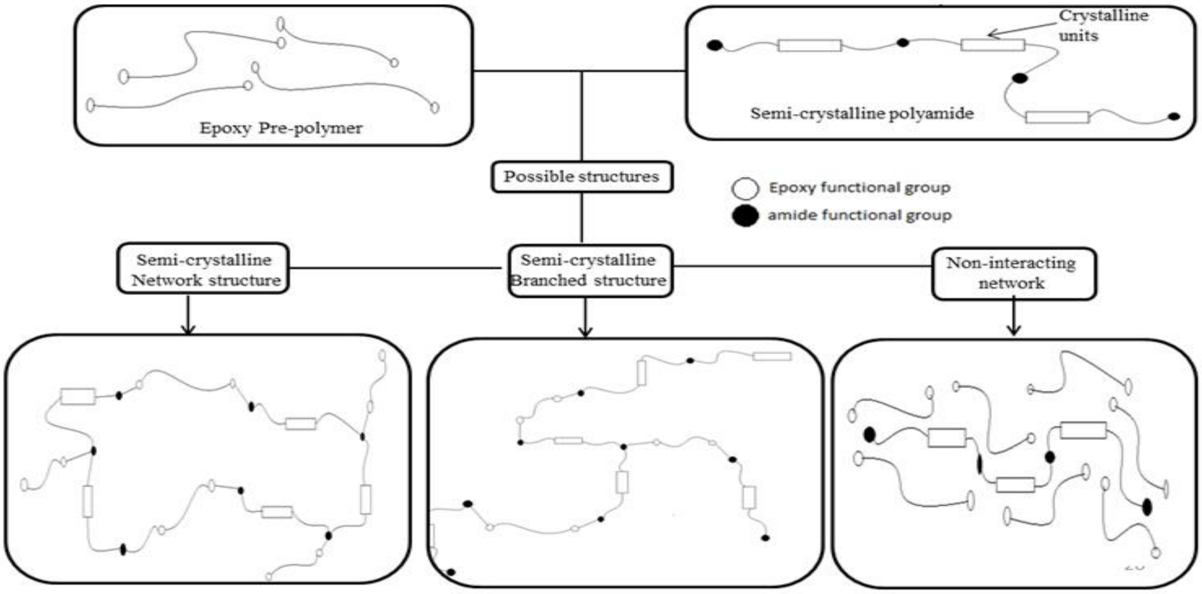

Figure 20 – Schematic of possible structures of modified epoxy

Table

Table 1 – The peak value of melting depression for different composition.

Composition	Melting Onset temperature (^{O} C)	Melting peak temperature (^{O} C)	Melting offset temperature (^{O} C)	T_g (^{O}C)
Neat Nylon-6	188	209	215	25
EPNY30	193	202	209	42
EPNY20	189	190	193	54
	194	196	198	
	200	206	210	
	210	211.7	213	
EPNY15	193	195	200	57
	202	206	212	
EPNY10	204	208	213	50
EPNY5	189	194	200	61
	202	208	214	

Journal of Thermal Analysis and Calorimetry, DOI 10.1007/s10973-014-3681-y, 2014

THERMAL BEHAVIOR AND STRUCTURE OF CLAY/NYLON-6 NANOCOMPOSITE SYNTHESIZED BY IN-SITU SOLUTION POLYMERIZATION

Aniket Vyas and Jude O. Iroh, Material Science and Engineering Program, College of
Engineering & Applied Science, University of Cincinnati, Cincinnati, OH 45221-0012, USA

Introduction

Nylon-6 is one of the most important member of the polyamide class of semi-crystalline polymers. The study of the structure and morphology of nylon-6 has always captivated polymer scientists and engineers. The interest in this area of sudy was heightened, when Toyota's central research and development laboratories synthesized first nylon-6-clay hybrid polymer in 1990s [1, 2]. Since then, nanosclae polymer-inorganic composites have been the focus of intense research. Such composites have found practical applications in sporting equipment and under-the hood automobile components [3]. Polymer-clay nanocomposites are the materials consisting of 1 nm thick aluminosilicate clay dispersed in polymer matrix. Such nanocomposites when compared to pure components, exhibits superior properties such as impact strength [4, 5], increased flame resistance [6], improved ablative performance [7], increased modulus [4, 8, 9], increased gas barrier [9], increased heat distortion temperature [4, 5, 10, 11] and resistance to small molecule permeation [8, 12].

Different synthesis and processing methods have been used to prepare polymer-clay nanocomposites, depending on the type of matrix, type of clay and the desired final structure. Nylon-6 and its nano-composites with layered silicates are generally produced by melt compunding using single and twin-screw extruders due to availbaility, simplicty and low cost [13], but such techniques for continuous processing have shortcomings. For instance, bulk polymerization is carried out at a very high temperature in a polar solvent (melted monomer), which acts as a strong basic medium. These conditions instigate unfavorable side reactions leading to formation of β-ketoimides and β-ketoamides. The high polymerization temperature can also cause thermal degradation of nylon-6 [13, 14] and occurrence of side reactions such as decarboxylation and disproportionation reactions. As a consequence, branching and crosslinking may occur [15-17], which may eventually lead to loss of crystallinity. To be specific, side reactions occur because of lack of proper dissipation of reaction heat during bulk polymerization, which is usually carried out in quasi-adiabatic conditions [15, 16].

To overcome these drawbacks, researchers developed an alternative route to synthesize nylon-6 via solution polymerization. A very small number of reports have been cited in literature on the use of addition polymerization of ε-caprolactam to synthesize nylon-6 in presence of an appropriate solvent. The presence of solvent as a continuous phase leads to "activated anionic mechanism" which provides quasi-isothermal conditions due to proper heat dissipation and allows working at low temperature with a very short reaction time [16]. These methods lead to formation of nylon-6 in granular or powder form which can be used in various applications such as flame spraying, electrostatic coating, paste production, dispersions, lacquer binder and adsorbents [17]. Recently, a huge interest in study of anionic polymerization of caprolactam at lab scale has raised, for its application in 3D prototyping [18].

Few researchers have demonstrated the synthesis of nylon-6 by solution polymerization [16, 17, 19-21] but use of such method to produce nylon-6/clay nanocomposite has not been reported yet. The present paper focuses on the synthesis of nylon-6 and it's composite with nano-clay by living anionic polymerization technique in solution. The presence of acidic (proton donating) solvent or solvents which solvate the ions poorly, terminates the polymerization reaction easily [22]. Therefore, a non-acidic solvent is desired for living polymerization. Considering these factors, ε-caprolactam was used as monomer, N-methylpyrollidone (NMP) was used as solvent due to its low toxicity, low VOC and non-acidic nature, montmorillonite 15A clay was chosen as reinforcing material, sodium hydride (NaH) was used as catalyst and N-acetyl caprolactam was used as initiator to synthesize nylon-6/clay nanocomposite.

Nylon-6/clay composite was obtained in a granular form after evaporation of solvent. The effect of clay on the thermal properties of nylon-6, such as glass transition temperature (T_g), melting temperature (T_m) and crystallization temperature ($T_{c)}$, were investigated using Differential Scanning calorimeter. At low concentration of nanoclay, a highly crystalline microstructure was observed with unusual morphology. The nanocomposites were studied for morphological and structural features using x-ray diffraction technique and scanning electron microscopy.

1. Experimental

2.1 Materials

ϵ-caprolactam, dry sodium hydride (95% purity), N-acetylcaprolactam and NMP solvent (99% purity) were purchased from Sigma-Aldrich, USA for solution polymerization of ε-caprolactam. Cloisite 15A clay was purchased from Southern Clay. All the reagents mentioned above are of analytical grade.

2.2 Procedure

2.2.1 Solution Synthesis of Nylon-6/Clay Nanocomposites

Polymerization was carried out in an oil bath assembly. 100 ml of NMP was taken in a 3 neck flask and monomer (ϵ-caprolactam) was added to it and stirred till it formed a colorless solution. It was followed by addition of montmorillonite 15A clay. Nitrogen supply was turned on and temperature was raised to 50°C. NaH (catalyst) was then added to the solution and stirred till it dissolved completely. This process of dissolution was accompanied by a series of color changes from colorless to dark blue which eventually turned black on complete dissolution. Temperature was then gradually raised to 160°C and N-acetyl Caprolactam (initiator) was added to the solution while maintaining the stirring. The color of solution gradually changed from black to blue. After addition of initiator, solution was stirred for 30-45 minutes. The Nitrogen supply was then turned off and the black solution gently turned into a dark orange yellow viscous solution indicating the completion of reaction terminated by air.

2.2.1 Preparation of Nylon-6/Clay Nanocomposite Granules

5 ml of nylon-6/clay suspension was taken in a Teflon mold and gradually heated up to 200°C for 24 hours in vacuum oven. This allowed full evaporation of the solvent and likewise nylon-6/clay granules were precipitated from the solution.

2.3 Characterization

Differential Scanning Calorimetry (DSC) was used to measure thermal properties of nylon-6/clay nanocomposite. DSC was performed at the heating rate of 5°Cmin^{-1} using DSC6200, Seiko Instruments Inc. The Aluminum crucible was used with the sample mass in range of 10-12 mg, and nitrogen gas was used as a purge gas.

Scanning Electron Microscope was a Philips model FEI XL 30 ESEM-FEG. The software used to capture images was Scandium. Aluminum stubs with carbon tape were used as sample holders and the sample was coated with Au-Pd before subjecting to SEM.

Wide angle X-ray diffraction (WAXD) was carried out using Philip X-Ray diffractometer. X-Ray diffraction tests were performed using Cu-K radiation source at a wavelength of 1.54 A^O between 2θ angles of 0 to 30^O.

The model used for TEM is JEOL 2100F with digital micrograph software with a voltage of 200Kv. A single tilt holder with samples disbursed on a lacey carbon grid.

3 Results and Discussion

3.1 Themal Behavior

In this section, thermal properties of neat nylon-6 and its nanocomposite with 15A clay is discussed. DSC is used to obtain information about the glass transition temperature (T_g), melting temperature (T_m) and crystallization temperature (T_c) of the polymer composites [23, 24]. The effect of quenching on individual polymer-clay systems and the modifications in thermal properties of nylon-6, such as T_g, T_m and T_c, on addition of clay are investigated. The experiment was carried out in 4 runs. The 1st run was to remove thermal history of polymer, where sample was heated just beyond T_g (around 40°C) and then cooled with liquid nitrogen to -5°C. The 2nd run was started from -5°C up to the melting point (T_m) of polymer sample (250°C). Then it was quenched in presence of liquid nitrogen, and the temperature was lowered to -5°C. The 3rd run was then started after quenching up to 250°C, to analyze the effect of quenching on T_g and T_m. Then the sample was allowed to cool naturally, followed by fourth run, in order to compare the thermal parameters with and without quenching.

3.1.1 *Nylon-6*

The DSC curve of neat nylon-6 samples for third run (after quenching) and fourth run (without quenching) is shown in Figure 1. A slight shift in T_g and T_m was observed, but no change in the position and nature of crystallization peak was observed. The T_c peak temperature remained constant at 170°C. crystallization onset temperature was around 176°C and the offset temperature at around 160°C. The peak was narrow and sharp, suggesting formation of polymer crsytals with a narrow distribution.

The comparison between melting peak of nylon-6 in second, third and fourth run are shown in Figure 2. Melting in second heating cycle belongs to the sample after it was precipitated from solution in the vaccum oven with prolonged heating. After complete melting in the second run, the sample was quenched with liquid nitrogen. The quenched sample was subjected to third heating cycle (3rd run). After complete melting in third run, it was allowed to cool naturally and the cooling cycle was traced. The fourth heating cycle (4th run) belongs to the non-quenched sample. The values for thermal parameters are shown in Table 1.

The melting temperature was highest in second run (212°C) which on further runs dropped to 209°C eventually. But the interesting phenomenon was observed in third run which belongs to the quenched sample. Two distinct melting peaks were observed at 201°C and 209°C. This can be possible only due to presene of different types of polymer crystals. Hene, it can be inferred that quenching or sudden cooling lead to formation of distribution of crystals of various types and size.

It is a well known fact that the crystallinity of solid depends upon the cooling history from the melt, and the crystallization decreases as the cooling rate increases [24-26]. Comparison of melting peak in second and third run suggests that crystallinity after quenching decreased significantly, which is evident by decrease in value of heat of fusion, which was in-turn more in fourth run compared to third run.

The presence of multiple melting endotherms has been shown previously for various polymers such as nylon-6,6 [27], poly (ether ether ketone) [28], nylon-10,12 [29] and poly(ethylene terephthalate) [30]. Li et. al [29] suggested that each melting endotherm has a different origin. The highest melting peak refers to the melting of recrystallized material while other melting endotherm corresponds to the melting of lamella with different thickness, developed under different crystallization conditions. Bell et.al [27] demonstrated that either of the two melting peaks observed can be converted to one by appropriate choice of annealing conditions. The two melting peaks belong to two separate morphological species – form I and form II, where form I is relativey fixed in melting temperature while form II varies with annealing conditions.

The presence of multiple peaks in semi-crystalline polymers has been demonstrated before, however, nothing significant has been reported in literature regarding such a phenomena in nylon-6. It has been cited in literature that multiple melting peaks are possible in nylon-6 when both type of crystal structures, α and γ are present [31]. In the present case, the form I can be considered to be crystals corresponding to peak at 209°C, as when sample was allowed to crystallize naturally, the peak at 201°C vanished and only one peak corresponding to 209°C remained in fourth run. The peak at 201°C can be referred to the crystals that formed due to faster cooling. For pure nylon-6, the γ-form of crystal is reported to have melting point about 8°C lower than α-form [32]. This suggests the possibality of fomation of γ-type crystals in nylon-6 after quenching. The crystal structure will be discussed in more detail in later sections.

The crystallization process in polymers is based on two steps, formation of nuclei and secondry nucleation. At lower temperature, a large number of small crystals are formed, as primary nucleation is greater then secondary nucleation. While at higher temperature, small number of large crystals are formed, as the rate of primary nucleation is low but the formation of secondry nuclei occurs faster [26]. In the present case, it is hypothized that when the neat nylon-6 sample was subjected to quenching after complete melting, large number of small crystals were formed along with few larger crystals, due to faster rate of cooling. As the melting point temperature is directly proportional to the size of crystals, it can be concluded that quenching lead to formation of different kinds of morpholgy with different crystal size. Larger crystals melted at 209°C while smaller crystals melted at 201°C.

In this section, the effect of quenching and natural cooling on a neat nylon-6 sample was discussed by different runs in DSC. In the following sub-sections, similar effects will be discussed for nylon-6/clay nanocomposite for different composition.

3.1.2 Nylon-6/clay(0.5%)

The complete DSC curve for nylon-6/clay nanocomposite, with clay loading of 0.5% by mass is shown in Figure 3. The parameters related to thermal properties, i.e T_g, T_m and T_c are clearly visible. The values of these parameters for different runs are shown in Table 2.

A little shift in the T_c peak was observed while cooling from melt in third and fourth run, but the shape and nature of peak almost remained same. The onset temperature for crystallization was around 185°C, peak temperature around 176-177°C and crystallization offset at 158°C.

The comparison between melting peaks of the nanocomposite for second, third and fourth run is shown in Figure 4. The temperature was highest in second run (218°C), when sample was freshlly prepared. After second run, the sample was quenched and in third run, T_m dropped to 216°C. After third run, the sample was allowed to cool naturally and the T_m increased to 217.6°C in fourth run. The shift in the melting temperature is in a very narrow range. This suggests that quenching did not have a profound effect on the crystalline morphology and structure of nanocomposite.

This is possibaly due to presence of 15A clay nano-particles that acted as an external nucleating agent for nylon-6 crystals to grow via secondry nucleations. It has been discussed before that at fast cooling rate, primary nucleation will be faster then secondry, leading to growth of large number of small nuclei. However, the present case seems to be a contradiction. It is possible only when in both the cases (quenching and natural cooling), secondry nucleation occurs.

In the case of nylon-6/clay (0.5%), small amount of nano-clay particles are already present in trace amount, which can act as external nucleating agent leading to commencement of secondry nucleation. The rate of primary nucleation is slow, but the formation of secondry nuclei follows at a much faster rate. In presense of external nucleating agent, secondry nucleation can take place easily. Hence, in both cases i.e. at fast cooling (quenching) and natural cooling, secondry nucleation was preferred and cooling rate was found to have no significant impact on crystal structure and thermal properties of nylon-6 in presnce of trace amount of nano-clay particles.

3.1.3 Nylon-6/clay(1%)

Figure 5 represents the comparison between third and fourth run of DSC for nylon-6/clay(1% by mass). The values for thermal parameters for different runs are listed in Table 3. The crystallization peak for nylon-6 with 1% clay loading by mass was broader compared to neat nylon-6 and nylon-6/clay (0.5 mass %). The possible reason can be that in the presence of clay platelets, crystal lamella organization is disrupted. This impedes large crystalline domains from forming due to steric hindrances, and leads to smaller, less ordered crystallites, and as a result, crystals with a great distribution of size and shape are produced.

The comparison between the melting peaks in second, third and fourth run is shown in Figure 6. When the composite was freshly processed in vaccum oven, it exhibited a high melting temperature with a peak at 219°C. After complete melting in the second run, sample was quenched. After recrystallization under fast cooling conditions, the melting temperature dropped to 204°C in third run. After complete melting in third run, sample was cooled naturally and recrystallization was allowed to take place on its own under normal conditions. In the fourth run, two melting peaks were observed, one at 210°C and the other at 200°C.

We speculate that when sample was prepared by precipitation from solution in oven at high temperature for prolonged period of time, it lead to formation of composite with high crystallinity evident by high melting temperature and large value of heat of fusion. After second run, when it was quenched, crystallization took place rapidly, but as clay particles were already present in the matrix acting as external nucleating agents for crystals, secondry nucleation was preferred, but the type of crystal structure was changed (compared to the fresh sample) as indicated by drop in melting temperature by 15°C. It is a well recognized fact that clay favours the formation of γ-type of crystals [3, 31]. Lincoln et al [3] reported that the addition of clay layers forces the amide groups of nylon-6 out of the plane formed by the molecular chains, which results in the conformational changes of the chains and restricts the formation of hydrogen-bonded sheets, hence, γ-form is favored. After complete melting in third run, sample was allowed to cool naturally. The recrystallization occurs again in presence of clay and in the next heating (fourth) run, two melting peaks are observed. This phenomena can be explained on basis of theory proposed by xie et al [31], in presence of clay layers, a part of highly oriented polymer chains my not be able to crystallize due to lack of space as it can be trapped between clay layers. This leads to a metastable crystal structure which is a partially disordered crystal structure of nylon-6, and it is a phase intermediate between α-form and γ-form [33, 34]. This metastable state is a non-equilibrium phase, the frozen-in stress could be located in this state and the recrystallization peak in third run (cooling cycle) belongs to formation of the metastable state. As a result, two melting peaks are observed in fourth run due to existance of series of crystal structures, which also undergo reorganization during DSC scan and varies continously in size and perefection.

3.1.4 Nylon-6/clay(5%) and Nylon-6/clay(10%)

The nylon-6/clay nanocomposite were prepared via in-situ solution polymerization of ε-caprolactam in presence of clay stacks in reactor. Semi-crystalline composites were obtained at lower concentration of clay i.e. 0.5% and 1% by mass, but when clay concentration was increased to 5% and 10%, melting and crystallization peak were not observed in DSC scans. It is spaculated that high amount of clay stacks during the ring opening anioninc addition polymerization reaction acts as hinderance to the addition reaction. Hence, large poymer chains with high molecular mass are not formed. This leads to decrease in crystallinity in nylon-6/clay (5% and10%) nanocomposite. The crystallinity decreased to such an extent that thermal transitions related to melting and crystallization broadened such that distinct peak was not observed. The effect of clay on molecular mass is discussed in later section.

3.2 Effect of Clay on Thermal Properties of Nylon-6

In this section, effects of clay concentration on the thermal properties of nylon-6 have been discussed. Each parameter, i.e., T_c, T_m and T_g are distinctly discussed. The observed values for these parameters are shown in table 4 for simplicity of comparison.

The effect of clay on the crystallization temperature of nylon-6 at 0.5% loading and 1% loading is shown in Figure 7. When the samples were allowed to cool naturally from the melt, a sharp narrow crystallization peak was observed with T_c at 170°C for neat nylon-6. On addition of clay to nylon-6 matrix during polymerization reaction at 0.5% loading, the T_c increased to 176°C. On further increasing clay to 1% by mass, the T_c dropped to 171°C. Moreover, the crystallization peak broadened comparatively, indicating formation of crystals with a wide distribution. Hence, it can be concluded that in presence of clay at very low concentration (0.5%), when nylon-6 is synthesized by solution polymerization, a composite with increased crystallinity is obtained. Further addition of clay leads to decrease in crystallinity. As the clay stacks are increased, they possess hindrance to the chain addition during polymerization step leading to formation of short polymer chains. Moreover, during crystallization from melt at higher concentration of clay, polymer chains may not be able to crystallize due to lack of space as it can be trapped between clay layers.

Figure 8 shows the comparison of melting temperature of nylon-6 with different clay loadings. Figure 8(a) refers to the samples, when they were freshly prepared by precipitation from solution in oven. Figure 8(b) refers to the samples that were quenched after melting in second run. Figure 8(c) refers to the samples that were recrystallized under natural cooling after melting in third run. When Samples were subjected to DSC just after processing, a single peak was observed in all the samples, suggesting that samples obtained were high in crystallinity with stable crystal structure. When these samples are quenched and re-melted, two melting peaks are observed for neat nylon-6 at 201°C and 209°C, while a single peak is observed for nylon-6/clay (0.5%) at 216°C and nylon-6/clay (1%) at 204°C. This indicates that in presence of clay, stable crystal structures are obtained on fast cooling due to preferred secondary crystals compared to mixture of α- and γ-crystals formed in neat nylon-6.

When these samples were allowed to cool naturally and re-melted as shown in Figure 8(c), single peak for nylon-6 re-emerged at 209.8°C and peak related to 201°C vanished. The γ-crystals that melted at 201°C recrystallized to form more stable α-crystals. For nanocomposite with 0.5% clay loading, position of melting peak remained almost unaffected at 217°C. However, for nylon-6/clay (1%) two melting peaks were observed. This is possibly due to presence of more clay particles which reduces the room for polymer chains to crystallize and gives rise to various metastable crystals. On further increasing clay concentration to 5 and 10%, crystallinity of nylon-6 was reduced significantly.

Hence, it can be concluded that 0.5% by mass is the optimum concentration for nylon-6/clay nanocomposite to be synthesized by solution polymerization, which constantly leads to formation of stable crystal structure with narrow distribution and high crystallinity, irrespective of slow or fast cooling conditions for crystallization.

Figure 9 represents the effect of clay on the T_g of nylon-6. A sharp fall in the base line was observed which occur near T_g. Such sharp and clean transition was not observed in the second and third run, probably due to thermal stresses.

A sharp transition in the baseline was observed for all the samples in fourth run. The T_g was found to be decreasing with increase in clay loading. The T_g for neat nylon-6 dropped from 26°C to 24^0C at 0.5% clay loading and to 18^0C at 1% clay loading. The range of temperature in which T_g transition occurred, was found to be decreasing with increase in clay percentage. The reinforcement of polymers by organoclay depends on the interaction of polymer matrix and the clay platelets [35]. There are two factors that can poosibaly contribute to lowering of T_g; 1) free volume existing at the polymer surface interface due to poor wetting and 2) plastcization of polymer due to incorporation of nanoclay [35].

3.3 X-Ray Diffraction

When nylon-6/clay composite granules are subjected to X-Ray diffraction, two kinds of peaks are observed. One corresponding to ordered clay stacks at lower angle and other corresponding to the polymers chains arranged in an orderly fashion to form crystals, at higher angle. The location of peak at a particular angle gives information about nature of crystalline form, d-spacing, length of crystals and stability of crystals.

The crystallite length and corresponding d-spacing were calculated using Scherrer equation and bragg's law respectively [36, 37]. The Scherrer equation is given as follows:

$$D(hkl) = \frac{K\lambda}{\beta(hkl)\,cos\theta} \qquad [1]$$

Where D (hkl) is the mean crystallite size along [hkl] direction, K is the shape factor (scherrer constant, value of 0.94 is used in this case), β(hkl) is the line broadening at half the max intensity in radians and θ is the half scattering angle. According to Bragg's law, d-spacing was calculated using the following equation:

$$n\lambda = 2dsin\theta \qquad [2]$$

Where n is a constant integer (1 in our case), λ is wavelength, d is d-spacing and θ is diffraction angle in degrees.

The x-ray diffraction pattern at lower angle for pristine 15A clay and nylon-6/clay composites is shown in Figure 10. The peak corresponding to pristine clay was found at 2θ angle of 2.5^0, but the peak position shifted to lower angle of 2.05^0 for composite. The decrease in the angle for peak location suggests that intercalated structure was obtained with increase in the distance of clay galleries. The peak location, d-spacing and crystallite length among clay galleries are shown in Table 5.

The increase or decrease in the d-spacing depends upon the processing technique used to obtain polymer/clay composite. Hegde et al [38] reported a slight increase in d-spacing at low clay concentration while slight decrease at higher concentration of clay for nylon-6/clay composites processed by melt compounding. Zhang et al [39] reported decrease in d-spacing for clay with increase in composition for composites processed by twin screw extruder. Swain and Isayev [40] demonstrated increase in d-spacing when composites are processed by continuous sonication process. The d-spacing increased by in-situ solution polymerization of ε-caprolactam in presence of clay. It is speculated that during polymerization reaction, a fraction of polymer chains enter the clay galleries which eventually crystallizes leading to formation of intercalated composite system. The d-spacing for clay increase from 34.48° to 43.25 A° for nylon-6/clay (0.5% by mass), but remains almost in the same range with further increase. Hence, the composition of the composite has no effect on the d-spacing of clay galleries after a threshold. It can be inferred that polymerization lead to increase in inter-gallery distance for clay up to a limit, but was not able to break the oriented or regular structure of clay, which is essential for exfoliation. On increasing clay to 5%, a new peak is observed at 3.23 which increases to 4.14 on increasing clay to 10% by mass, indicating that at high clay loading, the polymerization and crystallization process lead to change in the orientation of a fraction of clay stacks with decreased d-spacing.

Clay has a pronounced effect on the crystal structure of nylon-6 [34, 36]. Nylon-6 has two major crystalline forms, due to difference in packing of nylon-6 chains by hydrogen bonding. It may occur in an anti-parallel (α form) or parallel way (γ form). On subjecting nylon-6 to x-ray diffraction, the polymers crystals show a peak in diffraction pattern. Figure 11 is the X-Ray diffraction pattern for the polymer crystals of neat nylon-6 and its composites with clay at different loading. Along with a considerable effect on the d-spacing of clay galleries due to in-situ solution polymerization, a marked effect on crystalline form and structure of nylon-6 was also observed due to clay composition in intercalated composite system. Parameters related to crystal structure of nylon-6 such as peak position, d-spacing and crystal length is listed in Table 6.

α polymorph of nylon-6 crystal shows major peaks near 17.4°, 19.9° and 24°. [3, 41, 42] and γ polymorph usually shows peak at 18.2° and 21° [3, 41]. As the polymer was crystallized from solution, a mixture of both forms was observed in neat nylon-6 without clay. But α form was found to be dominating over γ form as indicated by the position of crystal peaks at 19.9^{o} corresponding to [200] plane and 24.1^{o} corresponding to [202] plane, while relatively small peaks were observed at 18.15^{o} and 21.6^{o} corresponding to [002] plane suggesting presence of γ phase in minority. But as the clay loading was increased, γ form began to stabilize gradually. When clay was introduced as 0.5% by mass, peaks related to α form were still dominant at 19.8^{o} and 24.09^{o}, but peaks corresponding to γ phase were narrow relative to neat nylon-6 with increased intensity suggesting formation stable γ form of crystals. On further increase in clay concentration to 1%, peak corresponding to α form at 24^{o} almost vanished and the one at 19.8^{o} reduced in intensity. Moreover, peak at 17.03^{o} and 18.15^{o} increased and new small peak at 22.8^{o} appeared. This suggests a swift transition from α to γ phase as the peak at 18.15^{o} grew up along with a small peak at 21.9^{o}. On further increasing clay upto 5 and 10 mass %, the overall crystallinity reduced substantially as indicated by relatively small peaks. Moreover, the peak at 18.15^{o} shifted to lower angle of 17.7^{o} and 17.3^{o}, i.e. d-spacing among crystals corresponding to this angle was increased. Few small crystalline peaks were observed at 17.7^{O}, 19.8^{O} and 21.2^{O} suggesting mixture of α and γ crystals. Hence, it can be concluded that at lower clay loading crystallinity increases with γ-crystals attaining stability, but as clay is further increased up to 5 and 10%, crystallinity of nylon-6 decreased.

The results obtained by XRD concerning dispersion of clay and crystallinity of nylon-6 were further supported by TEM. The dark shady lines represent layered clay platelets. TEM images of composites are shown in Figure 12.

3.4 Morphology

The morphology of nylon-6 and the composites with varying composition were observed under SEM. Observed morphologies are shown in Figure 13 at lower magnification and corresponding higher magnification. In case of nylon-6 without clay, synthesized by solution polymerization, small crystals dispersed in an amorphous matrix were observed throughout the sample. At higher magnification, large spherulites were observed grown radially outwards from a single point. Then, effect of clay was analyzed on subsequent samples. At a clay loading of 0.5% by mass, a highly crystalline and unique spherulitic morphology was observed at a lower magnification grown from a common center. At higher magnification, large crystals were observed but the appearance was different from that of neat nylon-6. They appeared to be more flat, like an array of ribbon tied at a common center. The unique flat appearance suggests that the crystallization process begin to take place inside the clay galleries which then continued outside clay in order to fulfill the space.

When clay was increased to 1 mass %, a morphology consisting of distinct crystalline zones were observed throughout the sample at lower magnification. The crystals appeared to be numerous but reduced in size. On closely observing at higher magnification, a noodle type crystalline morphology was observed, where cylindrical small crystals were observed distributed over a wide zone, unlike nylon-6 and it's composite with clay at 0.5 mass %. This suggests that on increasing clay particles, the amount of nucleating agents increased and various crystals had different origins, instead of a common center.

On further increasing clay to 5 and 10 mass %, a drastic change in the morphology was observed with significant reduction in crystals. At 5 mass % clay loading, a uniform morphology was observed at low magnification with cylindrical crystals protruding outwards. Large clay chunks were observed surrounded and encapsulated by nylon-6 crystals. Since the clay loading was high which was not exfoliated completely, it leads to reduction in the space for crystals to grow. Hence, the crystals that grew were found to be impinged on each other intensely as observed at higher magnification. At 10% clay loading, large clay stacks were observed with almost no crystallinity. At higher magnification small fiber like structures impinged into each other were observed surrounded by large clay chunks. This suggests that at higher concentration of clay, large aliphatic chains were not created due to stearic hindrance and no space was available for small chains to grow as crystals. Clay stack dominated in the nylon-6 matrix.

3.6 *Dilute Solution Viscometry – Molecular Mass Analysis*

The effect of clay concentration on the intrinsic viscosity [η] of nylon-6 was analyzed using ubbelhold viscometer. The intrinsic viscosity was obtained from a plot of Log (Rel η)/C and Sp η/C Vs. C, where C is the concentration in g/dl and η is the measure of viscosity. The following formulae were used in this experiment:

$$\text{Relative Viscosity (rel } \eta) = t/t_o \qquad [3]$$

Specific Viscosity (Sp η) = $(t - t_o)/t_o$ [4]

Where t is the elusion time of the solution and t_o is the elusion time of solvent.

By extrapolating the reduced viscosity plots to zero concentration, as shown in Figure 14(a-d), intrinsic viscosity were obtained for different clay/nylon-6 systems. The values of intrinsic viscosity were used to calculate viscosity average molecular mass for different systems by using Mark-Houwink equation:

$$[\eta] = KM^{\alpha} \quad [5]$$

Where the parameters K and α are Mark-Houwink constants, which depends upon the type of polymer and corresponding solvent. In the present case, nylon-6 was dissolved in conc. H_2SO_4. For this system $K = 3.32 \times 10^{-4}$ and $\alpha = 0.72$ [43]. The variation in the intrinsic viscosity and the calculated molecular mass as a function of clay concentration in nylon-6 matrix is shown in Figure 15a and 15b respectively. It was observed that molecular mass initially increased by 2.8% when 0.5 mass % clay was incorporated in nylon, but on further increase in clay concentration, molecular mass of clay began to fall sharply. It is spaculated that high amount of clay stacks during the ring opening anioninc addition polymerization reaction acts as hinderance to the addition reaction and growth of chains. Hence, at low clay concentration of clay, it is hypothesized that nylon chain growth occurs rapidly with intercalated clay platlets bein the part of chain therby increasing the molecular mass. While, at higher clay loading, chain growth is retared, hence, lower molecular mass. The values of intrisic viscosity and molecular mass are shown in Table 7.

4 Conclusion

In-situ solution polymerization was succesfully used to synthesize nylon-6/clay polymer nanocomposite containing intercalated clay. Thermal, and structural analysis of the nanocomposites suggested that the presence of low concentration of nanoclay lead to an increase in the crystallinity of nylon-6, while the presence of higher concentration of clay decreases crystallinity. Neat nylon-6 preferred to crystallize in α-form, however, at 0.5 mass % loading of clay nylon-6 crystallized partly in α-form an partly in γ-form. At higher mass % nylon-6 predominatly crystallized in the γ-form. Quenching of nylon-6 melt creates mixture of crystal structures constituted of α- and γ- forms. In the presence of clay, quenching does not produce any significant changes in nylon-6 crystal structure. When nylon-6 was recrystallized from melt under normal cooling, it retained the preferred α- crystalline form, but in presence of clay, a meta-stable phase was formed along with a mixture of the α and γ crystalline forms. In-situ solution polymerization in the presence of clay resulted in increased clay d-spacing. Lower concentration of clay increases the molecular mass of nylon-6, while at higher concentration, the molecular mass of nylon-6 decreases.

Acknowledgement

This study was funded by grants from office of naval research (ONR) # N00014-09-1-0980 and National Science Foundation (NSF) # CMMI-0758656. We would also like to thank Soumyarwit Manna at Advanced Material Characterization Center (AMCC), university of Cincinnati who assisted in capturing the SEM images.

References

[1] Kojima Y, Usuki A, Kawasumi M, Okada A, Kurauchi T, Kamigaito O. Synthesis of nylon 6–clay hybrid by montmorillonite intercalated with ϵ-caprolactam. J Pol. Sci. A: Pol. Chem. 1993;31(4):983-986.

[2] Yano K, Usuki A, Okada A, Kurauchi T, Kamigaito O. Synthesis and properties of polyimide–clay hybrid. J Pol. Sci. A: Pol. Chem. 1993;31(10):2493-2498.

[3] Lincoln DM, Vaia RA, Wang ZG, Hsiao BS. Secondary structure and elevated temperature crystallite morphology of nylon-6/layered silicate nanocomposites. Polym. 2001;42(4):1621-1631.

[4] Kojima Y, Usuki A, Kawasumi M, Okada A, Fukushima Y, Kurauchi T, et al. Mechanical properties of nylon 6-clay hybrid. J Mater. Res. 1993;8(05):1185-1189.

[5] Liu L, Qi Z, Zhu X. Studies on nylon 6/clay nanocomposites by melt-intercalation process. J App. Polym. Sci. 1999;71(7):1133-1138.

[6] Shanmuganathan K, Deodhar S, Dembsey N, Fan Q, Calvert PD, Warner SB, et al. Flame retardancy and char microstructure of nylon-6/layered silicate nanocomposites. J App. Polym. Sci. 2007;104(3):1540-1550.

[7] Vaia RA, Price G, Ruth PN, Nguyen HT, Lichtenhan J. Polymer/layered silicate nanocomposites as high performance ablative materials. App. Clay Sci. 1999;15(1–2):67-92.

[8] Usuki A, Koiwai A, Kojima Y, Kawasumi M, Okada A, Kurauchi T, et al. Interaction of nylon 6-clay surface and mechanical properties of nylon 6-clay hybrid. J of App Polym Sci. 1995;55(1):119-123.

[9] Somwangthanaroj A, Tantiviwattanawongsa M, Tanthapanichakoon W. Mechanical and Gas Barrier Properties of Nylon 6/Clay Nanocomposite Blown Films, Engineering Journal, 2012 DOI: 10.4186/ej.2012.16.2.93

[10] Ke Y, Long C, Qi Z. Crystallization, properties, and crystal and nanoscale morphology of PET–clay nanocomposites. J App Polym. Sci. 1999;71(7):1139-1146.

[11] Xie S, Zhang S, Wang F, Liu H, Yang M. Influence of annealing treatment on the heat distortion temperature of nylon-6/montmorillonite nanocomposites. Polym. Eng. and Sci. 2005;45(9):1247-1253.

[12] Singh-Beemat J, Iroh JO. Effect of clay on the corrosion inhibition and dynamic mechanical properties of epoxy ester–polyurea–polysiloxane hybrid coatings. Polym. Eng. and Sci 2012; 52(12):2611-2619

[13] Abdel Gawad A, Esawi AK, Ramadan A. Structure and properties of nylon 6–clay nanocomposites: effect of temperature and reprocessing. J Mater. Sci. 2010;45(24):6677-6684.

[14] Ryba J, Ujhelyiová A, Krištofič M, Vassová I. Thermal properties of PA 6 and PA 6 modified with copolyamides and layered silicates. J Therm. Anal. Calorim.2010;101(3):1027-1037.

[15] Ricco L, Russo S, Orefice G, Riva F. Anionic Poly(ε-caprolactam): Relationships among Conditions of Synthesis, Chain Regularity, Reticular Order, and Polymorphism. Macromol. 1999;32(23):7726-7731.

[16] Ricco L, Monticelli O, Russo S, Paglianti A, Mariani A. Fast-activated anionic polymerization of ε-caprolactam in suspension, 1. Role of the continuous phase on characteristics and properties of powdered PA6. Macrom. Chem. and Phy. 2002;203(10-11):1436-1444.

[17] Vasiliu-Oprea C, Dan F. On the relation between synthesis parameters and morphology of anionic polycaproamide obtained in organic media. I. Influence of the

Na[O(CH2)2OCH3]2AlH2/isophorone diisocyanate catalytic system. J App. Polym. Sci. 1996;62(10):1517-1527.

[18] Khodabakhshi K, Gilbert M, Fathi S, Dickens P. Anionic polymerisation of caprolactam at the small-scale via DSC investigations. J Therm. Anal. Calorim. 2013:1-9.

[19] Vasiliu-Oprea C, Dan F. On the relation between synthesis parameters and morphology of anionic polycaproamide obtained in organic media. II. Influence of the Na [O (CH2) 2OCH3]2AIH2/aliphatic diisocyanates catalytic systems. J App. Polym. Sci. 1997;64(13):2575-2583.

[20] Chrzczonowicz S, Wlodarczyk M, Ostaszewski B. Polymerization of ϵ-caprolactam and ζ-enantholactam in non-polar solvents. Die Makromolekulare Chemie. 1960;38(1):159-167.

[21] Dan F, Vasiliu-Oprea C. On the relationship between synthesis parameters and morphology of the anionic polycaproamide obtained in organic media. III. Macroporous powders obtained using CO2 and carbodiimides as activating compounds. J App. Polym. Sci. 1998;67(2):231-243.

[22] Szwarc M. /`Living/' Polymers. Nature. 1956;178(4543):1168-1169.

[23] Menczel J. The rigid amorphous fraction in semicrystalline macromolecules. J Therm. Anal. Calorim. 2011;106(1):7-24.

[24] Mao B, Cebe P. Avrami analysis of melt crystallization behavior of Trogamid. J Therm. Anal. Calorim. 2013;113(2):545-550.

[25] Brucato V, Crippa G, Piccarolo S, Titomanlio G. Crystallization of polymer melts under fast cooling. I: Nucleated polyamide 6. Polym. Eng. & Sci. 1991;31(19):1411-1416.

[26] Painter PC, Coleman MM. Fundamentals of Polymer Science: An Introductory Text, Second Edition: Taylor & Francis; 1998.

[27] Bell JP, Slade PE, Dumbleton JH. Multiple melting in nylon 66. J Polym. Sci. Part A-2: Polym. Phys. 1968;6(10):1773-1781.

[28] Blundell DJ. On the interpretation of multiple melting peaks in poly(ether ether ketone). Polym. 1987;28(13):2248-2251.

[29] Li Y, Zhu X, Tian G, Yan D, Zhou E. Multiple melting endotherms in melt-crystallized nylon 10,12. Polym. Intern. 2001;50(6):677-682.

[30] Zhou C, Clough SB. Multiple melting endotherms of poly(ethylene terephthalate). Polym. Eng. Sci. 1988;28(2):65-68.

[31] Xie S, Zhang S, Liu H, Chen G, Feng M, Qin H, et al. Effects of processing history and annealing on polymorphic structure of nylon-6/montmorillonite nanocomposites. Polym. 2005;46(14):5417-5427.

[32] Murthy NS, Aharoni SM, Szollosi AB. Stability of the γ form and the development of the α form in nylon 6. J Polym. Sci.: Polym. Phys. 1985;23(12):2549-2565.

[33] Holmes DR, Bunn CW, Smith DJ. The crystal structure of polycaproamide: Nylon 6. J Polym. Sci. 1955;17(84):159-177.

[34] Fornes TD, Paul DR. Crystallization behavior of nylon 6 nanocomposites. Polym. 2003;44(14):3945-3961.

[35] Paul DR, Robeson LM. Polymer nanotechnology: Nanocomposites. Polym. 2008;49(15):3187-3204.

[36] Arimoto H, Ishibashi M, Hirai M, Chatani Y. Crystal structure of the γ-form of nylon 6. J Polym. Sci. Part A: General Papers. 1965;3(1):317-326.

[37] Zhao Z, Yu W, Liu Y, Zhang J, Shao Z. Isothermal crystallization behaviors of nylon-6 and nylon-6/montmorillonite nanocomposite. Mater. Lett.. 2004;58(5):802-806.

[38] Hegde RR, Bhat GS, Deshpande B. Morphology and Properties of Nylon 6 Blown Films Reinforced with Different Weight Percentage of Nanoclay Additives. Inter. J Polym. Sci. 2012;2012:14.

[39] Zhang Y, Yang JH, Ellis TS, Shi J. Crystal structures and their effects on the properties of polyamide 12/clay and polyamide 6–polyamide 66/clay nanocomposites. J App. Polym. Sci. 2006;100(6):4782-4794.

[40] Swain SK, Isayev AI. PA6/clay nanocomposites by continuous sonication process. J of App. Polym. Sci. 2009;114(4):2378-2387.

[41] Li H, Wu Y, Sato H, Kong L, Zhang C, Huang K, et al. A New Facile Method for Preparation of Nylon-6 with High Crystallinity and Special Morphology. Macromol. 2009;42(4):1175-1179.

[42] Murthy NS, Minor H, Akkapeddi MK, Buskirk BV. Characterization of polymer blends and alloys by constrained profile-analysis of X-ray diffraction scans. J of Appl.Polym. Sci. 1990;41(9-10):2265-2272.

[43] Aharoni SM. n-Nylons, their synthesis, structure, and properties: J. Wiley & Sons; 1997.

Tables

Table 1: DSC parameters for neat nylon-6

	T_g /°C	T_m /°C	T_c/°C	ΔH_f /Jg^{-1} (app.)
Second Run	30.4	212.8	-	119.81
Third Run	15.4, 24.8	201.2, 209.8	170	72.58
Fourth Run	23.5	209.2	170	89.71

Table 2: DSC parameters for neat nylon-6/clay (0.5%)

	T_g /°C	T_m /°C	T_c/°C	ΔH_f / Jg^{-1} (app.)
Second Run	31	218	-	138.08
Third Run	13, 32	216	176	66.36
Fourth Run	25	217.6	177.1	90.01

Table 3: DSC parameters for neat nylon-6/clay (1%)

	T_g /°C	T_m /°C	T_c/°C	ΔH_f / Jg^{-1} (app.)
Second Run		219	-	136.51
Third Run	17.6	204	171.4	47.21
Fourth Run	16	200, 210	171.4	49.27

Table 4 – DSC parameters at different clay composition

Clay Composition	T_g /°C (4th run)	Tc /°C	T_m /°C (2nd run)	T_m /°C (3rd run)	T_m /°C (4th run)
0%	24	170	212.8	201.2, 209.8	209.2
0.5%	23	176	218	216	217.6
1%	18	171	219	204	200, 210

Table 5 – XRD peak location, d-spacing and crystallite size for nylon-6/clay composite system at lower angle (for nanoclay)

	2θ (⁰)	d-spacing/A⁰	Crystallite length/A⁰
Neat Clay 15A	2.5	34.48	103.48
Nylon-6/clay (0.5%)	2.05	43.25	113.35
Nylon-6/clay (1%)	1.95	45.26	125.19
Nylon-6/clay (5%)	1.95	45.26	137.42
Nylon-6/clay (10%)	2.05	43.25	131.73

Table 6 – XRD peak location, d-spacing and crystallite size for nylon-6/clay composite system at higher angle (for nylon crystals)

	2θ (⁰)	d-spacing/A⁰	Crystallite length /A⁰	Crystal Planes
Neat nylon-6 (α)	19.9, 24.1	4.45, 3.68	108.11, 80.12	[200], [202]
Neat nylon-6 (γ)	18.06, 21	4.90, 4.22	210.19, 191.86	[002]
Nylon-6/clay (0.5%) (α)	19.9, 24.1	4.45, 3.68	100.39, 93.33	[200], [202]
Nylon-6/clay (0.5%) (γ)	18.18, 21	4.87, 4.22	106.42, 136.15	[002]
Nylon-6/clay (1%) (α)	19.9	4.45	117.12	[200]
Nylon-6/clay (1%) (γ)	18.28, 21	4.84, 4.22	107.79, 159.28	[002]
Nylon-6/clay (5%) (α)	19.9	4.45	112.44	[200]
Nylon-6/clay (5%) (γ)	17.7	5.00	107.68	-
Nylon-6/clay (10%) (α)	19.9	4.45	124.01	[200]
Nylon-6/clay (10%) (γ)	17.3	5.12	209.97	-

Table 7 – Values of Intrinsic Viscosity and Molecular Weight

Clay Concentration (mass %)	Intrinsic Viscosity	Molecular Weight
0	0.45	10362.87
0.5	0.46	10659.03
1	0.22	4140.297
5	0.16	2752.46
10	0.08	1131.839

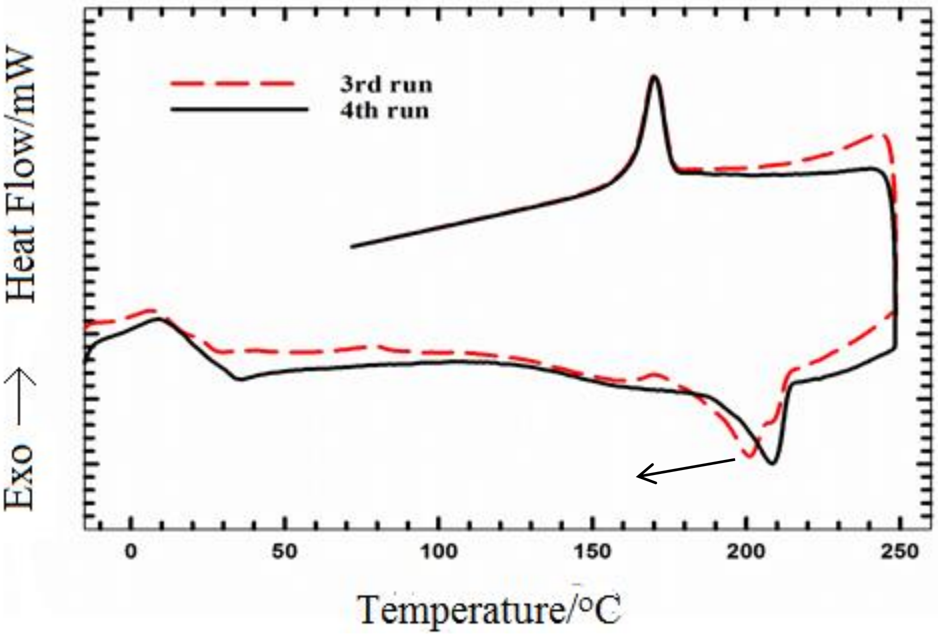

Figure 1 – DSC curve for neat nylon-6 showing T_g, T_m and T_c

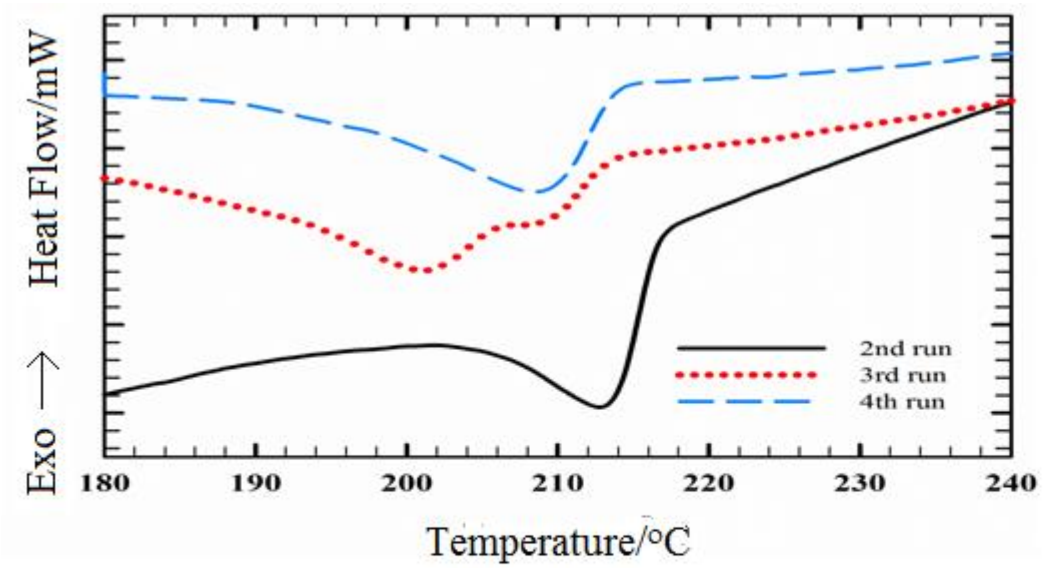

Figure 2 – DSC curve for neat nylon-6 showing T_m for different runs

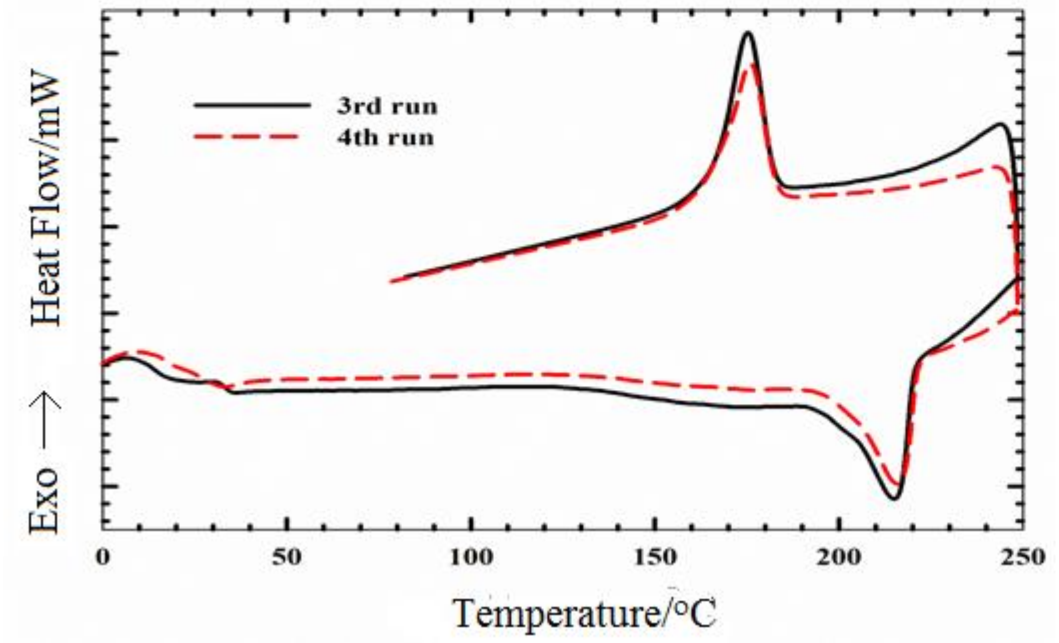

Figure 3 – DSC curves for nylon-6/clay (0.5%) nanocomposite showing T_g, T_m and T_c

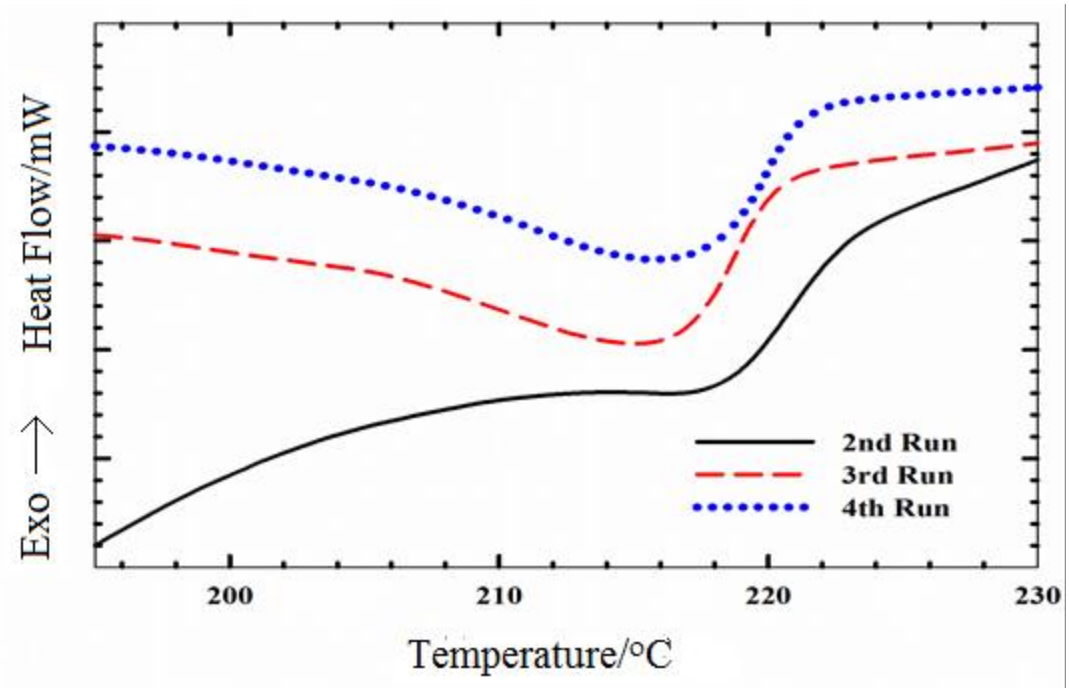

Figure 4 – DSC curve for nylon-6/clay (0.5%) nanocomposite showing T_m for different runs

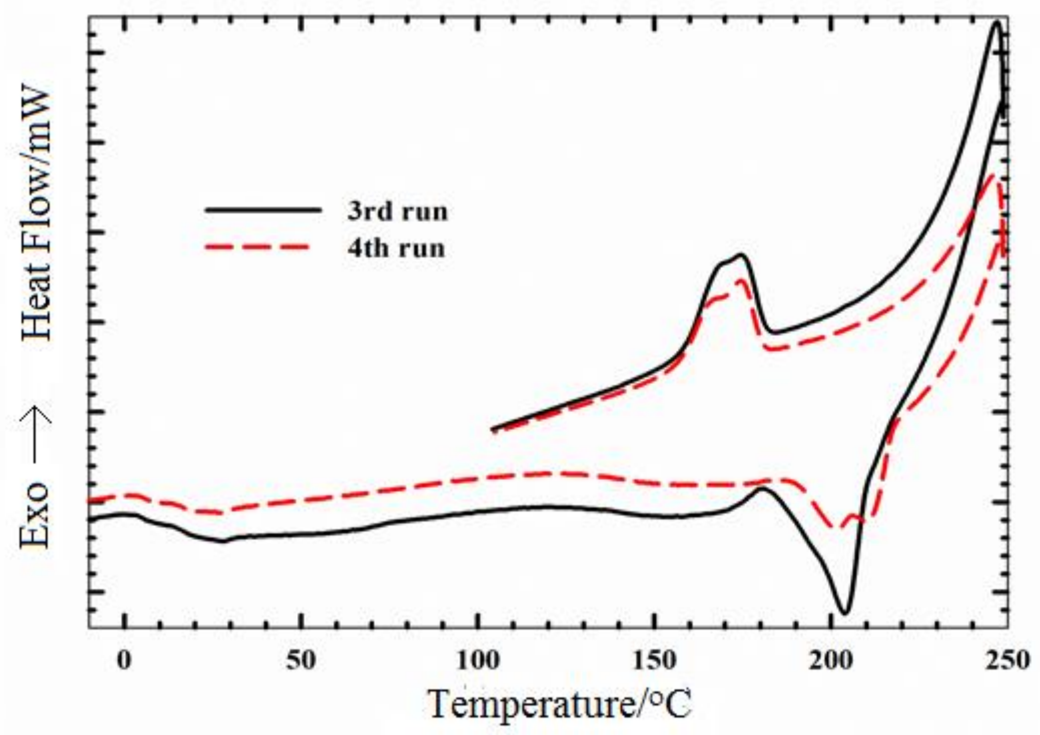

Figure 5 – DSC curve for nylon-6/clay (1%) nanocomposite showing T_g, T_m and T_c

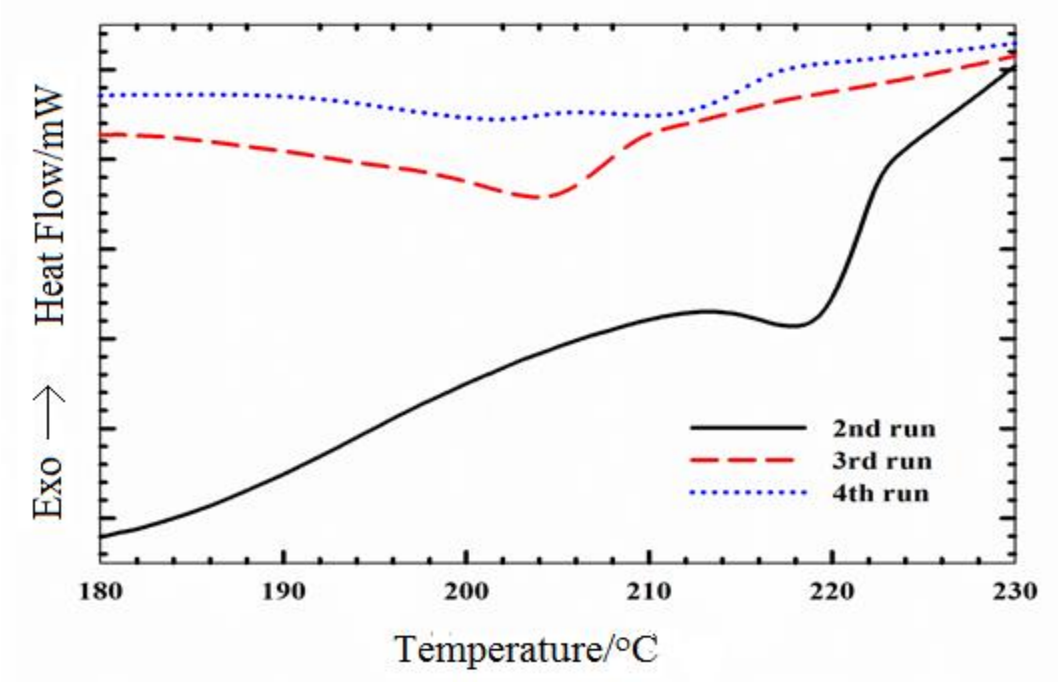

Figure 6 – DSC curve for nylon-6/clay (1%) nanocomposite showing T_m for different runs

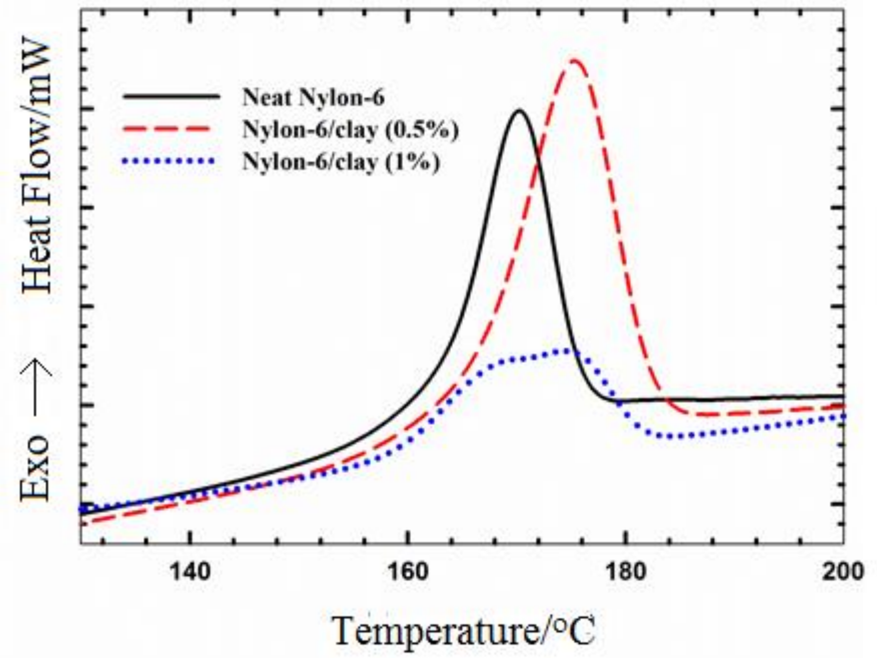

Figure 7 – DSC curve showing the crystallization peak for neat nylon-6 and its nanocomposites with clay

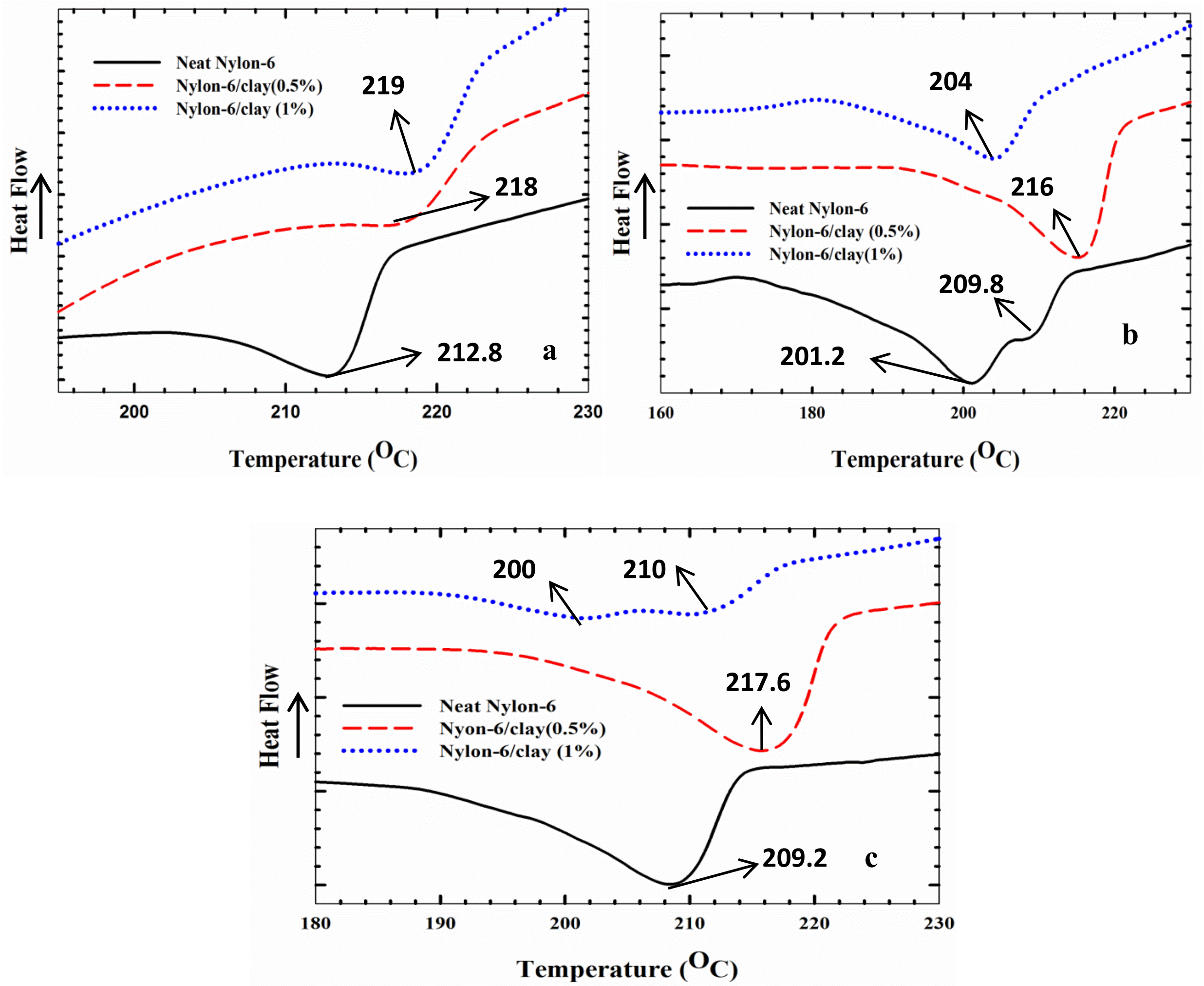

Figure 8 – DSC Thermogram showing the melting peak of nylon-6 and its nanocomposites with clay, (a) Second run, (b) Third run, (c) Fourth Run

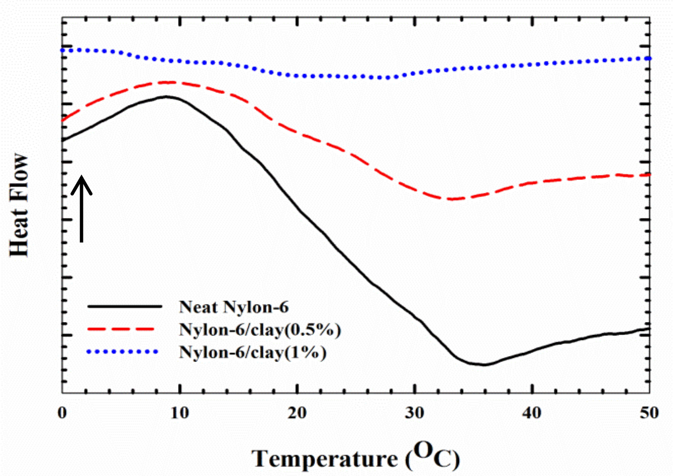

Figure 9 - DSC Thermogram showing the glass transition shift (T_g) of nylon-6 and its nanocomposites with clay

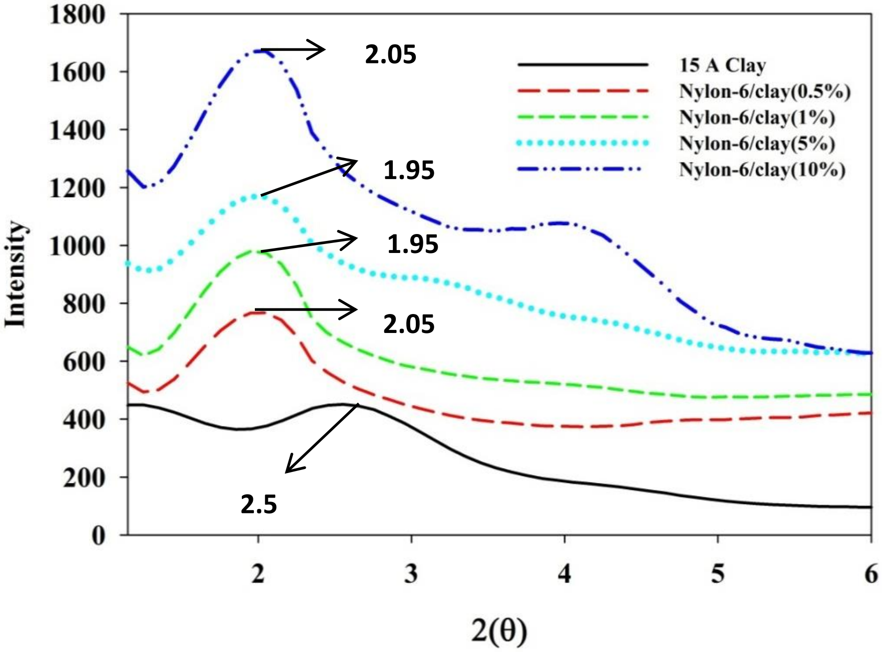

Figure 10 – X-ray diffraction pattern for nylon-6/clay composite at lower angle.

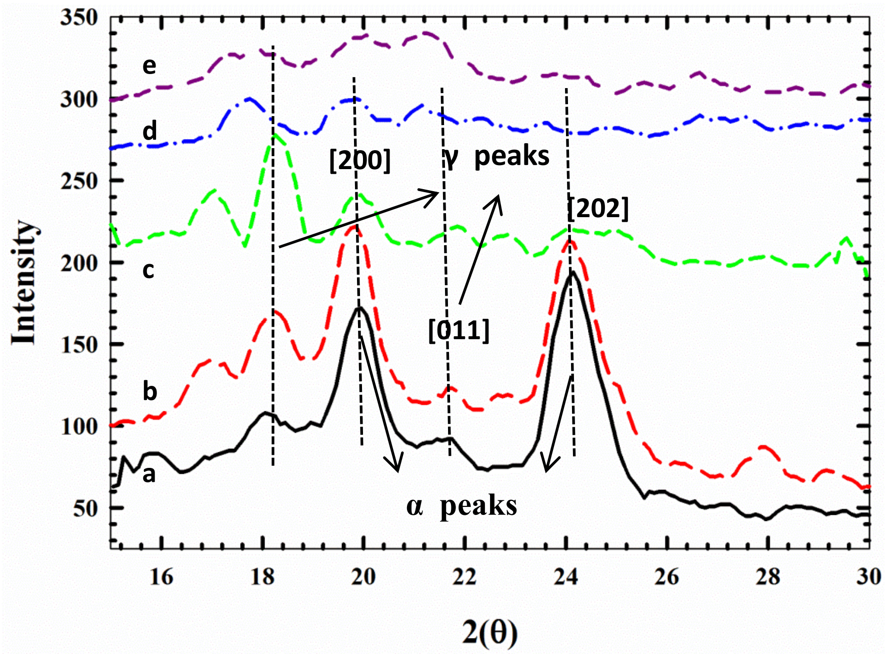

Figure 11 – X-ray diffraction pattern for nylon-6/clay composite at higher angle (a- neat nylon-6, b- nylon-6/clay(0.5%), c- nylon-6/clay(1%), d- nylon-6/clay(5%), e- nylon-6/clay(10%))

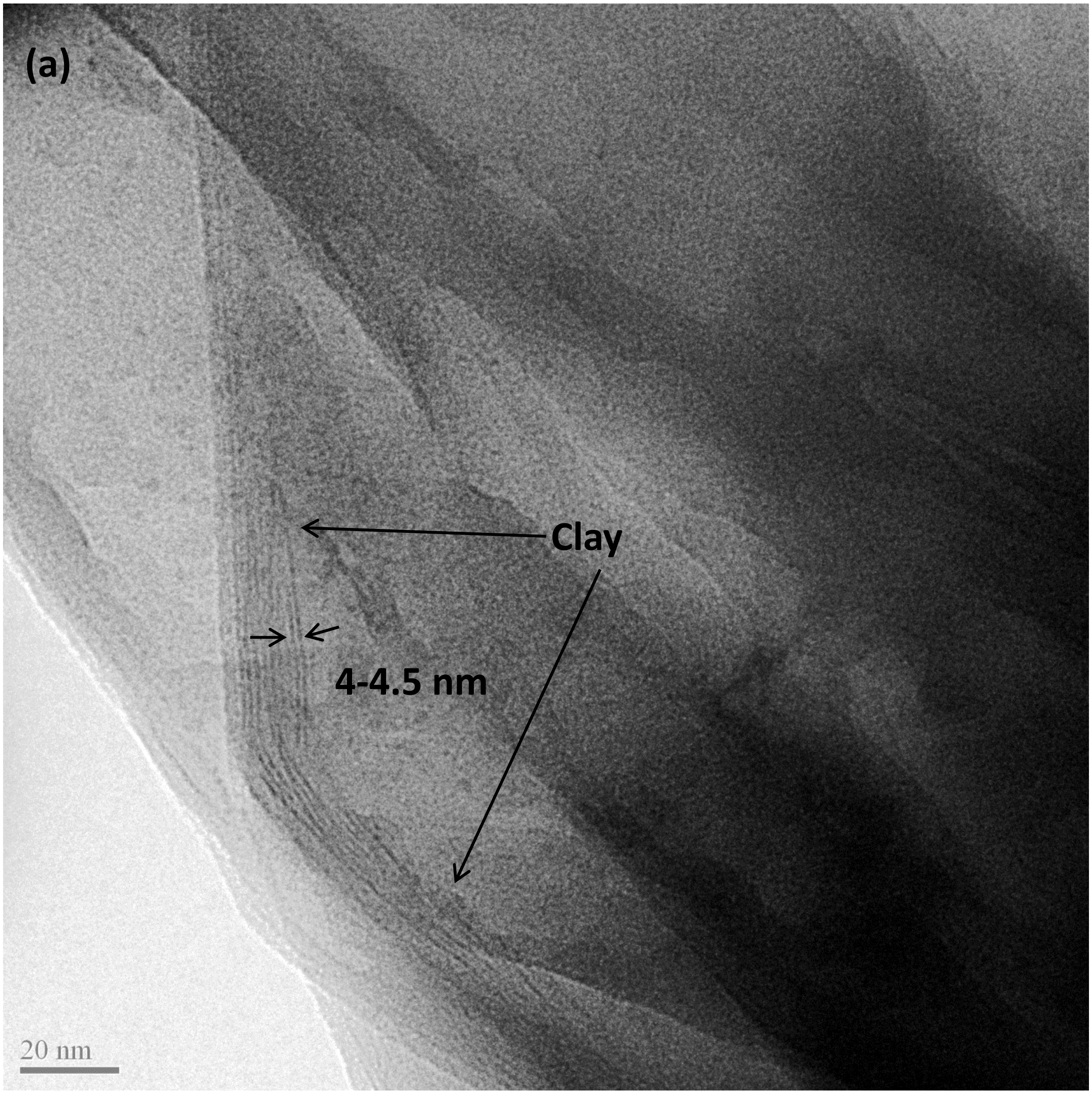
(a)
Clay
4-4.5 nm
20 nm

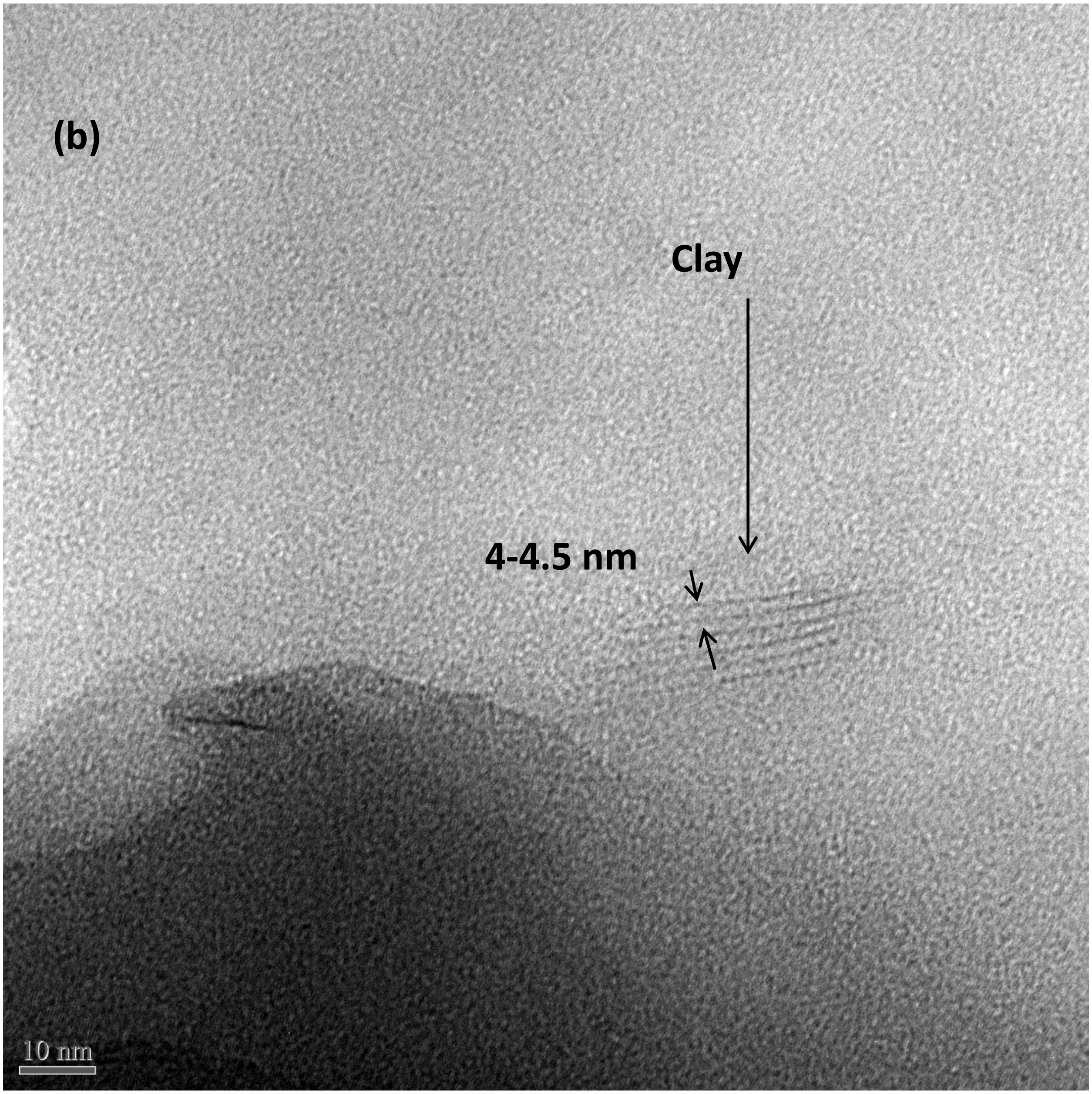

Figure 12 – TEM images for nylon-6/clay (a-5% and b-10%)

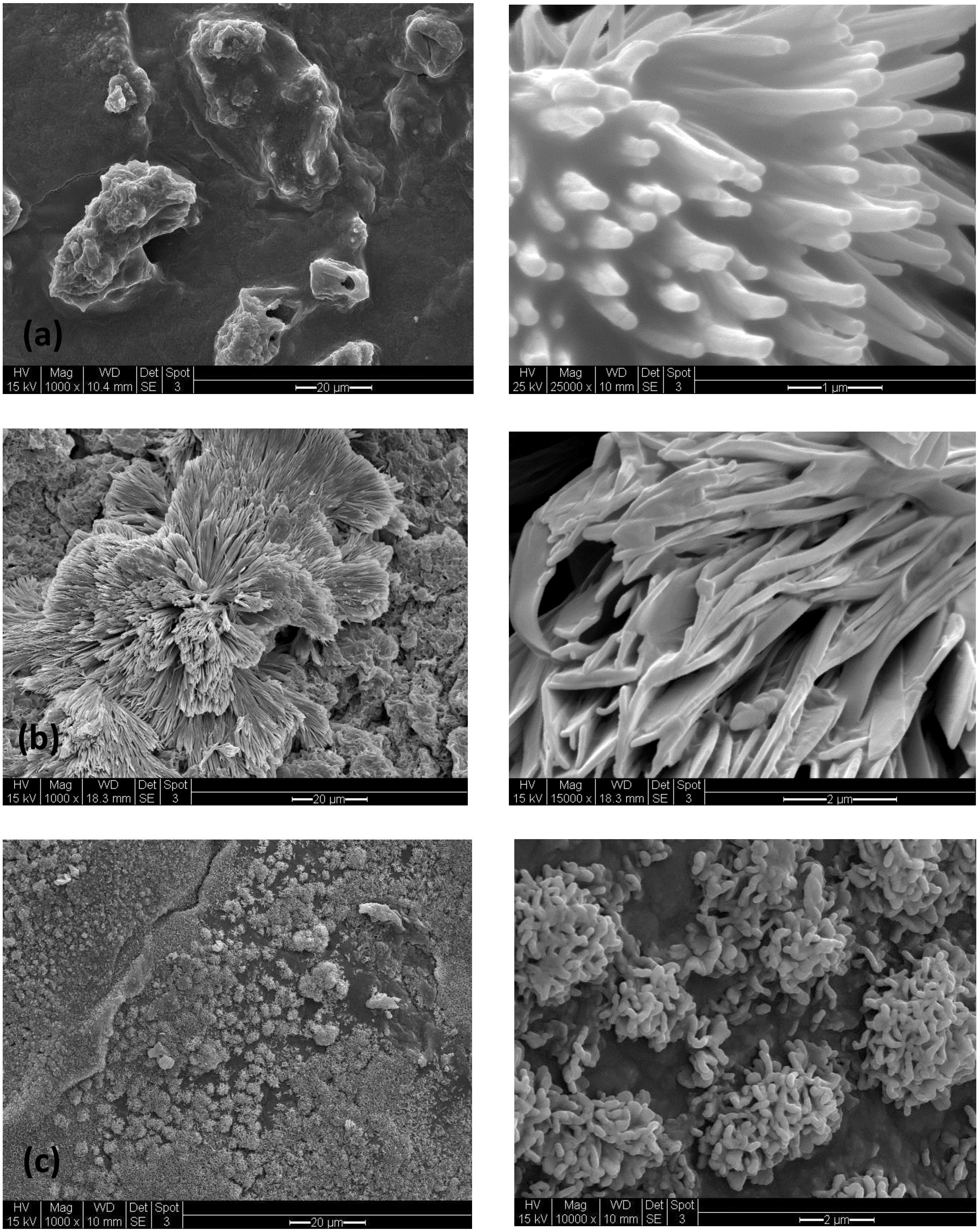
(a)
HV 15 kV | Mag 1000 x | WD 10.4 mm | Det SE | Spot 3 | 20 µm
HV 25 kV | Mag 25000 x | WD 10 mm | Det SE | Spot 3 | 1 µm
(b)
HV 15 kV | Mag 1000 x | WD 18.3 mm | Det SE | Spot 3 | 20 µm
HV 15 kV | Mag 15000 x | WD 18.3 mm | Det SE | Spot 3 | 2 µm
(c)
HV 15 kV | Mag 1000 x | WD 10 mm | Det SE | Spot 3 | 20 µm
HV 15 kV | Mag 10000 x | WD 10 mm | Det SE | Spot 3 | 2 µm

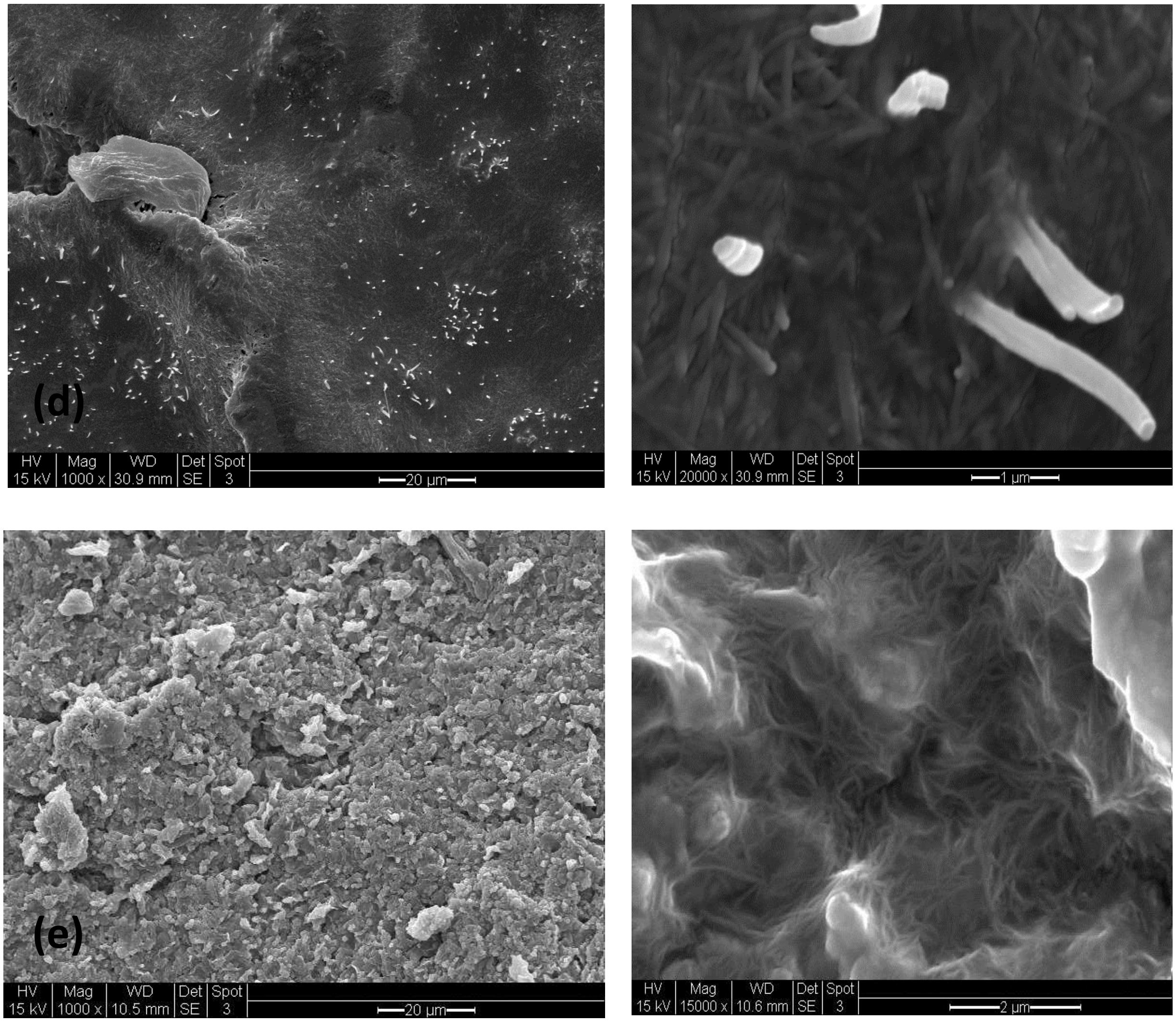

Figure 13 – SEM images for different composite systems (a – neat nylon-6, b- nylon-6/clay (0.5%), c- nylon-6/clay (1%), d- nylon-6/clay (5%), and e- nylon-6/clay (10%))

Polymer Composites (under review)

CLAY INDUCED THERMOPLASTIC CRYSTALS IN THERMOSET MATRIX: THERMAL, DYNAMIC MECHANICAL AND MORPHOLOGICAL ANALYSIS OF CLAY/NYLON-6-EPOXY NANOCOMPOSITES

Aniket Vyas, Jude O Iroh, Material Science and Engineering Program, College of Engineering and Applied Science, University of Cincinnati, Cincinnati, OH 45221-0012, USA

1. Introduction

Epoxy resin is an important and versatile material used in polymer industries. It is extensively used as coatings and adhesives in automotive, construction and aerospace segments because of its excellent physical, chemical and mechanical properties [1, 2]. It possess outstanding stiffness and strength that make it a useful matrix material in advanced structural composites [3].In spite of such desirable properties, epoxy resins are extremely brittle in nature due to highly cross-linked structure and glassy nature. Moreover, epoxy is also known to absorb moisture due to presence of hydroxyl groups [4]. Such shortcomings limit the use of epoxy resin in aerospace and automotive industries. Hence, an improvement in the toughness of epoxy resin is greatly desired in order to widespread it applications and increase service lifetime.

Toughening of epoxy has often been successful by incorporating rubber or thermoplastic polymer as second phase such as polysulfone, polyester [5], poly(ether-imides), poly(ϵ-caprolactone) [2] and polyamides [3, 6]. The thermoplastics polymers are preferred over rubber since they do not decrease the inherent properties of epoxy matrix as in case of rubbers [7, 8]. Thermoplastics provide a wider variety of toughening mechanisms such as (1) crack pinning, (2) particle bridging, (3) crack path deflection, (4) particle yielding, (5) particle-yielding induced shear banding, and (6) micro cracking [3, 9-11].

Among the thermoplastics, a special attention has been given to reinforcement of epoxy by polyamides or nylons. They are known to increase the toughness of epoxy not only by physical presence of crystals, but also by chemical interaction [12-14]. Kim et al [3] studied the effect of mixing temperature on morphology of blends and reported the effect of morphology on fracture toughness of composites.Cardwell and yee [6] reported that nylon particles toughen epoxy by crack bridging mechanism and large plastic deformation of nylon rich phase. Zhong et al [13] studied the kinetics of curing of epoxy by nylon. Wang et al [14] studied the thermo-mechanical properties of epoxy/nylon blends. All the above mentioned techniques consisted of few shortcomings such as use of corrosive (acid) or volatile (alcohol) solvent to dissolve nylon-6 or use of heat to mix it with epoxy.

Recently, our group reported a unique eco-friendly and facile processing method to prepare nlon-6/epoxy blends based on solution polymerization of nylon-6 [15, 16]. A remarkable semi-crystalline spherulitic morphology was achieved due to growth of crystals during curing of epoxy. It was proposed that nylon-6 crystals uses epoxy surface as template or a nucleating surface to grow on[16]. The effect of morphology on the dynamic mechanical properties, thermal behavior and rheological behavior was also discussed [15].

In the present article,advancement to the existing work is reported, where nylon-6 was first modified with nano clay during synthesis step and the clay modified nylon-6 was then incorporated in epoxy resin via reactive blending. Nano-clay was choice of filler as it has been reported to decrease the moisture uptake by nylon-6 significantly [17, 18]. Moreover, clay acts as nucleating agent for the growth of nylon-6 crystals [19]. Hence, presence of clay in nylon/epoxy system was expected to generate novel polymer architecture which could directly influence the properties.

2. Experimental

2.1. Materials

ϵ-caprolactam, dry sodiam hydride (95% purity), N-acetylcaprolactam and N-methylpyrollidone (NMP) solvent (99% purity) were purchased from Sigma-Aldrich, USA for solution polymerization ε-caprolactam. Cloisite 15A clay was purchased from southern clay. Polyfunctional Water Dispersible DGEBA based Epoxy resin (EPIREZ 5522-WY-55) was purchased from Hexion Chemicals, Houston, USA.

2.2. Procedure

2.2.1. Solution Polymerization of Nylon-6 in Presence of Clay

Initially, ε-caprolactam was added to NMP till it dissolved completely, followed by addition of 15A clay. Nitrogen supply was turned on and temperature was increased gradually from room temperature. NaH (catalyst) was then added to the solution and stirred till it dissolved completely at 50 ^{0}C. This process of dissolution was accompanied by a series of color changes from colorless to dark blue which eventually turned black on complete dissolution. Temperature was then raised to 160^{o}C and N-acetyl Caprolactam (initiator) was added to the solution. The color of solution gradually changed from black to blue. After addition of initiator, solution was stirred for 30-45 minutes. The Nitrogen supply was then turned off and the black solution gently turned into a dark orange yellow viscous solution indicating the completion of reaction terminated by air. Composite systems of nylon-6 modified by different loading of clay were synthesized. Clay loading was varied as 0.5%, 1%, 5% and 10% by weight.

2.2.2. Preparation of Clay/Nylon-6-Epoxy Blends

Epoxy was taken in a glass jar, suspension of nylon-6 modified by 0.5, 1, 5 and 10 weight % of 15A clay was added to it, maintaining the nylon-6/epoxy ratio by weight at 10/90 and 20/80. NMP was further added to dilute the solution to reduce the viscosity for ease of processing in order to have defect free films and coatings. The mixture was then stirred using mechanical stirrer for 1 hour at room temperature to obtain homogeneous solution and then ultra-sonicated for 5 minutes. Various compositions that were used in this study are listed in table 1.

2.2.3. Preparation of Clay/Nylon-6-Epoxy Films

8 ml of blend was taken and casted in 1.5'' × 1.5'' × ¼'' Teflon molds to form free standing films. The films were cured in vacuum oven in a stepwise manner, heating initially at 50 ^{O} C for 13 hours, 100 ^{O} C for 4 hours, 120 ^{O} C for 2 hours and finally 150 ^{O} C for 2 hours and were then cut with a sharp razor blade to obtain rectangular films.

The free standing films were quenched in liquid nitrogen and broken to see the cross-section of fractured surface under Scanning Electron Microscopy.

2.3. Characterization

The viscosity of blend was measured by shear viscometry using the Brookfield Viscometer. The Viscometer spindle speed was varied from 0.5 to 100 rpm and temperature was maintained at 25^{O}C.

Differential scanning Calorimeter (DSC) was used to measure thermal properties of Nylon 6 and modified epoxy. DSC was performed at the heating rate of 5^{O}C/min using DSC6200, Seiko

Instruments Inc. The samples were analyzed after complete melting and recrystallization to remove the thermal history.

Dynamic Mechanical Spectroscopy (DMS) was used to study the variation of storage modulus and tan δ of neat epoxy and epoxy/Nylon 6 composite films with respect to temperature. Dynamic Mechanical Analysis was performed between -20^{O}C to 140^{O}C by using DMS6000, Seiko Instruments Inc. The test was performed under tensile loading at a heating rate of 5^{O}C/min and a frequency of 1 Hz.

Scanning Electron Microscope was a Philips model FEI XL 30 ESEM-FEG. The software used to capture images was Scandium. Aluminum stubs with carbon tape were used as sample holders, and the sample was coated with Au-Pd before subjecting to SEM.

3. Results and Discussion

3.1. Rheological Behavior

The rheological behavior of various nylon-6/epoxy systems without clay is shown in Figure 1. The viscosity for all the systems was found to be increasing with increase in spindle speed, moreover the magnitude of the viscosity for the systems containing nylon-6 increased with respect to neat epoxy resin. A significant increase in viscosity by about 50% was observed for epoxy resin filled with 20 weight% of nylon-6. The possible reason for this can be shear-induced particle migration or in other words, under stress nylon-6 tends to crystallize and behave more like a solid then solution [15, 20, 21].

Then clay modified nylon-6 was incorporated in epoxy resin and the viscosity of resultant blend was measured. To observe the effect of clay on viscosity of blend, epoxy/nylon-6 ratio was kept almost constant with increasing amount of clay. At epoxy/nylon-6 ratio of 90:10 (Figure 2(a)), a shear thickening behavior was observed in the range of 0-100 rpm. When nylon-6 modified with 0.5 wt. % of clay was incorporated in epoxy resin (0.05% clay in overall system), a sudden rise in the viscosity was observed. On further increase in clay upto 0.1 wt.% in the system, the viscosity reduced and came close to that of nylon-6/epoxy system without clay. On further increasing clay upto 0.5 and 1 wt.%, viscosity begin to increase.

On further increasing nylon-6 in epoxy resin, changing the ratio to 80:20, a significant change in the rheological behavior was observed (Figure 2(b)). For the system containing 0.1 wt. % clay, the viscosity initially increased upto 480 cP at spindle speed of 2 rpm but begin to decrease on further increase in spindle speed. For all the system, viscosity initially increased and then began to show a decreasing trend with increasing spindle speed.

The clay is known to have different effects on the plasticization of polymers depending upon interaction between clay particles and matrix [22]. It may increase the plasticization as in case of poly(methylmethacryalte) or decrease it as in case of poly(2-vinylpyridine) [23]. Clay has been reported to lower the viscosity of epoxy ester previously [24]. In the present case, an increase in viscosity is observed with incorporation of clay over pristine sample, but the trend is not linear as a function of angular speed. Viscosity attains a maximum value at lowest loading of clay, decrease on further increase while increase again on further increasing clay. This is a 3-component system, where clay modified nylon-6 is blended with epoxy resin. Hence, Effect of clay on structure and properties of nylon-6 will naturally play an important role in deciding the properties of this system.

Viscosity of epoxy resin increases with addition of nylon-6 without clay, as under shear nylon-6 tends to crystallize. This suggests that crystallinity of nylon-6 is crucial in deciding the properties of resultant composite. Clay is known to have a significant effect on the crystalline properties of nylon-6 [17, 25, 26]. From viscosity results, it can be inferred that when nylon-6 is modified with 0.5 weight% of clay, the crystallinity of nylon-6 increases substantially while when it is modified with 1 wt.% clay, the crystallinity reduces such that viscosity approaches the nylon-6/epoxy sample without clay. Following the trend, crystallinity of nylon-6 should reduce significantly on further increasing clay such that matrix is primarily controlled by intercalated clay particles. These inferences were verified by thermal analysis of these composites as discussed in next section.

3.2. Thermal Behavior

The effect of clay concentration on the melting behavior of nylon-6 is shown in Figure 3(a). The melting point of neat nylon-6 was around 209 ^{0}C. When nylon-6 was synthesized in presence of 0.5 wt.% clay, the melting point increased to 217.6 ^{0}C. On further increasing clay to 1wt.%, the melting temperature decreased and showed multiple peaks at 200 ^{0}C and 210 ^{0}C. The multiple melting peaks indicate the presence of different polymorphs (α and γ type crystals) in the same sample, Melting peak was not observed for clay loading at 5 and 10 weight%. Fornes and Paul [27] has reported that crystallintiy of nylon-6 increases at lower loading whereas at higher loading polymer crystal growth retards. A similar phenomenon was observed for clay/nylon-6 composite prepared by in-situ solution polymerization. The melting point is dependent upon molecular weight and chain length of polymer, higher molecular weight leads to increase in melting point [20]. Hence it can be deduced that low amount of clay facilitated the polymerization and hence crystallization, while increasing clay concentration acted as hindrance to formation of polymer chains and reduced the crystallinity.

The effect of clay on melting of nylon-6 in epoxy resin matrix is shown in Figure 3(b), where epoxy to nylon-6 ratio is kept almost constant at 80:20 by weight. The sample without clay showed multiple melting points but a major peak was observed at 206 ^{0}C. At 0.5 wt.% clay loading, the melting point increased to around 210 ^{0}C, while at 1 wt.% clay loading, it decreased to 204 ^{0}C. The melting trend of nylon-6 in epoxy matrix followed the same fashion as in absence of epoxy. Presence of multiple peaks in nylon-6/epoxy composite without clay suggests that nylon-6 crystals used epoxy surface as a template to grow upon [16] but the composites containing clay showed a single peak suggesting, nylon-6 crystals preferred to use nano clay particles as nucleating agent over epoxy surface.

Hence it can be concluded that at very low level of clay (0.5 wt.%) , crystallinty of nylon-6 increases, which leads to rise in the viscosity of its blend with epoxy resin. On further increasing clay to 1wt. %, crystallinty reduces, thus when it is blended with epoxy resin, the viscosity reduces. On further increase in clay to 5 and 10 wt. %, the crystallinty of nylon-6 reduces drastically and matrix is dominated mostly by clay particles. The clay particles lead to increase in the viscosity of blend with respect to epoxy, as the filler is mostly clay instead of crystals.

3.3. Dynamic Mechanical Properties

The effect of clay on the dynamic mechanical properties of nanocomposite films is discussed in this section. Figure 4a and b represents the storage modulus and tan (δ) as a function of temperature respectively for epoxy films loaded with nylon-6 at 10 weight % with variation in clay weight %. The storage modulus begins from the glassy region with a high value at lower temperature and goes through a glass-rubber transition to a rubbery region at higher temperature. It was observed that as the nylon-6 modified with 0.5 and 1 weight% clay, the storage modulus in glassy region (0^{0}C) initially increased but at higher loading of clay where crystallinity decreased significantly and clay particle begin to dominate the matrix, the storage modulus begin to decrease (Figure 11c). A similar trend was observed for storage modulus in rubbery region (40^0C) where it increased initially where nylon-6 crystals were dominating over clay, but at higher loading of clay it begin to fall down (Figure 11d). Figure 11c represents T_g as a function of clay weight% for fixed nylon-6/epoxy composition. The T_g initially decreased from 38^0C for sample without clay to 18^0C for sample containing nylon-6 modified by 0.5weight% of clay (0.05% clay in system) which is possibly due to increased plasticization owing to high crystallinity of nylon-6. As the clay weight% was increased, the T_g begin to increase upto 35^0C as the crytallinity of nylon-6 begin to decrease.

In the glassy region, a material has the highest value of storage modulus which is largely independent of temperature, frequency, molecular weight between cross-links and crosslink functionality. This region occurs due to immobility of molecular chains within polymer network, due to close packing of molecular chains. The large scale molecular motion does not take place in this region[28]. On the other hand in rubbery region, material exhibit lowest storage modulus. In this state molecular chains are free from random coiling and hindrances and can slip past each other, but they are restricted only by crosslinks in the network [28, 29]. In the glass transition zone, storage modulus drops significantly from glassy to rubbery region due to large scale molecular motion of polymeric chains. The T_g is inferred by the peak in tan (δ) curve.

Wang et al [30] reported increase in storage modulus (glassy region) for epoxy resin in presence of clay while Wang and Chen [14] reported decrease in storage modulus (glassy region) in presence of nylon. A combined effect for three component system is shown in the present case when clay modified nylon-6 is incorporated in epoxy resin. At the same level of nylon-6 loading in epoxy, when clay was introduced at lower amounts, the stiffness of material increased. Although low level of clay increased the crystallinty of nylon-6 but at lower amount of clay, the interaction among different polymer chains increased causing reduction in mobility among polymer chains. At higher loading of clay, as nylon-6 crystals were not significantly present in the matrix, the interaction was mostly among clay particles (along with small nylon chains) and epoxy which increased the chain mobility leading to fall of storage modulus in glassy region. A similar trend was observed in rubbery region. Increased value of storage modulus at lower clay concentration suggests increased cross-link density while at higher clay concentration the crosslink density decreased. The plasticization effect of nylon-6 crystals on epoxy is clearly observed by variation in T_g. At lowest loading of clay, nylon-6 attained highest crystallinity which significantly reduced the T_g of epoxy but with increase in clay loading, as the crystallinity was reduced, the T_g began to increase.

3.4. Morphology

It is essential to understand the morphological evolution, because resultant morphology is the deciding factor behind physical and mechanical properties of polymer composites. The epoxy/nylon blends without clay have been reported before by our group [15, 16]. It was observed that as the epoxy/nylon blend is subjected to curing, nylon tends to crystalize in form of spherulites along with branching, growing radially outwards to occupy the free volume by using epoxy surface as heterogeneous template to grow upon. In the present case, clay was first introduced into nylon-6 during polymerization. The product was obtained as suspension. Since, clay facilitates crystallization of nylon [25], it is likely that nylon will tend to crystallize during and after polymerization before blending it with epoxy, as both process occurs simultaneously [31].Moreover, silicate layers present in clay can lead to a nucleation and growth of nylon crystals due to hydrogen bonds among nylon chains and silicates [32]. Hence, it can be inferred that nylon-6 will prefer to crystallize over clay particles instead of epoxy surface, as reported before for system without clay [16]. After curing the blend of clay modified nylon and epoxy, the crystal growth can occur in two conducts: at the surface and inside the bulk of matrix. The morphology at the surface and the bulk are discussed in separate sub-sections.

3.4.1 Surface Morphology of Coating

The morphology of surface of the coating is shown in Figure 5. When clay modified nylon-6 was blended with epoxy resin, and the resultant blend was subjected to curing, a unique morphology consisting of disordered symmetrical dendrites was observed at the surface. In case of nylon/epoxy blends without clay, the nylon crystals were found to grow in the cracks of brittle epoxy (see fig 5 ref 16) [16], but in the present case, cracks in the brittle epoxy can be clearly seen. This confirms the preference of crystals growth on clay as nucleating agent, instead of epoxy template. The cracks in brittle epoxy were more pronounced at nylon concentration of 10% and clay concentration of 0.1% by weight (fig 5a) then nylon concentration of 20% and clay concentration of 2% by weight (fig 5b).

The formation of crystals depends upon various thermodynamic and kinetic factors such as diffusion coefficient of atomic species, surface energies, temperature and concentration [20], but Granasy et al [33] reported that if the crystal growth mechanism is dependent on growth front nucleation (also called secondary nucleation), single crystal growth is transformed into polycrystalline growth. In the present case, since clay is acting as a nucleating agent, preferred mode of crystal growth is naturally secondary nucleation. The obtained morphology is the result of spectrum of structures generated by an interplay between ordering effect of crystallization and disordering effect of interfacial instabilities, during secondary nucleation [33]. Such morphologies have been reported previously for thin films of polymer blends [34], electrodeposited metal films [35] and single component polymer films [36]. The presence of clay as heterogeneous entity leads to polycrystalline growth, and the essential mechanism have been hypothesized to be stabilization of new crystals grains having the crystallographic orientation preferred by particles rather than the parent crystal. In other words, particulate additives, along with acting as a nucleating agent, can also perturb crystal growth, leading to evolution of irregular dendritic morphology [37]. Since the present morphological results are in accordance with the morphologies reported for crystal growth in presence of nanoparticles, it can be inferred that for a three component system consisting of clay modified nylon blended with epoxy resin, clay dominated the nucleation and crystal growth front of nylon. Moreover, at the surface, the crystallization was enhanced due to reduction in interfacial energy because when sample is cooled to crystallization temperature, surface is usually cooler [16, 38].

For epoxy/nylon(10%)/clay(0.1%), 1 weight % of clay was used for in-situ synthesis of nylon-6/clay composite, while for epoxy/nylon(20%)/clay(2%), 10 weight % of clay was used for in-situ synthesis of nylon-6/clay composite. Low concentration of clay in nylon-6 lead to increase in crystallinity in nylon-6, while higher concentration of clay decreased the crystallinity. Hence, it can be observed in fig 5a, each dendritic crystal’s diameter is in the range of 8-10 µm, and each branch is about 2-5 µm (Lower clay loading), while in fig 5b, growth was predominantly in transverse direction with length in range of 10-30 µm, with small branches in lateral direction of about 1-2.5 µm (higher clay loading). At lower clay and nylon loading (fig 5a), most of clay particles were consumed as nucleating agent for nylon, and crystals were not growing in the cracks of epoxy significant number of cracks were observed on surface. But at higher clay and nylon loading (fig 5b), no significant cracks were observed. It can be due to presence of large number of small chains of nylon and free nano clay particles that did not take part in crystallization process, that filed the epoxy resin matrix, evident by dark grainy background at the surface.

3.4.2 Bulk Morphology at Fractured Surface of Film

The morphology in the bulk of clay/nylon/epoxy film was observed after fracturing the film in liquid nitrogen. The effect of composition on nature and distribution of crystals in epoxy matrix was clearly visible. The SEM images of fractured surface of all the films are shown in Figure 6. It have been reported that interphasal morphology has a significant effect on the properties of composites [3, 39]. For Epoxy/nylon blends, new structure can be developed at interphase due to reaction between amide group of nylon and epoxide group of epoxy [40, 41]. A semi-IPN structure is obtained at the interphase. As the blend is subjected to curing, free nylon chains crystallizes in the matrix in form of isolated lamellae, in other words, the resultant morphology contains amorphous phase with irregular distribution of crystalline phase. It was observed that the nature of crystals, size of crystalline lamellae and distribution of crystal phases in amorphous phase depends upon composition. A variation in clay or nylon concentration in a 3-component system can cause significant change in morphology. Figure 6(a) is the SEM image of epoxy/nylon(20%)/clay(0.1%), where nylon-6 modified with 0.5 weight% of clay was blended with epoxy. Thermal behavior suggests that nylon-6 modified with 0.5% shown increased crystallinity, indicated by increase in melting temperature. Hence, nylon-6 modified with 0.5 weight% clay, wen blended with epoxy resin lead to very high number of crystalline zones in amorphous matrix. As can be seen in Figure 6a, a large number of small crystals can be observed encapsulated by epoxy resin. Ay higher magnification, a huge number of crystals were observed impinged into each other, possibly due to lack of space to accommodate such large number of crystals. Figure 6b is the SEM image of epoxy/nylon(10%)/clay(0.1%), which shows lesser number of crystalline zones in amorphous matrix. Moreover, growth of crystals was found to be in form of branched dendritic structure. The shape of crystals observed in the bulk and at the surface were very similar, suggesting similar growth mechanism in both the conducts, i.e. majority crystals preferred to grow over clay particles as nucleating agents instead of heterogeneous epoxy surface. The clay concentration on overall system was maintained at 0.1%

and nylon-6 was decreased from 20 to 10 weight%, it can be seen that relatively larger crystals were formed with less number of crystalline zones, as opposed to the prior case. Figure 6 c is the SEM image of epoxy/nylon(20%)/clay(2%). For this system, nylon-6 modified with 10 weight % of clay was blended with epoxy resin. Since the clay loading was high, crystallinty of nylon-6 was reduced significantly, which is further evident by lack of melting peak in DSC. The crystalline zones further decreased and a limited number of thin, small and feather-like crystals were observed inside the zones. A large number of particulate features were observed widely dispersed in the crystalline zone. This observation at bulk morphology is in accordance with the hypothesis proposed on basis of surface morphology of coating, due to large amount of clay; nano-particles unconsumed in the process of nucleation begins to fill the epoxy matrix.

4. Conclusion

A non-conventional method was explored for the synthesis of clay/nylon-6 composite suspension via in-situ solution polymerization. As the resultant composite was obtained as suspension, it became simple to efficiently blend it with water-based epoxy resin at room temperature, leading to formation of 3-component system comprising of clay, nylon and epoxy. Lower concentration of clay lead to increase in the crystallinity of nylon-6, while at higher concentration, crystallinity of nylon-6 reduced significantly. The properties of composite system were found to be dependent on crystalinty of nylon-6, which in turn was dependent on clay concentration. DSC analysis suggested that, the composite system was semi-crystalline in nature and at lower loading of clay, melting point increased while at higher concentration, melting point decreased. At very high concentration of clay, melting peak was not detected by DSC. From dynamic mechanical analysis, it was observed that storage modulus initially increased with increase in clay loading, but began to fall at higher concentration. On the contrary, T_g initially decreased with increase in clay due to high crystallinity and hence higher plasticization of epoxy due to clay/nylon system, but on further increasing concentration of clay, the T_g began to rise. All the prepared systems exhibited heterogeneity and the morphology changed significantly with variation in nylon-6 and clay concentration. During processing of composite coatings and films, the curing of epoxy and crystallization of nylon-6 via growth front nucleation occurred simultaneously, with clay particles acting as nucleating agents.

5. Acknowledgement

This study was funded by grants from office of naval research (ONR) # N00014-09-1-0980 and National Science Foundation (NSF) # CMMI-0758656. We would also like to thank Soumyarwit Manna at Advanced Material Characterization Center (AMCC), university of Cincinnati who assisted in capturing the SEM images.

6. References

7. 1. May, C. A., Epoxy Resins: Chemistry and Technology; M. Dekker, (1988).
8. 2. Barone, L.; Carciotto, S.; Cicala, G.; Recca, A., Polym. Eng. Sci. **46**, 1576 (2006).
9. 3. Kim, S.; Kim, J.; Lim, S. H.; Jo, W. H.; Choe, C. R., J App. Polym. Sci. **72**, 1055 (1999).
10. 4. Mallick, P. K., Fiber-Reinforced Composites: Materials, Manufacturing, and Design, Second Edition; Marcel Dekker, (1993).
11. 5. Kim, J.; Robertson, R. E., J Mater. Sci. **27**, 3000 (1992).
12. 6. Cardwell, B. J.; Yee, A. F., J Mater. Sci. **33**, 5473 (1998).
13. 7. Parker, D. S.; Yee, A. F., J Thermoplast. Comp. Mater **2**, 2 (1989).
14. 8. Bucknall, C. B.; Karpodinis, A.; Zhang, X. C., J Mater. Sci. **29**, 3377 (1994).
15. 9. PEARSON, R. A., SOURCES OF TOUGHNESS IN MODIFIED EPOXIES; University of MICHIGAN, (1990).
16. 10. Pearson, R. A.; Yee, A. F., Polym. **34**, 3658 (1993).
17. 11. Yee, A. F.; Pearson, R. A., J Mater. Sci. **21**, 2462 (1986).
18. 12. Gorton, B. S., J Appl.Polym. Sci. **8**, 1287 (1964).
19. 13. Zhong, Z.; Guo, Q., Polym. **39**, 3451 (1998).
20. 14. Wang, Y.-Y.; Chen, S.-A., Polym. Eng. Sci. **20**, 823 (1980).
21. 15. Vyas, A.; Iroh, J. O., J Appl. Polym. Sci. (2013) doi -10.1002/39574 .
22. 16. Vyas, A.; Iroh, J. O., Polymer Engineering & Science, (2013) DOI- 10.1002/pen 23616.
23. 17. Murase, S.; Inoue, A.; Miyashita, Y.; Kimura, N.; Nishio, Y., J Polym. Sci. B: Polym. Phy. **40**, 479 (2002).
24. 18. Okada, A.; Kawasumi, M.; Usuki, A.; Kojima, Y.; Kurauchi, T.; Kamigaito, O., MRS Online Proceedings Library 171, (1989).
25. 19. Wu, T.-M.; Liao, C.-S., Macromol. Chem.Phy. **201**, 2820 (2000).

26. 20. Painter, P. C.; Coleman, M. M., Fundamentals of Polymer Science: An Introductory Text, Second Edition; Taylor & Francis, (1998).
27. 21. Galindo-Rosales, F.; Rubio-Hernández, F.; Velázquez-Navarro, J., Rheol. Acta **48**, 699 (2009).
28. 22. Paul, D. R.; Robeson, L. M., Polym. **49**, 3187 (2008).
29. 23. Rittigstein, P.; Torkelson, J. M., J Polym. Sci. B: Polym. Phy. **44**, 2935 (2006).
30. 24. Singh-Beemat, J.; Iroh, J. O., Prog. in Org. Coat. **74**, 173 (2012).
31. 25. Hegde, R. R.; Bhat, G. S.; Deshpande, B., Int. J Polym. Sci. **2012**, 14 (2012).
32. 26. Kojima, Y.; Usuki, A.; Kawasumi, M.; Okada, A.; Kurauchi, T.; Kamigaito, O., J Polym. Sci. A: Polym. Chem. **31**, 983 (1993).
33. 27. Fornes, T. D.; Paul, D. R., Polímeros **13**, 212 (2003).
34. 28. Nakka, J. S., Ph.D. Thesis Technical University of Delft (2010).
35. 29. Menard, K. P., Dynamic Mechanical Analysis: A Practical Introduction, Second Edition; Taylor & Francis, (2008).
36. 30. Wang, K.; Chen, L.; Wu, J.; Toh, M. L.; He, C.; Yee, A. F., Macromol. **38**, 788 (2005).
37. 31. Wilfong, D. L.; Pommerening, C. A.; Gardlund, Z. G., Polym. **33**, 3884 (1992).
38. 32. Maiti, P.; Okamoto, M., Macromol. Mater. Eng. **288**, 440 (2003).
39. 33. Granasy, L.; Pusztai, T.; Borzsonyi, T.; Warren, J. A.; Douglas, J. F., Nat. Mater. **3**, 645 (2004).
40. 34. Ferreiro, V.; Douglas, J. F.; Warren, J. A.; Karim, A., Phys. Rev. **65**, 042802 (2002).
41. 35. Fleury, V., Nature **390**, 4 (1997).
42. 36. Beers, K. L.; Douglas, J. F.; Amis, E. J.; Karim, A., Langmuir **19**, 3935 (2003).
43. 37. Granasy Laszlo, P. T., Warren James A , Douglas Jack F, Borzsonyi Tamas, Ferreiro Vincent, Nat. Mater. **2**, 5 (2003).
44. 38. Schonhorn, H., Macromol. **1**, 145 (1968).
45. 39. Kim, J. K.; Robertson, R. E., J Mater. Sci. **27**, 161 (1992).
46. 40. Chang, F.-C.; Hwu, Y.-C., Polym. Eng. Sci. **31**, 1509 (1991).
47. 41. Maa, C.-T.; Chang, F.-C., J App. Polym. Sci. **49**, 913 (1993).

List of Figures

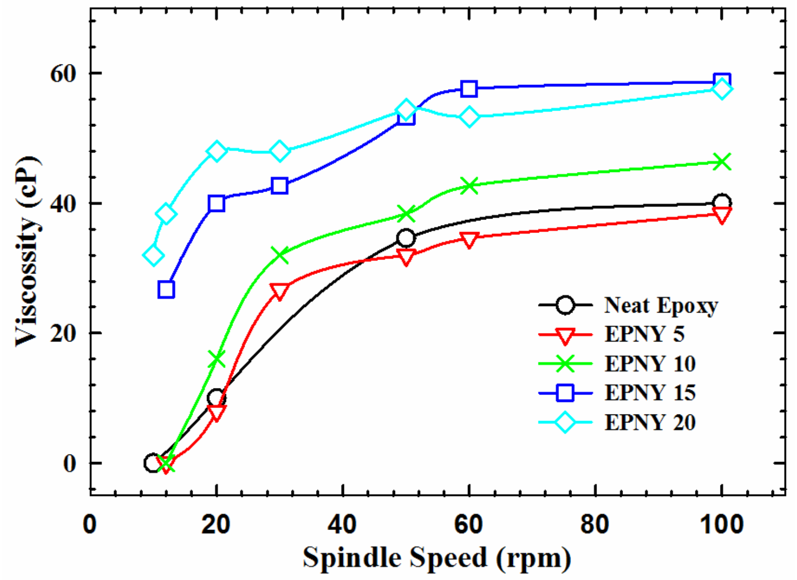

Figure 1 – Variation of viscosity with viscometer spindle speed for different composition of nylon-6 loaded epoxy resin

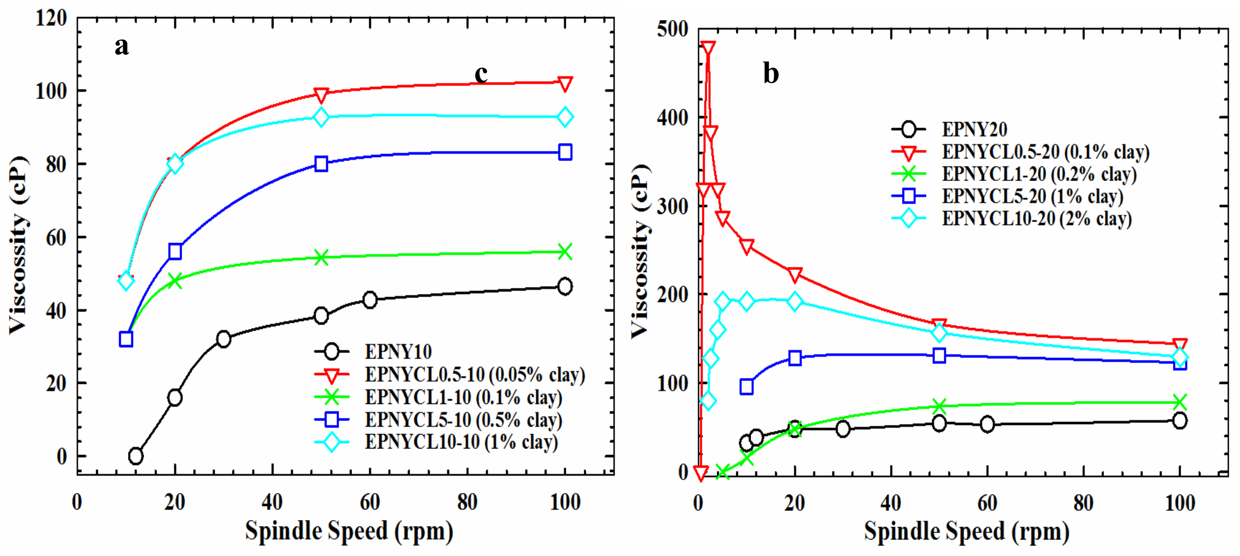

Figure 2 – Variation of viscosity with viscometer spindle speed for different loading of clay in nylon-6/epoxy system at (a) epoxy: nylon-6 (90:10), (b) epoxy: nylon-6 (80:20)

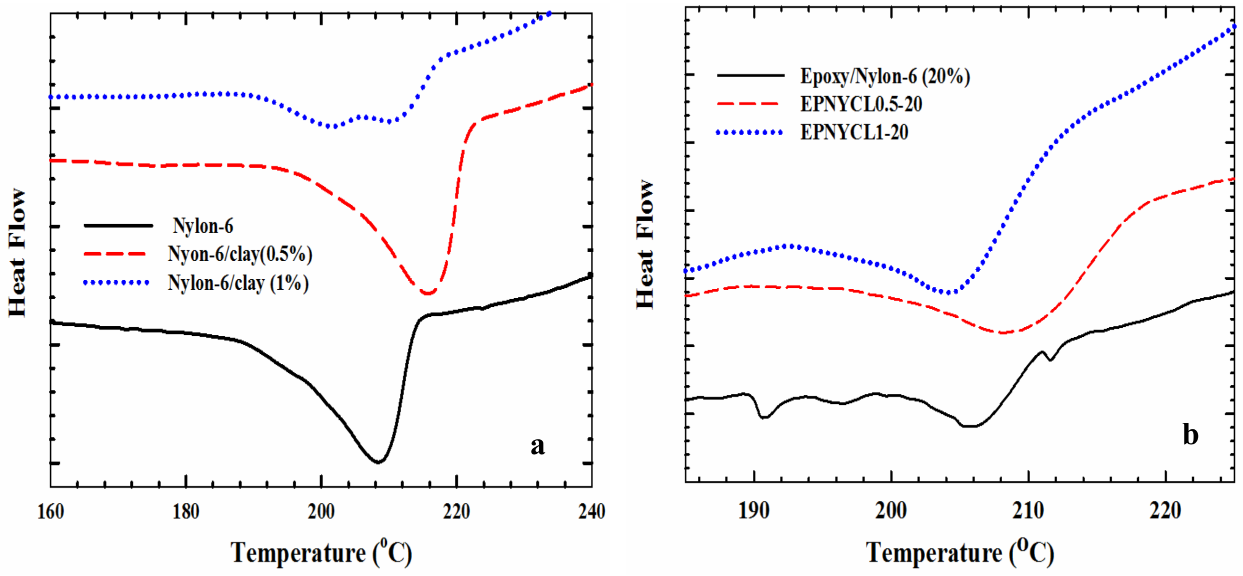

Figure 3 – DSC thermogram showing the effect of clay on melting of (a) Nylon-6 and (b) nylon-6 in epoxy resin at ratio of 80:20 (epoxy: nylon-6)

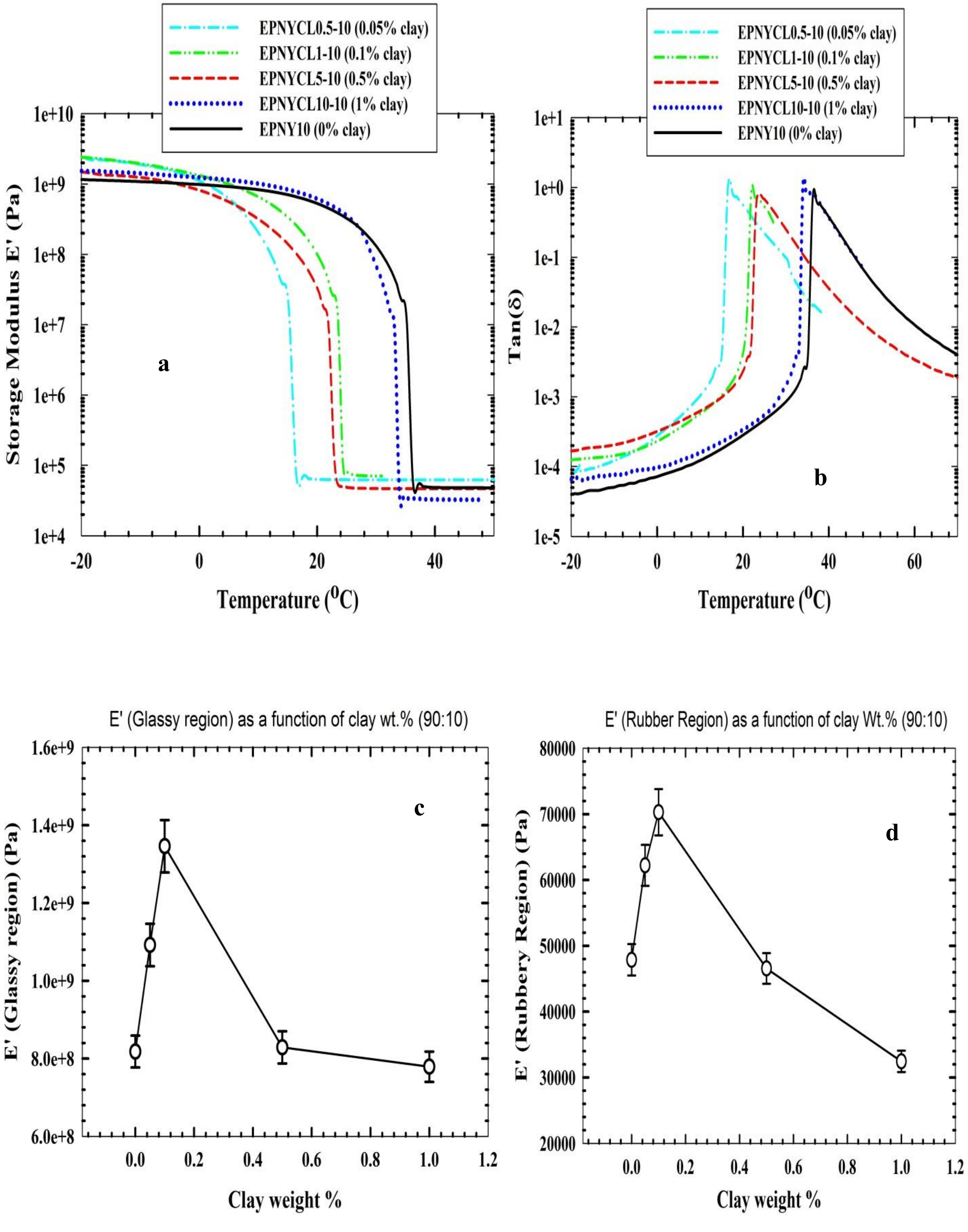
EPNYCL0.5-10 (0.05% clay)
EPNYCL1-10 (0.1% clay)
EPNYCL5-10 (0.5% clay)
EPNYCL10-10 (1% clay)
EPNY10 (0% clay)
Storage Modulus E' (Pa)
1e+10
1e+9
1e+8
1e+7
1e+6
1e+5
1e+4
a
-20
0
20
40
Temperature (°C)
EPNYCL0.5-10 (0.05% clay)
EPNYCL1-10 (0.1% clay)
EPNYCL5-10 (0.5% clay)
EPNYCL10-10 (1% clay)
EPNY10 (0% clay)
Tan(δ)
1e+1
1e+0
1e-1
1e-2
1e-3
1e-4
1e-5
b
-20
0
20
40
60
Temperature (°C)
E' (Glassy region) as a function of clay wt.% (90:10)
E' (Glassy region) (Pa)
1.6e+9
1.4e+9
1.2e+9
1.0e+9
8.0e+8
6.0e+8
c
0.0
0.2
0.4
0.6
0.8
1.0
1.2
Clay weight %
E' (Rubber Region) as a function of clay Wt.% (90:10)
E' (Rubbery Region) (Pa)
80000
70000
60000
50000
40000
30000
20000
d
0.0
0.2
0.4
0.6
0.8
1.0
1.2
Clay weight %

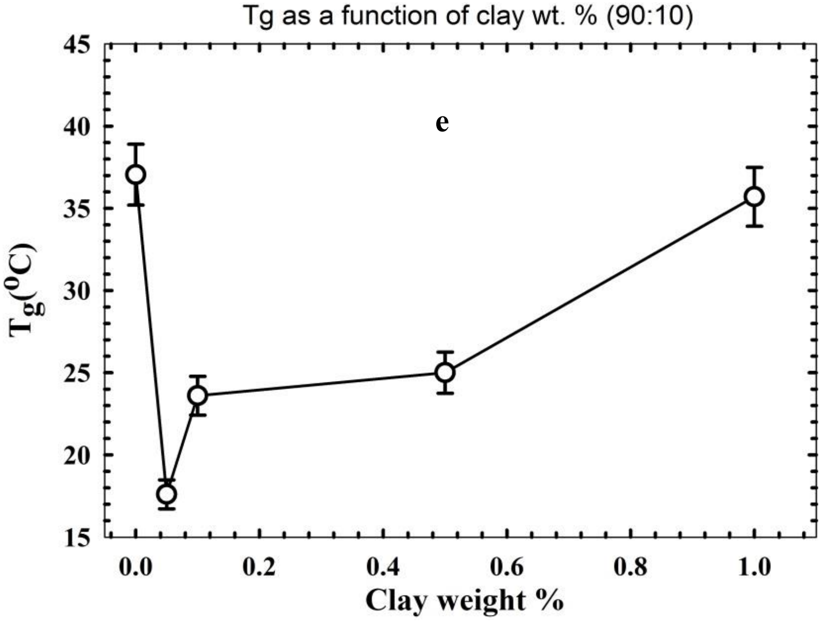

Figure 4 – Dynamic Mechanical Properties for clay/nylon 6-epoxy system for epoxy: nylon-6 weight ratio 90:10 (a) Storage modulus Vs. Temperature (b) Tan(δ) Vs. Temperature (c) Storage modulus in glassy region (0°C) as a function of clay weight % (d) Storage modulus in rubbery region (40°C) as a function of clay weight % (e) T_g as a function of clay weight%.

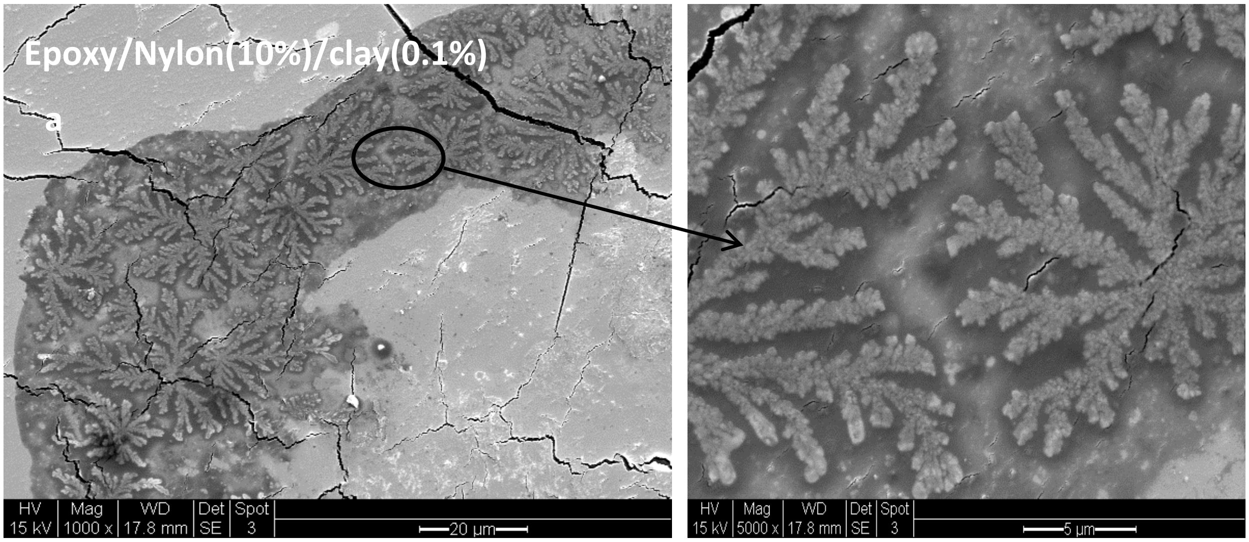

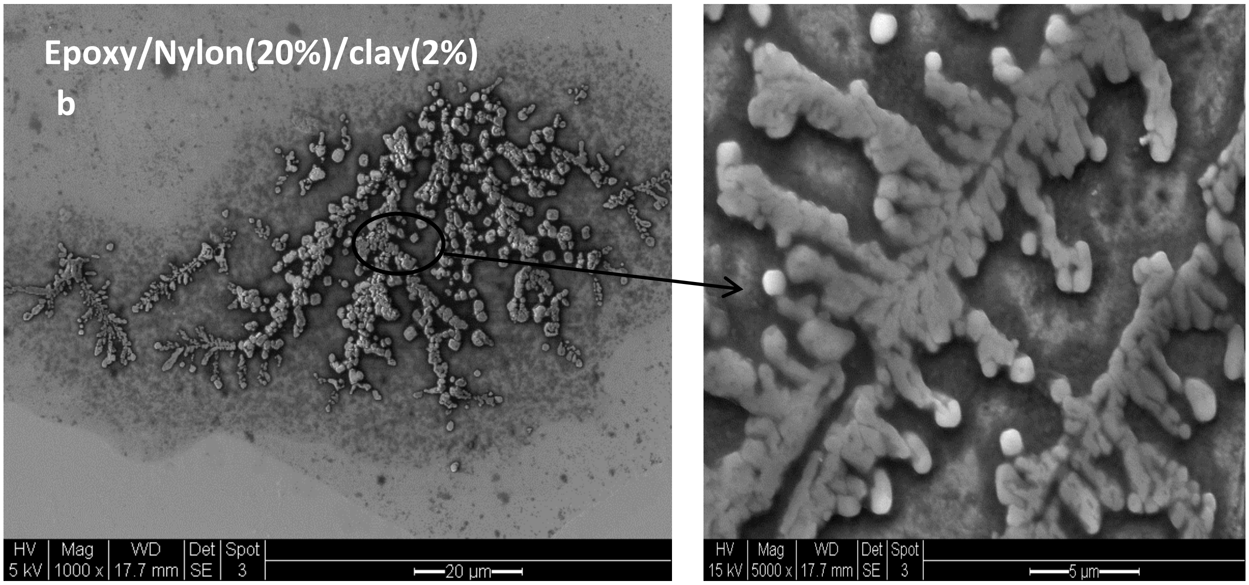

Figure 5 – SEM images of surface of coating (a) epoxy/nylon(10%)/clay(0.1%) (b) epoxy/nylon(20%)/clay(2%)

Progress in Organic Coatings (under preparation)

Novel Semi-Crystalline Hybrid Coatings: Corrosion Inhibition and Morphological Analysis of Clay/Nylon-6-Epoxy Nanocomposites

Aniket Vyas and Jude O. Iroh, Material Science and Engineering Program, College of Engineering & Applied Science, University of Cincinnati, Cincinnati, OH 45221-0012, USA

1. Introduction

With the development of polymers, a special attention has been paid to application of organic coatings to protect metal bodies from corrosion [1-5]. Various polymers have been investigated for their corrosion protection properties such as alkyd based coatings [6, 7], polyimide/polyaniline composite coatings [8], polyurethane films [9] and epoxy based coatings [2-4]. Epoxy resins are one of the most widely used polymers for corrosion protection. They are extensively used as coatings and adhesives in automotive, construction, and aerospace industries, due to their excellent thermal and mechanical properties, such as high stiffness, high strength, chemical resistance and dimensional stability with excellent adhesion to a variety of surfaces [10]. In spite of outstanding properties, there are few drawbacks associated with epoxy, such as inherit brittleness, low toughness, presence of micro-cracks and poor fracture resistance. To overcome these drawbacks, incorporation of second phase, such as rubber or thermoplastic polymers, has often been successful to enhance the toughness and lower the brittleness of epoxy. The epoxy–thermoplastic composites have been studied since the 1980s with considerable progress in property improvement [11-13].

Many engineering thermoplastics such as polysulfone [14], poly(ether-imides) [15], poly(ϵ-caprolactone) [16] and polyamides [13, 17] have been studied as alternate modifiers. These thermoplastics are found to be promising since they do not decrease the inherent properties of the epoxy matrix [11, 12]. Nylon-6 is a class of polyamide which has been known to toughen epoxy not only by physical mixing but also by chemical interactions [17, 18]. Most of the previous research in the area of epoxy-nylon blends have been focused on mechanical properties [19], miscibility and curing [18] and morphological evaluation [13] but very little attention has been paid to the corrosion resistance aspect of such thermoplastic reinforced epoxy based composite coating.

It has been reported that organic coatings increases the corrosion resistance of aluminum alloys, but the corrosion resistance decreases with increase in exposure time [1-3]. This is mainly due to hydrolytic degradation of coating exposed to corrosive electrolyte for prolonged period of time. Hydrolytic degradation increases pores and crevices in coatings, through which electrolyte can permeate leading to formation of corrosion product. Such products decrease the adhesion of coating to metal at the interface [4, 6, 7]. In the present case, epoxy and nylon-6 are used as two components of coating system, but both materials are known to absorb moisture [20, 21]. This can further attract hydrolytic degradation of coating.

In order to improve anticorrosion performance of coating, various nanoparticles such as nano-SiO_2 [22], nano-TiO_2 [23], nano-Al_2O_3 [24], nano-ZnO [4] and nano-clay [1-3] have been incorporated in coatings. Nano-clay has been reported to decrease the moisture uptake by nylon-6 significantly [25, 26]. The rate of water absorption was reported to be lowered by 40% in clay/nylon-6 hybrid compared to neat nylon-6 by Okada et al. [26]. Moreover, a co-relation between water absorption and crystallinity of polymer has been demonstrated by Lasoski et al. [27], where water absorption decrease almost linearly with increase in % crystallinity of unoriented polymer films. Becker et al. [28] reported that in case of clay/epoxy hybrid system, clay has no effect on water diffusion, but equilibrium water uptake was reduced in clay/epoxy systems compared to pristine epoxy.

Following the above stated facts to improve properties of epoxy based composite coatings, investigation of a novel three component systems consisting of clay, nylon-6 and epoxy are presented in this article. Initially, nylon-6 was synthesized via air terminated anionic living polymerization in solution. The resultant nylon-6 suspension was blended with epoxy and nylon-6 crystals were allowed to grow inside the epoxy matrix during curing process, in order to plasticize and improve the toughness. Then the nylon-6 was modified by clay during synthesis process. Clay is known to have a significant effect on the crystallinity and morphology of nylon-6 [29]. The clay modified nylon-6 was then incorporated in epoxy resin matrix. The effect of increasing clay concentration on corrosion inhibition, thermal properties and morphology of composite system at different ratio of epoxy: nylon-6 is presented in this paper.

2. Experimental

2.1 Materials

ϵ-caprolactam, dry sodiam hydride (95% purity), N-acetylcaprolactam and N-methylpyrollidone (NMP) solvent (99% purity) were purchased from Sigma-Aldrich, USA for solution polymerization ε-caprolactam. Cloisite 15A clay was purchased from southern clay. Polyfunctional Water Dispersible DGEBA based Epoxy resin (EPIREZ 5522-WY-55) was purchased from Hexion Chemicals, Houston, USA. The Al-2024-T3 was purchased from Q-labs, Cleveland, Ohio. All the reagents mentioned above are of analytical grade.

2.2 Synthesis of in-situ clay/nylon-6 composite

Initially, ε-caprolactam was added to NMP till it dissolved completely, followed by addition of 15A clay. Nitrogen supply was turned on and temperature was increased gradually from room temperature. NaH (catalyst) was then added to the solution and stirred till it dissolved completely at 50 ^{o}C. This process of dissolution was accompanied by a series of color changes from colorless to dark blue which eventually turned black on complete dissolution. Temperature was then raised to 160^{o}C and N-acetyl Caprolactam (initiator) was added to the solution. The color of solution gradually changed from black to blue. After addition of initiator, solution was stirred for 30-45 minutes. The Nitrogen supply was then turned off and the black solution gently turned into a dark orange yellow viscous solution indicating the completion of reaction terminated by air. Composite systems of nylon-6 modified by different loading of clay were synthesized. Clay loading was varied as 0.5%, 1%, 5% and 10% by weight.

2.3 Preparation of Clay/Nylon 6-Epoxy blends

Epoxy was taken in a glass jar, suspension of nylon-6 modified by 0.5, 1, 5 and 10 weight % of 15A clay was added to it, maintaining the nylon-6/epoxy ratio by weight at 10/90 and 20/80. NMP was further added to dilute the solution to reduce the viscosity for ease of processing in order to have defect free films and coatings. The mixture was then stirred using mechanical stirrer for 1 hour at room temperature to obtain homogeneous solution and then ultra-sonicated for 5 minutes. Various compositions that were used in this study are listed in table 1.

2.4 Sample Preparation

Composite coatings were formed via solution casting method. 2ml of blend was dropped on Al alloy panel and the coating was cured in a stepwise manner, heating initially at 70^{O}C for 3 hours, 100 ^{O}C for 2 hours, 120 ^{O}C for 2 hours and 150 ^{O}C for 2 hours. The resultant coating thickness was around 45-50 µm.

8 ml of blend was taken and casted in 1.5'' × 1.5'' × ¼'' Teflon molds to form free standing films. The films were cured in vacuum oven in a stepwise manner, heating initially at 50 ^{O} C for 13 hours, 100 ^{O} C for 4 hours, 120 ^{O} C for 2 hours and finally 150 ^{O} C for 2 hours and were then cut with a sharp razor blade to obtain rectangular films.

The free standing films were quenched in liquid nitrogen and broken to see the cross-section of fractured surface under Scanning Electron Microscopy.

2.5 Characterization

The corrosion protection properties were evaluated on the coated aluminum alloy (working electrode) in the testing solution of 3.5 weight% NaCl by using a cylindrical glass cells constantly clamped to the sample with an exposed area of 2.8 cm^{2}. Graphite rod was used as counter electrode. Direct current polarization curves were generated by applying a potential of 250 mV (-250 mV to + 250 mV) in both positive and negative direction from the open circuit potential against the saturated calomel electrode, SCE, at a scan rate of 2mV/s and the resultant current was measured. For Electrochemical Impedance Spectroscopy (EIS), the potential was applied in a range of +/- 10 mV from open circuit potential (OCP) against the saturated calomel electrode (SCE). OCP was measured and allowed enough time to stabilize before results were taken. The frequency was varied from 10^{6} to 10^{-2} Hz. Reference 3000 potentiostat from Gamry equipments, equipped with Gamry framework and echem analyst, was used to analyze the results from EIS.

Nicolet 6700 FT-IR instrument, equipped with a smart orbit ATR accessory with diamond crystal, was used to determine the chemical composition of the samples. ATR was performed over a wave number range between 4000 cm^{-1} and 400 cm^{-1}.

Differential scanning Calorimeter (DSC) was used to measure thermal properties of Nylon 6 and modified epoxy. DSC was performed at the heating rate of 5^{O}C/min using DSC6200, Seiko

Instruments Inc. The samples were analyzed after complete melting and recrystallization to remove the thermal history.

Scanning Electron Microscope was a Philips model FEI XL 30 ESEM-FEG. The software used to capture images was Scandium. Aluminum stubs with carbon tape were used as sample holders, and the sample was coated with Au-Pd before subjecting to SEM.

3. Results and Discussion

3.1 Direct Current Polarization

Potentiodynamic results for nylon-6/epoxy coatings with and without clay at a weight ratio 10/90 and 20/80, after 1 day and 2 months of exposure are shown in Figure 1 and 2 respectively. Different compositions including neat epoxy, nylon-6/epoxy and nylon-6/epoxy containing clay with varied concentration were compared for corrosion performance. The presence of clay in nylon-6/epoxy coatings resulted in a significant reduction in the corrosion current. The corrosion current density decreased from 10^{-6} A/cm^{-2} to 10^{-10} A/cm^{-2} as the clay concentration was increased. The values of corrosion current and corrosion potential for all the systems are listed in table 2 and 3.

Figure 1(a) show curves after 1 day of exposure. The neat epoxy and nylon-6/epoxy (10/90) showed corrosion current (I_{corr}) almost in the same range of around 10^{-6} - 10^{-7} A/cm^{-2} but with increase in clay I_{corr} decreased by two orders of magnitude and showed a minimum of 10^{-9} A/cm^{-2}. These coatings were kept exposed for two months and potentiodynamic curves obtained after two months are shown in Figure 1(b). The minimum corrosion current was shown by composite coating containing 1 weight% clay at around 10^{-10} A/cm^{-2}. Moreover, an increase in corrosion potential from -1.2 V to -0.9 V was also observed. Beemat and Iroh [3] have reported that the decrease in corrosion current density and increase in corrosion potential simultaneously, indicates that protection from corrosion by coatings is provided by both diffusion-controlled and activation-controlled mechanism. After 2 months of exposure, Al alloy substrate coated with neat epoxy and nylon-6/epoxy containing 0.05 wt. % and 0.5 wt. % clay began to show bending in anodic arms suggesting passivation behavior, which is shown by aluminum alloy due to formation of oxide layer.

Figure 2a shows DCP curves for composite systems with nylon-6/epoxy weight ratio of 20/80 after 1 day of exposure. A similar trend was observed where nylon-6/epoxy without clay showed an I_{corr} around 10^{-6} A/cm^{-2} which decreased by three order of magnitude to 10^{-9} A/cm^{-2} with incorporation for clay. After exposure for two months, obtained DCP curves are shown in Figure 2(b). A minimum I_{corr} of around 2.8×10^{-9} was observed for coating containing 0.2% clay. It was observed that for all the composite coatings, E_{corr} increased with exposure time, but for the neat epoxy coatings, it decreased with time. This suggests that neat epoxy coating failed earlier and the corrosion protection was controlled by passivation, where thin oxide layer began to form as a protective coating indicated by bending in anodic arm. The effect of clay concentration on the corrosion current of coatings is shown in Figure 3. At the nylon-6/epoxy ratio of 10/90, the I_{corr} decresed by almost 5 orders of magnitude upto clay weight concentration of 0.2%, which remained almost in the similar range on further increase (Figure 3(a)), but the coating containing 1 weight% clay showed decrease in corrosion current after 2 months of exposure. For nylon-6/epoxy weight ratio of 20/80, I_{corr} decreased significantly upto 0.2 clay weight%, and then slightly increased on further increase of clay as shown in Figure 3(b). The trend in corrosion current with variation in clay concentration remained same after exposure of two months, but the magnitude of current increased, suggesting decreasing anti-corrosion performance. These coatings were further evaluated by electrochemical impedance spectroscopy as discussed in next section.

3.2 Electrochemical Impedance Spectroscopy

Electrochemical Impedance Spectroscopy technique has been widely used recently to evaluate the anticorrosion performance of coatings [4, 8, 9]. The impedance value at the lowest frequency gives information about the coating resistance. Higher is the impedance; better is protection of substrate by coating.

Figure 4 and 5 are the Bode plots for neat epoxy, nylon-6/epoxy with and without clay, coated on aluminum alloy substrate exposed to 3.5% salt solution. Figure 4(a) represent the Bode plots for nylon-6/epoxy coatings at a weight ratio of 10/90 containing varied concentration of clay. The impedance value for neat epoxy at 0.01 Hz was around 4×10^{4} Ω after 1 day of exposure, while nylon-6/epoxy coatings showed an impedance value increased by 5 orders of magnitude around 1×10^{10} Ω. On increasing clay concentration, initially impedance decreased but at highest clay concentration of 1 weight % in the system, a higher value of impedance was observed. The Bode plots of coatings after exposure for two months are shown in Figure 4(b). The impedance for nylon-6/epoxy coating without clay dropped to $1\times10^{8}\ \Omega$, on the other hand, impedance value was substantially retained at $1\times10^{9}\ \Omega$ by coating containing 1 weight% clay. The impedance value as a function of exposure time is shown in Figure 5(a). It was observed that impedance value is retained by clay/nylon-6-epoxy coatings and drops slowly with exposure time, but at clay concentration of 1 weight %, the impedance value was highest at all times, while for coating without clay, impedance begin to decrease after 15 days of exposure.

Figure 5(a) represents Bode plots for coatings with nylon-6/epoxy weight ratio of 20/80. On the first day of exposure, nylon-6/clay coating (20%) without clay showed the highest value of impedance then all other coatings, but on second day impedance value decreased significantly as shown in impedance vs. exposure time plot in Figure 6(b). After 2 months of exposure, coatings containing 0.2% clay showed a maximum impedance of $1\times10^{8}\ \Omega$, where nylon-6/epoxy dropped to $8\times10^{5}\ \Omega$ and neat epoxy was around $1\times10^{4}\ \Omega$ as shown in Figure 5(b).

Figure 6 and 7 are the derivative plots for impedance as a function of exposure time and concentration of clay respectively. It can be seen in Figure 6(a) that coating containing 1 weight% of clay retained a maximum impedance value over a period of 2 months (nylon-6/epoxy = 10/90), while as the ratio was changed to 80/20, coatings containing 0.2 weight% clay showed the maximum impedance value. On analysis of impedance as a function of clay concentration, it was observed that at nylon-6/epoxy ratio of 10/90, the impedance first decreased upto 0.5 weight % clay but then increased and reached a maximum at 1 weight% as shown in Figure 7(a). On the other hand at ratio of 20/80 (Figure 7(b)), the coating without clay and with 2 weight% clay showed a higher value of impedance initially, but with the progress in exposure time, these coatings began to degrade an a maximum value was showed by coatings containing 0.2 weight % clay.

These results suggested that in a three component system, nylon-6/epoxy ratio, in other words, crystalline to amorphous part ratio has also a significant deciding factor for corrosion protection apart from clay concentration. At a ratio of 10/90, coating containing 1% clay showed the best performance ($Z=1\times10^{9}\ \Omega^{\text{and}}\ I_{\text{Corr}\,=}\ 1\times10^{-10}$ A/cm^{-2}, after 2 months of exposure), while at the ratio of 20/90, coatings containing 0.2% clay showed better corrosion performance ($Z=1\times10^{8}$

Ω and $I_{Corr} = 7\times10^{-9}$ A/cm^{-2}, after 2 months of exposure). The effect of clay on crystallinity is discussed in later section.

3.3 Functional Group Analysis by FTIR

Infra-red spectroscopy is a widely used technique to monitor the effect of corrosion on the coating at chemical level [3, 4]. Figure 8 a and b shows the FTIR spectra of neat epoxy, nylon-6/epoxy and clay/nylon-6/epoxy coating containing 10 weight% of nylon-6 and 1 weight% of clay, before and after exposure to a 3.5 weight% NaCl solution. It can be seen in figure that the coatings containing clay showed a significant reduction in the intensity for spectra, but for coatings not containing clay, the reduction in intensity was very minimal. The organoclay aliphatic group shows peak at 2925 and 2852 cm^{-1} and the silicon oxide shows a peak 1054 and 470 cm^{-1}. The peaks at 2925, 2852 and 1054 cm^{-1} were masked by epoxy but a prominent peak at 470 cm^{-1} was clearly observed. The intensity of the IR absorption peak at 465cm^{-1} was found to be increasing with increasing clay concentration, moreover after exposure intensity of clay peak at 465 relatively increased while overall intensity of the coatings decreased.

The major peaks associated with clay are observed at the wavenumber of 470cm^{-1} due to the Si-O-Si deformation [30] and Si-O out of plane vibration leads to a peak at 1118 and 980 cm^{-1} [31]. The neat epoxy sample, nylone-6 loaded epoxy and epoxy resin filled with clay modified nylon-6 were analyzed by FTIR. For pristine epoxy and mylon-6 filled epoxy, no peak was observed at 470, but as clay modified polyamide-6 was introduced to the system, a new peak at 470 was clearly observed. Figure 9(a) represents the FTIR for system focused at 470 cm^{-1} due to Si-O-Si deformation. Since, the system contained epoxy and polyamide, the peak at 1118 could not be clearly observed due to overlap. But with increase in clay loading at constant epoxy: nylon-6 ratio, a necking was observed at 980 which were consistent with increase in clay loading. Figure 9(b) represents the FTIR spectrum focused at shoulder peak at 980 cm^{-1} due to Si-O out of plane vibration.

The hydroxyl peak at 3361 cm^{-1} was examined for increment in absorption intensity for nylon-6/epoxy coatings with and without clay loading. The % increase in intensity before and after exposure to salt solution is shown in figure 10(a) for nylon-6/epoxy coatings and 10(a and b) for clay filled nylon-6/epoxy coatings at a weight ratio of 10/90 and 20/80 respectively. For epoxy coatings filled with nylon-6, an increase in the hydroxyl peak was observed upto 350%, suggesting high water absorption. But as clay was introduced, the % increase in peak related to water absorption decreased significantly. At a weight nylon-6/epoxy weight ratio of 10/90, the % increase in peak intensity decreased from around 350% without clay to almost 0% at clay loading of 0.1 weight %, which then increased to around 45% at clay loading of 1% (Figure 10b). A similar trend was observed for nylon-6/epoxy weight ratio of 20/80, where % increase in peak intensity decreased from 240% to 10% at clay concentration of 0.2 weight% and then increased upto 50% at clay concentration of 2 weight % (Figure 10c). This suggests that although nylon-6 and epoxy both absorbs moisture and possesses high water absorption properties, but when nano clay was incorporated in these coatings, the water uptake reduced dramatically.

3.4 Effect of Clay on Melting Behavior

The effect of clay concentration on the melting behavior of nylon-6 is shown in Figure 11(a). The melting point of neat nylon-6 was around 209 °C. When nylon-6 was synthesized in presence of 0.5 wt.% clay, the melting point increased to 217.6 °C. On further increasing clay to 1wt.%, the melting temperature decreased and showed multiple peaks at 200 °C and 210 °C. The multiple melting peaks indicate the presence of different polymorphs (α and γ type crystals) in the same sample, Melting peak was not observed for clay loading at 5 and 10 weight%. Fornes and Paul [32] has reported that crystallintiy of nylon-6 increases at lower loading whereas at higher loading polymer crystal growth retards. A similar phenomenon was observed in the present case for clay/nylon-6 composite prepared by in-situ solution polymerization. The melting point is dependent upon molecular weight and chain length of polymer, higher molecular weight leads to increase in melting point [33]. Hence it can be deduced that low amount of clay facilitated the polymerization and hence crystallization, while increasing clay concentration acted as hindrance to formation of polymer chains and reduced the crystallinity.

The effect of clay on melting of nylon-6 in epoxy resin matrix is shown in Figure 11(b), where epoxy to nylon-6 ratio is kept almost constant at 80:20 by weight. The sample without clay showed multiple melting points but a major peak was observed at 206 °C. At 0.5 wt.% clay loading, the melting point increased to around 210 °C, while at 1 wt.% clay loading, it decreased to 204 ^{o}C. The melting trend of nylon-6 in epoxy matrix followed the same fashion as in absence of epoxy.

Hence it can be concluded for nylon-6 modified with clay, that at very low level of clay (0.5 wt.%) , crystallinty of nylon-6 increases. On further increasing clay to 1wt. %, crystallinty reduces. On further increase in clay to 5 and 10 wt. %, the crystallinty is nylon-6 reduces drastically and matrix is dominated mostly by clay particles.

3.5 Morphology

In order to understand the effect of morphology on the corrosion inhibition properties of three component system, the morphology was observed at surface of coating and at the bulk by observing the surface of fractured composite film.

The neat epoxy coating is accompanied with sharp glassy cracks. We have reported a surface morphology of neat epoxy before with very sharp cracks in amorphous matrix, which were developed during the curing of epoxy coating. [34]. The fractured surface of neat epoxy film without nylon-6/clay is shown in Figure 17a, which is completely amorphous with no other moiety. As the nylon-6/epoxy coating was applied to substrate and heated, the curing of epoxy resin and crystallization of nylon-6 took place simultaneously. As a result, the cracks formed during curing were filled by nylon-6 crystals due to radial growth of crystals. This lead to increase in the durability and corrosion inhibition properties of epoxy as corrosive electrolyte could not percolate easily through the cracks of epoxy. The SEM micrograph of epoxy/nylon-6 coating surface is shown in Figure 12a, where crystals grown in cracks can be seen clearly. The morphology at the fractured surface is shown in Figure 13b, where numerous crystals grown inside the amorphous matrix were observed. It is hypothesized that, in nylon-6/epoxy composites without clay, epoxy surface can act as a heterogeneous surface which can be utilized by nylon-6 crystals as a nucleating site. Crystallization under such condition will be much more rapid due to reduction in interfacial energy. Moreover, when sample is cooled to crystallization temperature, the heterogeneous surface is usually cooler which will further enhance the crystallization process [35].

When clay was added as 0.05 weight % (nylon-6 modified by 0.5 weight% clay), It was observed that most nylon-6 crystals grew inside the matrix (Figure 13c) impinged into each other, while the part of matrix where crystal were not seen, cracks were observed. At the surface, crystals tending to protrude out of the epoxy matrix were observed, which may act as point defect as cracks were observed around those crystals (Figure 12b). It is easier for salt solution to pass through such cracks and pores in order to reach metallic substrate causing hydrolytic degradation and forming corrosion products which may eventually lead to delamination of coating as seen in optical micrograph. This phenomenon can be explained on basis of clay particles acting as nucleating agent. Unlike the composite system without clay, possibly nylon crystals preferred to grow upon clay particles instead of epoxy template which resulted in a different kind of morphology with various cracks.

As the clay was increased to 0.1% (nylon-6 modified by 1weight% of clay), a striking symmetrical morphology was observed at the surface as well is in bulk. Figure 12c is the surface morphology where nylon-6 crystals along with clay particles were organized in a symmetrical dendritic fashion with few small cracks. In the bulk of film (Figure 13d), a similar morphology was observed where crystals grew in form of pine leaf leading to a compact morphology, which possibly lead to better anti-corrosion properties. On further increasing clay to 0.5 weight%, crystallinity was reduced significantly and clay particles were present in agglomerated form, which lead to creation of cracks on the surface as shown in Figure 12d. A similar observation was made in the bulk were large agglomerates of clay, encapsulated by epoxy were observed with large cracks along the agglomerate boundaries (Figure 13e), due to which this sample showed relatively inferior anti-corrosion properties. At clay loading of 1 weight % in the system, no sharp cracks were observed along with uniform distribution of clay particle in the matrix indicated by small dots in the surface as shown in Figure 12e. Moreover, clay particles were organized in a symmetrical order possibly due to crystallization of short chains of nylon-6. Figure 13f represents the morphology in the bulk of film where distribution of large amount of clay particles is clearly visible along with few short crystals in form of a network, which is a possible reason for improved barrier properties of this coating.

In summary, at very low clay loading (0.5 weight % with respect to nylon-6), large crystals were produced leading to pores along the interface of nylon-6 crystals and epoxy chains. Moreover, large crystals acted as point defects leading to cracks in coatings which lead to poor corrosion inhibition. On further increasing clay (1 weight% with respect to nylon-6), crystals reduced in size and formed a symmetrical network of crystals and clay leading to improved barrier properties. On increasing clay further (5 weight% with respect to nylon-6), crystallinty of nylon-6 reduced and reinforcement was mostly by agglomerated clay particles. The agglomerations lead to increase in cracks and crevices which decreased the anti-corrosion properties. At higher concentration of clay, large amount of clay particles along with small network of crystals was observed in the epoxy matrix.

4. Conclusion

A novel semi-crystalline epoxy based coating consisting of organoclay modified nylon-6 have been successfully synthesized and applied onto aluminum alloy coupons. These coatings showed improved corrosion protection then neat epoxy indicated by lower corrosion current and higher impedance value. The coatings containing nylon-6 modified with 1 weight% and 10 weight% of nylon-6 showed a remarkable retention of corrosion resistance after 2 months of exposure of coated aluminum alloy substrate. Lower loading of clay increased the crystallinty of nylon-6, while at higher loading crystallinty decreased as indicated by melting behavior. The nylon-6 crystals were found to grow in the cracks and crevices of epoxy matrix as observed under SEM which increased the plasticization of epoxy, while presence of clay particles enhanced the barrier properties and reduced moisture uptake of coatings which was confirmed by FTIR.

5. Acknowledgement

This study was funded by grants from office of naval research (ONR) # N00014-09-1-0980 and National Science Foundation (NSF) # CMMI-0758656. We would also like to thank Soumyarwit Manna at Advanced Material Characterization Center (AMCC), university of Cincinnati who assisted in capturing the SEM images.

6. References

[1] J. Singh-Beemat, J.O. Iroh, Effect of clay on the corrosion inhibition and dynamic mechanical properties of epoxy ester–polyurea–polysiloxane hybrid coatings, Polymer Engineering & Science, (2012) n/a-n/a.

[2] J. Singh-Beemat, J.O. Iroh, The effect of morphology on the corrosion inhibition and mechanical properties of hybrid polymer coatings, Journal of Applied Polymer Science, 128 (2013) 1616-1624.

[3] J. Singh-Beemat, J.O. Iroh, Characterization of corrosion resistant clay/epoxy ester composite coatings and thin films, Progress in Organic Coatings, 74 (2012) 173-180.

[4] B. Ramezanzadeh, M.M. Attar, M. Farzam, A study on the anticorrosion performance of the epoxy–polyamide nanocomposites containing ZnO nanoparticles, Progress in Organic Coatings, 72 (2011) 410-422.

[5] T.T.X. Hang, T.A. Truc, M.-G. Olivier, C. Vandermiers, N. Guérit, N. Pébère, Corrosion protection mechanisms of carbon steel by an epoxy resin containing indole-3 butyric acid modified clay, Progress in Organic Coatings, 69 (2010) 410-416.

[6] S.K. Dhoke, A.S. Khanna, T.J.M. Sinha, “Effect of nano-ZnO particles on the corrosion behavior of alkyd-based waterborne coatings”, Progress in Organic Coatings, 64 (2009) 371-382.

[7] S.K. Dhoke, A.S. Khanna, Effect of nano-Fe2O3 particles on the corrosion behavior of alkyd based waterborne coatings, Corrosion Science, 51 (2009) 6-20.

[8] L. Liangcai, W. Ming, S. Huoming, L. Haiying, Q. Qingdong, D. Yuanlong, Preparation and EIS studies on polyimide/polyaniline blend film for corrosion protection, Polymers for Advanced Technologies, 12 (2001) 720-723.

[9] Y. González-García, S. González, R.M. Souto, Electrochemical and structural properties of a polyurethane coating on steel substrates for corrosion protection, Corrosion Science, 49 (2007) 3514-3526.

[10] P.F. Bruins, P.I.o. Brooklyn, Epoxy resin technology, Interscience Publishers, 1968.

[11] J.H. Hodgkin, G.P. Simon, R.J. Varley, Thermoplastic toughening of epoxy resins: a critical review, Polymers for Advanced Technologies, 9 (1998) 3-10.

[12] L. Barone, S. Carciotto, G. Cicala, A. Recca, Thermomechanical properties of epoxy/poly(ε-caprolactone) blends, Polymer Engineering & Science, 46 (2006) 1576-1582.

[13] S. Kim, J. Kim, S.H. Lim, W.H. Jo, C.R. Choe, Effects of mixing temperatures on the morphology and toughness of epoxy/polyamide blends, Journal of Applied Polymer Science, 72 (1999) 1055-1063.

[14] P.A. Oyanguren, M.J. Galante, K. Andromaque, P.M. Frontini, R.J.J. Williams, Development of bicontinuous morphologies in polysulfone–epoxy blends, Polymer, 40 (1999) 5249-5255.

[15] M. Wang, Y. Yu, X. Wu, S. Li, Polymerization induced phase separation in poly(ether imide)-modified epoxy resin cured with imidazole, Polymer, 45 (2004) 1253-1259.

[16] J.-L. Chen, F.-C. Chang, Phase Separation Process in Poly(ε-caprolactone)−Epoxy Blends, Macromolecules, 32 (1999) 5348-5356.

[17] B.S. Gorton, Interaction of nylon polymers with epoxy resins in adhesive blends, Journal of Applied Polymer Science, 8 (1964) 1287-1295.

[18] Z. Zhong, Q. Guo, Miscibility and cure kinetics of nylon/epoxy resin reactive blends, Polymer, 39 (1998) 3451-3458.

[19] Y.-Y. Wang, S.-A. Chen, Polymer compatibility: Nylon-epoxy resin blends, Polymer Engineering & Science, 20 (1980) 823-829.

[20] B. De'Nève, M.E.R. Shanahan, Water absorption by an epoxy resin and its effect on the mechanical properties and infra-red spectra, Polymer, 34 (1993) 5099-5105.

[21] E. Laredo, M. Grimau, F. Sánchez, A. Bello, Water Absorption Effect on the Dynamic Properties of Nylon-6 by Dielectric Spectroscopy, Macromolecules, 36 (2003) 9840-9850.

[22] E.V. Skorb, D. Fix, D.V. Andreeva, H. Möhwald, D.G. Shchukin, Surface-Modified Mesoporous SiO2 Containers for Corrosion Protection, Advanced Functional Materials, 19 (2009) 2373-2379.

[23] G.X. Shen, Y.C. Chen, L. Lin, C.J. Lin, D. Scantlebury, Study on a hydrophobic nano-TiO2 coating and its properties for corrosion protection of metals, Electrochimica Acta, 50 (2005) 5083-5089.

[24] S. Zhou, L. Wu, Development of Nanotechnology-Based Organic Coatings, Composite Interfaces, 16 (2009) 281-292.

[25] S. Murase, A. Inoue, Y. Miyashita, N. Kimura, Y. Nishio, Structural characteristics and moisture sorption behavior of nylon-6/clay hybrid films, Journal of Polymer Science Part B: Polymer Physics, 40 (2002) 479-487.

[26] A. Okada, M. Kawasumi, A. Usuki, Y. Kojima, T. Kurauchi, O. Kamigaito, Nylon 6–Clay Hybrid, MRS Online Proceedings Library, 171 (1989) null-null.

[27] S.W. Lasoski, W.H. Cobbs, Moisture permeability of polymers. I. Role of crystallinity and orientation, Journal of Polymer Science, 36 (1959) 21-33.

[28] O. Becker, R.J. Varley, G.P. Simon, Thermal stability and water uptake of high performance epoxy layered silicate nanocomposites, European Polymer Journal, 40 (2004) 187-195.

[29] T.-M. Wu, C.-S. Liao, Polymorphism in nylon 6/clay nanocomposites, Macromolecular Chemistry and Physics, 201 (2000) 2820-2825.

[30] T.M. Theophanides, Infrared Spectroscopy - Materials Science, Engineering and Technology, InTech, 2012.

[31] A.U. Dogan, M. Dogan, M. Onal, Y. Sarikaya, A. Aburub, D.E. Wurster, baseline studies of the clay minerals society source clays: specific surface area by the brunauer emmett teller (bet) method, Clays and Clay Minerals, 54 (2006) 62-66.

[32] T.D. Fornes, D.R. Paul, Formation and properties of nylon 6 nanocomposites, Polímeros, 13 (2003) 212-217.

[33] P.C. Painter, M.M. Coleman, Fundamentals of Polymer Science: An Introductory Text, Second Edition, Taylor & Francis, 1998.

[34] J.i. Aniket Vyas, Morphology and Structure of Nylon-6 crystallized in Epoxy resin Matrix, Polymer Engineering & Science, (2013) DOI: 10.1002/pen.23616.

[35] H. Schonhorn, Heterogeneous Nucleation of Polymer Melts on High-Energy Surfaces. II. Effect of Substrate on Morphology and Wettability, Macromolecules, 1 (1968) 145-151.

List of Figures:

Figure 1 – Direct Current Polarization Curves for Nylon-6/Epoxy (10%) with variation in clay weight% after (a) 1 day of exposure (b) 2 months of exposure

Figure 2 – Direct Current Polarization Curves for Nylon-6/Epoxy (20%) with variation in clay weight% after (a) 1 day of exposure (b) 2 months of exposure

Figure 3 – Corrosion current as a function of clay weight% in nylon-6/epoxy composite coatings at a weight ratio of (a) 10/90 and (b) 20/80

List of Tables

Table 3 - Parameters obtained from direct current polarization for nylon-6/epoxy (20/80)

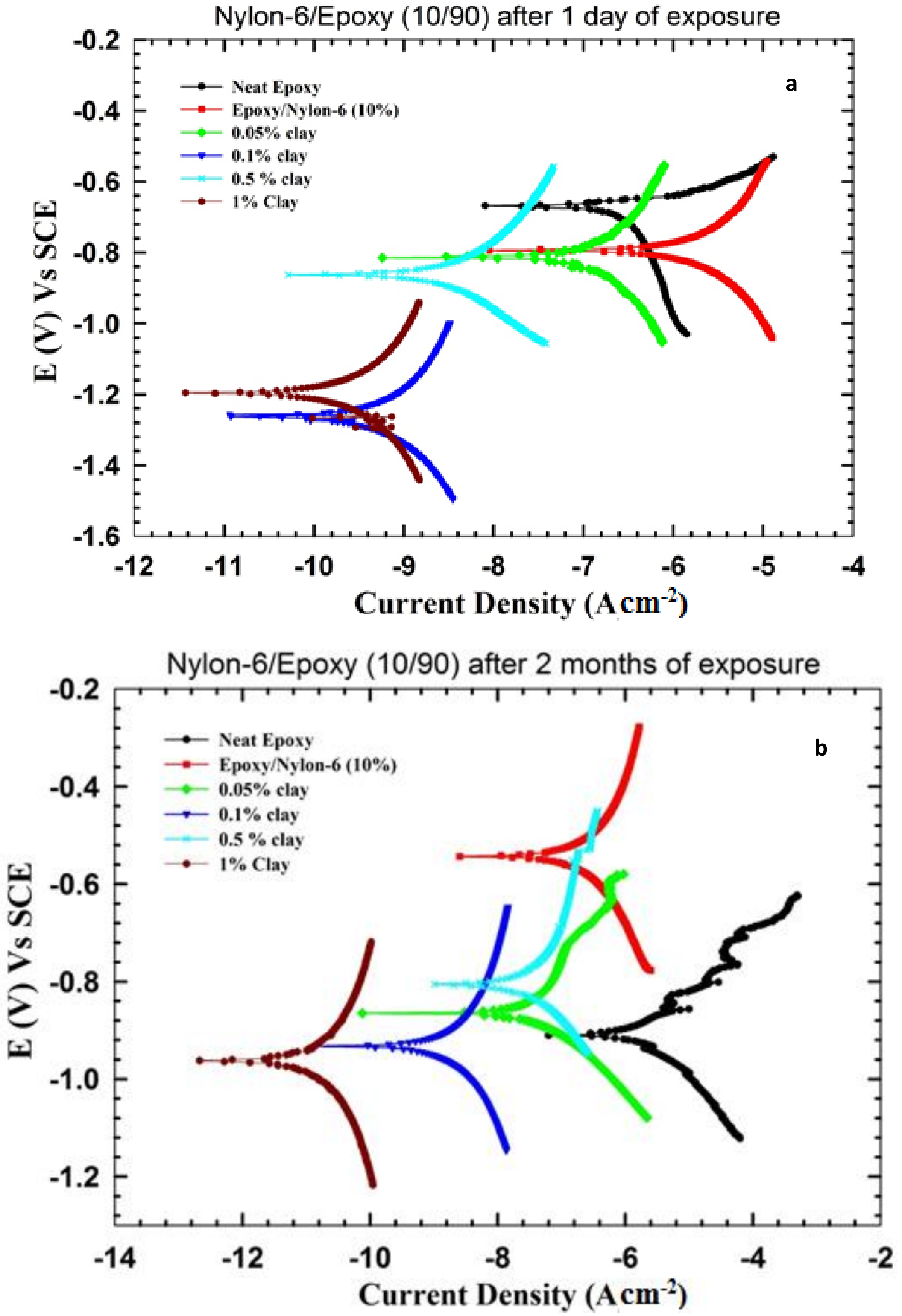

Figure 1 – Direct Current Polarization Curves for Nylon-6/Epoxy (10%) with variation in clay weight% after (a) 1 day of exposure (b) 2 months of exposure

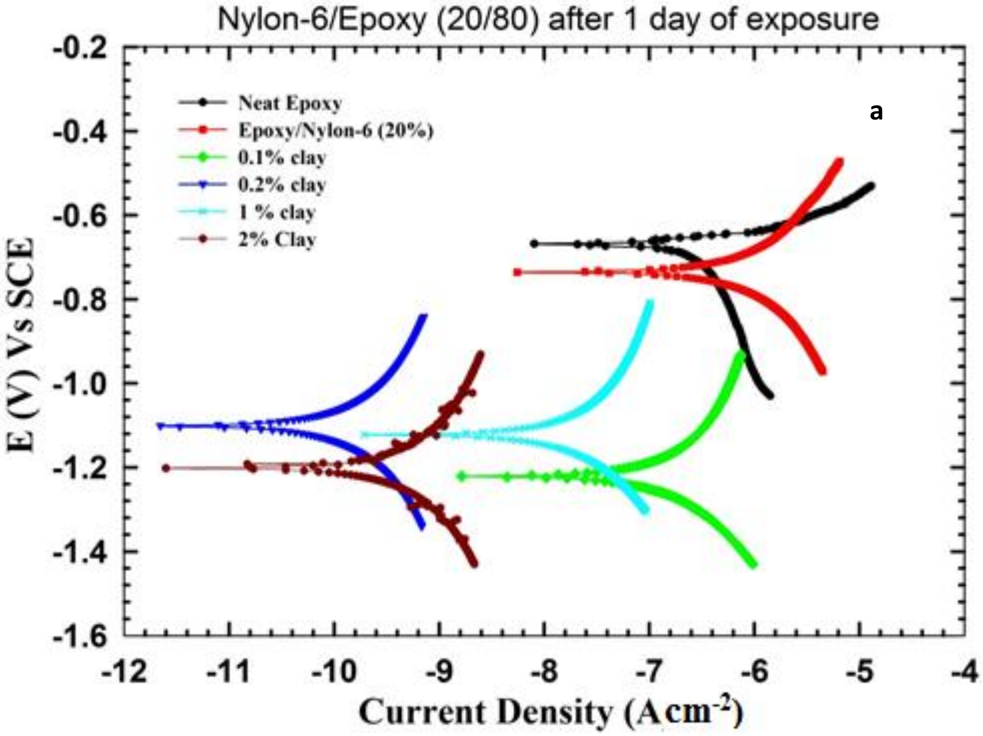

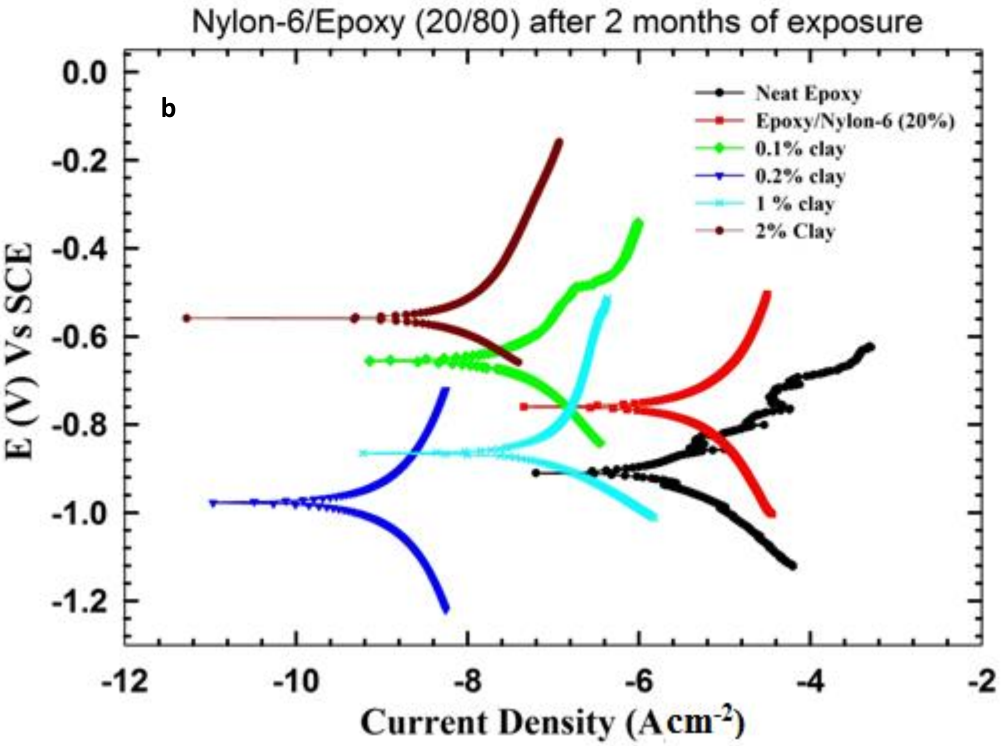

Figure 2 – Direct Current Polarization Curves for Nylon-6/Epoxy (20%) with variation in clay weight% after (a) 1 day of exposure (b) 2 months of exposure

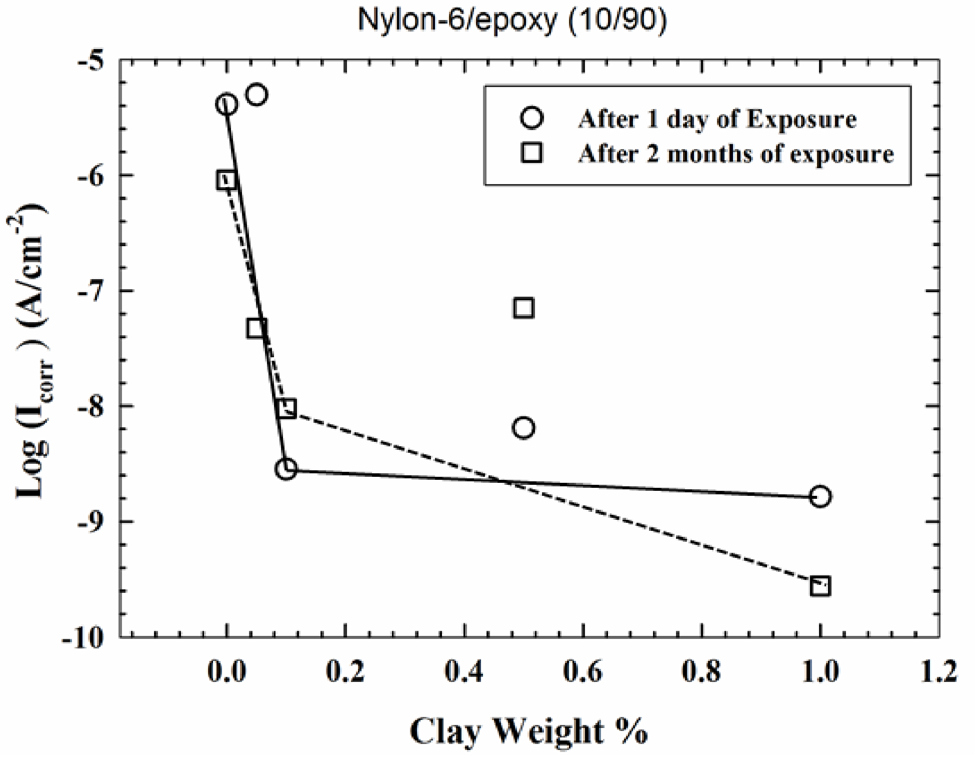

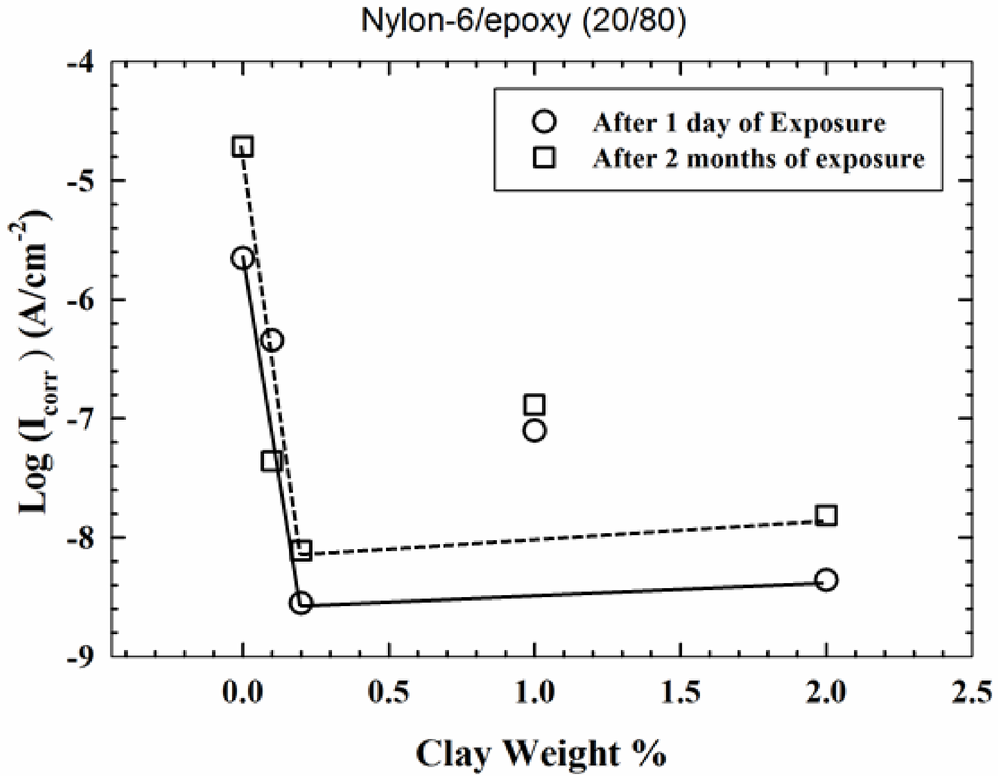

Figure 3 – Corrosion current as a function of clay weight% in nylon-6/epoxy composite coatings at a weight ratio of (a) 10/90 and (b) 20/80

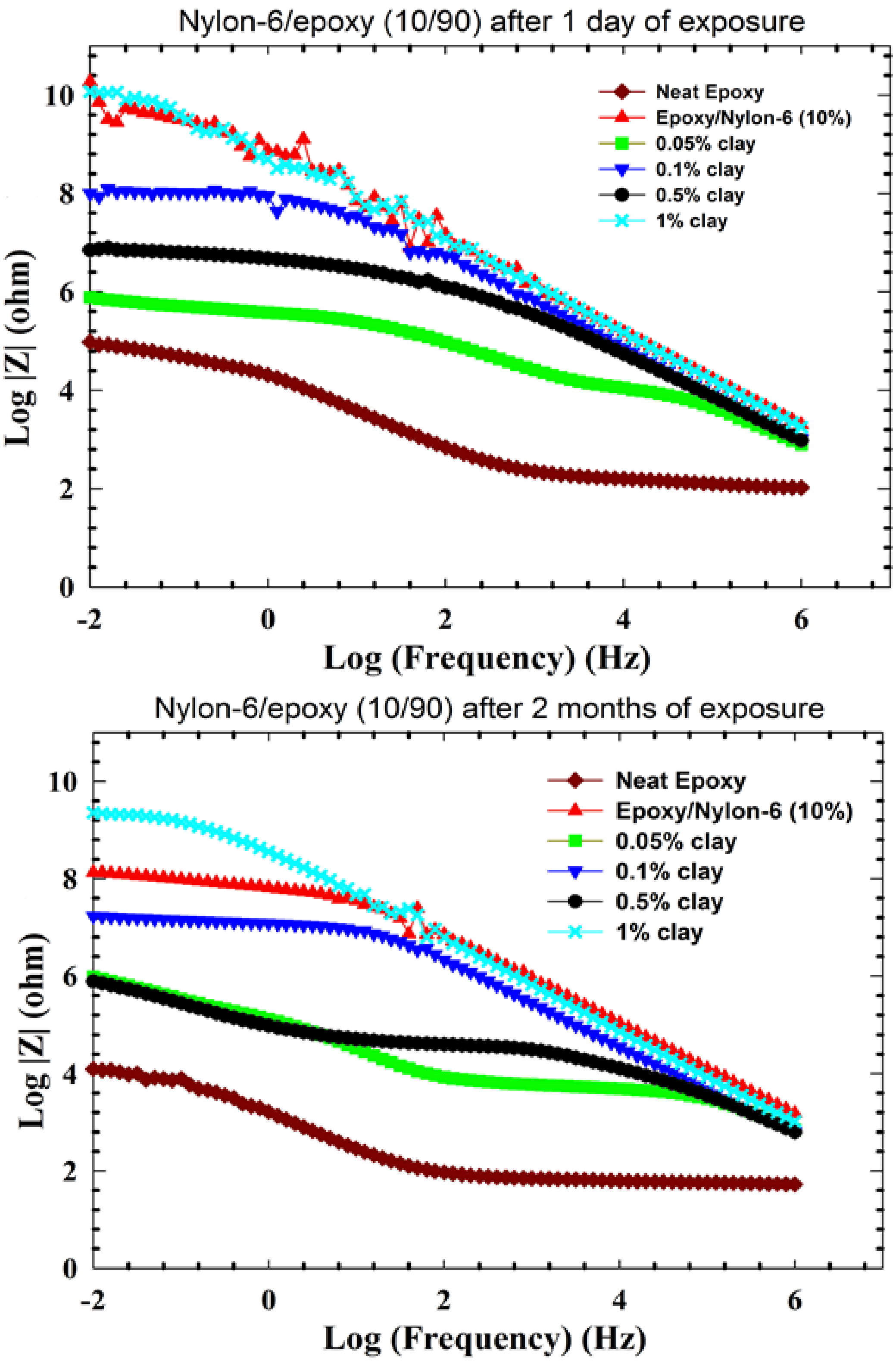

Figure 4 - Bode Plots for clay modified nylon-6 filled epoxy coatings after exposure to 3.5% salt solution for 2 months at epoxy: nylon-6 ratio of 90:10 (a) after 1 day of exposure (b) after 2 months of exposure

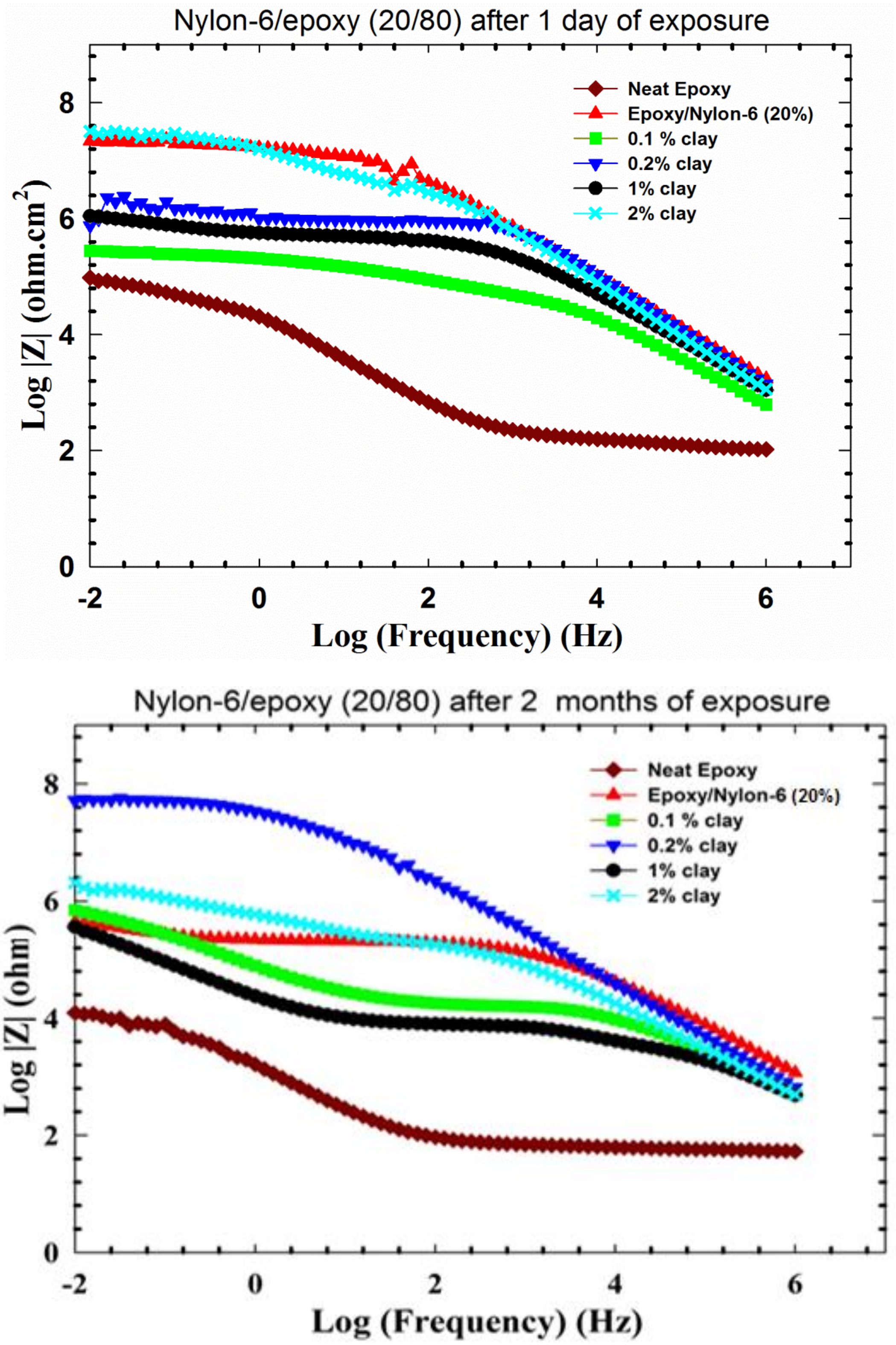

Figure 5 – Bode Plots for clay modified nylon-6 filled epoxy coatings after exposure to 3.5% salt solution for 2 months at epoxy: nylon-6 ratio of 80:20 (a) after 1 day of exposure (b) after 2 months of exposure

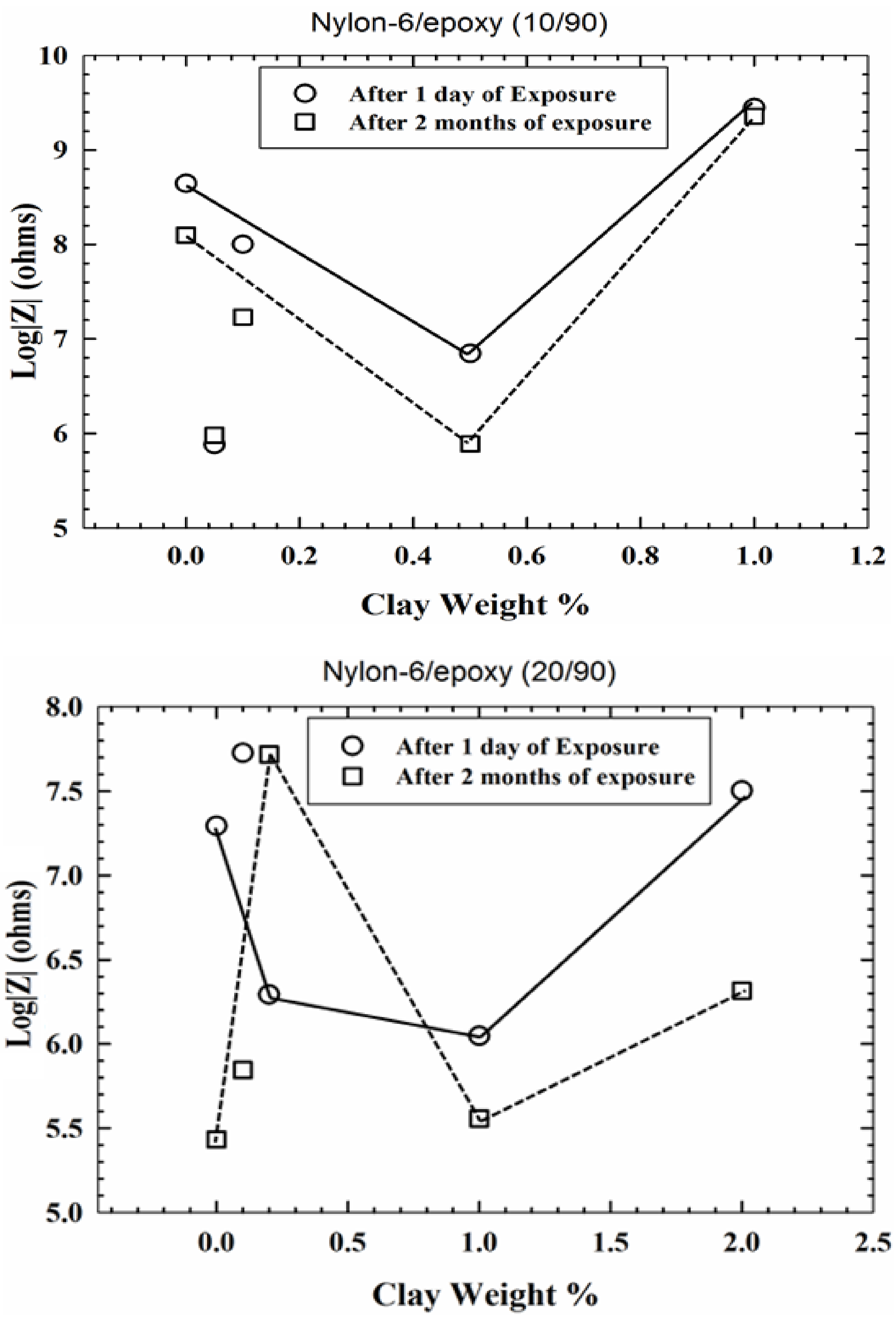

Figure 6 – Impedance as a function of clay weight% in nylon-6/epoxy composite coatings at a weight ratio of (a) 10/90 and (b) 20/80

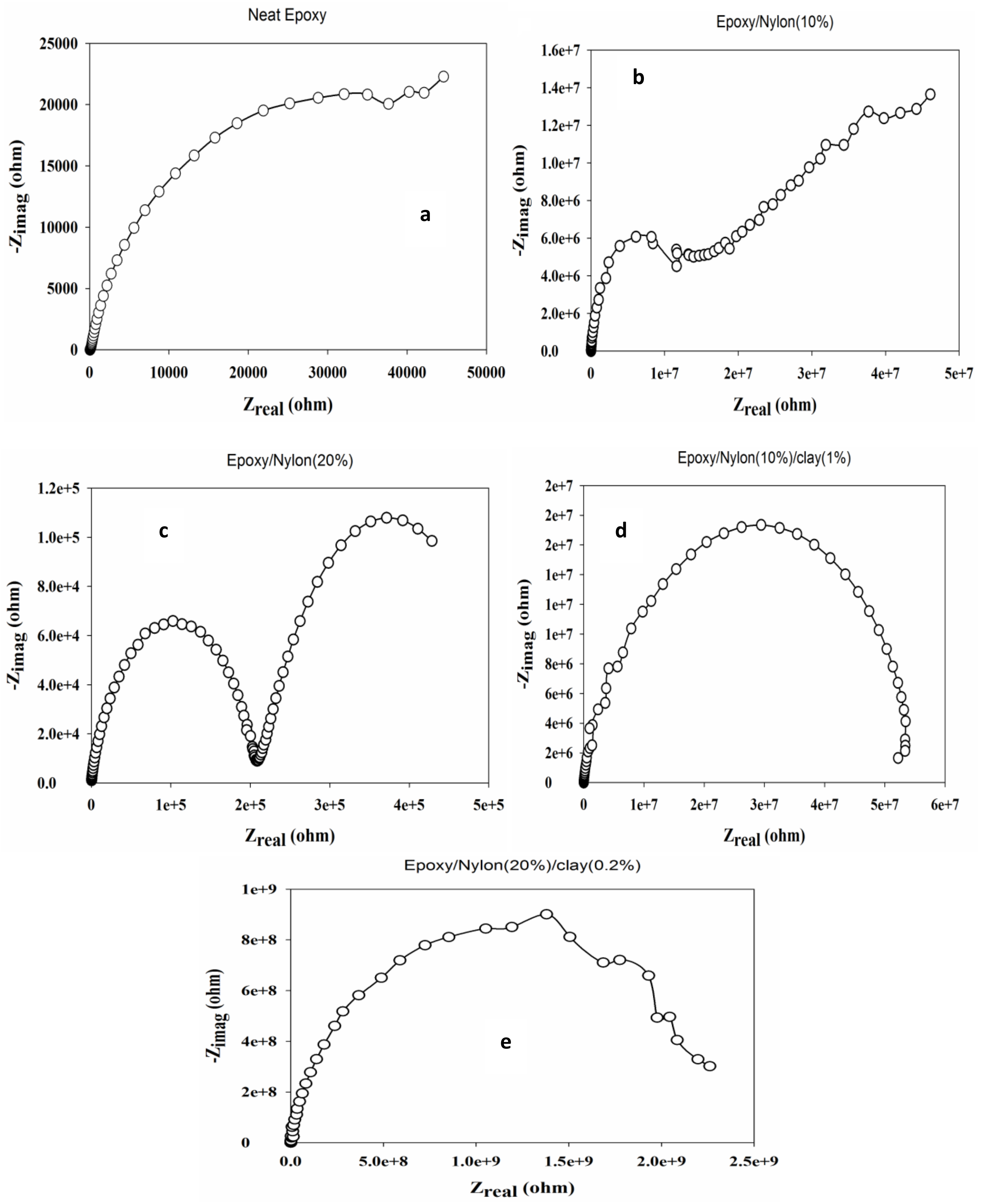

Fig 7 – EIS Nyquist Diagram for composite coating on Al alloy substrate after 2 months of exposure in 3.5 wt.% salt solution (a) neat epoxy (b) epoxy/nylon(10%) (c) epoxy/nylon(20%) (d) epoxy/nylon(10%)/clay(1%) (e) epoxy/nylon(20%)/clay(0.2%)

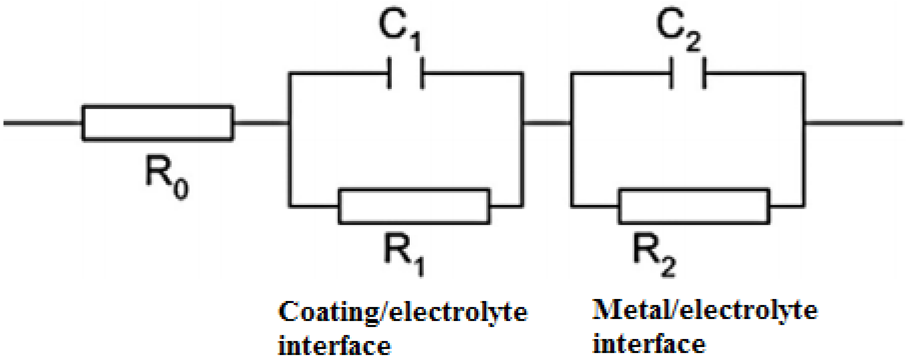

Figure 8 – Schematic diagram of equivalent electric circuit model

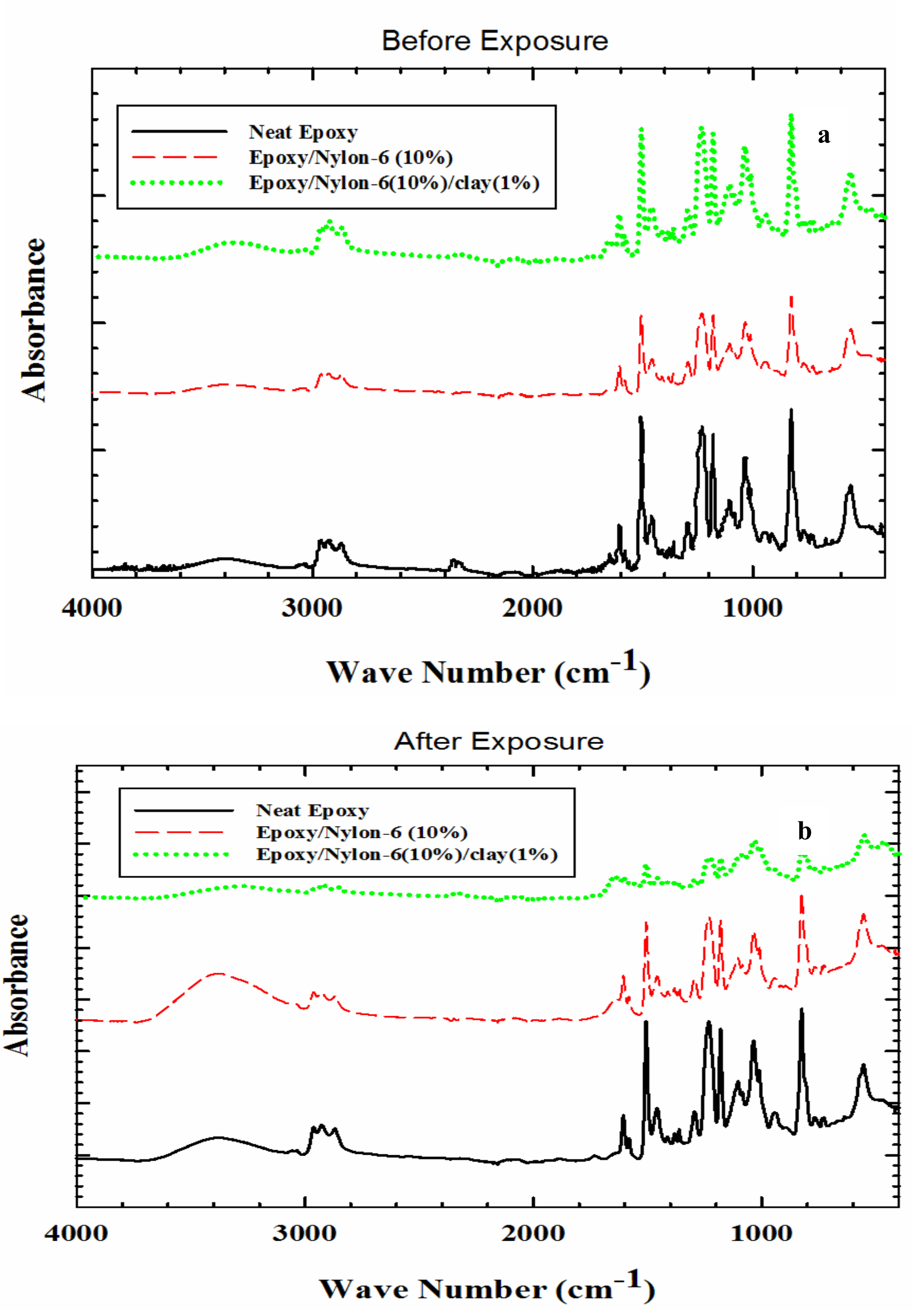

Figure 9 – FTIR spectrum of epoxy, epoxy/nylon-6 and epoxy/nylon-6/clay (a) before exposure (b) after 2 months of exposure to 3.5 weight% salt solution

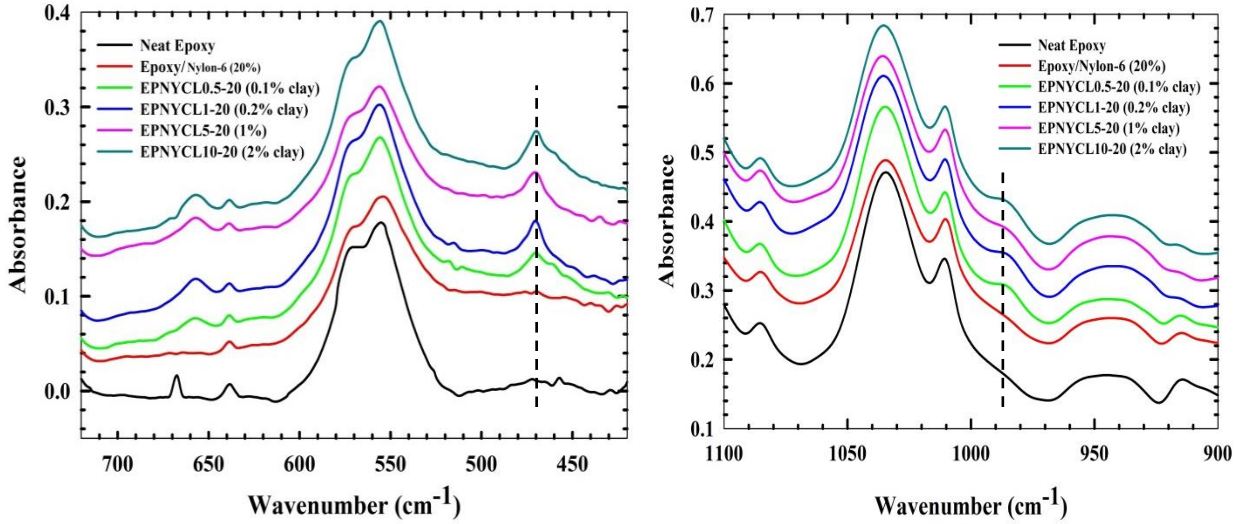

Figure 10 – FTIR spectrum for neat epoxy, polyamide-6/epoxy and clay/PA6-epoxy systems showing peak at (a) 470 cm^{-1} and (b) 980 cm^{-1}

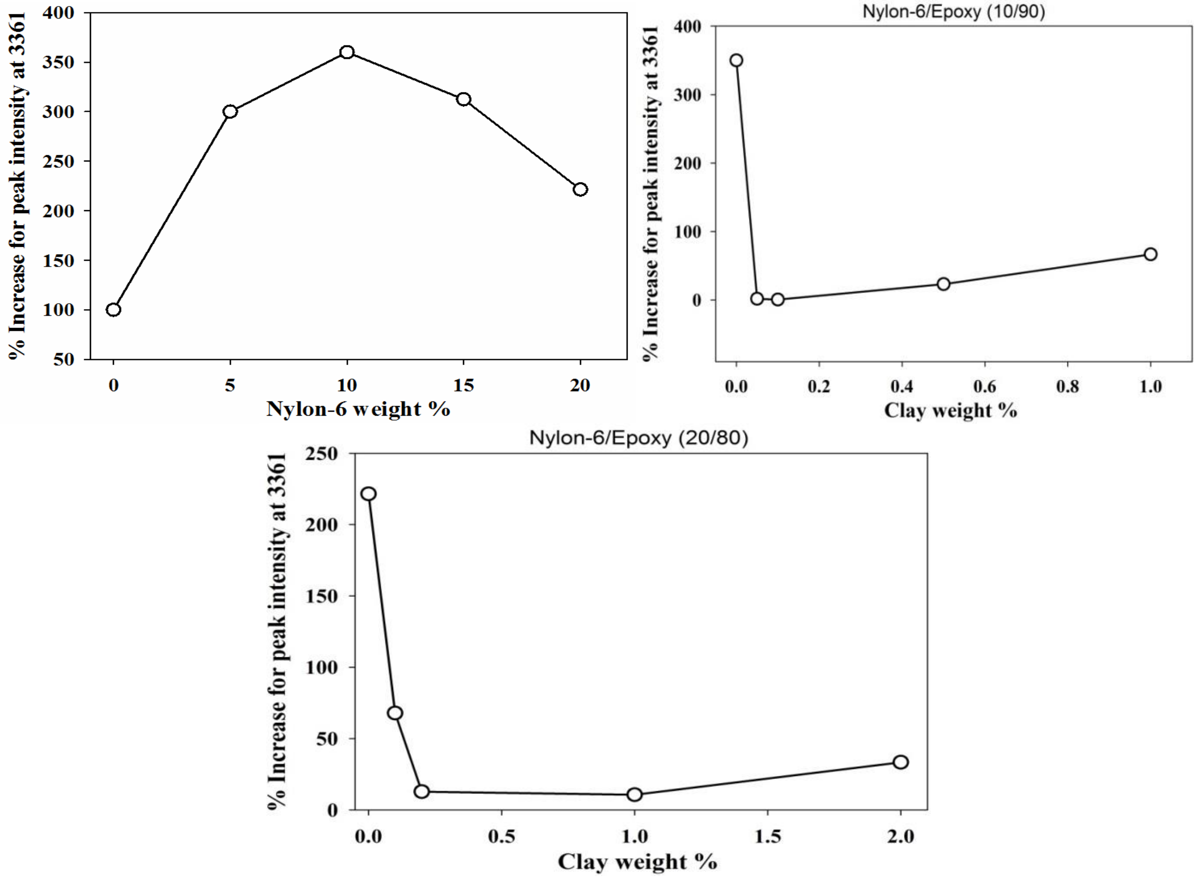

Figure 11 – percentage increase in the peak height of hydroxyl peak at 3361 cm^{-1} after exposure for (a) nylon-6/epoxy (b) clay/nylon-6(10%)/epoxy (c) clay/nylon-6(20%)/epoxy coatings

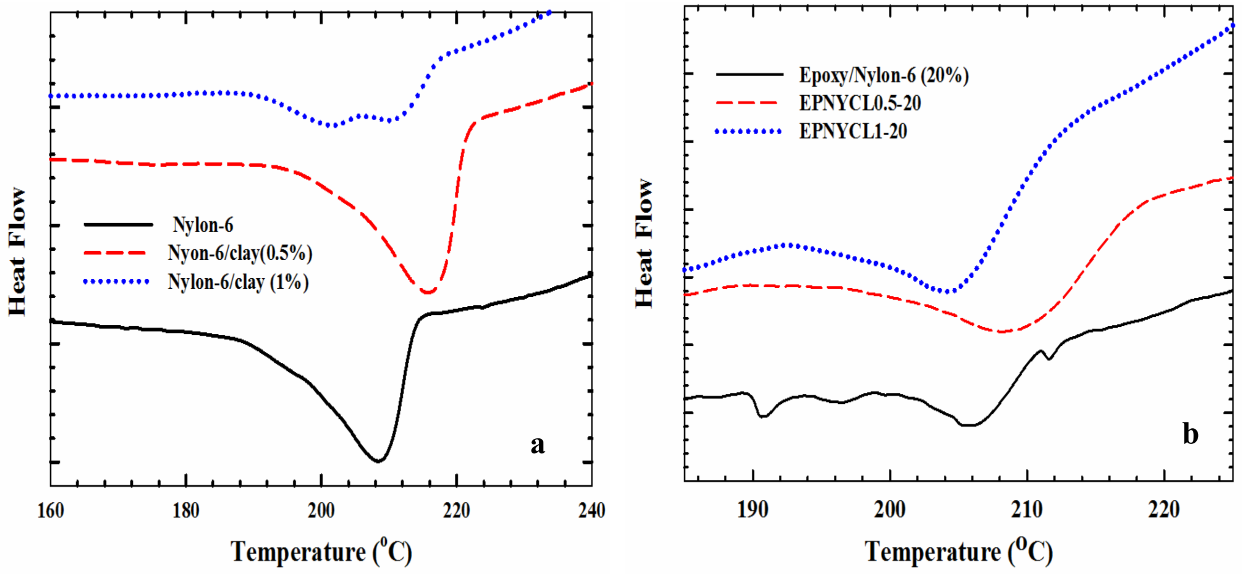

Figure 12– DSC thermogram showing the effect of clay on melting of (a) Nylon-6 and (b) nylon-6 in epoxy resin at ratio of 80:20 (epoxy: nylon-6)

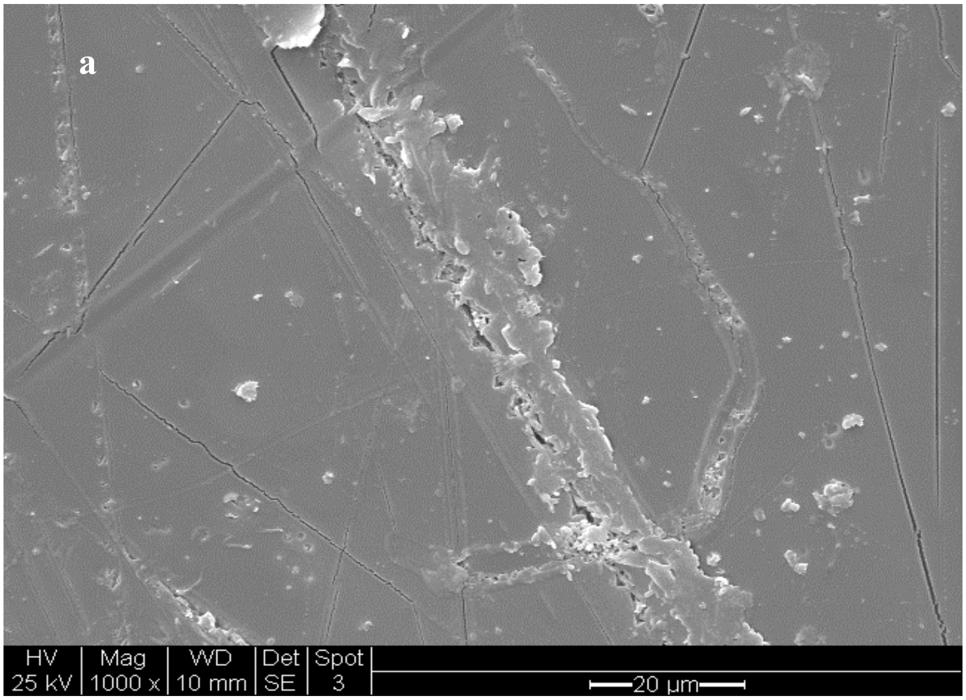

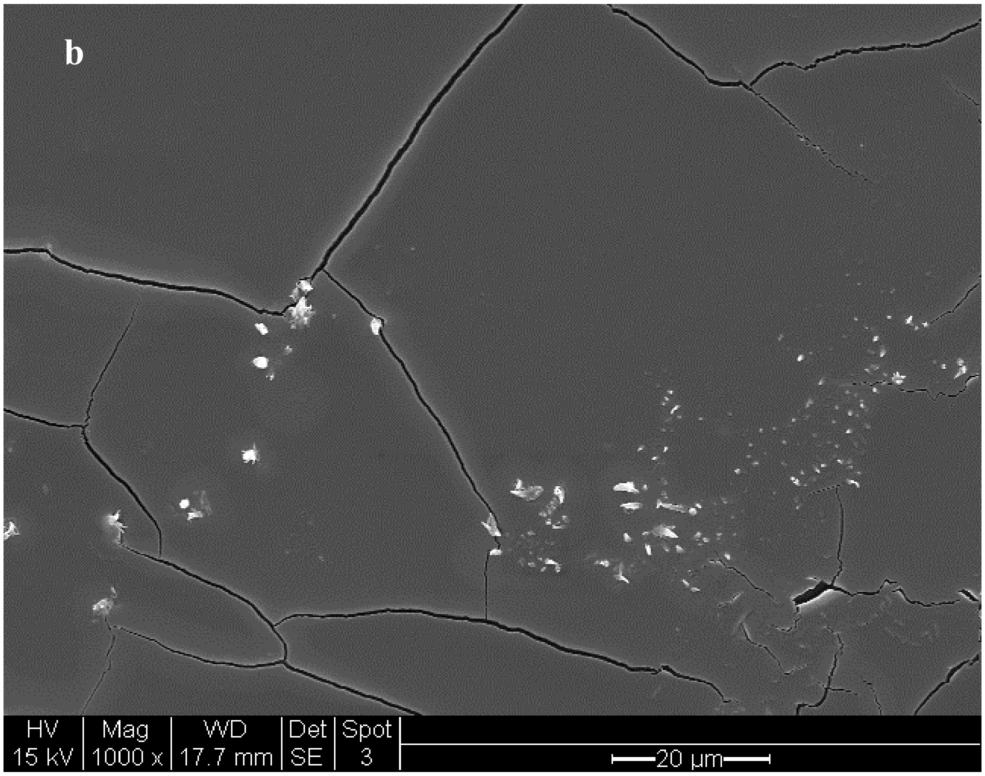
b
HV 15 kV
Mag 1000 x
WD 17.7 mm
Det SE
Spot 3
20 μm

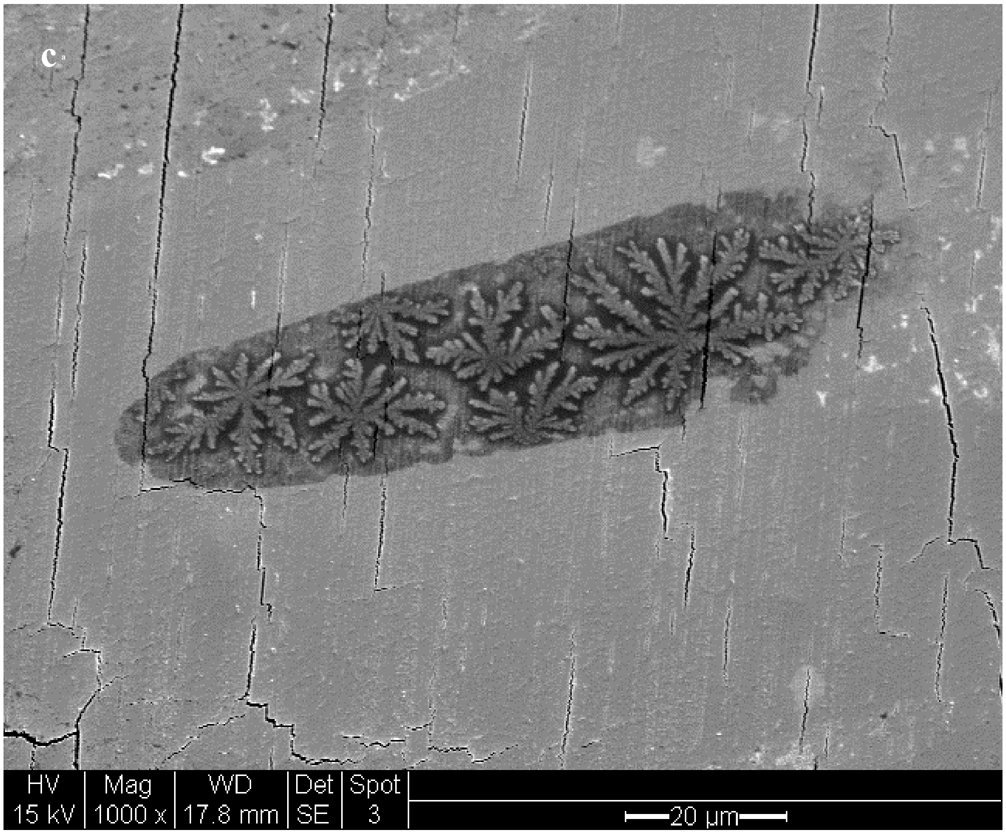
c
HV 15 kV
Mag 1000 x
WD 17.8 mm
Det SE
Spot 3
20 μm

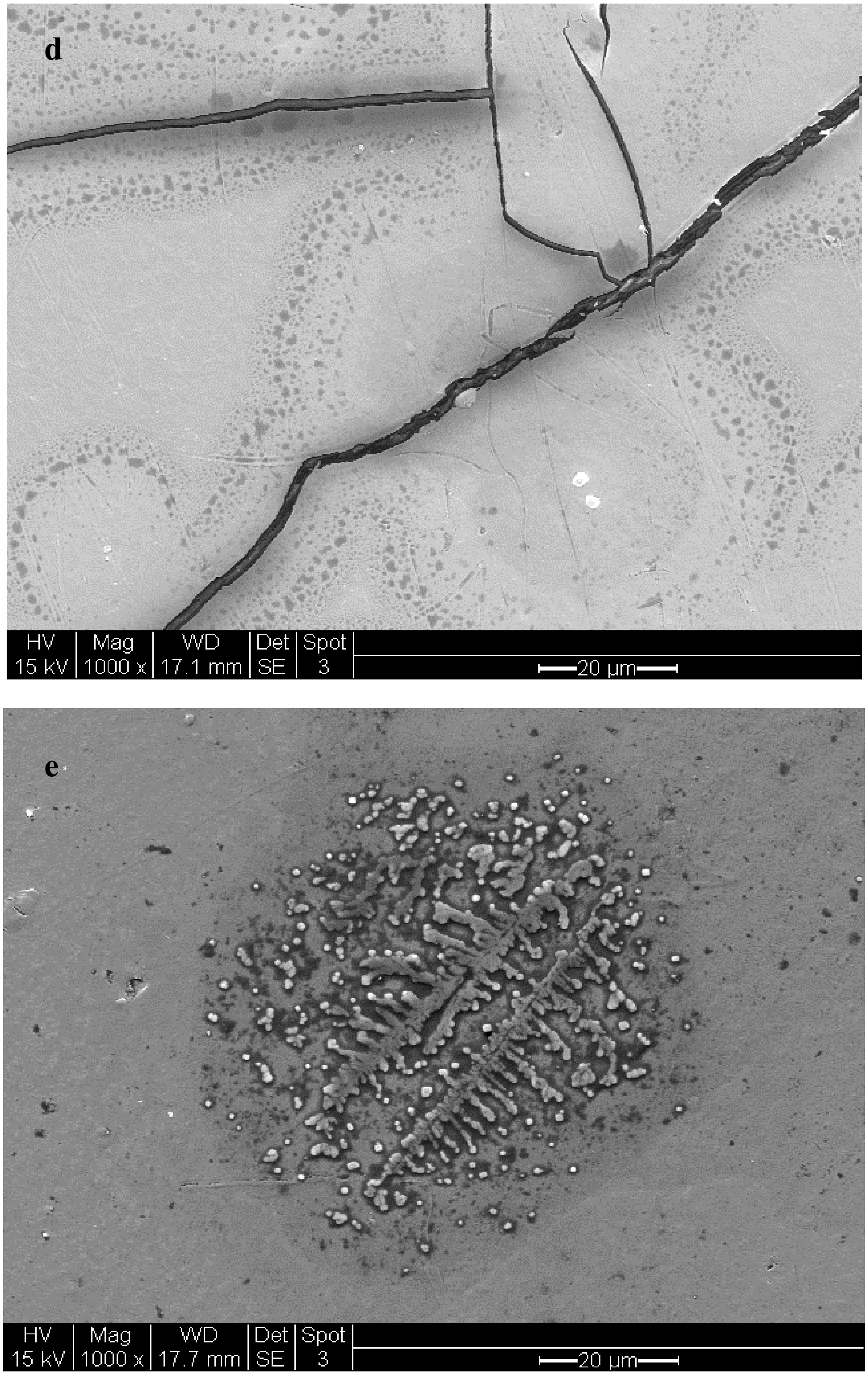

Figure 13 –SEM images of coating surface (a) Epoxy/Nylon-6 (10%), (b) Epoxy/Nylon-6 (10%)/clay(0.05%), (c) Epoxy/Nylon-6 (10%)/clay(0.1%), (d) Epoxy/Nylon-6 (10%)/clay(0.5%), (e) Epoxy/Nylon-6 (10%)/clay(1%)

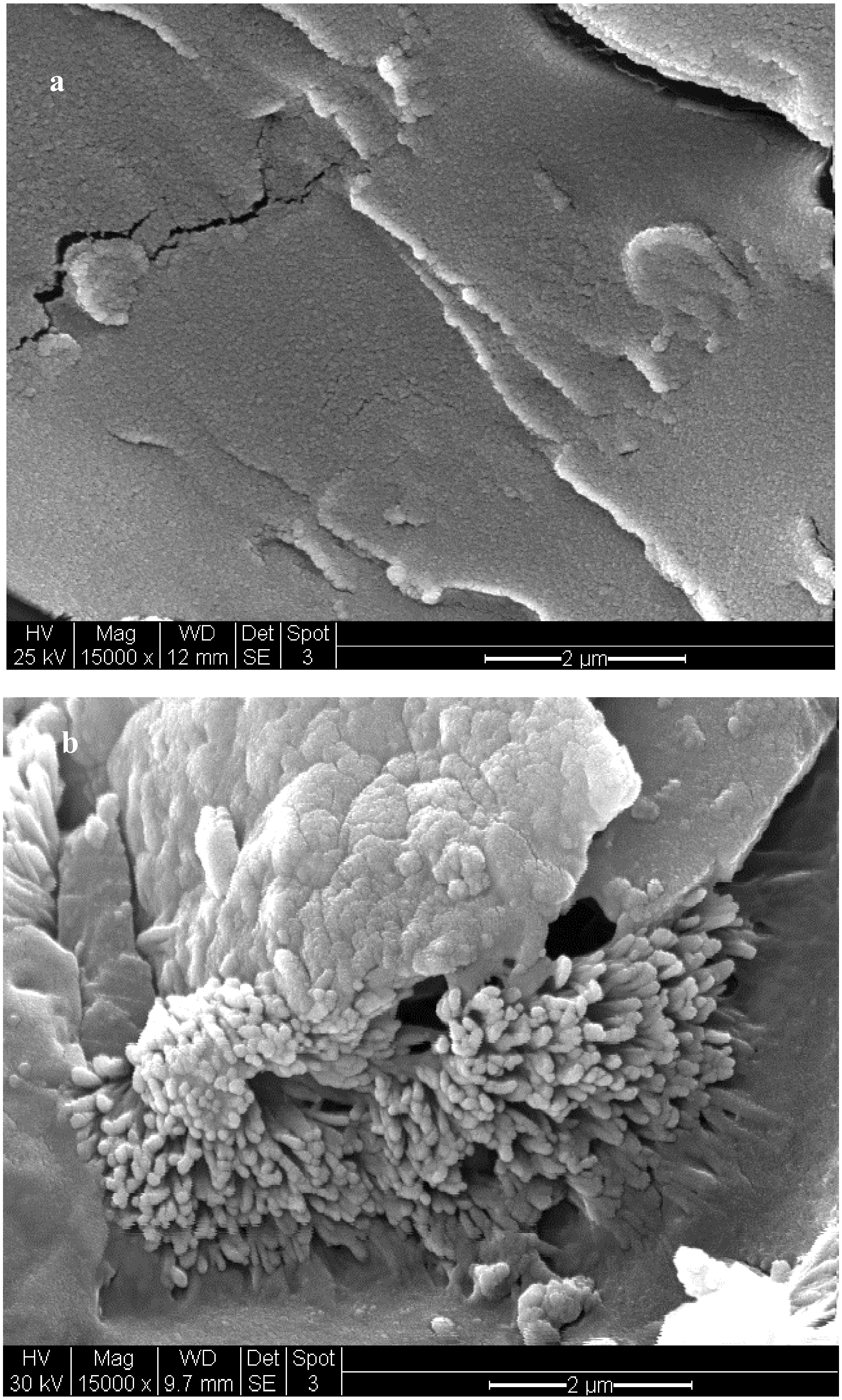
a
HV
25 kV
Mag
15000 x
WD
12 mm
Det
SE
Spot
3
2 µm
b
HV
30 kV
Mag
15000 x
WD
9.7 mm
Det
SE
Spot
3
2 µm

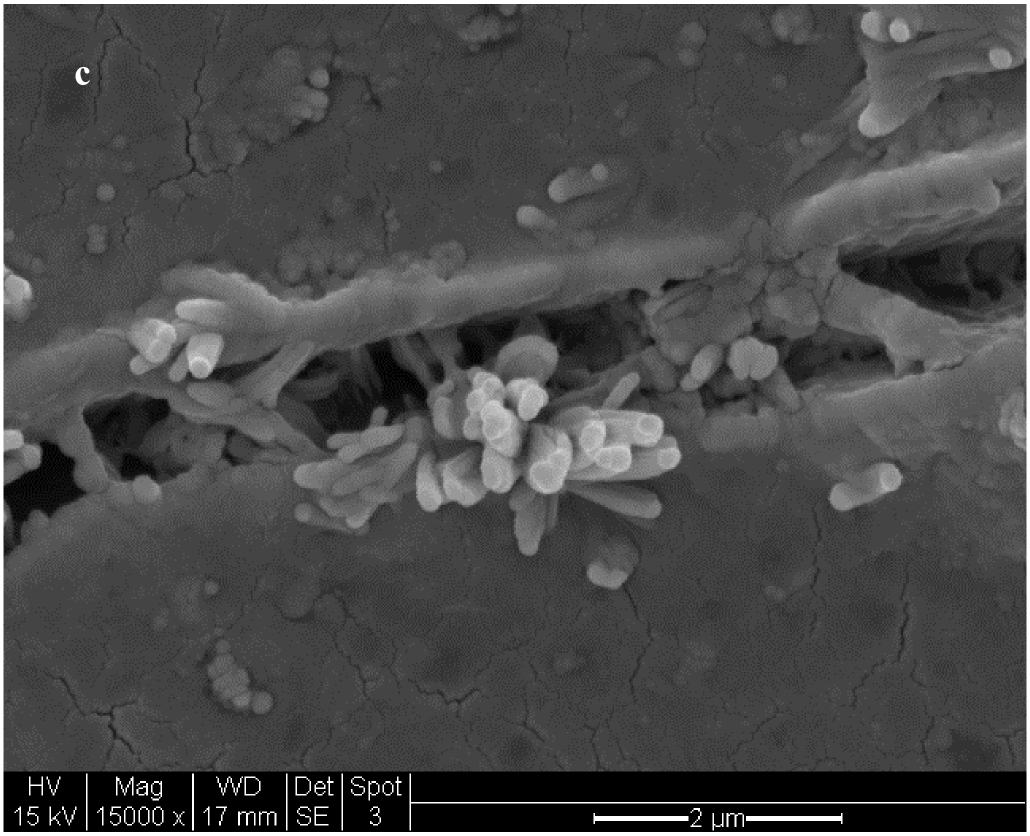
c
HV
15 kV
Mag
15000 x
WD
17 mm
Det
SE
Spot
3
2 µm

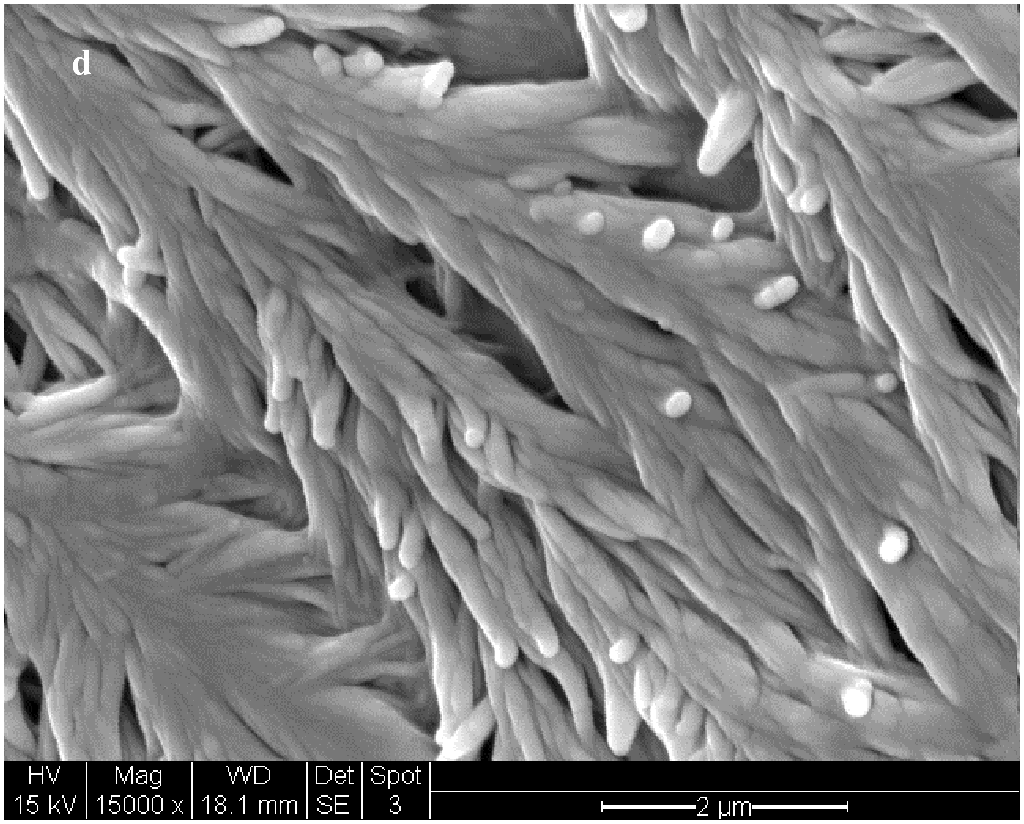
d
HV
15 kV
Mag
15000 x
WD
18.1 mm
Det
SE
Spot
3
2 µm

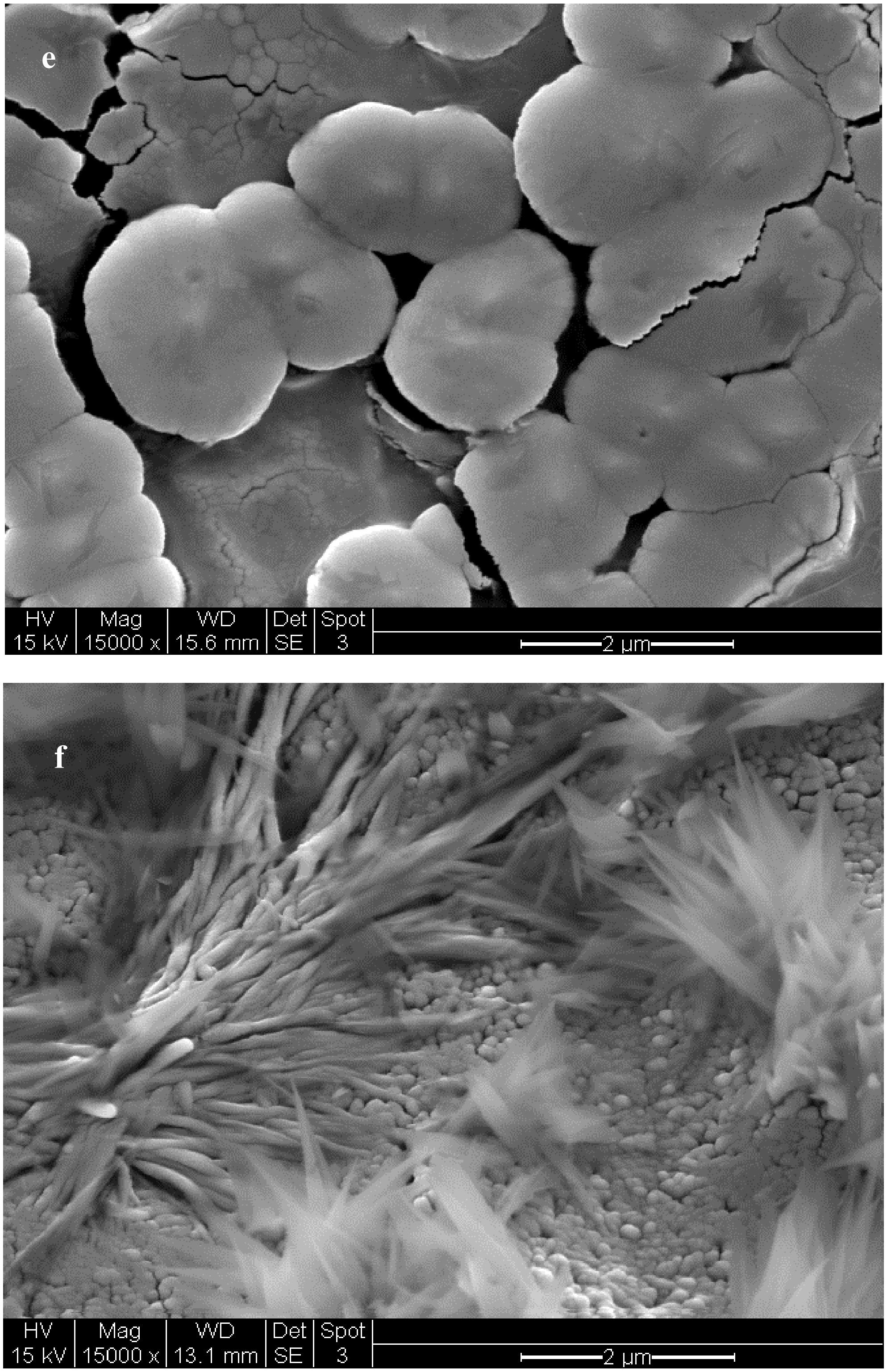

Figure 15 –SEM images of fractured surface of films (a) neat epoxy, (b) Epoxy/Nylon-6 (10%), (c) Epoxy/Nylon-6 (10%)/clay(0.05%), (d) Epoxy/Nylon-6 (10%)/clay(0.1%), (e) Epoxy/Nylon-6 (10%)/clay(0.5%), (f) Epoxy/Nylon-6 (10%)/clay(1%)

Table 1 - Various compositions prepared for clay/nylon-6-epoxy systems

Composition	% Epoxy	% Nylon-6	% Clay
EPNY5	95	5	0
EPNY10	90	10	0
EPNY15	85	15	0
EPNY20	80	20	0
EPNYCL0.5-10	90	9.95	0.05
EPNYCL0.5-20	80	19.9	0.1
EPNYCL1-10	90	9.9	0.1
EPNYCL1-20	80	19.8	0.2
EPNYCL5-10	90	9.5	0.5
EPNYCL5-20	80	19	1
EPNYCL10-10	90	9	1
EPNYCL10-20	80	18	2

Table 2 – Parameters obtained from direct current polarization for nylon-6/epoxy (10/90)

Compositions	I_{corr} (A/cm^{-2}) – after 1 day	E_{corr} (V) – after 1 day	I_{corr} (A/cm^{-2}) – after 2 months	E_{corr} (V) – after 2 months
Neat Epoxy	3.76×10^{-7}	-0.66	2.21×10^{-6}	-0.90
Nylon-6/Epoxy	4.08×10^{-6}	-0.79	9.05×10^{-7}	-0.54
0.05% clay	4.96×10^{-6}	-0.81	4.73×10^{-8}	-0.86
0.1% clay	2.84×10^{-9}	-1.26	9.49×10^{-9}	-0.93
0.5% clay	6.45×10^{-9}	-0.86	7.07×10^{-8}	-0.80
1% clay	1.64×10^{-9}	-1.20	2.78×10^{-10}	-0.96

Table 3 - Parameters obtained from direct current polarization for nylon-6/epoxy (20/80)

Compositions	**I_{corr} (A/cm^{-2}) – after 1 day**	**E_{corr} (V) – after 1 day**	**I_{corr} (A/cm^{-2}) – after 2 months**	**E_{corr} (V) – after 2 months**
Neat Epoxy	3.76×10^{-7}	-0.66	2.21×10^{-6}	-0.90
Nylon-6/Epoxy	2.22×10^{-6}	-0.73	1.94×10^{-5}	-0.76
0.1% clay	4.54×10^{-7}	-1.22	4.39×10^{-8}	-0.65
0.2% clay	2.80×10^{-9}	-1.10	7.76×10^{-9}	-0.97
1% clay	7.88×10^{-8}	-1.12	1.30×10^{-7}	-0.86
2% clay	4.29×10^{-9}	-1.20	1.54×10^{-8}	-0.55

Table 4 - Parameters obtained from EIS –Nyquist Plots after 2 months of exposure to 3.5 weight% NaCl solution for clay/nylon-6/epoxy coatings

	R_0 (Ω)	**R_1 (Ω)**	**C_1 (F)**	**R_2 (Ω)**	**C_2(F)**
Neat Epoxy	990	63.3×10^{3}	7.8×10^{-6}	3.1	3.2×10^{-12}
Epoxy/nylon(10%)	218.6	16.2×10^{6}	281.1×10^{-12}	11.2	8.9×10^{-15}
Epoxy/nylon(20%)	528.1	191.7×10^{3}	317.3×10^{-12}	17.3	54.9×10^{-15}
Epoxy/nylon(10%)/clay (1%)	198.6	32.4×10^{6}	693.6×10^{-12}	33.9×10^{3}	3.1×10^{-12}
Epoxy/nylon(10%)/clay(0.2%)	232.2	15.5×10^{6}	295.2×10^{-12}	1.8×10^{3}	9.3×10^{-12}